Simulation and Optimization of Medium Deep Borehole Thermal Energy Storage Systems

Dissertation

Doctoral thesis approved in fulfillment of the requirements
for the degree of Doktor-Ingenieur (Dr.-Ing.)
at the
Department of Material and Earth Sciences,
Technische Universität Darmstadt

TECHNISCHE
UNIVERSITÄT
DARMSTADT

Graduate School of
**Energy Science
and Engineering**

Submitted by

Daniel Otto Schulte, MSc
born on 19.09.1985 in Hagen, Germany

Date of thesis submission: 02.11.2016
Date of examination: 19.12.2016

Thesis approved by

Supervisor Prof. Dr. Ingo Sass
Co-supervisor Prof. Dr. Sebastian Geiger

Darmstadt, 20th December 2016

D17

Board of examiners

Head:	Prof. Dr. Andreas Henk
Supervisor:	Prof. Dr. Ingo Sass
Co-supervisor:	Prof. Dr. Sebastian Geiger
Examiner:	Prof. Dr.-Ing. Carl-Alexander Graubner
Examiner:	Prof. Dr. Matthias Hinderer

Declaration

I hereby declare that the presented dissertation is based on original research and is the result of my own work. I certify that this dissertation contains no material which has been accepted for the award of any other degree in my name, in any university or other tertiary institution and, to the best of my knowledge and belief, contains no material previously published or written by another person, except where due reference has been made in the text.

Darmstadt,   November 2nd, 2016

Abstract

In the heating and cooling sector, borehole heat exchangers (BHE) have become increasingly popular for supplying renewable energy. When grouped in compact arrays, BHEs represent suitable thermal energy storage systems for fluctuating heat sources such as solar energy or district heating grids. Tapping into greater depth allows for storage operation on a higher temperature level. This so-called medium deep borehole thermal energy storage (BTES) requires negligible groundwater flow in the reservoir rock and the thermal insulation of the upper part of the boreholes to meet legal requirements and to improve the BHEs' performance. Medium deep BTES is characterized by a slow thermal response and a large storage capacity, which makes it particularly suitable for seasonal heat storage applications.

However, the economic feasibility of these systems is compromised by high investment costs, especially by the expensive drilling of the boreholes. Therefore, a priori numerical simulations of the storage operation are imperative for the systems' planning and design. Only fully discretized models can account for depth-dependent borehole properties like insulated sections, but the model setup is cumbersome and the simulations come at high computational cost. Hence, these models are often not suitable for the simulation of larger installations and are difficult to handle in mathematical optimization applications. This thesis presents a versatile tool for the simulation and optimization of medium deep BTES systems. The Borehole Heat Exchanger Array Simulation and Optimization tool (BASIMO) includes models for the three most common BHE types: U-pipe, double U-pipe and coaxial pipe BHEs. In a dual-continuum approach, the simulator couples a numerical subsurface model with an analytical solution for the BHEs, which allows for the efficient, but detailed consideration of the relevant thermo-physical and operational parameters. With the presented tool, many aspects of BTES systems can be simulated and optimized.

The concept of medium deep BTES has not been put into practice so far. However, simulations yield promising results and show that large-scale medium deep BTES can achieve more than 80 % storage efficiency. The performance is sensitive to many geological, material and operational parameters, but also to the interaction between the BHE array and the downstream heating system. Therefore, future research should focus on coupled simulations including the above ground facilities and, more importantly, on the realization of field experiments including first and foremost a pilot plant, which could help to push this promising technology to economic viability.

Kurzfassung

Erdwärmesonden kommen zur Bereitstellung erneuerbarer Wärme und Kälte immer stärker zum Einsatz. Als engständige Sondenfelder stellen Erdwärmesonden Speichersysteme dar, die für Wärme aus fluktuierenden Quellen wie Solarthermie oder Nahwärmenetzen geeignet sind. Werden dabei im Untergrund von einem Sondenfeld größere Tiefen erschlossen, sind höhere Betriebstemperaturen im Wärmespeicher möglich. Solche sogenannten mitteltiefen Erdwärmesondenspeicher erfordern Standorte mit vernachlässigbar geringem Grundwasserfluss im Reservoir und eine thermische Isolierung im oberen Abschnitt der Bohrlöcher, um dem Grundwasserschutz gerecht zu werden und um die Entzugstemperaturen der Erdwärmesonden zu verbessern. Mitteltiefe Erdwärmesondenspeicher zeichnen sich durch ein verhältnismäßig träges thermisches Verhalten und hohe Speicherkapazitäten aus. Dadurch ist diese Technologie für die saisonale Speicherung von Wärme besonders geeignet.

Hohe Investitionskosten, besonders bedingt durch teure Bohrungen, stellen ein Risiko dar und können die Wirtschaftlichkeit eines Erdwärmesondenspeichers gefährden. Deshalb sind vorab numerische Simulationen des Speicherbetriebs zwingend für die Planung und Dimensionierung solcher Systeme erforderlich. Bisher konnten nur voll diskretisierte Modelle tiefenabhängige Eigenschaften wie die teilweise Isolierung des Bohrlochs berücksichtigen. Das Erstellen und die Simulation solcher Modelle sind jedoch aufwändig und sehr rechenintensiv. Daher sind voll diskretisierte Modelle für die Simulation großer Sondenfelder meist ungeeignet. Darüber hinaus ist eine mathematische Optimierung in den Simulationsprogrammen gewöhnlich nicht vorgesehen. In dieser Dissertation wird ein neues, vielseitiges Softwaretool vorgestellt, dass für die Simulation und Optimierung von mitteltiefen Erdwärmesondenspeichern geeignet ist. Das *Borehole Heat Exchanger Array Simulation and Optimization* (BASIMO) Tool kann Modelle mit den drei gängigen Erdwärmesondentypen U-Sonde, Doppel U-Sonde und Koaxialsonde, berechnen. In einem Zwei-Kontinuumsmodell wird die numerische Berechnung des Wärmetransports im Untergrund mit einer analytischen Lösung für die thermische Interaktion der Erdwärmesonden gekoppelt. Dies ermöglicht eine effiziente, aber detaillierte Modellierung der Erdwärmesonden, welche die relevanten thermo-physikalischen Material- und Betriebsparameter berücksichtigt. Mit dem diesem Simulationstool können viele Aspekte von Erdwärmesondenspeichern simuliert und optimiert werden.

Die mitteltiefe Speicherung von thermischer Energie mittels Erdwärmesonden wurde bisher noch nicht umgesetzt. Die Simulationen ergeben jedoch vielversprechende Ergebnisse: mit großen Sondenfeldern und entsprechend großen Wärmemengen, lassen sich Speichernutzungsgrade von über 80 % erzielen. Dabei ist die Leistung der Erdwärmesondenspeicher sowohl von geologischen, als auch von Material- und Betriebsparametern abhängig. Es zeigt sich aber, dass auch die dynamische Interaktion zwischen Erdwärmesondenspeicher und nachgeschaltetem Heizsystem eine große Rolle spielt. Zukünftige Forschung sollte sich deshalb auf gekoppelte Simulationen der Erdwärmesondenspeicher und der obertägigen Anlagen konzentrieren, vor allem jedoch auf die Umsetzung erster Demonstrationsprojekte, mit deren Hilfe diese vielversprechende Technologie zur Marktreife gebracht werden kann.

Acknowledgement

Preface

This PhD thesis is associated with the dissertation of my colleague Bastian Welsch within the joint project "Simulation and evaluation of coupling and storage concepts for renewable forms of energy for heat supply" (Simulation und Evaluierung von Kopplungs- und Speicherkonzepten regenerativer Energieformen zur Heizwärmeversorgung). The participating project partner was the local energy producer HEAG Südhessische Energie AG (HSE), now known as ENTEGA. The project (HA project no. 375/13-14) was funded within the framework of Hessen ModellProjekte, financed with funds of Energietechnologieoffensive Hessen – Projektförderung in den Bereichen Energieerzeugung, Energiespeicherung, Energietransport und Energieeffizienz. It was launched in 2013 and completed in 2015. My own research was funded through a scholarship by the Darmstadt Graduate School of Excellence Energy Science and Engineering (GSC 1070), which is financed by the Deutsche Forschungsgemeinschaft (DFG) in the framework of the Excellence Initiative.

The objective of the project was to develop simulation tools for coupled models, which consider the subsurface heat transport and the operation of above ground installations. The results were used to gather virtual experiences with medium deep borehole thermal energy storage (BTES) systems in order to prepare a proposal for the construction of a pilot facility. My accompanying research allowed for the in-house development of the simulation tool BASIMO (Borehole Heat Exchanger Array Simulation and Optimization) based on MATLAB instead of using the commercial software FEFLOW. This opened up possibilities to optimize the design of BTES systems mathematically and added value to the project beyond the initially proposed goals.

Here, I present a cumulative dissertation that includes the five publications following below. They reflect the course of my research and my growing contributions to the joint scientific effort. The publications listed below are attached as an appendix to this thesis. The accompanying manuscript contains verbatim sections of my first-author publications that are not explicitly referenced. As BASIMO was only publishable as a general synaptic description at the time this thesis was drafted, a comprehensive description of the simulator and the mathematical optimization approach is part of the presented enveloping manuscript together with a general introduction to the topic of medium deep BTES systems.

Appendix A: Bär K, Rühaak W, Welsch B, **Schulte DO**, Homuth S and Sass I (2015): Seasonal high temperature storage with medium deep borehole heat exchangers, Energy Procedia, v. 76, p. 351-360, doi:10.1016/j.egypro.2015.07.841.

Appendix B: Welsch B, Rühaak W, **Schulte DO**, Bär K and Sass I (2016): Characteristics of medium deep borehole thermal energy storage, International Journal of Energy Research, v. 40, no. 13, p. 1855-1868, doi: 10.1002/er.3570.

Appendix C: **Schulte DO**, Rühaak W, Oladyshkin S, Welsch B and Sass I (2016): Optimization of Medium-Deep Borehole Thermal Energy Storage Systems, Energy Technology, v. 4, p. 104-113, doi:10.1002/ente.201500254.

Appendix D: **Schulte DO**, Welsch B, Boockmeyer A, Rühaak W, Bär K, Bauer S and Sass I (2016) Modeling insulated borehole heat exchangers, Environmental Earth Sciences, v. 75, p. 1-12, doi:10.1007/s12665-016-5638-x.

Appendix E: **Schulte DO**, Rühaak W, Welsch B and Sass I (2016): BASIMO – borehole heat exchanger array simulation and optimization tool, Energy Procedia, v. 97, p. 210-217, doi:/10.1016/j.egypro.2016.10.057.

Appendix A is the first publication of the joint project "Simulation and evaluation of coupling and storage concepts for renewable forms of energy for heat supply" and lays the foundation for the research published in the papers mentioned hereafter. It introduces the concept of seasonal high temperature storage with medium deep borehole heat exchangers (BHE). The publication describes the key features of BTES and the general behavior of such systems. In a case study, different scenarios considering excess heat for storage from solar thermal collectors and a combined heat and power plant are assessed. Ultimately, the importance of prior detailed knowledge of the system specifications is pointed out. The authors emphasize the necessity of a priori numerical simulations for the determination of the eventual storage system design outlining the subsequent research.

Kristian Bär is the first author of this paper. He coordinated the project "Simulation and evaluation of coupling and storage concepts for renewable forms of energy for heat supply" and drafted the paper. He also gathered the data on the heat demand and designed the different heat supply scenarios for the case study. As a coauthor, I engaged in discussions with Kristian Bär, Bastian Welsch and Wolfram Rühaak on the aspects and requirements of numerical simulations of BTES. Furthermore, I developed the concept for the mathematical optimization and coupled simulation of these systems. Together with Bastian Welsch, I set up the numerical simulations and evaluated the results. Wolfram Rühaak supervised the numerical modeling and provided technical assistance. Bastian Welsch carried out field work and laboratory experiments for the site characterization of the case study. Sebastian Homuth gathered information on the required drilling technology and contributed to the manuscript accordingly. Ingo Sass supervised the project and the research. All coauthors engaged in early discussions, developed the concept of medium deep BTES and contributed to the revision of the manuscript.

Appendix B is a comprehensive preliminary parameter study on medium deep BTES. The study was carried out prior to the development of BASIMO with the commercial software FEFLOW to acquire basic knowledge of the general behavior of BTES systems and the dependency on several different system parameters. In more than 250 numerical simulations the effect of changing geometrical configurations of BTES systems as well as changing material and operational parameters on the long-term performance is investigated. The authors quantify and discuss the influence of the different variable parameters. Larger systems in particular show high potential for efficient seasonal storage of several GWh of heat with a recovery rate of more than 80 %.

Bastian Welsch is the first author of this paper. He set up all models and ran the numerical simulations. Also, he evaluated the results and drafted the manuscript. As a coauthor of this paper, I co-developed the experimental design of the numerical experiments together with Bastian Welsch and Wolfram Rühaak and helped to identify relevant model responses for the evaluation of the simulation results. Most notably, I was closely involved with the writing and editing of the manuscript. Wolfram Rühaak supervised the setup of the numerical models and provided technical assistance and engaged together with Kristian Bär and myself in early discussions on the general concept of seasonal heat storage. Furthermore, Kristian Bär coordinated the project "Simulation and evaluation of coupling and storage concepts for renewable forms of energy for heat supply", which provided the framework for this study. Ingo Sass supervised the project and the research. All coauthors contributed to the revision of the manuscript.

Appendix C is a description of the proxy model-based optimization approach, which can be adapted to many design aspects of medium deep BTES systems. Besides a basic description of the numerical methods applied for the simulation, the paper also includes a short summary on the arbitrary polynomial chaos expansion employed for the generation of the proxy model and the mathematical optimization algorithm used in the study. In an application example the ideal size of a BTES system is determined and the approximation error of the reduced model is discussed.

As the first author of this paper, I developed and programmed the numerical simulator, ran the proxy training simulations and the optimization, evaluated the results, calculated the approximation errors and drafted the manuscript. Wolfram Rühaak supervised the developments and assisted with the programming, especially with the matrix assembly routine, which had to be built in C++ for performance reasons. Furthermore, he engaged with me in countless discussions on many detailed programming aspects of the simulator. Sergey Oladyshkin provided a MATLAB script for the arbitrary polynomial chaos expansion and contributed to the manuscript accordingly. Bastian Welsch engaged in early discussions on the setup of the experimental design of simulation experiments and provided valuable ideas, as this issue was closely related to his own research (see above). He also contributed some of the figures. Ingo Sass supervised my research. All coauthors contributed to the revision of the manuscript.

Appendix D deals with the modeling of the partial insulation of BHEs within the borehole. This is an important feature of medium deep BTES systems, which has to be considered in numerical simulations. A borehole insulation can help to mitigate negative environmental impacts on shallow aquifers induced by high temperature heat storage. Furthermore, it can increase the performance of medium deep BHEs. Up to the publication of this paper, only fully discretized numerical models were able to adequately describe properties changing along the borehole length. In *Appendix D,* an existing analytical approach is improved to allow for the consideration of grout thermal conductivities and borehole diameters changing with depth. The improved solution is implemented in BASIMO and tested in a benchmark against a fully discretized model. An application example is given by determining the ideal length of a borehole insulation in a specific setup scenario by means of mathematical optimization. The benchmark and the application example are both discussed in terms of accuracy and significance of the results.

As the first author of this paper, I developed and programmed the improved analytical solution for partially insulated BHEs, implemented it into BASIMO, ran the simulations and the optimization for the application example, evaluated the results and drafted the paper. Bastian Welsch co-developed the improved analytical solution and provided high quality figures for the manuscript. Anke Boockmeyer provided the simulation results of a fully discretized OpenGeoSys model for the benchmark case. Wolfram Rühaak provided important suggestions and technical assistance for the implementation of the improved analytical solution into BASIMO. Kristian Bär engaged in early discussions on the necessity and the features of partially insulated boreholes. Sebastian Bauer and Ingo Sass supervised the work of Anke Boockmeyer and myself, respectively. All coauthors contributed to the revision of the manuscript.

Appendix E advertises BASIMO as a tool for BHE simulation and optimization applications. The structure of the program is explained and all important features of the simulator are briefly introduced. References to the aforementioned papers are given for more detailed descriptions.

Ultimately, *Appendix E* represents a brief synapsis of the development of BASIMO, which gives a good summary of my research's aspects.

In the course of my PhD research, I designed the concept and programmed the code of BASIMO. Furthermore, I tested the progressively improving code countless times to ensure numerical accuracy. As the responsible developer of BASIMO and as the first author of this paper, I wrote the manuscript and created all figures. Wolfram Rühaak supervised the overall development of BASIMO and supported my programming work. Bastian Welsch assisted with the testing and troubleshooting of the code. Ingo Sass supervised my research.

Furthermore, the research was presented on conferences and exhibitions in oral presentations and poster sessions, some including publication in the corresponding proceedings, listed below in chronological order:

Rühaak W, **Schulte DO**, Welsch B, Chauhan S, Bär K, Homuth S and Sass I (2014): Optimierung eines mitteltiefen Erdwärmesondenspeichers, *at* Tagung der Fachsektion Hydrogeologie in der Deutschen Gesellschaft für Geowissenschaften, Bayreuth, Germany, 29-31 May 2014.

Schulte DO, Chauhan S, Welsch B, Rühaak W and Sass I (2014): A MATLAB Toolbox for Optimization of Deep Borehole Heat Exchanger Storage Systems, *at* Computational Methods in Water Resources XX. International Conference, Stuttgart, Germany, 10-13 June 2014.

Welsch B, Rühaak W, **Schulte DO**, Bär K, Homuth S and Sass I (2015): Untersuchung des Leistungsvermögens mitteltiefer Erdwärmesondenspeicher mittels numerischer Modellierung, *at* Geotherm, Offenburg, Germany, 5-6 March 2015.

Schulte DO, Rühaak W, Chauhan S, Welsch B and Sass I (2015): A MATLAB Toolbox for Optimization of Deep Borehole Heat Exchanger Arrays, *in* Proceedings World Geothermal Congress, Melbourne, Australia, 19-25 April 2015.

Bär K, Homuth S, Rühaak W, **Schulte DO**, Welsch B and Sass I (2015): Coupled Renewable Energy systems for seasonal High Temperature Heat storage via Medium Deep Borehole Heat Exchangers, *in* Proceedings World Geothermal Congress, Melbourne, Australia, 19-25 April 2015.

Welsch B, Rühaak W, **Schulte DO**, Bär K, Homuth S and Sass I (2015): A Comparative Study of Medium Deep Borehole Thermal Energy Storage Systems Using Numerical Modelling, *in* Proceedings World Geothermal Congress, Melbourne, Australia, 19-25 April 2015.

Schulte DO, Rühaak W, Chauhan S, Welsch B and Sass I (2015): Simulation and Optimization of Deep Borehole Heat Exchanger Arrays, *at* Energy, Science & Technology International Conference and Exhibition – EST 2015, Karlsruhe, Germany, 20-22 May 2015.

Bär K, Welsch B, **Schulte DO**, Rühaak W, Homuth S and Sass I (2015): Coupled Renewable Energy Systems for Seasonal High Temperature Heat Storage via Medium Deep Bohrehole Heat Exchangers, *at* Energy, Science & Technology International Conference and Exhibition – EST 2015, Karlsruhe, Germany, 20-22 May 2015.

Welsch B, Rühaak W, **Schulte DO**, Bär K and Sass I (2015): A Comparative Study of Medium Deep Borehole Thermal Energy Storage Systems Using Numerical Modelling, *at* Energy, Science & Technology International Conference and Exhibition – EST 2015, Karlsruhe, Germany, 20-22 May 2015.

Bär K, Welsch B, **Schulte DO**, Rühaak W and Sass I (2015): Medium Deep High Temperature Heat Storage, *at* GeoEnergy 2015, Bergen, Norway, 2-3 September 2015.

Welsch B, **Schulte DO**, Rühaak W, Bär K and Sass I (2015): Technical and Economical Evaluation of Medium Deep Borehole Thermal Energy Storages, *at* FEFLOW 2015 Conference, Berlin, Germany, 21-23 September 2015.

Schulte DO, Rühaak W, Welsch B and Sass I (2015): BASIMO Borehole Heat Exchanger Array Simulation and Optimization Tool, *at* Geothermiekongress 2015, Essen, Germany, 2-4 November 2015.

Schulte DO, Rühaak W, Welsch B and Sass I (2015): Simulation unkonventioneller Erdwärmesonden-Anlagen, *at* Geothermiekongress 2015, Essen, Germany, 2-4 November 2015.

Sass I, Welsch B and **Schulte DO** (2016): Mitteltiefe Erdwärmesondenspeicher – Lösung für den Nutzungskonflikt Grundwasserschutz versus Geothermienutzung?, *in* Proceedings 7. Bochumer Grundwassertag, Bochum, Germany, 17 March 2016.

Schulte DO, Rühaak W, Welsch B, Bär K and Sass, I (2016): BASIMO - Borehole Heat Exchanger Array Simulation and Optimization Tool, *at* European Geoscience Union General Assembly 2016, Vienna, Austria, 17-22 April 2016.

Schulte DO, Rühaak W, Welsch B, Oladyshkin S and Sass I (2016): Optimization of Borehole Heat Exchanger Arrays, *at* European Geoscience Union General Assembly 2016, Vienna, Austria, 17-22 April 2016.

Welsch B, Rühaak W, **Schulte DO**, Bär K and Sass I (2016): Advanced Coupled Simulation of Borehole Thermal Energy Storage Systems and Above Ground Installations, *at* European Geoscience Union General Assembly 2016, Vienna, Austria, 17-22 April 2016.

Welsch B, Rühaak W, **Schulte DO**, Bär K and Sass I (2016): Sensitivity Analysis on the Performance of Medium Deep Borehole Thermal Energy Storage Systems, *at* European Geoscience Union General Assembly 2016, Vienna, Austria, 17-22 April 2016.

Welsch B, Rühaak W, **Schulte DO**, Bär K and Sass I (2016): Coupled Modelling and Optimization of Borehole Thermal Energy Storage and Above Ground Installations, *in* Proceedings 67. Berg- und Hüttenmännischer Tag, TU Bergakademie Freiberg, Germany, 8-10 June 2016.

Beside the research related to my dissertation, I published and contributed to the following papers:

Schulte DO, Ring U, Thomson SN, Glodny J and Carrad H (2014): Two-stage development of the Paparoa Metamorphic Core Complex, West Coast, South Island, New Zealand: Hot continental extension precedes sea-floor spreading by ~25 Myr, Lithosphere, v. 6, no. 3, p. 177-197, doi:10.1130/L348.1.

Willershausen I, Weyer V, **Schulte DO**, Lampe F, Buhre S and Willershausen B (2014): In Vitro Study on Dental Erosion Caused by Different Vinegar Varieties Using an Electron Microprobe, Clinical Laboratory, v. 60, no. 5, p. 783-790, doi:10.7754/Clin.Lab.2013.130528.

Willershausen I, **Schulte DO**, Azaripour A, Weyer V, Briseño B and Willershausen B (2015): Penetration Potential of a Silver Diamine Fluoride Solution on Dentin Surfaces. An Ex Vivo Study, Clinical Laboratory, v. 61, no. 11, p. 1695-1701, doi:10.7754/Clin.Lab.2015.150401.

Table of Contents

List of Figures

List of Tables

Index of Abbreviations and Symbols

Abbreviations

aPC	arbitrary polynomial chaos expansion
PCE	polynomial chaos expansion
BASIMO	borehole heat exchanger array simulation and optimization tool
BHE	borehole heat exchanger
BTES	borehole thermal energy storage
CHP	combined heat and power plant
DTH	down-the-hole
FEM	finite element method
GCI	grid convergence index
ROP	rate of penetration
TRCM	thermal resistance and capacity model

Formula symbols

$\mathbf{A}$	thermal conductivity matrix
$\mathbf{B}$	volumetric heat capacity matrix
b/$\mathbf{b}$	variable boundary / right-hand side
c	specific heat capacity
D	borehole diameter
d	norm of integration error
F	safety factor
f	solution to a numerical model
g	equaltiy constraint function
h	grid spacing / inequality constraint function
$\mathbf{J}$	Jacobian matrix
K	permability
L	length
M	total number of polynomials
N	total number of elements/subdomains
n	normal vector / total number of nodes
Q	heat
q	(heat) source / heat flux
R	residual error / set of real numbers
r	grid refinement ratio
S	storage coefficient
T/$\mathbf{T}$	temperature / temperature vector
$\hat{T}$	Dirichlet boundary condition
t	time
$\dot{V}$	volume rate
W	weight coefficient
x	first spatial dimension (global coordinate system), model input
y	second spatial dimension (global coordinate system)
Z	set of discrete numbers
z	third spatial dimension (global coordinate system) / depth
Γ	domain or element boundary

α	auxiliary variable for analytical BHE solution
β	auxiliary variable for analytical BHE solution
γ	auxiliary variable for analytical BHE solution
δ	auxiliary variable for analytical BHE solution
ε	error tolerance
ζ	third spatial dimension (local coordinate system)
η	second spatial dimension (local coordinate system), auxiliary variable
ξ	first spatial dimension (local coordinate system)
θ	time integration coefficient
κ	thermal diffusivity, auxiliary variable
λ	thermal conductivity
μ	auxiliary variable
ν	auxiliary variable
ρ	density
τ	auxiliary variable
ψ	approximation function
Φ	physical model approximation
Ψ	polynomial
Ω	domain or element
ω	weight function

Subscripts and superscripts

0	initial
b	borehole wall
cor	corrector
E	extraction
e	element
$eval$	evaluated
f	fluid
GC	grout change
in	inlet
l	lower variable boundary
n	(ortho)normal / time step / number of real variables
out	outlet
p	element node / number of discrete variables
pre	predictor
Q	heat
q	normal heat flux / Neumann boundary / replaced weight function
rep	representative
S	storage
s	solid rock
T	Dirichlet boundary
u	upper variable boundary
$spec$	specific
tot	total
$*$	optimal

Chapter 1: Introduction

1.1. Background

The public debate on renewable energies is often focused on electricity supply. Yet, countries in high latitudes spend vast amounts of energy on heating, especially in winter. For example, in Germany heating purposes alone account for more than half of the total end energy consumption (AGEB 2013). Consequently, there is a high potential for energy conservation in this sector. Renewable energy sources like solar collectors are increasingly used to cover the heat demand, to reduce the consumption of fossil fuels and to mitigate the CO_2 emissions (Bauer et al. 2010). Likewise, the increased use of district heating grids is supposed to play an important role in the future of renewable energies (Lund et al. 2010; Sass et al. 2015). The grids are often powered by combined heat and power plants (CHP). However, like the demand, the renewable heat supply is subject to seasonality. In summer, solar thermal collector panels provide excess heat, whereas the heating demand is low. Yet, during winter time, a secondary system has to provide heat when the situation is reversed. Moreover, electricity is needed throughout the year, but the seasonality of the heat demand forces CHPs to be run at reduced capacity and renders them inefficient during summer when the heat demand is low. Thus, a seasonal storage can enhance the efficiency of CHPs in district heating grids and solar collector systems by shifting excess heat to winter time.

Early considerations for solar thermal energy systems envisaged water tanks, but other technologies have been considered for seasonal heat storage as well (Schmidt et al. 2004; Dinçer & Rosen 2010; Pinel et al. 2011; Xu et al. 2014; Hesaraki et al. 2015). Because it is often the most expensive component in the system, it is imperative to exploit the decreasing price per storage volume with increasing size (Lindenberger et al. 2000). While water tanks require considerable space on the surface and cannot exploit this reverse correlation, borehole thermal energy storages (BTES) need only a small amount of space to tap into a large volume of subsurface rock. Borehole heat exchangers (BHE) penetrate the rock mass, which provides a high heat capacity and serves as a thermal storage. A BHE is a closed loop pipe system, which is fitted in a borehole. In many countries, the borehole has to be grouted. Depending on the temperature difference between the borehole wall and the fluid circulating in the BHEs, heat is transferred to or from the storage (Sass et al. 2016a). Additionally, geothermal heat feeds such a system. This combination of solar heat usage, seasonal storage and geothermal heat has already demonstrated as highly efficient with shallow BTES in practice in the recent past (Bauer et al. 2008; Bauer et al. 2010; Sibbitt et al. 2012; Mielke et al. 2014).

However, shallow aquifers are often used for the extraction of drinking water. In Germany and many other countries, legal regulations restrict alterations of groundwater that may have a negative impact on drinking water quality (Haehnlein et al. 2010). Thus, excessive heating, which can induce microbial growth, has to be prevented in these aquifers (Verein Deutscher Ingenieure 2001a, b, c; Griebler et al. 2015). Since solar collectors can provide a temperature output of 100 °C and above (Kalogirou 2004) and district heating grids operate at supply temperatures of ≳ 80 °C (Gadd & Werner 2014), storage of the excess heat in shallow BTES at such high temperature levels has to be regarded critically. Instead, the heat can be stored in greater depth. A thermally insulating grout in the upper section of the boreholes protects the topmost aquifer from excessive heating, while the bottom section is used for the heat exchange with the deeper subsurface (Appendix A and Appendix D). The use of geothermal energy at a depth, which significantly exceeds the typical BHE length of 100 m up to 1000 m,

is termed medium deep geothermics (Sass et al. 2016c). Consequently, BHE arrays used for heat storage at these depths are called medium deep BTES systems (Appendix A).

Drilling is one of the critical cost factors in the development of a geothermal reservoir (Blum et al. 2011). Deeper boreholes raise the costs for a high temperature underground storage system significantly. Consequently, the design of the BHE array has to be optimized for the heating purpose to avoid an oversized and therefore overpriced system. Numerical simulations can predict the performance of a planned system prior to the investment of building a storage and help to optimize its design. However, the corresponding numerical models have to include all parameters relevant to the heat transfer processes in the subsurface. Furthermore, they should be readily adaptable to be deployed in mathematical optimization.

Earlier optimization approaches used analytical two dimensional finite line source models (e.g. Molina-Giraldo et al. 2011; de Paly et al. 2012; Bayer et al. 2014), which represent oversimplifications of the actual BHEs. Simulators using fully discretized models, like OpenGeoSys (Kolditz et al. 2012), can consider all relevant thermo-physical properties of the BHEs. However, the full discretization of the boreholes results in high computational costs, which are only acceptable for models of very few BHEs, but not for entire BTES systems. Other models like the commercial simulator FEFLOW (Diersch 2014) capture the physical parameters of the borefield in high detail using fast analytical solutions, but the finite element mesh has to be created manually, which prohibits automatization necessary for mathematical optimization. Therefore, a simulation tool had to be developed that satisfies the following requirements: high physical detail of the model at acceptable computational speed and the capability for mathematical optimization.

This work presents the MATLAB-based *Borehole Heat Exchanger Array Simulation and Optimization* (BASIMO) tool, which can numerically simulate and optimize the three dimensional design of a medium deep BTES. Instead of using line source or cylindrical source models, the BHEs' thermal interactions are calculated by more detailed thermal resistance and capacity models (TRCM). Furthermore, for the first time, depth-dependent BHE properties like an insulation in the topmost part of the wellbore can be considered without a fully discretized model of the BHE. In this manuscript, the structure of the program and its features are described and application examples are given.

1.2. State of the Art

Beside the almost ubiquitous availability and the base load capability of geothermal energy, one of the key advantages is the low operational cost compared to the fuel cost of conventional energy sources. However, geothermal projects are characterized by expensive investments, which are mainly required for developing the geothermal reservoir. Especially for deeper boreholes, drilling can account for 50 % to 80 % of the total capital costs (Blum et al. 2011; Garms 2014; Hornich 2014; Stockhausen 2014). Therefore, affordable drilling technology is an important prerequisite for the economic feasibility of medium deep BTES systems.

1.2.1. Drilling

Shallow boreholes for geothermal applications are commonly drilled with pneumatic down-the-hole (DTH) hammers (Sanner 2012): pressurized air is channeled through the drill string and used for the propulsion of the hammer at the bottom of the borehole. In the annulus, the returning mixture of air and groundwater transports the cuttings to the surface. Pneumatic

DTH hammers are versatile tools, which can be used irrespectively of the rock strength and outperform regular polycrystalline diamond compact (PDC) or tricone drill bits in terms of their rate of penetration (ROP) (Buja 2009; Riechers 2011). Thus, pneumatic DTH hammers allow for much more efficient and economical drilling. However, the air pressure has to exceed the hydrostatic pressure at the bottom of the borehole. Therefore, depending on the groundwater level, the economical use of pneumatic DTH hammers is limited to depths of 200 m to 400 m. Beyond this point, the increasing energy demand, which is amplified by the compressibility and the low density of the pressurized air, render pneumatic DTH hammers inefficient (Foralith 1998; Wittig et al. 2015). Hence, conventional rotary drilling is the prevalent technology for deep geothermal applications, but it is also significantly more expensive (Bundesministerium für Umwelt Naturschutz und Reaktorsicherheit 2007).

In many European countries geothermal power plants can benefit from feed-in tariffs for renewable electricity (Cansino et al. 2010). Additionally, financial institutions like the German KfW bank offer low interest rate loans for deep drilling ventures (i.e. > 400 m depth) related to combined heat and power projects (KfW Bankengruppe 2009). This helps to compensate for the expensive drilling of the deep boreholes. Medium deep BTES systems only store and provide renewable heat. Yet, the promotion of renewable heat is lagging behind. Existing tax exemptions and subsidies mainly suit household-sized producers; only a few countries have introduced feed-in tariffs for renewable heat (Cansino et al. 2011). Consequently, a more competitive drilling technology is required for medium deep BTES applications.

Advances of the past two decades have led to the development of efficient hydraulic DTH hammers, which use a fluid working medium instead of pressurized air (Melamed et al. 1999; Tuomas 2004; Sanner 2012; Bruce et al. 2013; Wittig et al. 2015; Wassara 2016). The primary energy required for drilling, i.e. fuel, can be reduced by up to 76 % (Hornich 2014). In contrast to the pneumatic DTH technology, hydraulic hammers can operate at higher pressure and therefore in greater depth, while still maintaining a comparably high ROP (Homuth et al. 2016; Wassara 2016). Also, no fluid additives like bentonite are necessary, which makes it possible to apply this drilling method in water protection zones.

BTES applications impose high requirements on the verticality and the spacing of the boreholes. The minimum spacing for medium deep boreholes drilled with pneumatic DTH hammers can be considered to be as low as 10 m (Sass et al. 2016b). However, BTES systems require the boreholes to be parallel and approximately 5 m apart to ensure sufficient thermal interaction between the BHEs (Appendix B). This requirement can hardly be met with pneumatic DTH hammers. Yet, the up-hole velocity of water is much less than the velocity of compressed air expanding after passing through the DTH hammer (Wassara 2016). Thus, the annulus between the borehole wall and the drilling tool can be smaller and the bottom hole assembly can be equipped with tightly fitting stabilizers, which would otherwise lead to quick abrasion of the guide ribs, if they were exposed to the expanding air of a pneumatic hammer (Homuth et al. 2016; Wassara 2016). As a beneficial side effect, the hydrostatic pressure also stabilizes the borehole wall (Bruce et al. 2013). More importantly, however, this improves the straightness of the bore path. Therefore, hydraulic DTH hammers allow for significantly lower deviations from the vertical axis than pneumatic hammers (less than 10 % compared to ~35 %; Riechers 2011; Wittig et al. 2015). As a result, the reduced risk of intersecting bore paths permits closer borehole spacing. Nonetheless, a radial distance of only 5 m between neighboring boreholes still poses a substantial challenge, even with a hydraulic DTH hammer drilling, which can be considered as the most suitable drilling technology for medium deep BTES systems.

1.2.2. Borehole Thermal Energy Storage

Similar to BTES operation, the regular dual use of BHEs for heating and cooling corresponds to the seasonally alternating extraction and injection of heat from and to the ground. However, to qualify as an underground thermal energy storage, the subsurface has to be heated intentionally to increase the source temperature of the heat pump for a subsequent heating purpose (Sanner 2005). Shallow BHE arrays have been in use for the seasonal storage of heat since the 1970s and the 1980s (Givoni 1977; Andersson & Eriksson 1981; Beckmann & Gilli 1984). Extensive research on BTES was carried out across Europe, particularly in Scandinavian countries, culminating in the first large-scale pilot facility at the Luleå University in Sweden: It consisted of 120 BHEs of 65 m length (Nordell 1987, 1990). Many other installations followed, for example in the wake of the German research and development programs *Solarthermie2000* and *Solarthermie2000plus* on urban solar heat supply, which helped to push the technology of shallow BTES to economic viability (Mangold 2007). The BTES are typically used for the seasonal storage of solar heat and vary in size and design (Table 1). However, they are usually much bigger than common BHE installations of single households and supply heat for small communities. Mostly, the BHE arrays consist of boreholes, which are not deeper than 100 m. Storage systems in Lund, Sweden (Andersson et al. 2013), or Oshawa, Canada (Dinçer & Rosen 2007), are exceptions where the boreholes reach depths of 230 m and 200 m, respectively.

Table 1: Key data on a few representative BTES systems; *first year of operation; 1: (Bauer et al. 2013; Mielke et al. 2014), 2: (Bollin et al. 2013), 3: (Lundh & Dalenbäck 2008), 4: (Reuß 2008), 5: (Sibbitt et al. 2012), 6: (Sørensen 2013).

location	year built	heat demand [MWh]	storage volume [m³]	solar collector size [m²]	demand covered by renewables		buffer storage [m³]	heat pump [kW_th]
					planed	real		
Neckarsulm (Germany)[1,2]	1997	3000	63,400	5,884	50 %	55.8 %	200	512
Anneberg (Sweden)[3]	2001	550	60,000	3,000	60 %	70 %	0	none
Attenkirchen (Germany)[2,4]	2002	487	9,350	800	50 %	29 %	500	550
Okotoks (Canada)[5]	2006	528	35,000	2,290	90 %	97 %	240	none
Crailsheim (Germany)[1,2]	2007	4,100	39,000	7,410	50 %	35.8 %	580	485
Brædstrup (Denmark)[6]	2012	40,000	19,000	18,600	50 %	16.5 %*	5,500	1,200

1.2.3. Numerical Modeling

Along with the field experiments, the first numerical simulation approaches for BTES systems were published as well. For example, Lund & Östmann (1985) developed a model of a shallow BTES, which also considered convective heat flow in the storage region. Their study already included a rudimentary economical optimization of the system consisting of a BTES and a solar collector installation. Nordell (1994) built upon that and looked into the optimization of the storage layout under economical aspects, investigating the sensitivities of design parameters. More recent work applies mathematical optimization to reduce the risk of reservoir depletion by altering the geometry of the BHE array or by adapting the storage operation (De Ridder et al. 2011; Bayer et al. 2014).

All considerations on simulation-based BTES system optimization rely on calculation models for the heat transfer between the BHEs and the subsurface. The approaches and the level of detail captured by the existing models vary widely. Many analytical (Zeng et al. 2002; Lamarche & Beauchamp 2007; e.g. Bandos et al. 2009; Yang et al. 2009; Man et al. 2010; Molina-Giraldo et al. 2011) and numerical (Lee & Lam 2008; Al-Khoury et al. 2010; De Carli et al. 2010; Kim et al. 2010; Lazzari et al. 2010) methods have been proposed. Most of the former are based on the line source theory (Ingersoll & Plass 1948; Ingersoll et al. 1950) or the cylindrical source theory (Carlslaw & Jaeger 1986). These analytical solutions often treat BHEs as mere heat sources defined by a constant heat rate per borehole length, neglecting material properties or axial effects. Usually, these models only consider single BHEs in a homogeneous subsurface and a conduction-dominated regime. As they are easy to implement and exhibit much higher computational speed than the numerical solutions, they are commonly used for the evaluation of short-term interactions like thermal response tests (Lehr & Sass 2014).

However, BHE arrays consist of multiple boreholes, which are only a few meters apart. In the long term operation, the thermal interference between different BHEs and axial effects resulting from the convective heat transport within the BHE pipes become significant and have to be considered in simulations. Based on the line source theory, Claesson & Eskilson (1988) and Eskilson & Claesson (1988) developed a method to calculate a thermal response model by so-called dimensionless *g-functions*. With the resulting model, long-term simulations allowed for the consideration of thermal interference between the boreholes for given geometries of the BHE array. Hellström (1991) elaborated on his colleagues' work and provided an analytical solution based on simple thermal resistance models for different types of BHEs, which also account for convective heat transfer of the fluid in the pipes. Commonly used commercial software like EED (Hellström & Sanner 1994) still employ this method. However, for each borefield configuration, the g-functions have to be calculated separately. Thus, this approach lacks flexibility in the choice of the borefield geometry. Furthermore, the subsurface is still considered homogeneous and the model in itself is still steady-state. Transient simulation is only achieved by superposition of consecutive step pulses (Hellström 1991).

Many of these shortcomings can be addressed in a dual-continuum approach: the model of the BHEs and the surrounding subsurface is split (Shao et al. 2014). While the calculation of the heat transfer at the BHEs remains an analytical local steady-state solution, it is coupled to a numerical subsurface model, which allows for transient simulations and the consideration of a heterogeneous subsurface. Moreover, the thermal interference between the BHEs is determined by the numerical subsurface model rather than using array geometry specific g-functions. Numerical BHE models can be coupled as well (Al-Khoury et al. 2010), but only at significantly higher computational cost. The concept of coupling analytical or numerical BHE solutions with a separate subsurface model has been put into practice, for instance, in the software FEFLOW (Diersch et al. 2011b; Diersch 2014). It employs more advanced TRCMs for the BHEs (Bauer et al. 2011b; Diersch et al. 2011a) and calculates the subsurface heat and mass transport on a triangular prism mesh of finite elements. This approach represents the starting point for the development of BASIMO, which is presented in this thesis.

1.3. Characteristics of Medium Deep Borehole Thermal Energy Storage Systems

The principles of BTES have been briefly summarized by Reuss (2015) and Bauer (2011): in general, a BTES system consists of an array of boreholes, each fitted with a BHE. The number of BHEs, their radial distance and their length define the size of the storage. The BHEs have to

be located in a favorable distance of each other to grant thermal interference: BHEs that are too close to each other deplete the geothermal reservoir too quickly in winter, whereas BHEs that are too widely spaced cannot benefit from the heat stored in neighboring boreholes. A radial distance of about 5 m has proven to be ideal for typical operation scenarios with half-year charging and discharging cycles (Appendix B). BTES systems can only be insulated at the top, whereas the bottom and the sides remain without insulation. The heat losses of the storage are proportional to its enveloping surface, while the storage capacity correlates with its volume. Thus, a low surface-to-volume ratio is beneficial and results in a high storage efficiency (Appendix B). Therefore, BTES systems are typically large and consist of dozens of BHEs, which are arranged in a compact geometry. The resulting high capacity makes them particularly suitable for seasonal heat storage. Water tanks with a comparable heat storage capacity would require considerable space on the surface. Furthermore, a BTES system can be enlarged by drilling deeper or adding additional boreholes.

Despite the seemingly universal applicability of BTES, the hydrogeology on site is fundamentally important. While groundwater in a porous host rock can enhance the storage due to its high volumetric heat capacity, groundwater flow can reduce the BTES performance significantly or even render it entirely ineffective by increasing the heat losses due to convective heat transport (Appendix B). Although providing only a vague definition, Sanner & Stiles (1997) suggest that a BHE array can be considered as an underground thermal energy storage system, if less than 25 % of the annual thermal energy turnover is lost to the surrounding rock through heat dissipation. Hence, to prevent advective heat losses, BTES sites should have a low permeability and a negligible groundwater flow rate (Reuß 2015). Typically, permeability decreases with increasing depth and the related rock compaction, which prevents heat removal from the storage by groundwater flow. Furthermore, the stored heat will not dissipate as fast as in shallow depths due to a reduced lateral temperature gradient. Unfaulted crystalline basement rock, which can often be found under its sedimentary cover in medium and therefore reasonable depth, represents a good storage medium for BTES systems. In addition to an inherent low permeability, crystalline rocks rich in quartz like granite or granodiorite exhibit above average thermal conductivity (Table 2). This facilitates the conductive heat transport into and from the ground. Numerical simulations have shown that the thermal conductivity and the ground water flow in the BTES reservoir rock can have a significant influence on the storage efficiency (Appendix B). Hence, the influence of the location for a BTES system should not be disregarded.

Table 2: Typical thermo-physical and hydraulic properties for different crystalline rocks rich and poor in quartz from the Mid-German Crystalline High (after Bär 2012).

rock type	λ [W m^{-1} K]	κ [10^{-6} m^2 s^{-1}]	c [J kg^{-1} K^{-1}]	K [m^2]
amphibolite	1.88 ± 0.21	0.81 ± 0,14	813 ± 92	~10^{-16}-10^{-17}
gabbro	2.10 ± 0.19	1.01 ± 0,09	764 ± 53	~10^{-16}-10^{-17}
diorite	2.23 ± 0.18	1.03 ± 0,10	760 ± 59	~10^{-16}-10^{-17}
granodiorite	2.51 ± 0.33	1.26 ± 0,22	736 ± 68	~10^{-16}-10^{-17}
granite	2.58 ± 0.38	1.33 ± 0,25	753 ± 98	~10^{-16}-10^{-17}
gneiss	2.59 ± 0.25	1.33 ± 0,24	762 ± 106	~10^{-16}-10^{-17}

While medium deep BTES systems have several advantages over shallow ones, they still penetrate the topmost aquifers. In order to minimize the thermal impact on the shallow aquifers, a medium deep BTES system should be thermally insulated within the boreholes at the topmost part and reach a few hundred meters deep in order to provide enough heat exchange surface without insulation (Bär et al. 2015). Shallow BHEs are often polymer U-pipes or double U-pipes, whereas deeper BHEs are usually coaxial pipe systems with a high thermal conductivity outer steel pipe (Sass et al. 2016a). The inner pipe is insulated to reduce the thermal interaction between the up- and down-streaming fluids. In summer, the warm fluid is injected into the inner pipe for heat storage, while in winter the cold fluid is injected into the annular gap for heat extraction (Sass et al. 2016a). The insulating backfill material in the topmost part of the wellbore protects the topmost aquifer from excessive heating, but it can also increase the outlet temperature of medium deep BHEs (Appendix D). This enhances the performance of the heat pump and possibly allows for utilization with conventional radiator heating systems, which require a higher supply temperature (Bär et al. 2015).

Medium deep BTES are operated in seasonal charging and discharging cycles. Excess thermal energy is stored in summer. During winter it is extracted again for heating purposes. The performance is quantified by the heat, which is stored and extracted during each cycle (Figure 1a).

$$Q_{S/E} = \int_t \Delta T \cdot \rho_f \cdot c_f \cdot \dot{V} dt \qquad (1)$$

With $Q_{S/E}$: stored or extracted heat, ΔT: temperature difference between inlet and outlet, ρ_f: working fluid density, c_f: specific heat capacity of working fluid, $\dot{V}$: working fluid flow rate and t: time of operation. This defines the stored and extracted heat as the amount of thermal energy, which is rejected and absorbed by the fluid in the BHEs, respectively. The ratio of extracted heat to stored heat S defines the storage coefficient (Verein Deutscher Ingenieure 2001c), while the specific heat extraction rate Q_{spec} describes the system's efficiency of heat exchange between BHEs and the subsurface normalized by the total borehole length.

$$S = \left| \frac{Q_E}{Q_S} \right| \qquad (2)$$

$$Q_{spec} = \frac{Q_E}{L_{tot} \cdot t_E} \qquad (3)$$

With S: storage coefficient, $Q_{S/E}$: extracted and stored heat, Q_{spec}: specific heat extraction rate, L_{tot}: total drilled length and t_E: time of operation in heat extraction mode. In general, the difference between the inlet and outlet temperature of the working fluid in the BHEs decreases over the course of a charging or discharging cycle because of the continuous heat exchange with the reservoir (Figure 1b).
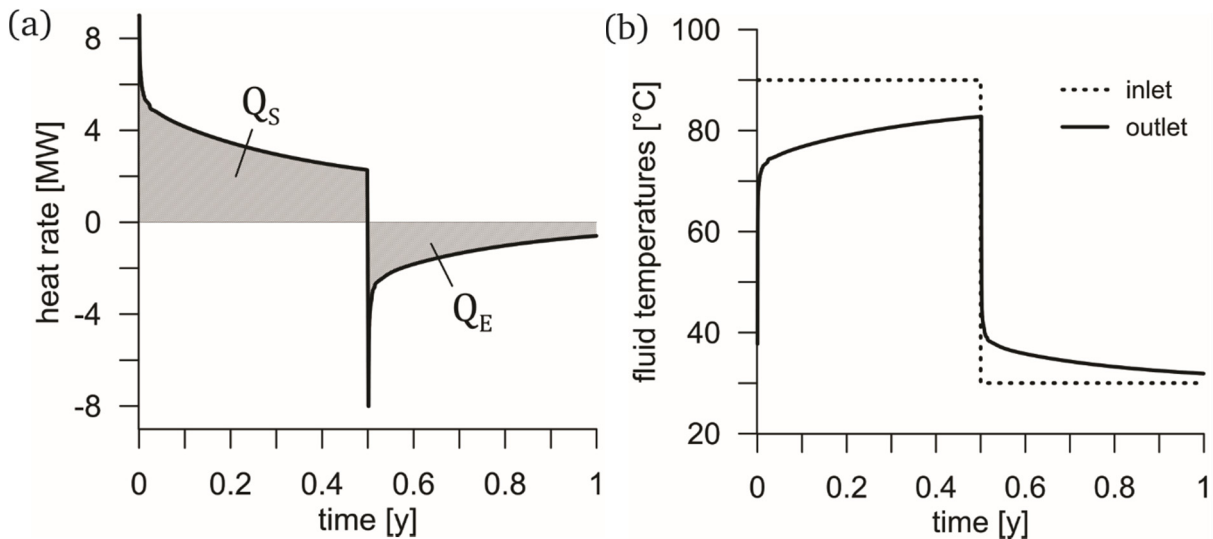
Figure 1: (a) Evolution of heat storage and extraction, Q_S: stored heat, Q_E: extracted heat; (b) Evolution of BHE inlet and outlet temperatures. (Schulte et al. 2016a; Welsch et al. 2016a)

Due to diffusion processes, not all of the stored heat can be recovered. Some of the thermal energy remains in the reservoir and begins to create a thermal plume in the subsurface. This thermal plume decreases the lateral temperature gradient between the BHEs and the surrounding rock, which leads to declining heat storage in summer, but enhanced heat extraction in winter (Figure 2). This effect builds up over the course of several charge and discharge cycles. As a result, the system efficiency improves, gradually approaching a balanced state. Yet, the trend persists even after many years of operation (Figure 2). However, typical BTES systems take about 3 to 6 years to achieve 80 % of their final storage efficiency (Appendix B).
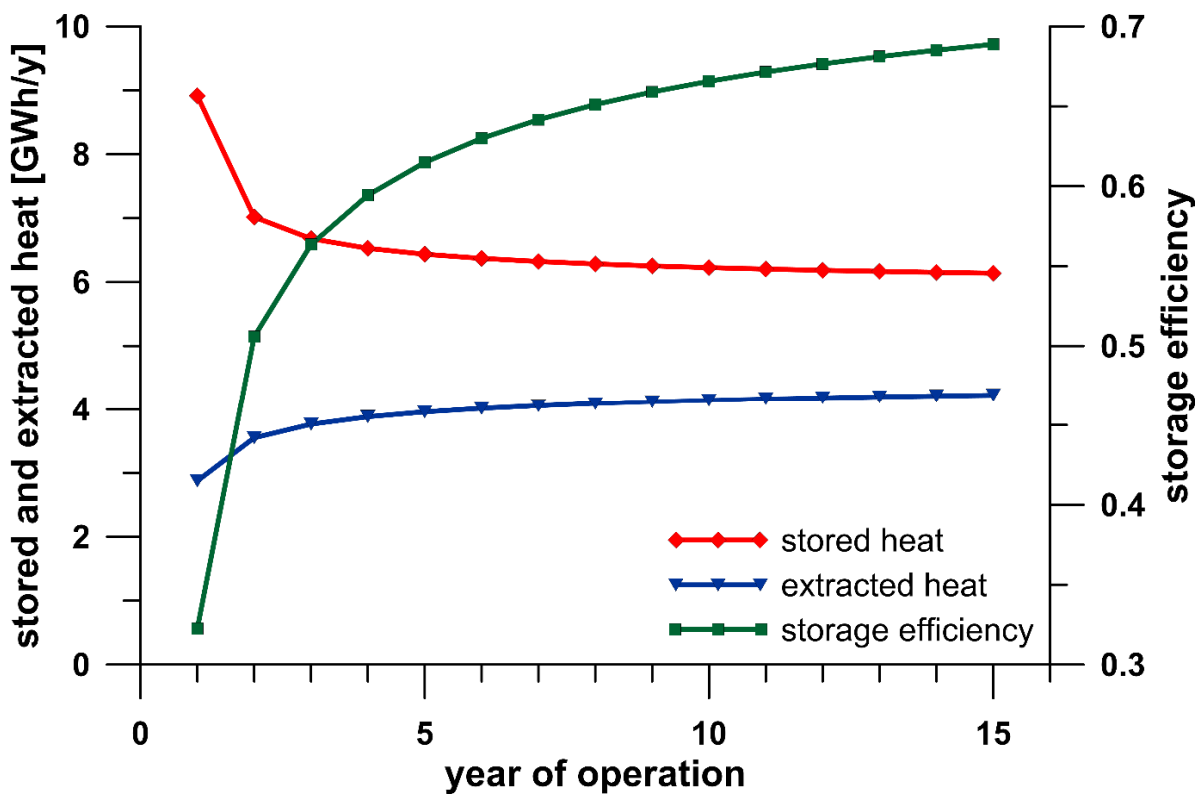
Figure 2: Evolution of storage performance; model: 19 coaxial BHEs, BHE length: 500 m, BHE spacing: 5 m, flow rate: 4 l/s, inlet temperature: 90 °C during storage and 30 °C during extraction. (Schulte et al. 2016a; Welsch et al. 2016a)

As mentioned above, the size and shape of the BTES define the surface-to-volume ratio and thereby the heat losses and the efficiency of the system. A comprehensive study (Appendix B) of the system parameters including the number, the length and the spacing of the BHEs confirms that large BTES systems are more efficient than small ones. Medium deep BTES systems, which are large enough to store and extract several GWh of heat per cycle can operate at storage efficiencies above 80 %. Furthermore, the study indicates that the storage efficiency is strongly dependent on the BHE inlet temperature during heat injection and extraction, respectively. This, in turn, relates to the return temperature of the building's heating system. Hence, the simulation of a BTES system can only be as good as the data provided from the building side, which controls the storage operation. However, building and storage constitute an interacting system. Therefore, as Welsch et al. (2016a) already pointed out, comprehensive considerations require coupled simulations of the storage and the building.

Chapter 2: Borehole Heat Exchanger Array Simulation Tool

As stated in Chapter 1, any consideration on the optimization of BTES systems relies on a simulation model. Until now, commercially available simulators have not included the means for mathematical optimization. Furthermore, they have often not captured the required level of physical detail of the BHE array design and operation for BTES applications. The necessity of a simulator for BTES systems, which allows for coupling with optimization algorithms or building simulation models, has been the motivation for the development of the *Borehole Heat Exchanger Array Simulation and Optimization* (BASIMO) tool. BASIMO was developed to meet the following requirements:

- Transient calculation of conductive heat transport in the subsurface
- Consideration of geological profiles
- Inclined boreholes
- Wide variety of BHE array geometries and arbitrary borehole locations
- Consideration of the most typical BHE types (U-pipe, double U-pipe and coaxial pipe)
- Detailed modeling with BHE material properties
- Consideration of insulated borehole sections
- BTES operation by predefined inlet temperature or heat load
- User-defined time series for operation input
- Detailed simulation output (subsurface and BHE outlet temperature time series)
- Coupling to mathematical optimization algorithms
- Coupling to building simulation models
- Reasonable computation time
- User-friendliness

With the focus on the mathematical optimization, MATLAB (The MathWorks 2015a) was chosen as a programming environment. In MATLAB, BASIMO is programmed as an accessible and modular code, which allows for future adaptations. Most importantly, however, BASIMO can be directly linked to the MATLAB Global Optimization Toolbox (The MathWorks 2015b), which provides multiple mathematical optimization algorithms and can be easily configured. Regardless of the optimization, BASIMO is also a versatile standalone simulator for BHE arrays in its own right.

The simulation of medium deep BTES operation comprises the calculation of the subsurface heat transport and the thermal interaction of the BHEs with the surrounding rock. Just like FEFLOW (see Chapter 1.2.3), BASIMO uses a dual-continuum approach, which splits the calculation of the heat transfer: the BHEs are modeled with the analytical local steady-state solution developed by Diersch et al. (2011a) and Bauer et al. (2011b). It is based on Eskilson & Claesson's (1988) concept, but is enhanced to account for thermally insulated sections of the borehole (Appendix D). The analytical BHE solution is coupled to a numerical model employing the finite element method in order to calculate the transient heat transport in the subsurface and the thermal interference between the BHEs. In the following, the structure and the features of BASIMO are explained in detail.

2.1. The Finite Element Method

The finite element method (FEM) is a numerical technique for the approximation of differential equations, which is used in various fields of applied science and engineering. For BASIMO, a

generalization of the standard Galerkin method of weighted residuals (Zienkiewicz et al. 2013) is applied in an adapted MATLAB (2015a) implementation for finite elements (Alberty et al. 1999). For brevity, the finite element method is described for two-dimensional problems in this chapter, whereas the simulator calculates three-dimensional heat transport.

2.1.1. Semidiscritization

The principles of the finite element method in heat transfer problems have been described by Reddy and Gartling (2010), which is the source for the summary of the method in Chapters 2.1 and 2.2: The basic idea is that the solution of a differential equation can be described as a linear combination of a priori unknown approximation functions and corresponding coefficients for the entire domain Ω of the problem. While the coefficients have to be determined to satisfy the differential equation, the approximation functions have to be chosen in a way that the boundary conditions of the problem are met. However, finding the appropriate approximation functions can be difficult, as most realistic problems describe geometrically complex regions. In order to account for different boundary conditions on different parts of the region (Figure 3a), the problem domain Ω with the boundary Γ has to be divided into N non-overlapping subdomains of simple geometric shapes, the so called finite elements Ω^e with respective boundaries Γ^e (Figure 3b).

$$\sum_{e=1}^{N} \Omega^e \cong \Omega ; \qquad \sum_{e=1}^{N} \Gamma^e \cong \Gamma \tag{4}$$

For each element the approximation functions are constructed separately. This way, any complex shape of the problem domain with arbitrary boundary conditions can be described and the solution of the differential equation can be approximated elementwise. For complex domain geometries, the sum of elements may not equal the actual domain exactly. The mismatch is called discretization error (Figure 3b). In general, a fine discretization, i.e. more, but smaller elements, results in a smaller discretization error compared to a mesh with fewer, but bigger elements. Alternatively, the discretization error can be reduced by using higher-order elements.

(a)

(b)
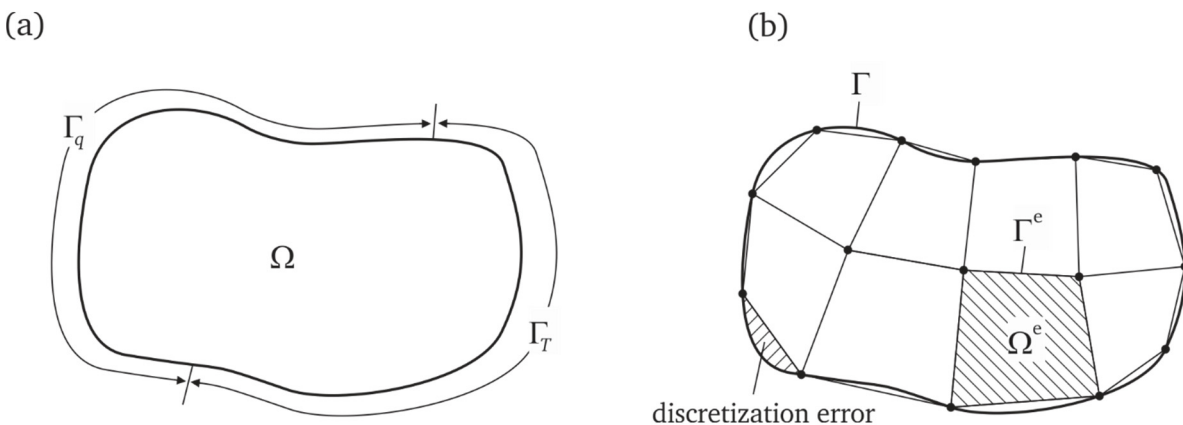
Figure 3: (a) problem domain with two types of boundary conditions; (b) subdivision of problem domain into finite elements.

The governing equation for the subsurface heat transport is heat diffusion according to Fourier's Law of heat conduction.

$$\rho_s c_s \frac{\partial T}{\partial t} = \nabla \cdot (\lambda_s \nabla T) + q_Q \quad \text{in } \Omega \tag{5}$$

With ρ_s: rock density, c_s: specific heat capacity of the rock, T: temperature, t: time, λ_s: thermal conductivity of the rock and q_Q: heat sources and sinks. Since low-permeable rock bodies with negligible groundwater flow are targeted for medium deep BTES, convective heat transfer is disregarded. Also, temperature dependency or anisotropy of material parameters is not taken into account. Equation (5) has to be solved for the place and time dependent temperature $T(x, y, t)$ in the model domain Ω. The initial conditions and the boundary conditions have to be considered. For conductive heat transport, the boundary conditions can be a temperature on Γ_T (i.e. Dirichlet boundary condition) or a heat flux normal to the domain boundary on Γ_q (i.e. Neumann boundary condition).

$$T(x, y, t = 0) = T_0(x, y) \qquad\qquad (x, y) \in \Omega \tag{6}$$

$$T(s) = \hat{T} \qquad\qquad s \in \Gamma_T \tag{7}$$

$$q_n = \lambda \left(\frac{\partial T}{\partial x} n_x + \frac{\partial T}{\partial y} n_y \right) = \hat{q}_n(s) \qquad\qquad s \in \Gamma_q \tag{8}$$

T_0 describes the initial temperature distribution in the model domain Ω, $\hat{T}$ is the Dirichlet boundary condition, q_n is the Neumann boundary condition (defined for a Cartesian coordinate system) and n_x and n_y are the components of the unit vector perpendicular on the boundary Γ. Γ_T and Γ_q are disjunct parts of the domain boundary Γ, which have to fulfill the following conditions:

$$\begin{aligned} \Gamma_T \cup \Gamma_q &= \Gamma \\ \Gamma_T \cap \Gamma_q &= \varnothing \end{aligned} \tag{9}$$

Considering a steady-state problem without any sources for simplicity at first, the time derivative term and the source term can be set to zero. The governing equation is then reduced to the Laplace equation:

$$\frac{\partial}{\partial x} \left(\lambda_s \frac{\partial T}{\partial x} \right) + \frac{\partial}{\partial y} \left(\lambda_s \frac{\partial T}{\partial y} \right) = 0 \tag{10}$$

Then, the sought solution of the differential equation $T(x, y)$ can be approximated for each finite element by a Lagrange interpolation

$$T(x, y) \approx T^e(x, y) = \sum_{p=1}^{n} T_p^e \psi_p \qquad\qquad (x, y) \in \Omega^e \tag{11}$$

Where $T^e(x, y)$ is the approximation of $T(x, y)$ for the finite element Ω^e and T_p^e denote the initially undetermined temperature values at the n element nodes. The ψ_p are the corresponding interpolation functions of the element. Each element node has one

corresponding function, which takes on $\psi_p = 1$ at the respective node p and $\psi_p = 0$ at all other nodes. Hence, the interpolation functions depend on the number of nodes n and the shape of the finite elements. They will be discussed in more detail in section 2.2.

The replacement of T in (10) by T^e results in a residual error $R^e(x, y)$, because T^e is only an approximation.

$$\frac{\partial}{\partial x}\left(\lambda_s \frac{\partial T^e}{\partial x}\right) + \frac{\partial}{\partial y}\left(\lambda_s \frac{\partial T^e}{\partial y}\right) = R^e(x, y) \tag{12}$$

The method of weighted residuals requires this error to vanish, if the residuals are weighted by functions ω and integrated over the subdomain of the element Ω^e. The resulting statement is called the *weak form*. The governing differential equation is not fulfilled precisely in every point anymore, but only in a weighted-integral sense over the subdomain Ω^e.

$$\iint\limits_{\Omega^e} \omega R^e \, dx \, dy = 0 \tag{13}$$

Inserting the residual error (12) of the differential equation (10) in the weak form gives the weighted-residual statement (14). Considering the approximation of T^e according to (11), the functions ψ_p have to be differentiable twice with respect to x and y, whereas the weight functions ω are not subject to differentiation.

$$\iint\limits_{\Omega^e} \omega \left[\frac{\partial}{\partial x}\left(\lambda_s \frac{\partial T^e}{\partial x}\right) + \frac{\partial}{\partial y}\left(\lambda_s \frac{\partial T^e}{\partial y}\right)\right] dx \, dy = 0 \tag{14}$$

This requirement limits the choice of interpolation functions to polynomials of second-order or higher. However, in the weak form, integration-by-parts following Green's first identity (Strauss 2007) can *weaken* this continuity requirement by shifting the differentiation partially from T^e to ω.

$$\iint\limits_{\Omega^e} \omega \frac{\partial}{\partial x}\left(\lambda_s \frac{\partial T^e}{\partial x}\right) dx \, dy = -\iint\limits_{\Omega^e} \lambda_s \frac{\partial \omega}{\partial x}\frac{\partial T^e}{\partial x} dx \, dy + \int\limits_{\Gamma^e} \omega \lambda_s \frac{\partial T^e}{\partial x} n_x \, ds$$

$$\iint\limits_{\Omega^e} \omega \frac{\partial}{\partial y}\left(\lambda_s \frac{\partial T^e}{\partial y}\right) dx \, dy = -\iint\limits_{\Omega^e} \lambda_s \frac{\partial \omega}{\partial y}\frac{\partial T^e}{\partial y} dx \, dy + \int\limits_{\Gamma^e} \omega \lambda_s \frac{\partial T^e}{\partial y} n_y \, ds \tag{15}$$

In the differential equation, temperature T^e is the dependent unknown and therefore termed the *primary variable*. The boundary integrals on the right-hand side in (15) contain the expression for the heat flux q_n normal to the element boundary Γ^e (8), which is denoted as *secondary variable*. Applying these relations on the weighted-residual statement (14) and rearranging the equation gives the following description of the weak form.

$$\iint\limits_{\Omega^e} \left(\lambda_s \frac{\partial \omega}{\partial x}\frac{\partial T^e}{\partial x} + \lambda_s \frac{\partial \omega}{\partial y}\frac{\partial T^e}{\partial y}\right) dx \, dy = \int\limits_{\Gamma^e} q_n \omega \, ds \tag{16}$$

The left-hand side of this expression can be expanded by inserting the approximation for T^e. It is obvious, that now the functions ψ_p only need to be differentiable once. Hence, interpolation functions ψ_p, which are linear in both x and y will be sufficient.

$$\iint\limits_{\Omega^e} \left[\lambda_s \left(\sum_{p=1}^{n} T_p^e \frac{\partial \psi_p}{\partial x} \right) \frac{\partial \omega}{\partial x} + \lambda_s \left(\sum_{p=1}^{n} T_p^e \frac{\partial \psi_p}{\partial y} \right) \frac{\partial \omega}{\partial y} \right] dx\, dy = \int\limits_{\Gamma^e} q_n \omega\, ds \tag{17}$$

Since the temperatures T_p^e are located at the n nodes of the element Ω^e and since they are not functions of x and y, they can be excluded from the integral expression.

$$\sum_{p=1}^{n} \left[\iint\limits_{\Omega^e} \left(\lambda_s \frac{\partial \psi_p}{\partial x} \frac{\partial \omega}{\partial x} + \lambda_s \frac{\partial \psi_p}{\partial y} \frac{\partial \omega}{\partial y} \right) dx\, dy \right] T_p^e = \int\limits_{\Gamma^e} q_n \omega\, ds \tag{18}$$

The resulting algebraic equation contains n unknowns: the node temperatures T_p^e. Thus, a system of n independent equations is required to solve for the unknown temperatures T_p^e. The equations must hold for any weight function ω. Therefore, in the Galerkin method the interpolation functions ψ are chosen as weight functions. Substitution of ω by interpolation functions denoted as ψ_q provides the qth of n statements for the system of equations:

$$\sum_{p=1}^{n} \left[\iint\limits_{\Omega^e} \left(\lambda_s \frac{\partial \psi_p}{\partial x} \frac{\partial \psi_q}{\partial x} + \lambda_s \frac{\partial \psi_p}{\partial y} \frac{\partial \psi_q}{\partial y} \right) dx\, dy \right] T_p^e = \int\limits_{\Gamma^e} q_n \psi_q\, ds$$

or $\tag{19}$

$$\sum_{p=1}^{n} A_{pq}^e T_p^e = b_q^e$$

where A_{pq}^e and b_q^e are here defined by

$$A_{pq}^e = \iint\limits_{\Omega^e} \left(\lambda_s \frac{\partial \psi_p}{\partial x} \frac{\partial \psi_q}{\partial x} + \lambda_s \frac{\partial \psi_p}{\partial z} \frac{\partial \psi_q}{\partial z} \right) dx\, dy$$

$$b_q^e = \int\limits_{\Gamma^e} q_n \psi_q\, ds \tag{20}$$

The system of the n equations can be rewritten in matrix notation:

$$\mathbf{A^e T^e = b^e} \tag{21}$$

where $\mathbf{A^e}$ is the quadratic thermal conductivity matrix and $\mathbf{b^e}$ is the right-hand side, which contains the boundary-normal heat fluxes.

Returning back to a problem, which captures transient heat conduction with internal heat generation, the description of the weak statement for steady-state (16) expands by a capacity and a source term following the same derivation as described above:

$$\iint_{\Omega^e} \left(\rho_s c_s \frac{\partial T^e}{\partial t} \psi_q + \lambda_s \frac{\partial \psi_q}{\partial x} \frac{\partial T^e}{\partial x} + \lambda_s \frac{\partial \psi_q}{\partial y} \frac{\partial T^e}{\partial y} \right) dx\, dy = \iint_{\Omega^e} q_Q \psi_q\, dx\, dy + \int_{\Gamma^e} q_n \psi_q\, ds$$

or (22)

$$\sum_{p=1}^{n} B_{pq}^e \frac{dT_p^e}{dt} + \sum_{p=1}^{n} A_{pq}^e T_p^e = b_q^e$$

where B_{pq}^e, A_{pq}^e and b_q^e are defined by

$$B_{pq}^e = \iint_{\Omega^e} \rho_s c_s \psi_p \psi_q\, dx\, dy$$

$$A_{pq}^e = \iint_{\Omega^e} \left(\lambda_s \frac{\partial \psi_p}{\partial x} \frac{\partial \psi_q}{\partial x} + \lambda_s \frac{\partial \psi_p}{\partial z} \frac{\partial \psi_q}{\partial z} \right) dx\, dy$$

(23)

$$b_q^e = \iint_{\Omega^e} q_Q \psi_q\, dx\, dy + \int_{\Gamma^e} q_n \psi_q\, ds$$

Subsequently, the system of equations can be expressed in a short matrix notation, which is called the *finite element model* of the governing differential equation (5):

$$\mathbf{B^e \dot{T}^e + A^e T^e = b^e} \tag{24}$$

where $\mathbf{B^e}$ is the heat capacity matrix, $\mathbf{A^e}$ is the thermal conductivity matrix and $\mathbf{b^e}$ is the right-hand side now containing heat source terms and boundary conditions on the element boundary Γ^e. In BASIMO, an analytical solution for the thermal interaction of the BHEs calculates the resulting heat source terms contained in $\mathbf{b^e}$ (Chapters 2.1.3 and 2.3).

2.1.2. Assembly

The finite element model can be obtained for every element Ω^e of the domain. It is generally possible to combine differently shaped elements in one finite element mesh (Figure 4). Two rules have to be considered in the process:

1. Neighboring elements have the same temperature at the nodes they share (i.e. continuity of the primary variable)
2. The heat fluxes across the boundary of neighboring elements cancel each other out (i.e. balance of the second variable)
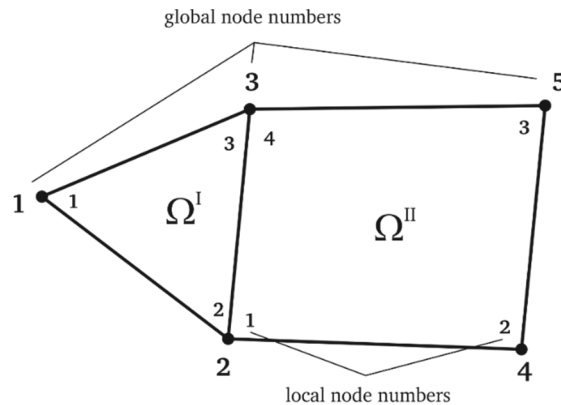
Figure 4: Assembly of a triangular (Ω^I) and a quadrilateral element (Ω^{II})

After all finite element models are obtained, one global system of equations is assembled. It contains one equation for every node in the finite element mesh. As neighboring elements share some of their nodes (25), the respective finite element models (24) contribute to the corresponding nodal equations in the global system: the temperature nodes are replaced by global nodes (26-27) and the rearranged subsystems are summed up in the global matrix equation (28). An example for the assembly of a steady-state finite element model (21) consisting of a triangular and a quadrilateral element is given with reference to Figure 4:

$$T_1^I = T_1 \; ; T_2^I = T_1^{II} = T_2 \; ; T_3^I = T_4^{II} = T_3 \; ; T_2^{II} = T_4 \; ; T_3^{II} = T_5 \tag{25}$$

$$\Omega^I: \begin{pmatrix} A_{11}^I & A_{12}^I & A_{13}^I \\ A_{21}^I & A_{22}^I & A_{23}^I \\ A_{31}^I & A_{32}^I & A_{33}^I \end{pmatrix} \begin{pmatrix} T_1^I \\ T_2^I \\ T_3^I \end{pmatrix} = \begin{pmatrix} b_1^I \\ b_2^I \\ b_3^I \end{pmatrix} \Rightarrow \begin{pmatrix} A_{11}^I & A_{12}^I & A_{13}^I & 0 & 0 \\ A_{21}^I & A_{22}^I & A_{23}^I & 0 & 0 \\ A_{31}^I & A_{32}^I & A_{33}^I & 0 & 0 \\ 0 & 0 & 0 & 0 & 0 \\ 0 & 0 & 0 & 0 & 0 \end{pmatrix} \begin{pmatrix} T_1 \\ T_2 \\ T_3 \\ T_4 \\ T_5 \end{pmatrix} = \begin{pmatrix} b_1^I \\ b_2^I \\ b_3^I \\ 0 \\ 0 \end{pmatrix} \tag{26}$$

$$\Omega^{II}: \begin{pmatrix} A_{11}^{II} & A_{12}^{II} & A_{32}^{II} & A_{14}^{II} \\ A_{21}^{II} & A_{22}^{II} & A_{23}^{II} & A_{24}^{II} \\ A_{31}^{II} & A_{32}^{II} & A_{33}^{II} & A_{34}^{II} \\ A_{41}^{II} & A_{42}^{II} & A_{34}^{II} & A_{44}^{II} \end{pmatrix} \begin{pmatrix} T_1^{II} \\ T_2^{II} \\ T_3^{II} \\ T_4^{II} \end{pmatrix} = \begin{pmatrix} b_1^{II} \\ b_2^{II} \\ b_3^{II} \\ b_4^{II} \end{pmatrix} \Rightarrow \begin{pmatrix} 0 & 0 & 0 & 0 & 0 \\ 0 & A_{11}^{II} & A_{14}^{II} & A_{12}^{II} & A_{13}^{II} \\ 0 & A_{41}^{II} & A_{44}^{II} & A_{42}^{II} & A_{43}^{II} \\ 0 & A_{21}^{II} & A_{24}^{II} & A_{22}^{II} & A_{23}^{II} \\ 0 & A_{31}^{II} & A_{34}^{II} & A_{32}^{II} & A_{33}^{II} \end{pmatrix} \begin{pmatrix} T_1 \\ T_2 \\ T_3 \\ T_4 \\ T_5 \end{pmatrix} = \begin{pmatrix} 0 \\ b_1^{II} \\ b_4^{II} \\ b_2^{II} \\ b_3^{II} \end{pmatrix} \tag{27}$$

$$\Omega^{I+II}: \begin{pmatrix} A_{11}^I & A_{12}^I & A_{13}^I & 0 & 0 \\ A_{21}^I & A_{22}^I + A_{11}^{II} & A_{23}^I + A_{14}^{II} & A_{12}^{II} & A_{13}^{II} \\ A_{31}^I & A_{32}^I + A_{41}^{II} & A_{33}^I + A_{44}^{II} & A_{42}^{II} & A_{43}^{II} \\ 0 & A_{21}^{II} & A_{24}^{II} & A_{22}^{II} & A_{23}^{II} \\ 0 & A_{31}^{II} & A_{34}^{II} & A_{32}^{II} & A_{33}^{II} \end{pmatrix} \begin{pmatrix} T_1 \\ T_2 \\ T_3 \\ T_4 \\ T_5 \end{pmatrix} = \begin{pmatrix} b_1^I \\ b_2^I + b_1^{II} \\ b_3^I + b_4^{II} \\ b_2^{II} \\ b_3^{II} \end{pmatrix} \tag{28}$$

For the transient case, the assembly is carried out accordingly and results in the following matrix equation describing the entire domain Ω:

$$\mathbf{B\dot{T}} + \mathbf{AT} = \mathbf{b} \tag{29}$$

BASIMO performs the assembly of the matrices $\mathbf{A}$ and $\mathbf{B}$ prior to the simulation. As the heat source terms of the BHEs are time dependent, $\mathbf{b}$ has to be calculated every time step (Chapter 2.4).

2.1.3. Time Integration

After the semi-discretization (i.e. spatial discretization) of the differential equation, the time derivative can be approximated by a time integration scheme, as well. The time interval of interest, which is to be integrated, is subdivided into discrete segments termed $\Delta t = t^{n+1} - t^n$, where t marks the time and n denotes the time step number. For transient heat transport, the temperature $\mathbf{T}$ and the temperature rate $\dot{\mathbf{T}}$ are expected to vary. Hence, Δt has to be chosen, so that the variation can be adequately captured and described by an approximation like the

left-sided first order derivative $\dot{\mathbf{T}}^{n+1} = (\mathbf{T}^{n+1} - \mathbf{T}^n)/\Delta t$ or other finite difference approximations. As the initial conditions $\mathbf{T_0}$ have to be defined according to (6), the finite element model (29) can be evaluated for all subsequent time steps $n+1$ using the aforementioned time derivative approximation. Depending on the choice of the approximation, different formulas for the calculation of the solution vector $\mathbf{T}$ are obtained. In BASIMO, the generalized trapezoid method is applied:

$$\frac{1}{\Delta t} \mathbf{B} \left(\mathbf{T}^{n+1} - \mathbf{T}^n \right) + \theta \, \mathbf{A} \mathbf{T}^{n+1} = \mathbf{b} - \left(1 - \theta \right) \mathbf{A} \mathbf{T}^n \tag{30}$$

With $0 \leq \theta \leq 1$, the generalized trapezoid rule allows for the employment of the explicit forward Euler ($\theta = 0$) and the implicit backward Euler ($\theta = 1$) scheme, which are first-order accurate in time. Simply put, the value of θ defines the point in the time interval between t^n ($\theta = 0$) and t^{n+1} ($\theta = 1$) where the matrix equation is evaluated and the temperature $\mathbf{T}$ is determined:

$$\mathbf{T}^{eval} = \left(1 - \theta \right) \mathbf{T}^n + \theta \, \mathbf{T}^{n+1} \tag{31}$$

While the forward Euler scheme does not require solving the system of equations by inverting a matrix and is therefore easily implemented, the explicit nature of the method implies stability conditions, which restrict the time step size, the thermal diffusivity and the mesh spacing (Hughes 1977). Hence, BASIMO applies the Crank-Nicolson time integration scheme ($\theta = 1/2$) by default, as it is unconditionally stable like the backward Euler method, but is also second-order accurate in time. However, it is possible to impose the forward or backward Euler scheme by a user-defined value for θ, if desired. For the Crank-Nicolson method, the generalized trapezoid rule produces:

$$\left(\frac{1}{\Delta t} \mathbf{B} + \frac{1}{2} \mathbf{A} \right) \mathbf{T}^{n+1} = \left(\frac{1}{\Delta t} \mathbf{B} - \frac{1}{2} \mathbf{A} \right) \mathbf{T}^n + \mathbf{b} \tag{32}$$

In BASIMO, heat source terms are calculated and added to the boundary integrals in $\mathbf{b}$ (equation 23), to link the BHEs to the numerical subsurface model: fed with inlet temperature and flow rate data, an analytical solution provides the temperature distribution in the inlet and outlet pipes in predefined depth levels. It takes into account all thermal and hydraulic parameters of the BHE materials and the borehole wall temperature. In the finite element mesh, the BHEs are discretized as vertical lines of mesh nodes. The temperature at these nodes defines the borehole wall temperature and is passed to the analytical solution. In return, the analytical solution sets heat sources in $\mathbf{b}$ for the corresponding vector components. The calculation of the nodal heat sources is based on the thermal resistances within the BHEs and the difference between the borehole wall temperature and the calculated BHE fluid temperature at the respective nodes (Chapter 2.3). This results in a contribution to the right-hand side term of the respective equations (Diersch 2014). As the heat source terms depend on the temperature, which is the solution vector, the system of equations is non-linear:

$$\mathbf{B}\dot{\mathbf{T}} + \mathbf{A}\mathbf{T} = \mathbf{b}(\mathbf{T}) \tag{33}$$

In order to take into account the non-linearity, the system is solved by applying a Picard iteration procedure. The matrix equation (33) is solved for $\mathbf{T}$ using two separate time integration methods instead of one. The respective schemes update each other until they converge on a solution. An initial value for the solution (i.e. the temperature $\mathbf{T}$) is required to start the iterative process. Typically, it can be obtained by applying the explicit forward Euler

method (Gresho et al. 1980). BASIMO uses the Adams-Bashforth predictor instead, which estimates a solution for $\mathbf{T}^{n+1}$ as $\mathbf{T}_{pre}^{n+1}$ based on the temperature rate defined at two previous time steps termed acceleration vectors $\dot{\mathbf{T}}^n$ and $\dot{\mathbf{T}}^{n-1}$ (Gresho et al. 1980; Gresho et al. 2008):

$$\mathbf{T}_{pre}^{n+1} = \mathbf{T}^n + \frac{\Delta t_n}{2}\left[\left(2 + \frac{\Delta t_n}{\Delta t_{n-1}}\right)\dot{\mathbf{T}}^n - \left(\frac{\Delta t_n}{\Delta t_{n-1}}\right)\dot{\mathbf{T}}^{n-1}\right] \tag{34}$$

where $\Delta t_n = t_{n+1} - t_n$ and $\Delta t_{n-1} = t_n - t_{n-1}$. As this is also an explicit method, no matrix inversion is required for the calculation. Hence, estimating $\mathbf{T}_{pre}^{n+1}$ at first is computationally inexpensive. Then, BASIMO solves the matrix equation (33) for $\mathbf{T}_{cor}^{n+1}$ as the *true* solution of $\mathbf{T}^{n+1}$ using the Crank-Nicolson scheme as a corrector. For that, the source terms in $\mathbf{b}(\mathbf{T})$ are determined assuming the predicted values of $\mathbf{T} = \mathbf{T}_{pre}^{n+1}$ to factor in the non-linearity. Subsequently, the acceleration vectors are updated based on the corrector's solution for the next predictor step according to:

$$\dot{\mathbf{T}}^{n+1} = \frac{\Delta t_n}{2}\left(\mathbf{T}^{n+1} - \mathbf{T}^n\right)\dot{\mathbf{T}}^n \tag{35}$$

This loop is repeated until a user-defined maximum number of iterations or an error tolerance between corrector and predictor solution is reached.

Furthermore, using a predictor-corrector method also allows for the implementation of an automated and adaptive time step control (Reddy & Gartling 2010). According to Gresho et al. (1980; 2008), the size of the next time step Δt_{n+1} can be determined by evaluating the integration error of the predictor and the corrector solution considering a user defined error tolerance ε:

$$\Delta t_{n+1} = \Delta t_n \sqrt[3]{\left(b \frac{\varepsilon}{d_{n+1}}\right)} \tag{36}$$

Where Δt_n is the current time step and $b = 3(1 + \Delta t_{n-1}/\Delta t_n)$. The denominator d_{n+1} is defined as a norm of the integration error by

$$d_{n+1} = \frac{1}{\sqrt{n}T_{rep}}\sqrt{\sum_{i=1}^{n}\left(T_{cor}^{n+1} - T_{pre}^{n+1}\right)^2} \tag{37}$$

Here, n is the total number of nodes in the entire mesh and T_{rep} is a value representative for the temperature scale of the problem. As this scale can shift significantly from heat storage to heat extraction operation, BASIMO calculates T_{rep} at each time step as the midpoint between the maximum and the minimum temperature occurring in the mesh.

The predictor (34) cannot be computed at the beginning of the simulation, because the acceleration vectors are not available at this point. Hence, BASIMO initializes each simulation by calculating the first five time steps only using the corrector (30) as prescribed by the user-defined value for θ. The time step size for the initial steps is constant and should be very small. This allows for the calculation of the acceleration vectors. Subsequently, BASIMO switches to the predictor-corrector method and the automatic time stepping takes control.

2.2. Unstructured Tetrahedron Mesh

Most of the available simulation tools like EED (Hellström & Sanner 1994) restrict the BHE array to a set of predefined geometrical arrangements. Furthermore, the models of BHE arrays are usually limited to vertical boreholes. Some available solutions can merely consider a single inclined BHE. Others can handle arrays, but use a priori calculated g-functions introduced by Eskilson (1987), which again restricts the models to predefined geometries (e.g. Lamarche 2011). Even the sophisticated FEM-based commercial simulator FEFLOW (Diersch 2014) only just introduced unstructured grids in the latest release 7.0, which potentially allows for arbitrary bore paths. However, the workflow of the model setup is not suitable for mathematical optimization problems that affect the finite element mesh. Furthermore, the validity of the implemented BHE solution has yet to be tested for deviated boreholes. This leaves only simulators like OpenGeoSys (Kolditz et al. 2012) with a full discretization of the BHEs for modeling inclined boreholes and arbitrary BHE array geometries. Nevertheless, the setup of fully discretized models is cumbersome and the simulation of entire BHE arrays is computationally expensive. Therefore, one of the simulator's development requirements is the ability to model BHEs with as few geometric restrictions as possible. Hence, BASIMO uses tetrahedral elements generated by TetGen (Si 2010) to create an unstructured finite element mesh. The one-dimensional discretization of the bore path is defined as a polyline of neighboring grid nodes. The analytical BHE solution coupled to these polylines is not affected by the bore path, as the temperature at the nodes and the distance between the nodes are the only relevant parameters. Consequently, even modeling bore paths with a curvature is potentially feasible. This allows BASIMO to simulate arrays of inclined boreholes, which is an increasingly popular application for BHEs in densely populated urban areas with limited space (Cui et al. 2006; Bussmann et al. 2015).

2.2.1. Interpolation Functions

Modeling inclined boreholes and the steep temperature gradients, which occur in the direct vicinity of the BHEs, imply that structured grids with a rigid mesh spacing are unsuitable. Unstructured grids with mesh refinements in regions of high temperature gradients require the finite elements to vary in size and shape. Assuming a reference geometry for a standard tetrahedron, any distorted shape, which preserves the topology, can be obtained by coordinate transformation. The four nodes defining the reference tetrahedron are described using a local coordinate system denoting the three dimensions in space as ξ, η, ζ ranging from 0 to 1 (Figure 5).
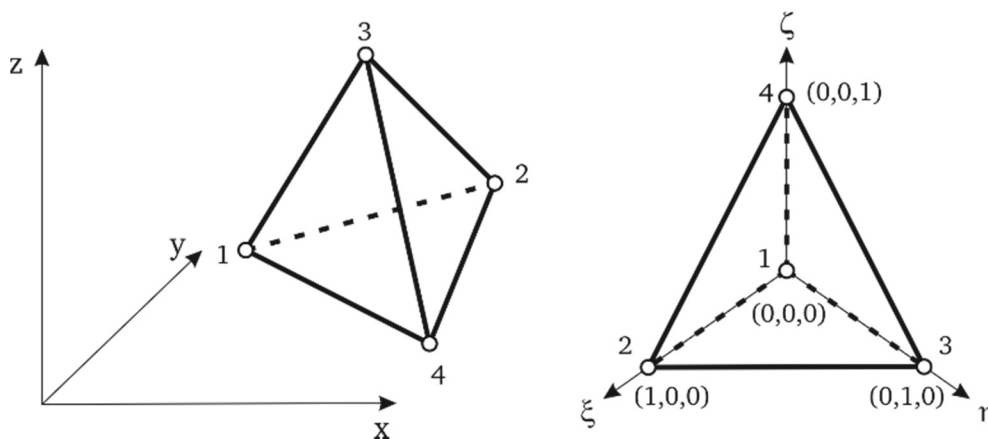
Figure 5: Linear tetrahedron in the global (left) and local (right) coordinate system, after Diersch (2014)

BASIMO uses linear tetrahedral elements, which are defined by their four corner points. The temperature is interpolated at these nodes. Hence, Lagrange polynomials suffice to describe the approximation functions ψ_p of the temperature T^e at the elements' nodes (11). These functions satisfy two criteria: their value is 1 at the corresponding node and 0 at all the others. Furthermore, for each finite element, the sum of all approximation functions' values is 1. Also, they are linear in all three dimensions, as required, to ensure continuity of the first order derivatives of the weak form (22) and all variable terms are linearly independent. The four approximation functions for the reference tetrahedron are according to Diersch (2014):

$$
\begin{aligned}
\psi_1 &= 1 - \xi - \eta - \zeta \\
\psi_2 &= \xi \\
\psi_3 &= \eta \\
\psi_4 &= \zeta
\end{aligned}
\tag{38}
$$

2.2.2. Coordinate Transformation

The temperature approximation functions refer to the local coordinate system. Hence, a transformation rule between the global and the local coordinate system (39) is required to use the approximation functions in the coefficient matrices (23). Doing so, the interpolation of the temperature T^e is extended to the coordinates:

$$
x = \sum_{p=1}^{n} x_p^e \psi_p^e(\xi, \eta, \zeta), \quad y = \sum_{p=1}^{n} y_p^e \psi_p^e(\xi, \eta, \zeta), \quad z = \sum_{p=1}^{n} z_p^e \psi_p^e(\xi, \eta, \zeta)
\tag{39}
$$

Where n is the number of nodes of the element Ω^e and x_p, y_p and z_p are the respective global coordinates. As the number of nodes describing the geometry of the finite element equals the number of nodes to interpolate the variable (i.e. the temperature), the elements are termed isoparametric.

In order to evaluate the coefficient matrices (23) of the finite element model, the spatial derivatives of the interpolation functions have to be determined. Based on the chain rule of differentiation, the following relations can be derived for three-dimensional isoparametric elements (Reddy & Gartling 2010):

$$
\begin{pmatrix}
\dfrac{\partial \psi_p}{\partial \xi} \\[2ex]
\dfrac{\partial \psi_p}{\partial \eta} \\[2ex]
\dfrac{\partial \psi_p}{\partial \zeta}
\end{pmatrix}
=
\begin{pmatrix}
\dfrac{\partial x}{\partial \xi} & \dfrac{\partial y}{\partial \xi} & \dfrac{\partial z}{\partial \xi} \\[2ex]
\dfrac{\partial x}{\partial \eta} & \dfrac{\partial y}{\partial \eta} & \dfrac{\partial z}{\partial \eta} \\[2ex]
\dfrac{\partial x}{\partial \zeta} & \dfrac{\partial y}{\partial \zeta} & \dfrac{\partial z}{\partial \zeta}
\end{pmatrix}
\begin{pmatrix}
\dfrac{\partial \psi_p}{\partial x} \\[2ex]
\dfrac{\partial \psi_p}{\partial y} \\[2ex]
\dfrac{\partial \psi_p}{\partial z}
\end{pmatrix}
= \mathbf{J}
\begin{pmatrix}
\dfrac{\partial \psi_p}{\partial x} \\[2ex]
\dfrac{\partial \psi_p}{\partial y} \\[2ex]
\dfrac{\partial \psi_p}{\partial z}
\end{pmatrix}
\tag{40}
$$

Where $\mathbf{J}$ is the Jacobian matrix of the transformation from global (x, y, z) to local coordinates (ξ, η, ζ). The components of $\mathbf{J}$ can be calculated based on the transformation relationship defined in (39):

$$\frac{\partial x}{\partial \xi} = \sum_{p=1}^{n} x_p^e \frac{\partial \psi_p}{\partial \xi} ; \qquad \frac{\partial y}{\partial \xi} = \sum_{p=1}^{n} y_p^e \frac{\partial \psi_p}{\partial \xi} ; \qquad \frac{\partial z}{\partial \xi} = \sum_{p=1}^{n} z_p^e \frac{\partial \psi_p}{\partial \xi}$$

$$\frac{\partial x}{\partial \eta} = \sum_{p=1}^{n} x_p^e \frac{\partial \psi_p}{\partial \eta} ; \qquad \frac{\partial y}{\partial \eta} = \sum_{p=1}^{n} y_p^e \frac{\partial \psi_p}{\partial \eta} ; \qquad \frac{\partial z}{\partial \eta} = \sum_{p=1}^{n} z_p^e \frac{\partial \psi_p}{\partial \eta} \qquad (41)$$

$$\frac{\partial x}{\partial \zeta} = \sum_{p=1}^{n} x_p^e \frac{\partial \psi_p}{\partial \zeta} ; \qquad \frac{\partial y}{\partial \zeta} = \sum_{p=1}^{n} y_p^e \frac{\partial \psi_p}{\partial \zeta} ; \qquad \frac{\partial z}{\partial \zeta} = \sum_{p=1}^{n} z_p^e \frac{\partial \psi_p}{\partial \zeta}$$

Ultimately, explicit expressions for the derivatives of the approximation functions in the global coordinate system can be obtained by inverting the Jacobian matrix $\mathbf{J}$. For $\mathbf{J}^{-1}$ to exist, the determinant of the Jacobian must not be zero at any point of the finite element volume Ω^e.

$$\begin{pmatrix} \dfrac{\partial \psi_p}{\partial x} \\ \dfrac{\partial \psi_p}{\partial y} \\ \dfrac{\partial \psi_p}{\partial z} \end{pmatrix} = \mathbf{J}^{-1} \begin{pmatrix} \dfrac{\partial \psi_p}{\partial \xi} \\ \dfrac{\partial \psi_p}{\partial \eta} \\ \dfrac{\partial \psi_p}{\partial \zeta} \end{pmatrix} ; \qquad \det(\mathbf{J}) \neq 0 \qquad (42)$$

For brevity, these expressions are not listed here, but can be found for example in Diersch (2014). After the integrands of (22) have been transformed, the limits of the integration have to be adapted, as well. The differential elemental volume transforms from global to local coordinates $0 \leq \xi, \eta, \zeta \leq 1$ according to:

$$dx \, dy \, dz = \det(\mathbf{J}) \, d\xi \, d\eta \, d\zeta \qquad (43)$$

2.2.3. Numerical Integration

The transformation of the integrals for each element Ω^e to the associated reference tetrahedron geometry in the local coordinate system results in algebraic expressions, which are too complex to be evaluated analytically. However, they can be integrated applying numerical techniques. Essentially, a polynomial function f, which is to be integrated, is evaluated at specific sampling points i. Each sampling point has a weight coefficient W_i that is multiplied with the corresponding function value. The sum of the products represents an approximation of the integral. Considering f as an abbreviation for a transformed integral argument, this results in the following formula:

$$\int_0^1 \int_0^{1-\xi} \int_0^{1-\xi-\eta} f(\xi, \eta, \zeta) \, d\xi \, d\eta \, d\zeta = \sum_{i=1}^{m} W_i \, f(\xi_i, \eta_i, \zeta_i) \qquad (44)$$

The available numerical methods differ from each other with respect to the coordinates of the sampling points and the associated weight coefficients. The Gauss-Legendre quadrature (Zienkiewicz et al. 2013) is applied, as it provides the highest possible accuracy with the least number of sampling points. Quadrature points with corresponding coordinates and weights for linear tetrahedral elements, as well as a more detailed description of the entire finite element method can be found; for example, in Reddy & Gartling (2010), Zienkiewicz et al. (2013) or Diersch (Diersch 2014).

2.3. Analytical Solution for Borehole Heat Exchangers

In the past, BHEs rarely exceeded 100 m depth. Therefore, no partial thermal insulation was necessary. On the contrary, due to the small temperature differences between the heat carrier fluid and the borehole wall, a high thermal conductivity of a single grout was favorable along the entire borehole. Consequently, simulation models did not need to account for grout thermal conductivities or borehole diameters changing with depth. Based on Eskilson and Claessons's solution (1988), Bauer et al (2011b) and Diersch et al. (2011a) developed a thermal resistance and capacity model (TRCM) which reduces a BHE to a one-dimensional discretization of nodes in a finite element mesh. This model accounts for a detailed description of the geometry of different BHE types and their material parameters. While it is more accurate than many line source models as it calculates depth-dependent grout and fluid temperatures within the BHE, it cannot accommodate changing borehole diameters or backfill material properties along the borehole length. Thus, up to now only fully discretized 3D numerical models have been able to simulate BHEs with vertically varying thermal conductivities. However, these models are laborious to set up, require expensive computations and lack the efficiency of fast analytical solutions, especially for larger models with multiple BHEs as needed for BTES systems.

For BASIMO, Eskilson and Claessons's solution was improved to a model, which considers boreholes with an upper and a bottom section, both with different borehole diameters and different thermal conductivities of the backfill material represented in a TRCM. This approach is independent from the specific BHE type and can handle coaxial, U-pipe and double U-pipe BHEs.

2.3.1. Ordinary BHEs

Eskilson and Claesson's analytical BHE solution (1988) describes the fluid temperature in the downstream and upstream pipes T_{in} and T_{out} in °C as two codependent functions of depth z (in the range of $\zeta = 0$ to the total borehole length L) and the current borehole wall temperature T_b at time t.

$$T_{in}(z,t) = T_{in}(0,t)f_1(z) + T_{out}(0,t)f_2(z) + \int_0^z T_b(\zeta,t)f_4(z-\zeta)d\zeta \tag{45}$$

$$T_{out}(z,t) = -T_{in}(0,t)f_2(z) + T_{out}(0,t)f_3(z) - \int_0^z T_b(\zeta,t)f_5(z-\zeta)d\zeta \tag{46}$$

The functions f_1, f_2, f_3, f_4 and f_5 are given by the following expressions:

$$f_1(z) = e^{\beta z}\left[\cosh(\gamma z) - \delta \sinh(\gamma z)\right]$$

$$f_2(z) = e^{\beta z}\frac{\beta_{12}}{\gamma}\sinh(\gamma z)$$

$$f_3(z) = e^{\beta z}\left[\cosh(\gamma z) + \delta \sinh(\gamma z)\right] \tag{47}$$

$$f_4(z) = e^{\beta z}\left[\beta_1 \cosh(\gamma z) - \left(\delta\beta_1 + \frac{\beta_2\beta_{12}}{\gamma}\right)\sinh(\gamma z)\right]$$

$$f_5(z) = e^{\beta z}\left[\beta_2 \cosh(\gamma z) + \left(\delta\beta_2 + \frac{\beta_1\beta_{12}}{\gamma}\right)\sinh(\gamma z)\right]$$

The functions' auxiliary variables α, β, β_1, β_2, β_{12}, γ and δ, which are based on the TRMCs of the involved BHE components, are calculated according to the BHE type after Bauer (2011) and Bauer et al. (2011b), whereas the derivation of the functions $f_1 - f_5$ can be found in Eskilson and Claesson (1988). The auxiliary variables summarize the interaction of the different thermal resistances in the TRCM. That way, U-pipe double U-pipe and coaxial BHEs can be considered by the analytical solution. Since the solution describes only local steady-state conditions, time t is omitted from the following equations for better readability. The analytical solution has to be linked to a numerical subsurface model by deriving a heat source term from the difference between the borehole wall temperature and the fluid temperature (Diersch et al. 2011a) to account for transient heat transport in the subsurface. Then, the numerical model calls the analytical solution every time step, providing the time-dependent borehole wall temperature.

As the upstream and downstream pipes form a closed loop, the fluid temperature must be the same at the bottom. Hence, equations (45) and (46) can be equalized at $z = L$ and resolved for $T_{out} = T_{out}(z = 0)$ for a given inlet temperature of the BHE $T_{in} = T_{in}(z = 0)$:

$$T_{out} = T_{in}\frac{f_1(L) + f_2(L)}{f_3(L) - f_2(L)} + \int_0^L \frac{T_s(\zeta)f_4(L-\zeta) + f_5(L-\zeta)}{f_3(L) - f_2(L)}d\zeta \tag{48}$$

2.3.2. Partially Insulated BHEs

Determining the outlet temperature T_{out} is the imperative first step, as equations (45) and (46) require both the inlet and the outlet temperature of the BHE to calculate the depth-dependent temperature profile in the downstream and upstream pipes. However, equation (48) shows that the solution for the outlet temperature integrates functions f_4 and f_5 over the entire borehole length L. Likewise, functions f_1, f_2 and f_3 depend on the total borehole length L as well. Hence, borehole properties changing with depth cannot be accounted for in this equation, as they are constants in the auxiliary variables of the functions $f_1 - f_5$. Instead, a BHE with a borehole insulation in the upper part requires a split calculation.
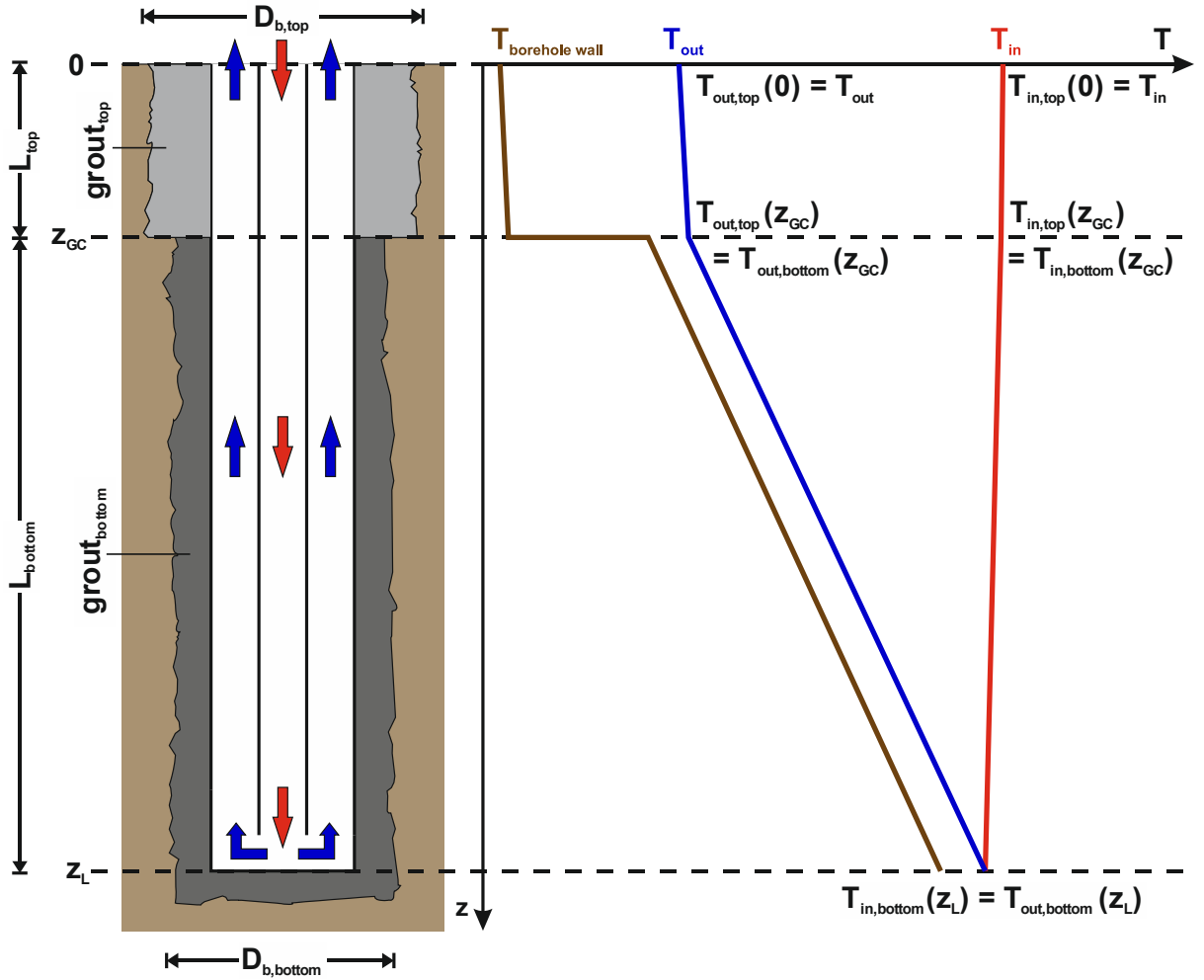
Figure 6: Sketch of a coaxial BHE (centered inlet) with the insulated borehole section and the corresponding temperature profile for heat storage operation (Schulte et al. 2016b).

As the design splits the BHE into two sections with different grout properties and drilling diameters (Figure 6), equations (45) and (46) apply for the upper and lower section separately. This allows for an independent consideration of different TRCMs with different auxiliary variable values for the functions $f_1 - f_5$ in each section. The downstream and upstream pipes are connected in the bottom section. Therefore, equations (45) and (46) cannot be equalized for the bottom of the upper part at the interface between the two different grout types at depth z_{gc} to derive equation (48). However, at the interface the fluid temperatures $T_{in,top}(z_{gc})$ and $T_{out,top}(z_{gc})$ of the upper section of the wellbore are equal to the inlet and outlet temperatures $T_{in,bottom}$ and $T_{out,bottom}$ of the bottom section.

$$
\begin{aligned}
T_{in,bottom} &= T_{in,top}\left(z_{GC}\right) \\
T_{out,bottom} &= T_{out,top}\left(z_{GC}\right)
\end{aligned}
\tag{49}
$$

Equation (48) is still valid for the bottom section, but the inlet and outlet temperatures are unknown. Thus, substitution according to (49) gives

$$T_{out,bottom} =$$

$$T_{in,bottom} \frac{f_{1,bottom}\left(L_{bottom}\right)+f_{2,bottom}\left(L_{bottom}\right)}{f_{3,bottom}\left(L_{bottom}\right)-f_{2,bottom}\left(L_{bottom}\right)} + \int\limits_{z_{GC}}^{z_L} \frac{T_s(\zeta)f_{4,bottom}\left(L_{bottom}-\zeta\right)+f_{5,bottom}\left(L_{bottom}-\zeta\right)}{f_{3,bottom}\left(L_{bottom}\right)-f_{2,bottom}\left(L_{bottom}\right)} d\zeta$$

$$\equiv \hspace{6cm} (50)$$

$$T_{out,top}\left(z_{GC}\right)=$$

$$T_{in,top}\left(z_{GC}\right)\frac{f_{1,bottom}\left(L_{bottom}\right)+f_{2,bottom}\left(L_{bottom}\right)}{f_{3,bottom}\left(L_{bottom}\right)-f_{2,bottom}\left(L_{bottom}\right)} + \int\limits_{z_{GC}}^{z_L} \frac{T_s(\zeta)f_{4,bottom}\left(L_{bottom}-\zeta\right)+f_{5,bottom}\left(L_{bottom}-\zeta\right)}{f_{3,bottom}\left(L_{bottom}\right)-f_{2,bottom}\left(L_{bottom}\right)} d\zeta$$

Inserting (45) and (46) for $T_{in,top}(z_{GC})$ and $T_{out,top}(z_{GC})$ the resulting equation can be solved for $T_{out,top}$:

$$T_{out,top} = T_{in,top}\frac{\kappa+\nu \int\limits_{0}^{z_{GC}} T_b(\zeta)f_{4,top}\left(L_{top}\right)d\zeta + \int\limits_{0}^{z_{GC}} T_b(\zeta)f_{5,top}\left(L_{top}\right)d\zeta + \mu}{\tau} \hspace{2cm} (51)$$

with

$$\kappa = \nu\, f_{1,top}\left(L_{top}\right)+f_{2,top}\left(L_{top}\right)$$
$$\tau = f_{3,top}\left(L_{top}\right)-\nu\, f_{2,top}\left(L_{top}\right)$$
$$\mu = \int\limits_{z_{GC}}^{z_L} \frac{T_b(\zeta)\left(f_{4,bottom}\left(L_{bottom}\right)+f_{5,bottom}\left(L_{bottom}\right)\right)}{f_{3,bottom}\left(L_{bottom}\right)-f_{2,bottom}\left(L_{bottom}\right)} d\zeta \hspace{2cm} (52)$$
$$\nu = \frac{f_{1,bottom}\left(L_{bottom}\right)+f_{2,bottom}\left(L_{bottom}\right)}{f_{3,bottom}\left(L_{bottom}\right)-f_{2,bottom}\left(L_{bottom}\right)}$$

Subsequently, the depth-dependent temperature profiles in the downstream and upstream pipes can be calculated with (45) and (46) using $T_{in,top}$ and $T_{out,top}$ for the upper insulated section of the wellbore and $T_{in,bottom} = T_{in,top}(z_{GC})$ and $T_{out,bottom} = T_{out,top}(z_{GC})$ for the lower section. The new solution now takes into account borehole properties changing with depth and can be coupled to the numerical subsurface model as described in Diersch et al. (2011a).

2.4. Program Structure

BASIMO has an intricate structure of subroutines and input files. Their relationships are shown in Figure 7. The main code initializes the model and computes the numerical solution, while the subroutines organize the model input and output, as well as the analytical solution for the BHEs. Numerical and model parameters are defined in self-explaining Excel sheets to ensure user-friendliness. The finite element mesh is generated by a small separate MATLAB program, which calls for user input to define the geometry of the BHE array. At this point, BASIMO does not check for faulty user inputs. Hence, it is important to make sure the model input is sensible. A short description of each subroutine and input/output file is given below. A copy of BASIMO is provided with the digital supplement of this thesis.
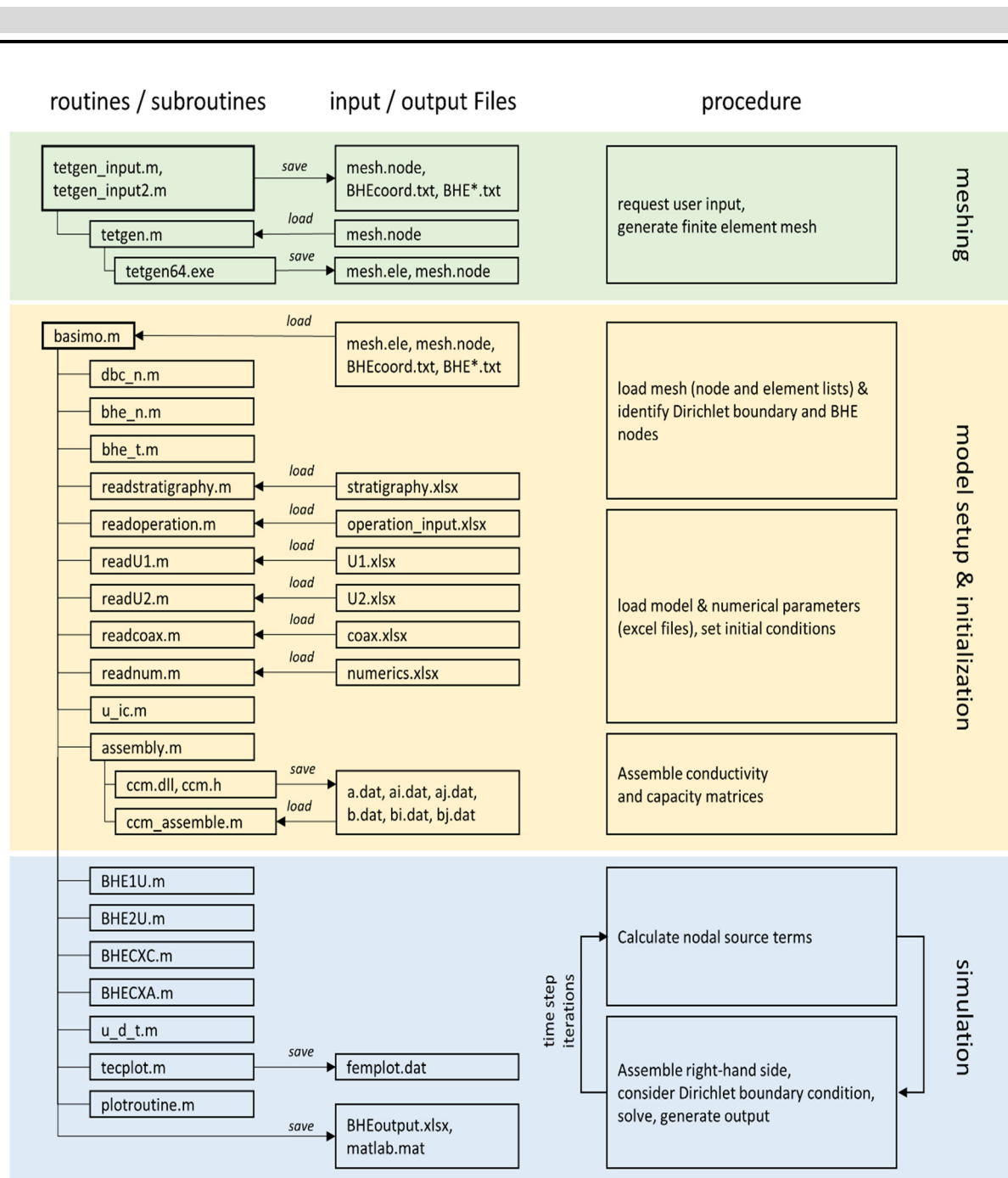
Figure 7: Tree diagram illustrating the structure of BASIMO and the relation between the involved subroutines.

2.4.1. Input and Output files

mesh.ele and mesh.node

These text files are generated with TetGen (Si 2010) and comprise the spatial discretization of the model as lists of elements and nodes. The list of elements assigns four global node numbers to each tetrahedral finite element, while the list of nodes provides Cartesian coordinates for each node. The latter are required for the coordinate transformation described in Chapter 2.2.2.

BHEcoord.txt

BHEcoord.txt lists the x and y coordinates of the topmost node for each BHE. Consequently, the file provides the number of BHEs, which defines how many BHE*.txt files have to be loaded.

BHE.txt*

The nodes representing a bore path have to be identified in BASIMO to couple the numerical model and the analytical solution correctly. For each BHE, a BHE*.txt file provides a list of nodal coordinates, where * denotes the serial number of the BHE.

stratigraphy.xlsx

BASIMO can consider a basic stratigraphic profile with individual values of density, specific heat capacity and thermal conductivity for each layer. The layers are numbered from top to bottom and defined by their respective bottom depth. The values are taken into account in the assembly process for calculating the conductivity and capacity matrices (Chapter 2.1.2). At least one entry is required.

operation_input.xlsx

A table in the operation_input.xlsx file provides a time series for the operation of the BHE array. The time series is defined by time intervals, which are described by the table's lines. The intervals' length is set by the time stamp marking the end of the respective increment. For every interval, the user can specify the BHE type (i.e. U-pipe, double U-pipe, coaxial pipe with centered inlet or with annular inlet) and choose between a given heat load or an inlet temperature. Obviously, changing the BHE type during the operation is only intended for the change of flow direction in coaxial pipes. At this point, BASIMO only supports parallel operation of the BTES array. Hence, the settings are applied to all BHEs alike. At least one entry is required. The specified values are included in the calculation of the auxiliary variables of the analytical solution for BHEs (Chapter 2.3)

U1.xlsx, U2.xslx and coax.xlsx

With these Excel files, the user can specify the material and geometric parameters within the U-pipe, double U-pipe and coaxial BHEs. Depending on the first entry in operation_input.xlsx, BASIMO loads the corresponding Excel sheet. Each borehole is necessarily represented in it's own column in this table. Thus, borehole diameters, pipe diameters, pipe thicknesses, shank spaces and thermo-physical properties of the pipe material, the grout and the working fluid can be assigned separately to each BHE. Additional columns are ignored by BASIMO. The coax.xlsx file serves for both central and annular inlet operation. Based on the values in the table, BASIMO calculates the auxiliary variables for the analytical solution (Chapter 2.3) according to the specified BHE type.

numerics.xlsx

In numerics.xlsx, a few adjustments can be made to the simulator itself, which affect the time integration (Chapter 2.1.3). The user can define the time integration coefficient θ, the error tolerance ε for the time step control and for the Picard iteration, the maximum number of Picard iterations, the initial time step size, the maximum time step growth factor and the maximum time step size. Furthermore, numerics.xlsx contains two switches for a graphical output during the simulation, and the output of a solution vector – i.e. subsurface the temperature field – time series for post-processing purposes.

a.dat, ai.dat, aj.dat, b.dat, bi.dat and bj.dat

These text files contain the assembled thermal conductivity matrix **A** and the heat capacity matrix **B** (see Chapter 2.1.2). The matrices are stored in the compressed row storage format

(Barrett et al. 1994). Hence, a.dat and b.dat contain the values of **A** and **B**, whereas ai.dat, aj.dat, bi.dat and bj.dat include the row pointers and column indices.

BHEoutput.xlsx

At the end of the simulation, BASIMO saves a BHEoutput.xlsx file. The table contains the outlet temperature of each BHE determined by the analytical solution (Chapter 2.3) at every computed time step.

femplot.dat

Depending on the settings in numerics.xlsx, femplot.dat is a text file containing the solution vector of the final time step or a time series with time steps of one day length. Furthermore, it includes all information on the finite element mesh, which are required for the visualization of the temperature field. The file is formatted for use with the post-processing software Tecplot 360 2013R1 (Tecplot 2013).

matlab.mat

For debugging purposes, BASIMO saves the entire workspace after the simulation in a file labeled matlab.mat.

2.4.2. Subroutines

tetgen_input.m and tetgen_input2.m

The tetgen_input.m and tetgen_input2.m files contain separate MATLAB programs, which create the finite element mesh for arrays of vertical and inclined BHEs, respectively. In general, BASIMO allows for arbitrary borehole paths. Even a curved borehole can be approximated by a polyline. BASIMO only requires a list of the BHE node coordinates, ordered from top to bottom. However, creating an input routine for arbitrary geometries is a task of its own. Hence, BASIMO comes with these two programs, which offer a range of BHE array geometries. Experienced MATLAB users can create their own input routines for the mesh generation to suit their specific requirements.

Both routines define a box model at first. Subsequently, polylines consisting of nodes are added, which represent the one-dimensional discretization of the BHEs. Along with the polylines, the neighboring nodes are defined as well. Diersch et al. (Diersch et al. 2011b) showed that the BHE nodes and their neighbors should be kept at a specific distance to ensure numerical accuracy. The tetgen_input.m routine creates an array of vertical boreholes. The array layout is based on predefined templates, which determine the respective locations of the BHEs by constant angular relationships (Figure 8). A user input is required to set the number of BHEs (maximum of 20), their length and their radial distance towards each other. The tetgen_input2.m routine generates a BHE array of inclined boreholes with one central vertical BHE. In addition to the number of BHEs, their length and their radial distance at the surface, the user also has to define the inclination angle: The deviated boreholes dip away radially from the center of the array (cf. Appendix E).

In the end, both subroutines generate a list of coordinates containing the corners of the box model and the BHE polylines with the respective neighbor nodes. This list is saved as a text file labeled mesh.node and passed to tetgen.m. Furthermore, separate coordinate lists of the BHE nodes (without their neighbors) are saved as text files labeled BHE*.txt, where * is replaced by the serial number of the respective BHE. Next, the x and y coordinates of the topmost BHE

nodes are saved in BHEcoord.txt. The latter files are loaded in basimo.m to determine the number of BHEs and to identify the BHE polylines.

tetgen.m and tetgen64.exe

After the box model and the BHEs are defined, tetgen.m is executed. This function simply executes the tetgen64.exe (the 64-bit built of TetGen, Si 2010) twice. In the first run, the nodes stored in mesh.node are connected to form a preliminary mesh of finite elements, which is saved as mesh.ele. This grid contains only the nodes previously defined in tetgen_input.m or tetgen_input2.m. As a consequence, many of the resulting elements have ill-shaped geometries, which would results in erroneous calculations. Hence, tetgen64.exe is run a second time, now provided with the additional information on the preliminary elements and parameters for mesh optimization. TetGen improves the element geometries by adding Steiner points and re-meshing the grid (for more detail, see Si 2010). During this procedure, the original nodes remain at their position. The resulting mesh consists of well-shaped Delaunay-triangulated tetrahedral elements and is saved to mesh.node and mesh.ele overwriting the previously generated files.
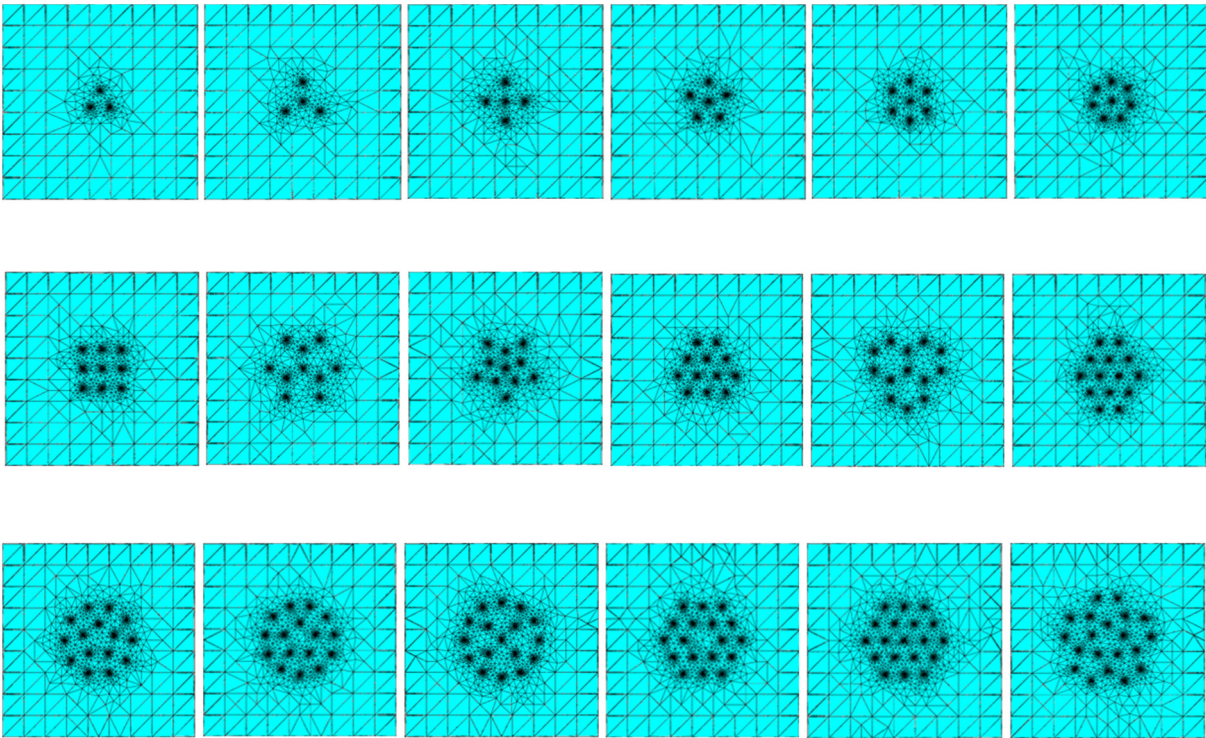
Figure 8: Templates for the arrangements of vertical BHEs in the discretized tetrahedron mesh (overhead perspective) generated with tetgen_input.m; model edge length: 100 m.

basimo.m

This file is the main routine of BASIMO. The program loads the finite element mesh and the model parameters from the respective files and initializes the simulation before running it (Figure 7). The code of basimo.m contains the time integration of the finite element model and controls the Picard iterations, as well as the automatic time stepping described in Chapter 2.1.3. Many subroutines are called for the model initialization, the calculation of the heat sources and for the simulation output, which are described in brief below.

dbc_n.m

By evaluating the z-coordinate, this subroutine identifies all nodes at the top and the bottom of the model domain and marks them as Dirichlet boundary nodes.

bhe_n.m

The bhe_n.m subroutine compares the coordinates of the mesh nodes to those provided by the coordinate lists for the BHE nodes in the BHE*.txt files previously loaded in basimo.m. Matching coordinate tuples are identified as BHE nodes in the finite element mesh. Possible rounding errors that may prevent the coordinates from matching exactly are compensated by searching for the nearest neighboring mesh point.

bhe_t.m

Based on the previously identified BHE nodes, this subroutine determines the length of the edges between the nodes.

readstratigraphy.m

This subroutine reads the stratigraphy.xlsx file and assigns the bulk values for density, specific heat capacity and thermal conductivity to vectors, which are later used in the assembly of the conductivity and heat capacity matrices.

readoperation.m

This subroutine reads the operation_input.xlsx file and stores the table as a matrix. Later, the predictor-corrector method progresses through the operation time series table line by line.

readU1.m, readU2.m and readcoax.m

Depending on the first entry in the operation time series, these subroutines load the U1.xlsx, the U2.xlsx or the coax.xlsx file and store the contained BHE parameters in a matrix. Since the values in the operation table apply for every BHE all the same, BASIMO can only call one of these functions during the model initialization. The individual BHEs, however, can have varying parameters defined in the columns of the respective Excel file.

readnum.m

BASIMO calls readnum.m to load the numerical parameters stored in the numerics.xlsx file. The values are stored in a structured variable, which BASIMO refers back to during the numerical computation.

u_ic.m

The u_ic.m subroutine imposes the initial temperature field on the subsurface model, considering a geothermal gradient of 0.03 K/m and a surface temperature of 10 °C to satisfy Equation (6) (Chapter 2.1.1). Experienced MATLAB users can change these values in the code of the subroutine.

assembly.m

The assembly.m file is a subroutine, which handles the assembly of the heat capacity and the thermal conductivity matrices (see Chapter 2.1.2). The two following nested functions are called in assembly.m.

ccm.dll, ccm.h and helper.h

The original assembly routine provided by Alberty et al. (1999) is computationally too expensive for large three-dimensional models. Hence, the assembly is carried out outside of MATLAB using ccm.dll, ccm.h and helper.h. They constitute a C/C++ library published in Rühaak et al. (2014). It is called in assembly.m to compute the numerical integration (see chapter 2.2.3) of the finite elements. The library call returns the heat capacity and the thermal

conductivity matrices in the compressed row storage format (Barrett et al. 1994) and saves them in separate text files labeled a.dat, ai.dat, aj.dat, b.dat, bi.dat and bj.dat.

ccm_assemble.m

The output of ccm.dll has to be converted to MATLAB's native matrix format. Therefore, assembly.m calls the ccm_assemble.m subroutine, which loads the text files generated by the C/C++ library and compiles them into matrices in MATLAB.

BHE1U.m, BHE2U.m, BHECXC.m and BHECXA.m

These functions are the analytical solutions for U-pipe, double U-pipe and coaxial BHEs with centered or annular inlet described in Chapter 2.3. Depending on the operation time series table, the according function is called each time step to calculate the heat source terms for the numerical model. If the switch for graphical output in numerics.xlsx is set to 1, a temperature profile of the central BHE is plotted each time step. For BHE arrays, the profile for the fourth BHE is also plotted. Experienced MATLAB users can choose another borehole by changing the referring serial number of the BHE.

u_d_t.m

BASIMO calls u_d_t.m at each time step to calculate the right-hand side of the numerical equation (30) when solving for $\mathbf{T}^{n+1}$. The subroutine imposes the Dirichlet boundary condition on equations corresponding to the top and on the bottom mesh nodes of the subsurface model, which were earlier identified by dbc_n.m, to satisfy Equation (7) (Chapter 2.1.1).

tecplot.m

If the switch for the solution vector time series in numerics.xlsx is set to 1, tecplot.m saves the temperature field of the subsurface to femplot.dat every time BASIMO has elapsed one day of simulation time. Experienced MATLAB users can change the interval in basimo.m.

plotroutine.m

If the switch for graphical output in numerics.xlsx is set to 1, basimo.m calls this function every time step after the solution of the numerical equation. It plots the time step size against the time step number, as well as the central BHE's inlet and outlet temperature against time. For BHE arrays, the inlet and outlet temperature is also plotted for the fourth BHE. Experienced MATLAB users can choose another borehole by changing the referring serial number of the BHE.

Chapter 3: Mathematical Optimization of Medium Deep BTES systems

A comprehensive introduction to mathematical optimization is given by Burkhard & Zimmermann (2012): on a basic level, the mathematical optimization of a restricted problem requires an objective function f that provides a numerical response based on an input x under consideration of certain constraints and boundaries. Such a function can be anything from a simple polynomial to a complex simulation program. Optimization methods minimize the function value by choosing an optimal x^*. Therefore, the response of the objective function has to be a scalar value for the algorithm to be able to compare it. The function input x can be a set of multiple variables $x = (x_1, x_2, \ldots, x_n) \in R^{n-p} \times Z^p$ including p discrete values, which influence the response of f. The formal notation of an optimization problem reads as

$$\min_{x \in R^{n-p} \times Z^p} f(x)$$

subject to

$$g(x) = 0 \tag{53}$$
$$h(x) \leq 0$$
$$b_l \leq x \leq b_u$$

Where $g(x)$ and $h(x)$ represent equality and inequality constraint functions, whereas b_l and b_u are the lower and the upper boundary of x. It is worth noting, that mathematical optimization is subdivided into the fields of discrete (Dück 1977) and non-linear optimization (Ulbrich & Ulbrich 2012), which exclusively deal with discrete or real values for $x = (x_1, x_2, \ldots, x_n) \in R^{n-p} \times Z^p$, respectively. The consideration of mixed-integer problems is attained through combinations of discrete and non-linear methods (Kallrath 2013).

3.1. Mathematical Optimization in MATLAB

The MATLAB Global Optimization Toolbox (The MathWorks 2015b) used in BASIMO offers several algorithms that pursue different strategies to find the optimal x^*, which provides the lowest objective function value. Algorithms, which are able to handle functions with more than one variable x are called multivariate, whereas those that optimize multiple objective functions sharing the same input are termed multi-objective optimization algorithms (Burkard & Zimmermann 2012).

In MATLAB, many algorithms include user-defined bounds and constraints to restrict the feasible set for possible values for x (Kelley 1999; Fletcher 2000). Bounds are defined by mere lower and upper values of x, whereas functions determine additional, more complex constraints. For optimization applications dealing with an engineering problem, such bounds and constraints are important to limit the parameters to a physically meaningful space or to include additional considerations that may decrease the possible choice of parameter values. Depending on the optimization problem, the BASIMO response can be used in an objective function or in a constraint function.

Many optimization algorithms apply an iteration scheme to converge on the sought solution (Kelley 1999). This implies that depending on that scheme and the complexity of f and the constraints g and h, the algorithm requires multiple evaluations of the objective function and the related constraint functions. In some cases the number of iterations can be very large, involving hundreds of function calls. If a single evaluation of the objective function or the

constraint function takes a long time, this can result in an unacceptably exaggerated total computation time.

Typically, numerical simulations assessing the performance of BTES systems have to consider several years of operation. Even commercial simulators, which exploit more sophisticated mathematical methods than BASIMO, require considerable computation time for this task. This limits the direct use of BASIMO in an objective or in a constraint function mostly to very simple optimization problems, where only a few iterations are required to converge on an optimal solution.

This problem can be bypassed by using a proxy model instead. Proxy models are analytical functions derived from a previously defined set of numerical experiments. The resulting analytical function returns an approximated objective function value as a response to a set of input variables $x = (x_1, x_2, \ldots, x_n) \in R^{n-p} \times Z^p$, but in contrast to the numerical model it can be evaluated in a split second.

A MATLAB program provided along with BASIMO generates a proxy model from a set of training simulations. The program only requires a table containing the input variables and corresponding model responses of the training simulations (Appendix C). The applied method is briefly explained below. Afterwards, two short examples for an optimization directly calling BASIMO and a proxy-based optimization using two different optimization algorithms are given.

3.2. Proxy-based Optimization

The physical model described in Chapter 2 is used to construct a proxy model based on the theory of polynomial chaos expansion (PCE). The basic idea of PCE was introduced by Wiener (1938) and comprises the construction of the proxy model (response surface) of the original model with the help of an orthonormal polynomial basis of the parameter space. In simple words, the dependency of the model output on all input variables is approximated by projection onto a high-dimensional polynomial. The key attractive features of all PCE techniques are the high-order approximation of the model combined with its computational speed.

Formally, the vector of n input variables $x = (x_1, \ldots, x_n)$ is considered for the physical model $\Phi(x)$. The proxy model has to capture the influence of all inputs x on the model output Φ. According to PCE theory, the model output Φ can be approximated by polynomials $\Psi_i(x)$ with $i = 1, \ldots, M$.

$$\Phi(x) \approx \sum_{i=1}^{M} c_i \Psi_i(x) \tag{54}$$

The number M of polynomials $\Psi_i(x)$ and corresponding vector of real coefficients c_i depends on the total number of analyzed input parameters n and on the order d of the polynomial representation and is determined as (Oladyshkin & Nowak 2012):

$$M := \frac{(n+d)!}{(n! \cdot d!)} - 1 \tag{55}$$

The coefficients c_i quantify the dependency between the physical model output and the input x for each desired point in the parameter space, resulting in a surrogate for model $\Phi(x)$.

For BASIMO, a recent generalization of the PCE technique known as the arbitrary polynomial chaos (aPC) is applied (Oladyshkin & Nowak 2012). In aPC, the multi-dimensional orthonormal polynomial basis Ψ is constructed for arbitrary probability distribution shapes of input variables and, in addition, even works with unknown distribution shapes when only a few statistical moments can be inferred from limited data or from expert elicitation. To project the medium deep BTES model response onto an orthogonal polynomial basis, a uniform distribution is assumed for the modeling variables, which is simply dictated by equal interest to all possible outcomes of the physical model. The orthogonal polynomial basis of order d can be constructed according to equation (4) in Oladyshkin & Nowak (2012).

In order to determine the unknown coefficients c_i of the proxy model the original model is run at least once, but preferably more often, for every input variable using so-called training simulations with various sets of the input variables (cf. Chapter 4.2.3 and Appendix C). Such training simulations are used to create an initial proxy model for the following optimization procedure. However, to assure robustness of the overall modeling procedure, the quality of the proxy model is improved by incorporating additional simulations: specifically, the performance of the ideal design found by the optimization algorithm is validated by an additional numerical simulation. The corresponding approximation error of the proxy model must not be bigger than 1 %. If the verification simulation results in a violation of this criterion, it is used as an additional training simulation for refinement of the proxy model. Thus, a new projection of the model onto the orthonormal basis is performed using all cumulatively available training simulations within the least-squares collocation method (Moritz 1978; Chen et al. 2009). The process is then repeated starting with the optimization, which uses the refined proxy model for the constraint function until the error criterion is not violated anymore (Figure 9). From the practical point of view, the computational costs of the framework are dominated by the model calls required for constructing the surrogate model.
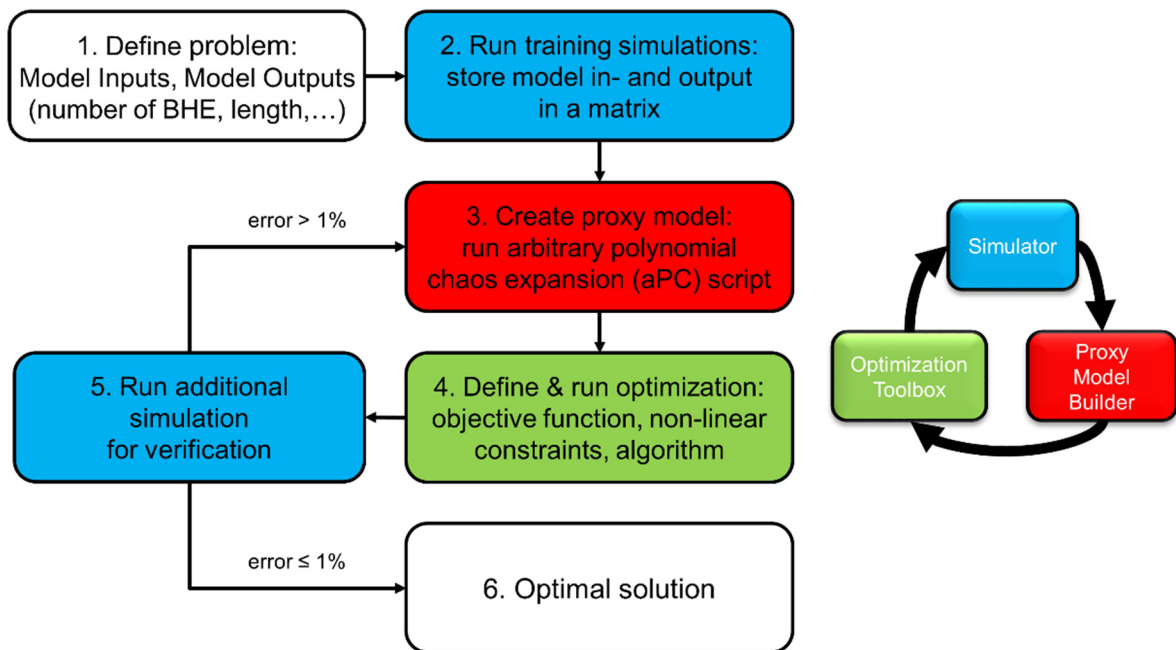

Figure 9: Flowchart illustrating the optimization procedure employing the aPC method (after Schulte et al. 2016a).

Chapter 4: Application of BASIMO

Before deploying BASIMO, the code is tested to attain confidence in the simulation results. Due to the large uncertainties of subsurface parameters, field data of existing BTES sites or even single BHEs are unsuitable for a basic model validation. Instead, numerical verifications and benchmarks are performed to evaluate the accuracy of the simulator. The successful tests allow for the application of BASIMO.

4.1. Verification and Validation

For most of the second half of the past century, the scientific computing community has been debating an exact definition of *verification* and *validation* (Oberkampf & Roy 2012). Here, the terms refer to the definition given in the *guide for verification and validation in computational solid mechanics* of the American Society of Mechanical Engineers (ASME). According to this guide, *verification* denotes "the process of determining that a computational model accurately represents the underlying mathematical model and its solution" (ASME 2006), whereas *validation* is "the process of determining the degree to which a model is an accurate representation of the real world from the perspective of the intended uses of the model" (US Department of Defense 1994; ASME 2006). In other words, verification assess the mathematical correctness, whereas validation evaluates the physical correctness (Roache 1998; Oberkampf & Roy 2012).

As Oberkampf & Roy (2012) pointed out, the hydrology community addressed the difficulty of model validation related to the typically limited knowledge of subsurface parameters. Despite the fact that BASIMO cannot be applied to hydrological problems, the same difficulties apply. Due to the predominant geological uncertainty of subsurface conditions, the parameters and boundary conditions required for model validation cannot be obtained with sufficient accuracy. Even the reference data set of the laboratory sandbox experiment of Beier et al. (2013) does not provide all the necessary parameters such as heat capacities, as their work focused on applications for thermal response tests rather than full-scale subsurface simulators. Therefore, BASIMO's capability to accurately represent the operation of BHEs are evaluated by comparison of benchmark simulations with the well-established software tools FEFLOW (Diersch 2014) and OpenGeoSys (Kolditz et al. 2012) instead. Nevertheless, the numerical part of BASIMO, i.e. the model for the conductive heat transport in the subsurface, is also verified.

4.1.1. Verification

If a mathematical model has been implemented correctly into a numerical code, the discretization error should decrease with an increasingly finer grid. As a result, the numerical solution converges on the true solution, if the spatial and temporal discretization is sufficiently fine. This test of grid convergence is a common way of verifying scientific computing code (Oberkampf & Roy 2012). Therefore, a grid convergence study was carried out to verify the FEM implementation in BASIMO following the recommendations for uniform reporting of grid refinement studies by Roache (1994). Evaluating the convergence of the numerical implementation requires the comparison of two solutions f_1 and f_2 on two different grids with discrete spacings h_1 (fine grid) and h_2 (coarse grid), which determine the grid refinement ratio $r = h_2 / h_1$. The most common approach is the grid doubling of the spatial and temporal domain with uniform spacings for h_1 and h_2 so that $r = 2$.

For this purpose, a model is created, to simulate the conductive heat transport induced by an infinite line source. In the model, the source is defined as a vertical line of evenly spaced nodes with a constant source term equating to 100 W m⁻¹ of heat input (Figure 10a and Figure 10b). Exploiting the symmetry of the problem, only a quarter of the domain has to be modeled. The thermo-physical parameters of the model domain are chosen to match the properties of stainless steel at a temperature of 300 K (Haynes et al. 2016). In order to model an infinite line source, vertical heat fluxes have to be inhibited. Therefore, boundary conditions are set at the top and bottom face of the grid. There, the temperature is set to be equal to the neighboring node. As a result, vertical temperature gradients emerging at the edge of the model are removed, mimicking an infinite domain in the vertical direction (Figure 10c) by imposing Neumann boundary conditions. All relevant model parameters are summarized in Table 3.

Table 3: Parameters of the verification model used to test the grid convergence, *according to Haynes et al. (2016).

Parameter	Value(s)	Unit
Model size	1 x 1 x 1	m
Grid spacing	$\frac{1}{8}, \frac{1}{16}, \frac{1}{32}$	m
Simulation time	86400	s
Time step size	8, 4, 2	s
Line source	100	W m⁻¹
Initial temperature	300	K
Specific heat capacity*	533	J kg⁻¹ K⁻¹
Density*	7722	kg m⁻³
Thermal conductivity*	17.31	W m⁻¹ K⁻¹

The model is discretized on different grids (Table 3, Figure 10a and Figure 10b) with a refinement ratio of $r = 2$ between each mesh. As the time domain has to be considered as well, constant time steps are used according to the refinement ratio instead of automatic time stepping. Subsequently, the heat conduction induced by the line source is simulated for one day on each grid (Figure 10c). At the end of the simulation, the temperature field is evaluated on the median plane of the model at distinct observations points in 25 cm, 50 cm and 75 cm distance of the line source (Figure 10a and Figure 10b). The root mean squared value of the temperatures acquired at these locations is used as the respective solution f of each model to calculate the grid convergence index (GCI). With a safety factor of $F = 3$ and under consideration of both the grid refinement ratio r and the order p of the numerical method, Roache (1994) defines the GCI for the fine grid as:

$$\text{GCI}_{\text{fine grid}} = F \left| \frac{f_2 - f_1}{f_1} \right| \frac{1}{r^p - 1} \tag{56}$$

The errors of the Crank-Nicolson time integration scheme and of the linear tetrahedral finite elements employed in BASIMO (Chapters 2.1 & 2.2) have a second order rate of convergence (Zienkiewicz et al. 2013). If the grid spacing is halved, theoretically, the error of the result will be decreased by a factor of four. Therefore, the GCI can be calculated with $p = 2$. In the verification simulations of BASIMO, this results in a GCI value of 0.007 % for the fine grid solution.

The GCI is based on a generalized form of the Richardson Extrapolation (Richardson & Gaunt 1927), which is an estimate of the exact solution of the mathematical model. However, it is not possible to predict whether the estimated solution is above or below the exact solution. Thus, the error derived from the Richardson Extrapolation will match the true error only with 50 % certainty (Oberkampf & Roy 2012). By including the safety factor F, the GCI can be regarded as an error band with 95 % confidence (Roache 1994). This safety factor can be reduced to a less conservative value of $F = 1.25$, if the observed order of accuracy matches the theoretical one (Roache 1998).
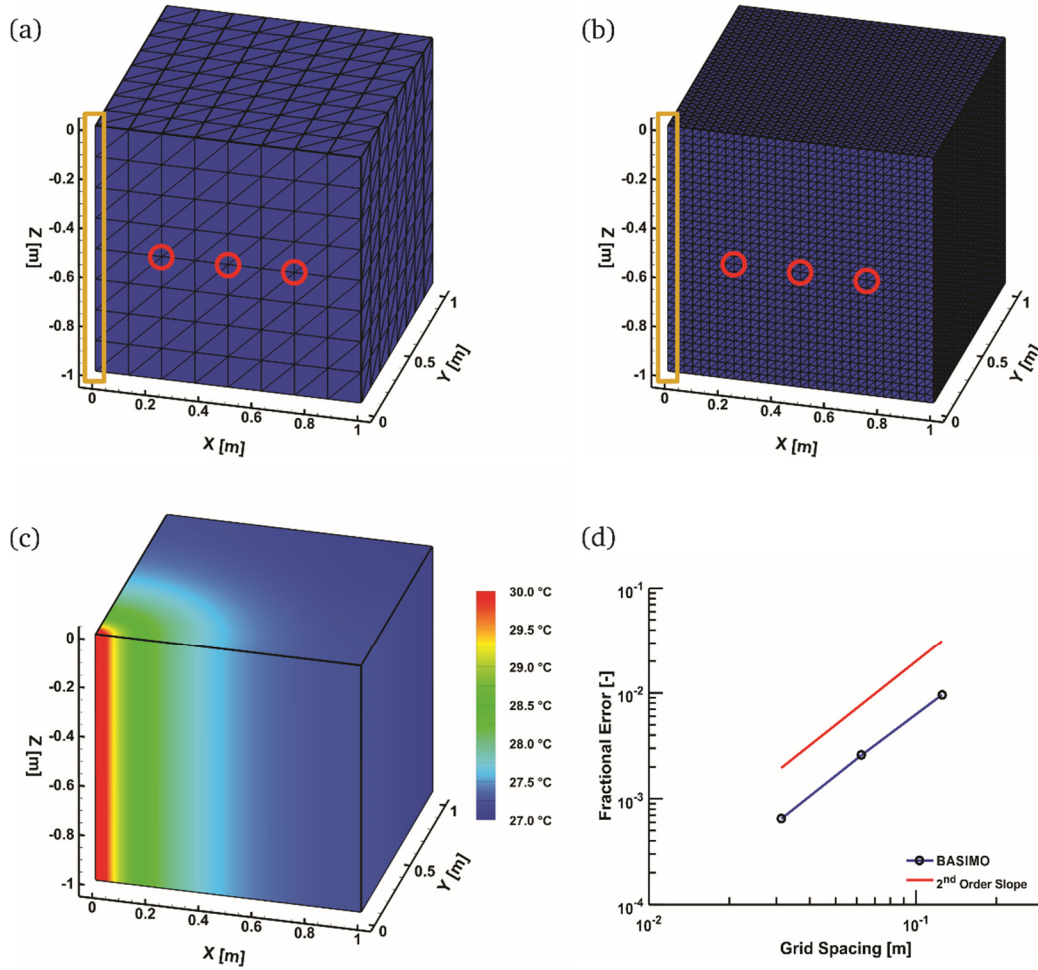
Figure 10: Setup and results of the code verification: (a) fine grid and (b) coarse grid discretization of the model domain (medium grid not shown), red circles mark the observation points where the solution is evaluated, the orange rectangle marks the heat source nodes; (c) resulting temperature distribution and (d) the discretization error plotted in a double logarithmic graph.

The discretization errors of the systematically refined models should fall on a straight line, if plotted against the grid spacing in a double logarithmic graph. The slope of this line describes the observed order of accuracy (Oberkampf & Roy 2012). As mentioned before, the theoretical order of accuracy of the FEM scheme is $p = 2$ due to the rate of error convergence of the time integration method and the finite element type implemented in BASIMO. However, the actual value of the discretization error remains unknown without having an exact solution to compare the numerical results with. For simplicity, an approximated solution is used instead (Oberkampf & Roy 2012). Since the GCI value is already very low, the Richardson Extrapolation can provide

an estimate on the true solution with sufficient accuracy. The resulting line traced by the discretization errors almost perfectly parallels the second order slope (Figure 10d). Consequently, the observed order of accuracy matches the theoretical one. Hence, the factor of safety can be reduced to $F = 1.25$ (Roache 1998), which lowers the GCI for fine grid solution below 0.003 %. Considering the accuracy of subsurface temperature measurements, this represents a very good value for the accuracy of the FEM solution.

4.1.2. Benchmark

A sound validation of a scientific code has to show that it can correctly simulate the physics of the problem it was designed to describe. Therefore, the complete code of BASIMO including the analytical BHE solution has to be tested after the successful verification of the FEM implementation. As available field data are unsuitable for validation, the results of benchmark simulations computed with BASIMO and other well-established scientific code are compared against each other.

The first benchmark model is set up to simulate one year of BTES operation (Appendix C). It comprises a BHE array with six coaxial BHEs in a circular arrangement with a seventh BHE in the center. A thermal insulation of the boreholes is not considered at first. Heat is stored for 182 days with a constant inlet temperature of 80 °C with injection rate of 0.0025 m³ s⁻¹ and is subsequently extracted for 183 days with an inlet temperature of 30 °C. All relevant model parameters are summarized in Table 4.

Table 4: Model parameters and BHE properties for the first benchmark model.

Parameter	Value(s)	Unit
Model size	100 x 100 x 150	m
Constant surface temperature boundary condition	10	°C
Geothermal gradient	0.03	°C m⁻¹
Rock thermal conductivity	2.6	W m⁻¹ K⁻¹
Rock volumetric heat capacity	2.08	MJ m⁻³ K⁻¹
Number of BHEs	7	
BHE length	100	m
BHE radial distance	5	m
Borehole diameter	0.1522	m
Grout thermal conductivity	1.73	W m⁻¹ K⁻¹
Outer pipe, outer diameter	0.127	m
Outer pipe, wall thickness	0.0056	m
Outer pipe, thermal conductivity (steel)	54	W m⁻¹ K⁻¹
Inner pipe, diameter	0.087	m
Inner pipe, wall thickness	0.0055	m
Inner pipe, thermal conductivity (polyethylene)	0.05	W m⁻¹ K⁻¹
Heat carrier fluid dynamic viscosity	0.000504	kg m⁻¹ s⁻¹
Heat carrier fluid volumetric heat capacity	4.05	MJ m⁻³ K⁻¹
Heat carrier fluid thermal conductivity	0.65	W m⁻¹ K⁻¹

Inlet temperature during storage operation	90	°C
Inlet temperature during extraction operation	30	°C
Injection rate	0.0025	m³ s⁻¹

The benchmark model is simulated with BASIMO and with the commercial software FEFLOW (Diersch 2014). Both simulators provide a time series of the BHEs' outlet temperatures. A mere visual assessment (Figure 11) shows that BASIMO's results are in good agreement with FEFLOW. However, as other scientists point out, the analytical solution lacks accuracy in highly transient situations (Diersch et al. 2011b). These situations occur when the BTES system undergoes abrupt temperature changes, i.e. when the operation switches from heat storage to heat extraction. Since this only affects very short time spans compared to the overall operation time, the error is hardly discernable in the visualization (Figure 11). Hence, the error between the two results is subsequently quantified in a second benchmark with the final code of BASIMO, which also considers thermally insulated boreholes (Appendix D). The benchmark model is provided in the digital supplement together with the FEFLOW simulation results.
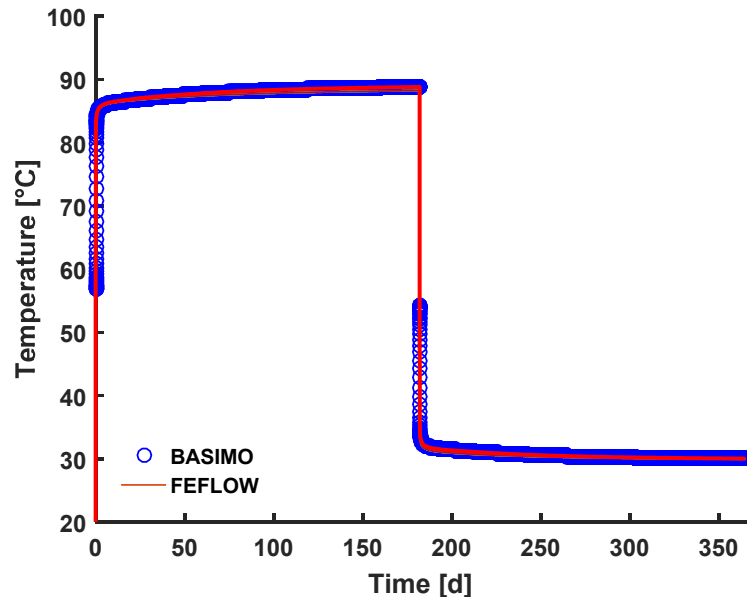
Figure 11: Comparison of BHE outlet temperatures of the central pipe of a BHE array calculated with BASIMO and with FEFLOW (after Schulte et al. 2016a).

After extending the analytical BHE solution to include partially insulated boreholes, BASIMO is tested in a second benchmark case (Appendix D). It is compared against a simulation of a fully discretized detailed numerical 3D model using OpenGeoSys (OGS, Kolditz et al. 2012). Instead of considering a small BHE array, the second benchmark case only includes one partially insulated coaxial BHE of 100 m length. The thermal insulation is realized by an enlarged borehole diameter filled with a low thermal conductivity grout in the upper 30 m of the borehole. In the simulation, heat is stored for 182 days with an inlet temperature of 90 °C and a flow rate of 2.5 l/s. Subsequently, the heat extraction period lasts 183 days with the same flow rate and an inlet temperature of 5 °C. The change of the flow direction from the centered inlet for heat storage to the inlet through the annular gap for heat extraction is considered. A detailed description of the model setup can be found in Appendix D.

In the benchmark, the temporal evolutions of the outlet temperatures is compared against each other. As the simulators use independent time-stepping schemes, results are saved after one day and after 10 days of storage and extraction operation, respectively, to ensure at least two comparison points per period. The results show that the improved analytical solution lacks the accuracy to match the fully discretized model for the early time steps during transient input situations (Figure 12a and Figure 12c), but achieves a very good fit after a few hours of simulation time (Figure 12b and Figure 12d). After ten days of operation, the temperature difference is less than 0.14 °C. At the end of the storage and extraction periods, the BHE outlet temperature differs less than 0.02 °C between the BASIMO and the OGS model.
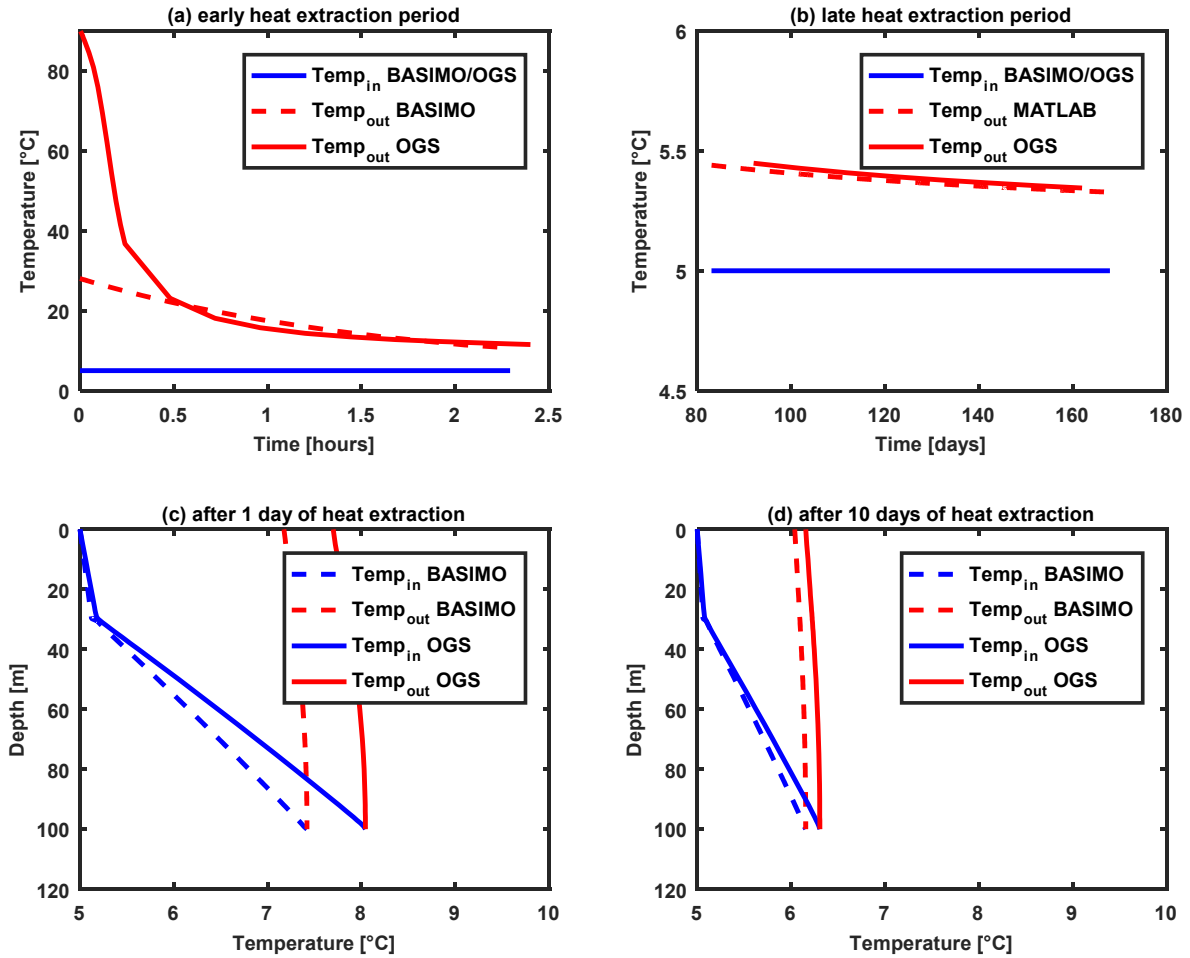
Figure 12: Comparison of the BHE model responses. Top: (a) short-term and (b) long-term evolution of the BHE outlet temperature. Bottom: BHE temperature profiles after (c) one day and after (d) ten days of heat extraction (after Schulte et al. 2016b).

It is not possible to quantify the difference in the outlet temperature for the entire time domain without interpolation of the results due to the different time-stepping schemes. Hence, the heat balance Q, which represents the heat exchanged with the subsurface and requires the integration for the storage and the extraction period, is evaluated:

$$Q = \int \left(T_{in} - T_{out} \right) \cdot f \cdot \rho_f \cdot c_f \cdot t \, dt \qquad (57)$$

with T_{in}: inlet temperature, T_{out}: outlet temperature, f: flow rate of the heat carrier fluid, ρ_f: density of the heat carrier fluid, c_f: specific heat capacity of the carrier fluid and t: time. The results of the benchmark and the relative difference of the models are summarized in Table 5.

The amount of transferred heat differs by 1.6 % and 5 % during storage and extraction, respectively. Considering only the first ten days of the storage and extraction periods, increased errors of 6.8 % and 13.54 % indicate the strong influence of the analytical solution's inaccuracy during the first time steps, whereas the remaining storage and extraction periods yield smaller deviations (Table 5). The benchmark model is provided in the digital supplement of the thesis together with the OGS simulation results.

Table 5: Results of the second benchmark simulation (after Schulte et al. 2016b).

Period	Q_{BASIMO} [MWh]	Q_{OGS} [MWh]	Deviation: $(Q_{OGS}-Q_{BASIMO})/Q_{OGS}$
Storage$_{total}$	106.57	108.29	1.6 %
Storage$_{0-10 days}$	8.34	8.95	6.8 %
Storage$_{10-182 days}$	98.24	99.34	1.1 %
Extraction$_{total}$	-23.55	-24.77	5.0 %
Extraction$_{182-192 days}$	-3.84	-4.45	13.54 %
Extraction$_{192-365 days}$	-19.70	-20.33	3.1 %

4.2. Application Examples

Three application examples are given to illustrate the capabilities of BASIMO. The first example illustrates the simulation of an insulated BHE, while the other two cases demonstrate univariate optimization directly calling BASIMO and multivariate proxy-based optimization. In the two optimization examples, different algorithms are applied using BASIMO as the objective function or as a constraint function (Table 6).

Table 6: Differences of optimization examples computed with BASIMO.

	Optimization (direct call of BASIMO)	Proxy-based Optimization
use of BASIMO	objective function	constraint function
algorithm	single-variable minimization with bounds	genetic algorithm
variables	1 (univariate)	2 (multivariate)
bounds	yes	yes
constraints	no	yes

4.2.1. Assessing the Effect of Partial Borehole Insulation

As mentioned in Chapter 1, the thermal insulation of the upper part of the borehole is a characteristic feature of medium deep BTES systems: An enlarged borehole diameter filled with a low thermal conductivity backfill material increases the thermal resistance between the pipes and the borehole wall. This prevents advective heat losses caused by groundwater flow and protects the groundwater in the upper aquifer from excessive heating. However, the thermal insulation of a borehole section has not been put into practice so far. Therefore, there is no data on the effect that a partial insulation would take.

The effect can be assessed by revisiting the second benchmark simulation, which considered a 100 m BHE with a thermal insulation in the upper 30 m of the borehole. A cross section of the model (Figure 13) illustrates the subsurface temperature distribution after 182 days of heat storage and subsequent 183 days of heat extraction (model details can be found in Appendix D):

A heat plume measuring approximately 20 m in diameter has developed around the bottom section of the BHE, due to the fact that only a part of the stored heat could be retrieved. However, in close proximity to the BHE, the subsurface has been cooled even below the undisturbed temperature conditions during heat extraction. In contrast to that, the insulation of the BHE has effectively inhibited any major thermal influence on the upper part of the model. As a result, the subsurface temperature distribution remains undisturbed in this zone, preventing a potentially negative impact on the upper aquifer.
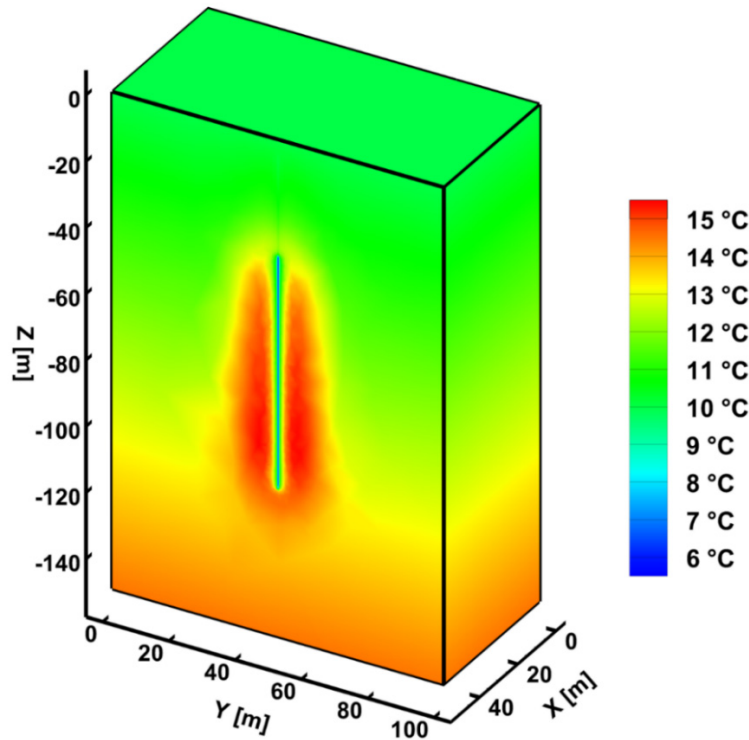
Figure 13: Subsurface temperature distribution of a single BHE with partial borehole insulation (upper 30 m) after one heat storage and extraction cycle.

4.2.2. Finding the Ideal Length for an Insulated Section of a Medium Deep BHE

In a synthetic example, a single medium deep double U-pipe BHE is to be fitted with a borehole insulation in the upper section (Appendix D). For double U-pipe BHEs, the full length of the downstream and upstream pipes acts as a heat exchange surface with the surrounding rock and the grout material. Thus, double U-pipe BHEs suffer growing heat losses in the upstream pipes with increasing borehole length: the heat extracted at the bottom of the BHE is lost to the cooler shallow subsurface and the cooler downstream pipes (Figure 14a). An insulation of the upper section of the borehole can decrease these losses (Figure 14b). As a result, the outlet temperature of the BHE is higher, which can increase the efficiency of a heat pump coupled to the system. Evidently, an entirely insulated borehole will perform worse than a BHE without any insulation. Hence, an ideal length of borehole insulation must exist.

BASIMO is used to simulate 30 days of constant heat extraction and serves directly as the objective function of a basic algorithm contained in the MATLAB Optimization Toolbox (The MathWorks 2015b) for finding the minimum of a single-variable function on a fixed interval by combining a gold-section search with parabolic interpolation (Brent 1973; Forsythe et al. 1977). The input variable x for the objective function is the length of the insulated section,

which is bounded by the depth of the borehole L. At each function call, BASIMO simulates the 30-day operation of the BHE with the respective insulation length and returns the final outlet temperature to the optimization algorithm. Therefore, the optimization problem reads as

$$\max_{x \in R} \quad BASIMO(x)$$

subject to (58)

$$0 \le x \le L$$

For the specific scenario of a 400 m deep BHE and a constant heat extraction rate of 20 kW, the algorithm converges on an insulation length of $\sim$142 m as an optimal solution after 15 iterations (Figure 15a). The insulation increases the outlet temperature by approximately 1.7 °C compared to a BHE without insulation (Figure 15b). Considering an ideal Carnot heat pump, which raises the temperature to a target level of 35 °C, this equates to an increase of the theoretical maximum coefficient of performance of about 5 %. A more detailed description of the application example including all relevant model and BHE parameters, as well as boundary conditions, can be found in Appendix D. A copy of the optimization setup is provided in the digital supplement of the thesis.
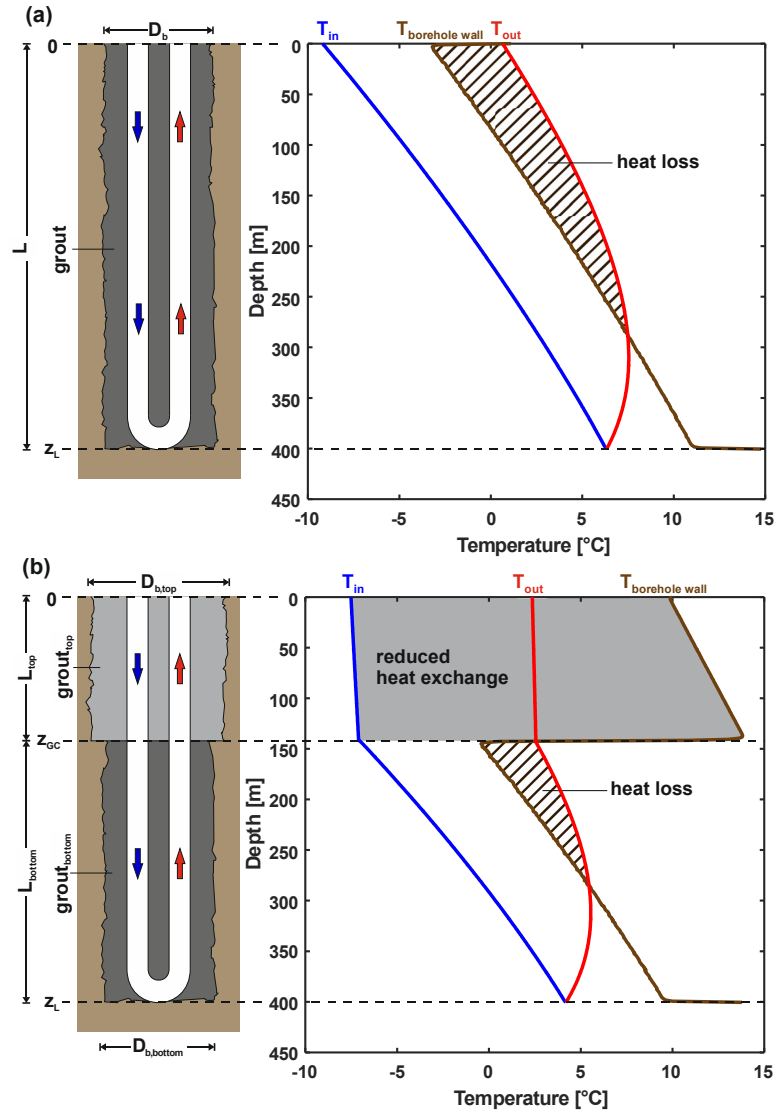

Figure 14: Temperature profiles of (a) a medium deep double U-pipe BHE without insulation and (b) an insulated double U-pipe BHE assuming equal heat extraction rates and equal boundary conditions (Schulte et al. 2016b).
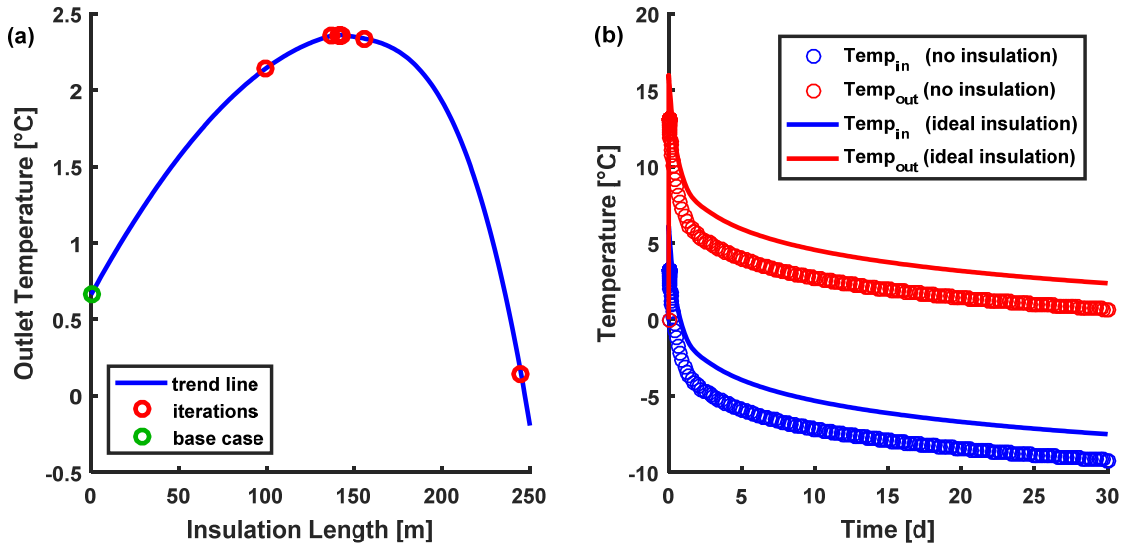
Figure 15: Optimization results: (a) outlet temperature after 30 days of operation for each iteration, (b) inlet and outlet temperature evolution of the base case (i.e. no insulation) and the ideally insulated BHE (Schulte et al. 2016b).

4.2.3. Minimizing the Required Borefield Size

The thermal interaction of the BHEs is sensitive to many design parameters, and the non-linear increase of BTES system performance over the first couple of years prohibits the estimation of the required array size by a rule of thumb. Therefore, simulations, which take into account the strong dependency on the specific heat load profile, are imperative. In the second application example (Appendix C), BASIMO is used to determine the minimum required size of a BHE array, which has to cover a specific heat demand based on a basic biannual operation scenario with constant inlet temperatures and flow rates during the heat storage and extraction periods.

As the radial distance is fixed, the size of the array is defined by the number and depth of the boreholes. Hence, the objective function is simply the product of the number of BHEs and the BHE length. This equates to the total drilled length, which is to be minimized to reduce the costs. As the drilling costs can increase disproportionately with depth (Tester et al. 2005), in this example, the BHE length is additionally penalized against the number of BHEs. Therefore, the objective function reads as

$$f(x) = x_1 \cdot x_2 \cdot e^{a \cdot x_2} \tag{59}$$

where x_1 is the number of BHEs, x_2 is the borehole length and a is a scaling factor for the penalty on x_2. The objective function $f(x)$ does not contain BASIMO, but is a mere algebraic function, which can be evaluated very quickly.

The performance of BTES systems improves markedly over the first few cycles. Later, this trend levels off. Preliminary simulations indicate that medium deep BTES systems attain 80 % of their final efficiency after 3 to 6 years (Appendix B). A system, which already meets the heat demand after the first year, would turn out to be distinctly oversized after prolonged operation. Therefore, the BTES system has to cover the heat demand only after seven years. The heat to be supplied represents a constraint to the optimization algorithm: the BTES system cannot be indefinitely small, as this would lead to a vanishingly low performance. Used as a constraint function g, BASIMO has to determine the heat supply after seven years for each BTES system

that the optimization algorithm evaluates by choosing a combination of the variable $x = (x_1, x_2)$. Only combinations of (x_1, x_2), which represent a BTES system large enough to meet the predefined heat demand Q, are allowed as a solution. Therefore, the optimization problem reads as

$$\min_{x_1 \in Z,\, x_2 \in R} \quad f(x) = x_1 \cdot x_2 \cdot e^{a \cdot x_2}$$

subject to
$$g(x) := BASIMO\,(x_1, x_2) \geq Q$$

(60)

Determining the BTES system performance for seven years results in large numerical efforts. Assuming that the optimization will need a large number of iterations to converge on a solution, and taking into account that the constraint function has to be evaluated for each iteration, the total computation time is expected to be unacceptably long. Therefore, BASIMO has to be replaced as a constraint function by a proxy model generated with the aPC method. As described in Chapter 3.2, the proxy model is based on a set of training simulations. The design of the numerical experiments has to ensure that each input variable's domain of definition is adequately covered by the training simulations (Siebertz et al. 2010) to allow for higher-order approximations.

In the application example, the parameter space encompasses four to ten BHEs of 100 to 500 m length, which also represents the bounds of the optimization problem. The parameter combinations are determined using a full factorial design (Siebertz et al. 2010), which samples the first variable (i.e. number of BHEs) at seven levels and the second variable (i.e. BHE length) at nine levels. Consequently, the training simulations provide 63 combinations of (x_1, x_2) and the corresponding amount of heat delivered in the seventh extraction cycle as a model response. The inputs and outputs of BASIMO are used to create the aPC proxy model. A fourth-order polynomial grants high accuracy without overfitting the training simulations. The resulting proxy model is used as a constraint function g in the optimization algorithm instead of BASIMO.

Two scenarios are considered in the application example. In both cases, the value of the constraint function g has to exceed $Q = 500$ MWh as the minimum heat extraction. This resembles roughly the annual heat demand of a midsized energetically modernized office building. The second scenario includes, in addition, a constraint of 200 m on the minimum BHE depth to take into account a fictional legal requirement. In both cases, the objective of the algorithm is to determine the smallest possible BTES system that still provides enough heat to cover the annual demand. Denoting the proxy model generated from the training simulations as aPC, the optimization problems read as:

scenario 1

$$\min_{x_1 \in Z,\, x_2 \in R} \quad f(x) = x_1 \cdot x_2 \cdot e^{a \cdot x_2}$$

subject to
$$aPC(x_1, x_2) \geq Q$$
$$4 \leq x_1 \leq 10$$
$$100 \leq x_2 \leq 500$$

scenario 2

$$\min_{x_1 \in Z,\, x_2 \in R} \quad f(x) = x_1 \cdot x_2 \cdot e^{a \cdot x_2}$$

subject to
$$aPC(x_1, x_2) \geq Q$$
$$4 \leq x_1 \leq 10$$
$$200 \leq x_2 \leq 500$$

(61)

x_2 is the BHE length, whereas x_1 is the number of BHEs and therefore always an integer value. The aPC proxy model implies a relaxation of the integer condition of x_1. Hence, the resulting

response surface includes real values for x_1, which are not physical representations of the actual model. Nevertheless, the optimization has to treat x_1 as a discrete variable, which limits the choice of algorithms. Genetic algorithms (Goldberg 1989) can solve mixed-integer optimization problems, that is, the variables are real and integer values. Hence, the optimal design for the BTES system is determined with a genetic algorithm, which is included in the MATLAB Global Optimization Toolbox (The MathWorks 2015b).

For both scenarios in the application example, the potential solutions have to be on the intersection of the response surface of the aPC model and the 500 MWh plane (Figure 16). The algorithm tends to choose more, but shorter BHEs due to the objective function's penalty on the borehole length. Therefore, the genetic algorithm converges on the edge of the parameter space for x_1 at 10 BHEs, each 134.5 m deep. However, this configuration violates the constraints of the second scenario. Hence, the smallest possible BHE array, which considers the fictional legal requirement, consists of 7 BHEs, each 220 m deep. In both cases, the genetic algorithm performs several thousand evaluations of the objective and constraint functions, which underlines the importance of using a fast proxy model instead of a comparably slow numerical simulator.

In the second scenario, the verification of the found solution marginally violates the approximation quality criterion. Hence, the proxy model is refined with the additional numerical simulation according to the procedure described in Chapter 3.2. Thereafter, the adjusted solution is successfully verified. A more detailed description of the application example including all relevant BHE parameters and boundary conditions can be found in Appendix C. A copy of the optimization setup is provided in the digital supplement of the thesis.
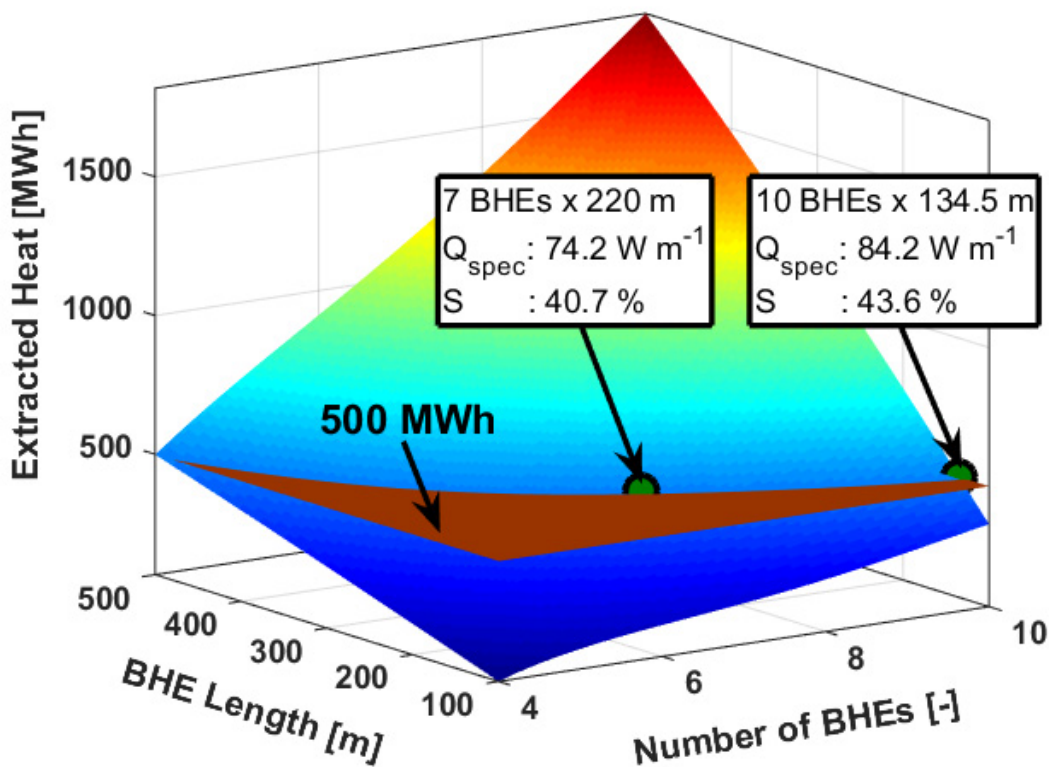

Figure 16: Response surface of the aPC model showing the heat recovered in the 7th extraction cycle depending on the size of the BHE array and the two optimal solutions on the intersection with the 500 MWh plane (Schulte et al. 2016a).

Rigorous testing indicates that BASIMO is suitable for the simulation of medium deep BTES systems. In particular, the FEM implementation proves to calculate the conductive heat transport in the subsurface well. The achieved overall accuracies are comparable to other well-established scientific codes. It is only on short time scales that BASIMO fails to match the results of simulators using fully discretized models like OpenGeoSys. This leaves room for further improvement of the analytical solution for the BHEs. Bauer (2011) and Bauer et al. (2011a) already described how it can be improved to better capture transient behavior of BHEs. Yet, the current code is sufficiently accurate on longer time scales. The seasonal storage and extraction cycles require the simulation of the BTES operation for many years. Therefore, the shortcomings of BASIMO in transient situations on short time scales have only a small effect and the resulting errors can be considered as negligible.

Nevertheless, the first simulations of medium deep BTES systems yield promising and interesting results. Exploiting the heat capacity of the large volume of the rock mass, heat storage can be accomplished in the subsurface at efficiencies above 80 % after a few years of operation (Appendix B). Due to the comparably slow conduction-dominated transport in the subsurface, the heat cannot dissipate before it is retrieved in the subsequent cycle, which compensates for the lack of lateral insulation and reduces the heat losses. In contrast to water tanks, BTES systems can also be employed in confined urban areas without wasting valuable space. Water tanks are equally efficient, but require substantial dimensions to achieve comparable storage capacities. This makes medium deep BTES particularly suitable for on-site storage of large quantities of heat on a seasonal time scale.

Yet, seasonally fluctuating sources like CHP-powered district heating grids and solar thermal installations deliver heat at a high temperature level. The simulation of a one-year storage operation with a single BHE already indicates that high temperature heat storage generates a local, yet considerable heat plume in the subsurface, which represents a significant disturbance of the natural temperature regime. This effect can be expected to be even stronger for BTES systems consisting of large BHE arrays. The developing heat plume is the main reason for the notable increase of storage efficiency in the first few years of operation. However, legal authorities restrict the use of BHEs, which can cause alterations of the groundwater that may have a negative impact on drinking water quality (Verein Deutscher Ingenieure 2001a; Haehnlein et al. 2010; Griebler et al. 2015). Thus, excessive heating of the subsurface has to be regarded critically, if the aquifer used for drinking water extraction is affected. Typically, this problem concerns the shallow aquifers.

Therefore, medium deep BTES systems evade the problem by storing the heat at greater depth. Since the BHEs still penetrate the upper aquifer used for drinking water extraction, the borehole section in question has to be fitted with thermal insulation. The simulation results show that such an insulation can effectively inhibit both heating and cooling of the surrounding rock and prevent a potentially negative impact on the drinking water quality. Instead, the heat exchange is limited to the deeper part of the BHEs. As a beneficial side effect, the reduction of the heat losses in the upper section results in an increased return temperature of the heat carrier fluid. If the length of the insulated section is optimized, this temperature gain can improve the heating system's efficiency significantly (Appendix D).

Consequently, tapping into medium depth allows for operation of the storage system at a higher temperature level without the ecological risk that existing shallow BTES face. As a result of the higher temperature level, the heat pumps require less power or become dispensable altogether. Hence, the benefits of medium deep BTES are twofold: on the one hand, the higher temperature level of medium deep BTES systems increases the efficiency of the downstream heating system. On the other hand, the large capacities and the slow thermal response facilitate the storage of heat from renewable sources or district heating grids in summer on a seasonal scale. Since this is typically excess heat, the consumption efficiency of the primarily produced thermal energy is increased as well. CHPs can produce electricity in summer, raising the total annual operation hours without wasting the heat; whereas solar thermal installations can cover the heat demand not only in summer, but ideally throughout the year. Moreover, BTES profits from the geothermal heat, which also feeds the storage system. Even if the heat extraction exceeds the previous storage due to climatic variations, BTES systems can still provide the required heat, merely by increasing the power consumption.

However, the simulations confirm that the size of medium deep BTES systems is crucial. Only large BHE arrays with a compact layout of the borefield can achieve high storage efficiencies (Appendix B and Appendix C). Hence, medium deep BTES is not suitable for small-scale applications. The technology's full potential is only exploited if the heat supply and demand amount to several GWh of thermal energy. Consequently, the heat demand of only 500 MWh, which was assumed in the second application scenario, resulted in relatively low storage efficiencies. The same goes for the different scenarios which were envisaged in Appendix A, where a single medium-sized office building is to be fit with a medium deep BTES system. Such a case can only serve as a pilot plant to prove the concept in the field. In real-life applications, medium deep BTES systems should be connected to a heating grid with multiple heat consumers rather than supplying only a single building with heat.

Considering the higher investment costs for sufficiently large medium deep BHE arrays and the associated financial risk, this emphasizes the importance of reliable tools for performance prediction and determination of the best system design. As outlined before, mathematical optimization has to evaluate the system model multiple times, changing the relevant model variables at each iteration. This implies that simulation-based optimization requires models that can be altered automatically and quickly, while still allowing for high detail like including BHE material properties and operational parameters.

The in-house development of a simulator was motivated by the lack of such a tool suitable for the assessment of medium deep BHE arrays in BTES applications. To this end, BASIMO fulfills the main requirements: key features like partially insulated or inclined boreholes as well as all relevant thermo-physical parameters can be considered in detail. In contrast to fully discretized models, BASIMO is capable of simulating entire BHE arrays by adopting a dual-continuum approach and thereby reducing the computational cost. At the same time, BASIMO still maintains sufficient accuracy and exhibits a high level of agreement with other simulators like FEFLOW or OpenGeoSys (Appendix C and Appendix D), which can potentially perform the same simulations. Yet, the model setup is cumbersome and can only be automated to a limited degree, which renders these tools useless for applications in mathematical optimization. BASIMO, however, is specifically tailored to serve as a constraint or objective function.

As the development of BASIMO accompanied a research project on the "simulation and evaluation of coupling and storage concepts for renewable forms of energy for heat supply"

(Preface), it became evident that the BHE array and the facilities on the surface represent an interacting entity. Simulations of BTES systems, which only take into account the storage itself and neglect the dynamic interdependency with the variable heat demand and supply, can only provide an estimate on the overall system performance. Feedback mechanisms between the storage and other components can have significant impact on the state variable (i.e. temperature) at various points in the system. Consequently, comprehensive models of BTES systems have to consider the heat demand of the building and include its heating facilities. Since BASIMO is already designed to be used as a function with optimization algorithms, it is particularly suitable to be linked to other software tools. Therefore, the development of BASIMO is a good starting point for coupled simulations of BTES systems including the facilities on the surface.

The focus of the simulator's development on capturing high model detail prevented the consideration of uncertainty. A single simulation can only reflect the behavior of one possible realization of a geological model. Nevertheless, the subsurface conditions are usually subject to geological uncertainty, which requires a multitude of different model realizations to be accounted for. One of the important geological parameters is groundwater flow, as it can influence the system performance considerably, but it can be neglected in typical BTES applications (Appendix B). Hence, BASIMO disregards convective heat transport in the subsurface to simplify the numerical calculations. If groundwater flow cannot be ruled out in a specific scenario, heat convection has to be implemented in the FEM calculation.

In other words: provided with a set of boundary and initial conditions, simulations with BASIMO return a deterministic solution. Randomness is not involved. However, in reality some model parameters are subject to uncertainty, which can take significant effect on the simulation results and should not be underestimated. For instance, the fractional deviations determined in the second benchmark simulation for the heat storage period (1.6 %) and the heat extraction period (5 %) are smaller than the uncertainties of all thermo-physical parameters of crystalline rocks ($\gtrsim$ 7 %) given in Chapter 1.3 (Table 1). Another important uncertainty for BTES systems is the drill path of the boreholes. While hydraulic DTH hammers significantly improve the control on the borehole verticality, it is still very difficult to ensure the designated drill path accurately: under favorable conditions, bore paths deviate from the vertical axis by up to ~10 % (Riechers 2011; Wittig et al. 2015). This means that parameter uncertainty often outweighs the numerical inaccuracy of BASIMO. With many – possibly interacting – parameters affected by uncertainties combined, it becomes very difficult to assess their impact on the BTES system performance. This indicates the importance of considering geological uncertainty in numerical simulations, which is a research topic in its own right. Even so, uncertainty can be factored in in the aPC proxy model. In petroleum engineering, proxy model-based approaches are applied to consider geological uncertainties in reservoir modeling and operations optimization (Yang et al. 2011). This approach can potentially be applied to the simulation and optimization of medium deep BTES systems under geological uncertainty in the future.

Chapter 6: Outlook

BASIMO allows for unprecedented detail in numerical simulations of BTES systems, which has been matched only by fully discretized models up to now. The presented application scenarios provide only a brief insight to the full potential of the simulator. Many characteristics of the physical domain can be considered, except for groundwater flow. The latter is disadvantageous for BTES and is therefore currently neglected in BASIMO, but future improvements of the code should include the implementation of advective heat transport in the FEM solution. Also, the analytical solution should be extended to consider the transient behavior of BHEs on short time scales. Furthermore, the simulator should allow for serial interconnection of single BHEs, which would be more realistic (Mielke et al. 2014), instead of operating all BHEs in parallel. This would facilitate an increased accuracy and complete BASIMO as a BHE array simulation tool for general purposes, which are not limited to BTES applications.

Calculations with BASIMO are in good agreement with other simulators, but they still lack validation with field data. In addition, the simulations still rely on many assumptions and simplifications. Future research has to focus on the realization of field experiments. Before building a pilot plant, where many parameters are fraught with uncertainty, a sandbox test rig of a single BHE can provide the data basis required for proper validation of the code. To that end, it has to be fitted with multiple temperature sensors in various distances of the BHE pipes. Furthermore, it is important to keep the uncertainty of all material parameters at a minimum. Only if the experiments are performed under controlled conditions can the data be used for the validation of BASIMO and other potential simulation tools.

In most countries, the legal approvability of medium deep BTES systems will depend on the environmental sustainability. This is determined by its ability to protect the shallow aquifers from critical thermal influences. However, so far the concept of partial thermal borehole insulation has only been demonstrated in the presented simulations. As a next step, its effectivity has to be quantified and proven in practice. Furthermore, the technical implementation of partial borehole insulation has yet to be devised. Thus, partial thermal borehole insulation could be included in the test rig to prove its ability in inhibiting heat exchange with the ground.

The potential test rig should be designed similarly to the sandbox experiment of Beier et al. (2011) with a few adaptions to include an insulated section: A coaxial BHE is used instead of a U-pipe BHE. In order to allow for a thermally insulated section, a total length of ~25 m is suggested. The coaxial BHE and the grout are installed in a steel pipe, which represents the borehole. For the insulated section, this pipe has to have an enlarged diameter. In either section, the pipe's contribution to the thermal resistance of the grout should be negligible due to the high thermal conductivity of steel. The assembly is embedded in loose sand to permit easy access and relatively effortless changes to the experiment. This allows for the use of fiber-optic cables as temperature sensors providing continuous measurements along the entire borehole length (Lehr & Sass 2014) not only within the BHE, but also in various distances to the outer steel pipe. The entire setup is encased in a double-walled container. An air conditioning system is connected to the spacing to control the temperature boundary condition of the experiment at all times. Consequently, the inner wall should have a low thermal resistance, whereas the outer wall should be insulated to reduce the influence of room temperature variations. A conceptual sketch of the potential test rig is shown in Figure 17.

Including the borehole insulation into the sandbox experiment allows for tentative testing of different thermally insulating materials. In shallow applications, the development of grout materials focused on increasing the thermal conductivity rather than decreasing it. Expanding foams like polyurethane are already in use for the sealing of wellbores in other applications (Zawislanski & Faybishenko 1999). Because they are watertight and have a thermal conductivity as low as $0.04\ \mathrm{W\,m^{-1}\,K^{-1}}$, expanding foams are potential candidates for an effective thermal borehole insulation. All the same, their low density and their comparably low compressive strength imply challenges for application below the groundwater level (Black 1977). Hence, the technical application of thermally insulating grouts for BHEs has yet to be developed.
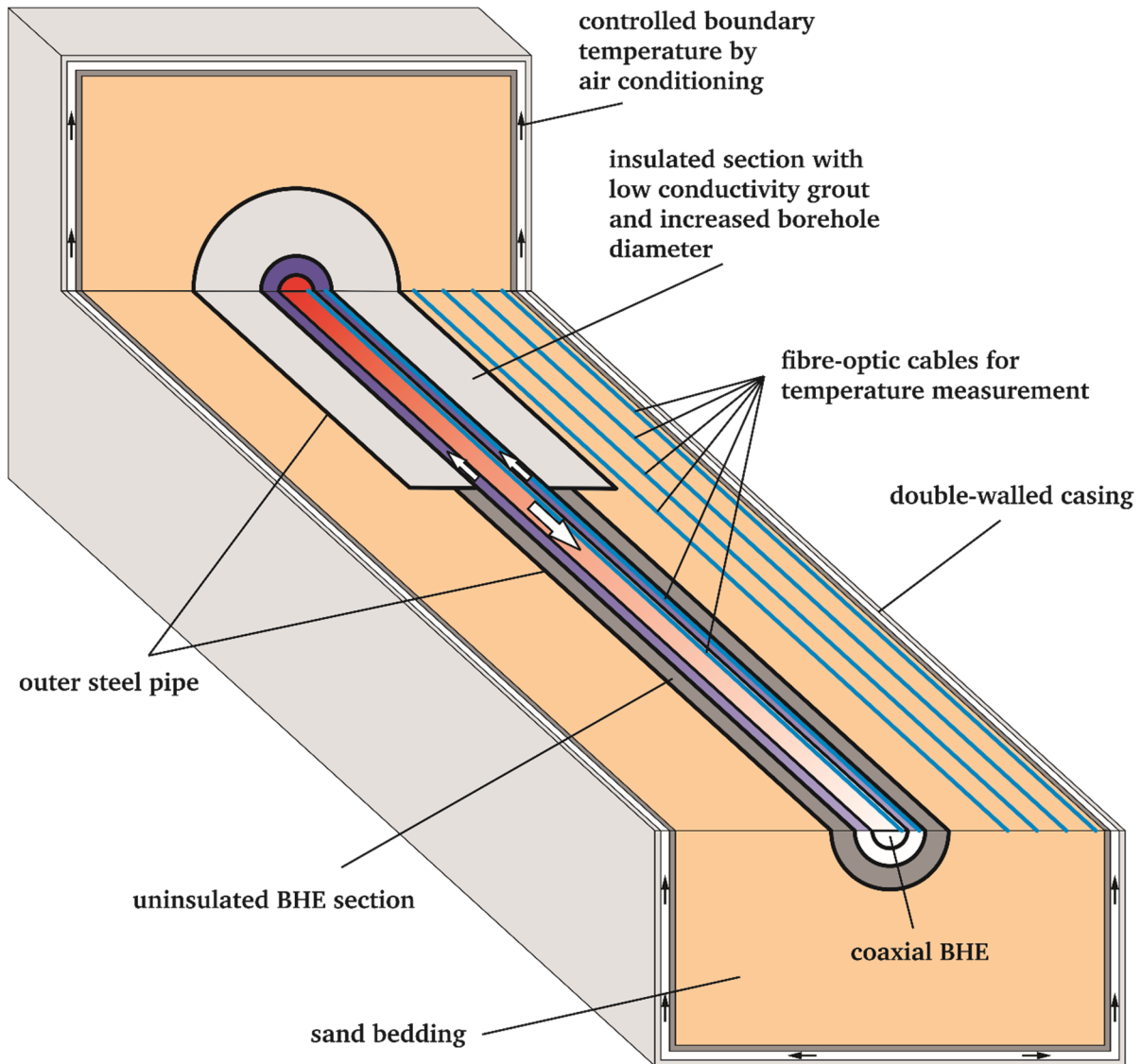
Figure 17: Conceptual sketch: cross section of a potential sandbox experiment (dimensions not to scale); coaxial BHE with centered inlet in heat storage operation, low thermal conductivities in light grey, high thermal conductivities in dark grey.

Technical details aside, medium deep BTES has not been put into practice so far. The concept remains to be demonstrated in a pilot plant. To that end, it is crucial to fit such a pilot plant with an ample number of sensors within the BHE array, but also in all components of the downstream heating system like buffer storages or heat pumps. In the wake of the joint project "Simulation and evaluation of coupling and storage concepts for renewable forms of energy for

heat supply" first numerical investigations were carried out (Formhals 2015). BASIMO was coupled with the commercial software SimulationX (ITI 2015) to model a BTES system for a mid-sized office building including a heat pump, buffer storage and a CHP-powered and solar-assisted local heating grid. Taking into account these components significantly increased the model's complexity. The results indicate that the system is sensitive to the control of the heat and mass flows and to the interconnection scheme of the components. This reflects the interdependency of the involved heat transfer processes and underlines the importance of coupled simulations. Ongoing and future research (Welsch et al. 2016b) will focus on the importance of the comprehensive considerations of medium deep BTES systems, which includes the surface facilities.

Consequently, close monitoring of a pilot plant's entire system is imperative for the calibration of coupled simulations. With experiments on the operation of a pilot BTES plant and with reliable coupled models, future research can focus on the optimization of the whole system. This will ultimately help to push the promising technology of medium deep borehole thermal energy storage to economic viability.

References

AGEB AE (2013): Anwendungsbilanzen für die Endenergiesektoren in Deutschland in den Jahren 2011 und 2012 mit Zeitreihen von 2008 bis 2012, Bundesministerium für Wirtschaft und Technologie

Al-Khoury R, Kölbel T and Schramedei R (2010): Efficient numerical modeling of borehole heat exchangers, Computers & Geosciences, v. 36, no. 10, p. 1301-1315.

Alberty J, Carstensen C and Funken S (1999): Remarks around 50 lines of Matlab: short finite element implementation, Numerical Algorithms, v. 20, no. 2-3, p. 117-137.

Andersson O, Ekkestubbe J and Ekdahl A (2013): UTES (Underground Thermal Energy Storage) - Applications and Market Development in Sweden, Journal of Energy and Power Engineering, v. 7, no. 4, p. 669-678.

Andersson S and Eriksson A (1981): Seasonal Storage in Hard Rock — Multiple Well System, *in* Proceedings Thermal Storage of Solar Energy International TNO-Symposium, Amsterdam, Netherlands, 5–6 November 1980: Dordrecht, Springer, p. 249-258.

ASME (2006): Guide for verification and validation in computational solid mechanics: ASME V&V 10-2006, New York, NY, USA., American Society of Mechanical Engineers, p. 28.

Bandos TV, Montero Á, Fernández E, Santander JLG, Isidro JM, Pérez J and de Córdoba PJF (2009): Finite line-source model for borehole heat exchangers: effect of vertical temperature variations, Geothermics, v. 38, no. 2, p. 263-270.

Bär K (2012): Untersuchung der tiefengeothermischen Potenziale von Hessen, PhD thesis, Fachbereich Material- und Geowissenschaften, Technischen Universität Darmstadt, xxvi + 268 p.

Bär K, Rühaak W, Welsch B, Schulte D, Homuth S and Sass I (2015): Seasonal High Temperature Heat Storage with Medium Deep Borehole Heat Exchangers, Energy Procedia, v. 76, p. 351-360.

Barrett R, Berry M, Chan T, Demmel J, Donato J, Dongarra J, Eijkhout V, Pozo R, Romine C and van der Vorst H (1994): Templates for the Solution of Linear Systems: Building Blocks for Iterative Methods, Philadelphia, USA, Society for Industrial and Applied Mathematics, Miscellaneous Titles in Applied Mathematics v. 43, 142 p.

Bauer D (2011): Zur thermischen Modellierung von Erdwärmesonden und Erdsonden-Wärmespeichern, PhD thesis, Fakultät Energie-, Verfahrens- und Biotechnik, Universität Stuttgart, xiv + 121 p.

Bauer D, Heidemann W and Diersch HJG (2011a): Transient 3D analysis of borehole heat exchanger modeling, Geothermics, v. 40, no. 4, p. 250-260.

Bauer D, Heidemann W, Marx R, Nußbicker-Lux J, Ochs F, Panthalookaran V and Raab S (2008): Solar unterstützte Nahwärme und Langzeit-Wärmespeicher, Forschungsbericht zum BMU-Vorhaben 0329607J (Juni 2005 bis Juli 2008), Institut für Thermodynamik und Wärmetechnik, Universität Stuttgart

Bauer D, Heidemann W, Müller-Steinhagen H and Diersch HJG (2011b): Thermal resistance and capacity models for borehole heat exchangers, International Journal of Energy Research, v. 35, no. 4, p. 312-320.

Bauer D, Marx R, Nußbicker-Lux J, Ochs F, Drück H and Heidemann W (2013): Wissenschaftlich-technische Begleitung des Förderprogramms Solarthermie2000plus zu solar unterstützter Nahwärme und Langzeit-Wärmespeicherung FKZ 0329607P, Institut für Thermodynamik und Wärmetechnik, Universität Stuttgart

Bauer D, Marx R, Nußbicker-Lux J, Ochs F, Heidemann W and Müller-Steinhagen H (2010): German central solar heating plants with seasonal heat storage, Solar Energy, v. 84, no. 4, p. 612-623.

Bayer P, de Paly M and Beck M (2014): Strategic optimization of borehole heat exchanger field for seasonal geothermal heating and cooling, Applied Energy, v. 136, p. 445-453.

Beckmann G and Gilli PV (1984): Thermal Energy Storage: Basics, Design, Applications to Power Generation and Heat Supply, Springer-Verlag Wien, 232 p.

Beier R, Acuna J, Mogensen P and Palm B (2013): Borehole resistance and vertical temperature profiles in coaxial borehole heat exchangers, Applied Energy, v. 102, p. 665 - 675.

Beier RA, Smith MD and Spitler JD (2011): Reference data sets for vertical borehole ground heat exchanger models and thermal response test analysis, Geothermics, v. 40, no. 1, p. 79-85.

Black JH (1977): Polyurethane foam — A useful new borehole grout, Journal of Hydrology, v. 32, no. 1, p. 183-188.

Blum P, Campillo G and Kölbel T (2011): Techno-economic and spatial analysis of vertical ground source heat pump systems in Germany, Energy, v. 36, no. 5, p. 3002-3011.

Bollin E, Huber K and Mangold D (2013): Solare Wärme für große Gebäude und Wohnsiedlungen, Fraunhofer IRB Verlag, 159 p.

Brent RP (1973): Algorithms for Minimization without Derivatives, Mineola, New York, Dover Publications, 206 p.

Bruce DA, Lyon R and Swartling S (2013): The History of Down-The-Hole Drilling and the Use of Water-Powered Hammers, *in* Proceedings Association of State Dam Safety Officials Annual Conference, Providence, Rhode Island, USA, 8-12 September 2013.

Buja HO (2009): Handbuch der Baugrunderkundung: Geräte und Verfahren, Wiesbaden, Vieweg+Teubner Verlag, 586 p.

Bundesministerium für Umwelt Naturschutz und Reaktorsicherheit BMU (2007): Tiefe Geothermie in Deutschland, Berlin, Bundesministerium für Umwelt, Naturschutz und Reaktorsicherheit (BMU), Referat Öffentlichkeitsarbeit.

Burkard ER and Zimmermann U (2012): Einführung in die Mathematische Optimierung, Berlin, Heidelberg, Springer, 328 p.

Bussmann G, Bracke R, Eicker T, Wittig V, Tuente H, Gueldenhaupt J, Groening L, Kiel F, Maeggi K and Montag B (2015): Geostar - a Scalable Borehole Heat Exchanger Plant for Growing District Heating Systems and Constricted Large Urban Infrastructures, *in* Proceedings World Geothermal Congress, Melbourne, Australia, 19-25 April 2015.

Cansino JM, Pablo-Romero MdP, Román R and Yñiguez R (2010): Tax incentives to promote green electricity: An overview of EU-27 countries, Energy Policy, v. 38, no. 10, p. 6000-6008.

Cansino JM, Pablo-Romero MdP, Román R and Yñiguez R (2011): Promoting renewable energy sources for heating and cooling in EU-27 countries, Energy Policy, v. 39, no. 6, p. 3803-3812.

Carlslaw HS and Jaeger JC (1986): Conduction of Heat in Solids, Oxford, Clarendon Press, 510 p.

Chen J-S, Wang L, Hu H-Y and Chi S-W (2009): Subdomain radial basis collocation method for heterogeneous media, International Journal for Numerical Methods in Engineering, v. 80, no. 2, p. 163-190.

Claesson J and Eskilson P (1988): Conductive heat extraction to a deep borehole: Thermal analyses and dimensioning rules, Energy, v. 13, no. 6, p. 509-527.

Cui P, Yang H and Fang Z (2006): Heat transfer analysis of ground heat exchangers with inclined boreholes, Applied Thermal Engineering, v. 26, no. 11–12, p. 1169-1175.

De Carli M, Tonon M, Zarrella A and Zecchin R (2010): A computational capacity resistance model (CaRM) for vertical ground-coupled heat exchangers, Renewable Energy, v. 35, no. 7, p. 1537-1550.

de Paly M, Hecht-Méndez J, Beck M, Blum P, Zell A and Bayer P (2012): Optimization of energy extraction for closed shallow geothermal systems using linear programming, Geothermics, v. 43, p. 57-65.

De Ridder F, Diehl M, Mulder G, Desmedt J and Van Bael J (2011): An optimal control algorithm for borehole thermal energy storage systems, Energy and Buildings, v. 43, no. 10, p. 2918-2925.

Diersch HJG (2014): FEFLOW Finite Element Modeling of Flow, Mass and Heat Transport on Porous and Fractured Media, Berlin, Heidelberg, Springer-Verlag, 384 p.

Diersch HJG, Bauer D, Heidemann W, Rühaak W and Schätzl P (2011a): Finite element modeling of borehole heat exchanger systems: Part 1. Fundamentals, Computers & Geosciences, v. 37, no. 8, p. 1122-1135.

Diersch HJG, Bauer D, Heidemann W, Rühaak W and Schätzl P (2011b): Finite element modeling of borehole heat exchanger systems: Part 2. Numerical simulation, Computers & Geosciences, v. 37, no. 8, p. 1136-1147.

Dinçer I and Rosen MA (2007): A Unique Borehole Thermal Storage System at University of Ontario Institute of Technology, in Paksoy, H. Ö., ed., Thermal Energy Storage for Sustainable Energy Consumption: Fundamentals, Case Studies and Design, Dordrecht, Springer Netherlands, p. 221-228.

Dinçer İ and Rosen MA (2010): Thermal Energy Storage, John Wiley & Sons, Ltd, 620 p.

Dück W (1977): Diskrete Optimierung, Wiesbaden, Vieweg+Teubner Verlag, 139 p.

Eskilson P (1987): Thermal analysis of heat extraction boreholes, PhD thesis, Institute of Technology, Department of Mathematical Physics, Lund University, Sweden, 6 p.

Eskilson P and Claesson J (1988): Simulation model for thermally interacting heat extraction boreholes, Numerical Heat Transfer, v. 13, no. 2, p. 149 - 165.

Fletcher R (2000): Practical Methods of Optimization, John Wiley & Sons, Ltd, 450 p.

Foralith AG (1998): Innovative Bohrtechniken; ein Weg zur Erhöhung der Wirtschaftlichkeit geothermischer Bohrungen, Studie im Auftrag des Bundesamtes für Energiewirtschaft

Formhals J (2015): Gekoppelte Simulation von Erdsonden-Wärmespeichern und solar unterstützten Nahwärmenetzen, unpublished MSc thesis, Geothermal Science and Technology, Technische Universität Darmstadt, x+72 p.

Forsythe GE, Malcolm MA and Moler CB (1977): Computer Methods for Mathematical Computations, Prentice Hall Professional Technical Reference, 259 p.

Gadd H and Werner S (2014): Achieving low return temperatures from district heating substations, Applied Energy, v. 136, p. 59-67.

Garms H-J (2014): Finanzierung, in Bauer, M., Freeden, W., Jacobi, H., and Neu, T., eds., Handbuch Tiefe Geothermie: Prospektion, Exploration, Realisierung, Nutzung, Berlin, Heidelberg, Springer, p. 527-541.

Givoni B (1977): Underground longterm storage of solar energy—An overview, Solar Energy, v. 19, no. 6, p. 617-623.

Goldberg DE (1989): Genetic Algorithms in Search, Optimization and Machine Learning, Addison-Wesley Longman Publishing Co., Inc., 372 p.

Gresho P, Lee R, Sani R and Stullich T (1980): On the Time-Dependent FEM Solution of the Incompressible Navier-Stokes Equations in Two and Three Dimensions, in

Taylor, C., and Morgan, K., eds., Recent Advances in Numerical Methods in Fluids, Volume 1, Swansea, Pineridge Press.

Gresho PM, Griffiths DF and Silvester DJ (2008): Adaptive Time-Stepping for Incompressible Flow Part I: Scalar Advection-Diffusion, Society for Industrial and Applied Mathematics Journal on Scientific Computing, v. 30, no. 4, p. 2018-2054.

Griebler C, Kellermann C, Stumpp C, Hegler F, Kuntz D and Walker-Hertkorn S (2015): Auswirkungen thermischer Veränderungen infolge der Nutzung oberflächennaher Geothermie auf die Beschaffenheit des Grundwassers und seiner Lebensgemeinschaften – Empfehlungen für eine umweltverträgliche Nutzung, Texte 54/2015, Umweltbundesamt

Haehnlein S, Bayer P and Blum P (2010): International legal status of the use of shallow geothermal energy, Renewable and Sustainable Energy Reviews, v. 14, no. 9, p. 2611-2625.

Haynes WM, Lide DR and Bruno TJ (2016): CRC handbook of chemistry and physics : a ready-reference book of chemical and physical data, Boca Raton, CRC Press, Taylor & Francis Group, 2652 p.

Hellström G (1991): Ground Heat Storage. Thermal Analyses of Duct Storage Systems. Theory., PhD thesis, University of Lund, Department of mathematical physics, Lund, Sweden., 262 p.

Hellström G and Sanner B (1994): Software for dimensioning of deep boreholes for heat extraction, *in* Proceedings Calorstock '94, Espoo, Finnland, 22-25 August 1994, p. 195-202.

Hesaraki A, Holmberg S and Haghighat F (2015): Seasonal thermal energy storage with heat pumps and low temperatures in building projects—A comparative review, Renewable and Sustainable Energy Reviews, v. 43, p. 1199-1213.

Homuth S, Hornich W, Krenn H, Sass I and Spahn T (2016): DTH fluid drill hammer method for medium deep geothermal energy drilling, OIL GAS European Magazine, v. 132, no. 3, p. 39-41.

Hornich W (2014): Hydraulische Imlochhammerbohrungen - eine technische Perspektive für Geothermievorhaben., *at* 9. Tiefengeothermie-Forum, Darmstadt, Germany, 30 September 2014.

Hughes TJR (1977): Unconditionally stable algorithms for nonlinear heat conduction, Computer Methods in Applied Mechanics and Engineering, v. 10, no. 2, p. 135-139.

Ingersoll RL, Adler FT, Plass HJ and Ingersoll AC (1950): Theory of earth heat exchangers for the heat pump, ASHVE Transactions, v. 56, p. 167-188.

Ingersoll RL and Plass HJ (1948): Theory of the ground pipe source for the heat pump, ASHVE Transactions, v. 54, p. 339-348.

ITI (2015): SimuationX (Software), Dresden, Germany, ITI GmbH.

Kallrath J (2013): Gemischt-ganzzahlige Optimierung: Modellierung in der Praxis, Wiesbaden, Springer Fachmedien Wiesbaden, 381 p.

Kalogirou SA (2004): Solar thermal collectors and applications, Progress in Energy and Combustion Science, v. 30, no. 3, p. 231-295.

Kelley CT (1999): Iterative methods for optimization, Philadelphia, USA, Society for Industrial and Applied Mathematics, Frontiers in applied mathematics, v. 18, 180 p.

KfW Bankengruppe (2009): KfW Renewable Energies Programme (KfW-Programm Erneuerbare Energien - Premium - Tiefengeothermie), 272-282, KfW Bankengruppe, https://www.kfw.de/inlandsfoerderung/Unternehmen/Energie-

Umwelt/F%C3%B6rderprodukte/Erneuerbare-Energien-Tiefengeothermie-(272-282)/, accessed 19.10.2016.

Kim EJ, Roux JJ, Rusaouen G and Kuznik F (2010): Numerical modelling of geothermal vertical heat exchangers for the short time analysis using the state model size reduction technique, Applied Thermal Engineering, v. 30, no. 6-7, p. 706-714.

Kolditz O, Bauer S, Bilke L, Böttcher N, Delfs JO, Fischer T, Görke UJ, Kalbacher T, Kosakowski G, McDermott CI, Park CH, Radu F, Rink K, Shao H, Shao HB, Sun F, Sun YY, Singh AK, Taron J, Walther M, Wang W, Watanabe N, Wu Y, Xie M, Xu W and Zehner B (2012): OpenGeoSys: an open-source initiative for numerical simulation of thermo-hydro-mechanical/chemical (THM/C) processes in porous media, Environmental Earth Sciences, v. 67, no. 2, p. 589-599.

Lamarche L (2011): Analytical g-function for inclined boreholes in ground-source heat pump systems, Geothermics, v. 40, no. 4, p. 241-249.

Lamarche L and Beauchamp B (2007): New solutions for the short-time analysis of geothermal vertical boreholes, International Journal of Heat and Mass Transfer, v. 50, no. 7–8, p. 1408-1419.

Lazzari S, Priarone A and Zanchini E (2010): Long-term performance of BHE (borehole heat exchanger) fields with negligible groundwater movement, Energy, v. 35, no. 35, p. 4966-4974.

Lee CK and Lam HN (2008): Computer simulation of borehole ground heat exchangers for geothermal heat pump systems, Renewable Energy, v. 33, no. 6, p. 1286-1296.

Lehr C and Sass I (2014): Thermo-optical parameter acquisition and characterization of geologic properties: a 400-m deep BHE in a karstic alpine marble aquifer, Environmental Earth Sciences, v. 72, no. 5, p. 1403-1419.

Lindenberger D, Bruckner T, Groscurth HM and Kümmel R (2000): Optimization of solar district heating systems: seasonal storage, heat pumps, and cogeneration, Energy, v. 25, no. 7, p. 591-608.

Lund H, Möller B, Mathiesen BV and Dyrelund A (2010): The role of district heating in future renewable energy systems, Energy, v. 35, no. 3, p. 1381-1390.

Lund PD and Östman MB (1985): A numerical model for seasonal storage of solar heat in the ground by vertical pipes, Solar Energy, v. 34, no. 4, p. 351-366.

Lundh M and Dalenbäck JO (2008): Swedish solar heated residential area with seasonal storage in rock: Initial evaluation, Renewable Energy, v. 33, no. 4, p. 703-711.

Man Y, Yang H, Diao N, Liu J and Fang Z (2010): A new model and analytical solutions for borehole and pile ground heat exchangers, International Journal of Heat and Mass Transfer, v. 53, no. 13-14, p. 2593-2601.

Mangold D (2007): Seasonal Storage - a German success story, Sun & Wind Energy, no. 1, p. 48-58.

Melamed Y, Kiselev A, Gelfgat M, Dreesen D and Blacic J (1999): Hydraulic Hammer Drilling Technology: Developments and Capabilities, Journal of Energy Resources Technology, v. 122, no. 1, p. 1-7.

Mielke P, Bauer D, Homuth S, Götz A and Sass I (2014): Thermal effect of a borehole thermal energy store on the subsurface, Geothermal Energy, v. 2, no. 1, p. 1-15.

Molina-Giraldo N, Blum P, Zhu K, Bayer P and Fang Z (2011): A moving finite line source model to simulate borehole heat exchangers with groundwater advection, International Journal of Thermal Sciences, v. 50, no. 12, p. 2506-2513.

Moritz H (1978): Least-squares collocation, Reviews of Geophysics, v. 16, no. 3, p. 421-430.

Nordell B (1987): The borehole heat store in rock at the Luleå University of Technology constructional and operational experience: The Lulevärme Project 1982-1985

Nordell B (1990): A borehole heat store in rock at the University of Lulea: the Lulevarme project, 1982-1988 / Bo Nordell, Stockholm, Sweden, Swedish Council for Building Research, Document (Statens rad for byggnadsforskning (Sweden)) ; 1990:D12., 56 p.

Nordell B (1994): Borehole Heat Store Design Optimization, PhD thesis, Luleå University of Technology, Sweden., 196 p.

Oberkampf WL and Roy CJ (2012): Verification and validation in scientific computing, Cambridge, Cambridge University Press, 767 p.

Oladyshkin S and Nowak W (2012): Data-driven uncertainty quantification using the arbitrary polynomial chaos expansion, Reliability Engineering & System Safety, v. 106, p. 179-190.

Pinel P, Cruickshank CA, Beausoleil-Morrison I and Wills A (2011): A review of available methods for seasonal storage of solar thermal energy in residential applications, Renewable and Sustainable Energy Reviews, v. 15, no. 7, p. 3341-3359.

Reddy JN and Gartling DK (2010): The Finite Element Method in Heat Transfer and Fluid Dynamics, CRC Press, 524 p.

Reuß M (2008): Tätigkeitsbericht 2008 - ZAE Bayern, Würzburg, Bayerisches Zentrum für Angewandte Energieforschung e.V.

Reuß M (2015): The use of borehole thermal energy storage (BTES) systems, *in* Cabeza, L. F., ed., Advances in Thermal Energy Storage Systems, Woodhead Publishing, p. 117-147.

Richardson LF and Gaunt JA (1927): The Deferred Approach to the Limit. Part I. Single Lattice. Part II. Interpenetrating Lattices, Philosophical Transactions of the Royal Society of London. Series A, Containing Papers of a Mathematical or Physical Character, v. 226, no. 636-646, p. 299-361.

Riechers J (2011): Innovatives hydraulisches Bohrverfahren für die oberflächennahe Geothermie als Alternative zum pneumatischen Bohrstandard., unpublished BSc thesis, Internationales Geothermiezentrum, Hochschule Bochum.

Roache PJ (1994): Perspective: A Method for Uniform Reporting of Grid Refinement Studies, Journal of Fluids Engineering, v. 116, no. 3, p. 405-413.

Roache PJ (1998): Verification and Validation in Computational Science and Engineering, Albuquerque, NM, USA, Hermosa Publishers, 464 p.

Rühaak W, Bense VF and Sass I (2014): 3D hydro-mechanically coupled groundwater flow modelling of Pleistocene glaciation effects, Computers & Geosciences, v. 67, p. 89-99.

Sanner B (2005): Examples of GSHP and UTES Systems in Germany, *in* Proceedings World Geothermal Congress, Antalya, Turkey, 24-29 April 2005.

Sanner B (2012): Shallow Geothermal Drilling, *in* Proceedings International Geothermal Days, Oradea, Romania, 6-7 June 2012.

Sanner B and Stiles L (1997): Status of seasonal cold storage in ground source heat pumps, *in* Proceedings Megastock '97, Sapporro, Japan, 18-21 June 1997.

Sass I, Bracke R and Rühaak W (2015): Urban Heating, *in* Proceedings World Geothermal Congress, Melbourne, Australia, 19-24 April 2015.

Sass I, Brehm D, Coldewey WG, Dietrich J, Klein R, Kellner T, Kirschbaum B, Lehr C, Marek A, Mielke P, Müller L, Panteleit B, Pohl S, Porada J, Schiessl S, Wedewardt M and Wesche D (2016a): Shallow Geothermal Systems - Recommendations on Design, Construction, Operation and Monitoring, Berlin, Ernst & Sohn, 276 p.

Sass I, Heldmann C-D and Lehr C (2016b): Exploitation of a Marble Karst Reservoir for a medium deep Borehole Heat Exchange System in Tux, Tyrol, Grundwasser, v. 21, no. 2, p. 137-145.

Sass I, Welsch B and Schulte DO (2016c): Mitteltiefe Erdwärmesondenspeicher - Lösung für den Nutzungskonflikt Grundwasserschutz versus Geothermienutzung?, *in* Proceedings 7. Bochumer Grundwassertag, Bochum, Germany, 17.03.2016.

Schmidt T, Mangold D and Müller-Steinhagen H (2004): Central solar heating plants with seasonal storage in Germany, Solar Energy, v. 76, no. 1–3, p. 165-174.

Schulte DO, Rühaak W, Oladyshkin S, Welsch B and Sass I (2016a): Optimization of Medium-Deep Borehole Thermal Energy Storage Systems, Energy Technology, v. 4, no. 1, p. 104-113.

Schulte DO, Welsch B, Boockmeyer A, Rühaak W, Bär K, Bauer S and Sass I (2016b): Modeling Insulated Borehole Heat Exchangers, Environmental Earth Sciences, v. 74, no. 10, p. 1-12.

Shao H, Schelenz S, Kist N, Shim BO, Boockmeyer A and Kolditz O (2014): Numerical Modeling of Borehole Heat Exchangers (BHEs) and its interactions with the surrounding soil, *at* 3rd European Geothermal Workshop, Karlsruhe, Germany, 15-16 October 2014.

Si H (2010): Constrained Delaunay tetrahedral mesh generation and refinement, Finite Elements in Analysis and Design, v. 46, no. 1–2, p. 33-46.

Sibbitt B, McClenahan D, Djebbar R, Thornton J, Wong B, Carriere J and Kokko J (2012): The Performance of a High Solar Fraction Seasonal Storage District Heating System – Five Years of Operation, Energy Procedia, v. 30, p. 856-865.

Siebertz K, van Bebber D and Hochkirchen T (2010): Statistische Versuchsplanung - Design of Experiments (DoE), Berlin, Heidelberg, Springer-Verlag.

Sørensen PA (2013): Final Report - Boreholes in Brædstrup, Skørping, Denmark, PlanEnergi, http://www.energinet.dk/SiteCollectionDocuments/Danske%20dokumenter/Forskning%20-%20PSO-projekter/10496%20-%20Slutrapport%20Boreholes%20in%20Br%C3%A6dstrup.pdf, accessed 24/10/2016.

Stockhausen S (2014): Fördermöglichkeiten, *in* Bauer, M., Freeden, W., Jacobi, H., and Neu, T., eds., Handbuch Tiefe Geothermie: Prospektion, Exploration, Realisierung, Nutzung, Berlin, Heidelberg, Springer Berlin Heidelberg, p. 543-558.

Strauss WA (2007): Partial Differential Equations: An Introduction, Wiley, 464 p.

Tecplot (2013): Tecplot 360 2013R1 (Software), Bellevue, Washington, Tecplot, Inc.

Tester JW, Drake EM, Driscoll MJ, Golay MW and Peters WA (2005): Sustainable Energy: Choosing Among Options, MIT Press, 846 p.

The MathWorks (2015a): MATLAB 2015b (Software), Natick, Massachusetts, The MathWorks, Inc.

The MathWorks (2015b): MATLAB 2015b Global Optimization Toolbox (Software), Natick, Massachusetts, The MathWorks, Inc.

Tuomas G (2004): Effective use of water in a system for water driven hammer drilling, Tunnelling and Underground Space Technology, v. 19, no. 1, p. 69-78.

Ulbrich M and Ulbrich S (2012): Nichtlineare Optimierung, Basel, Springer Basel, Mathematik Kompakt, 148 p.

US Department of Defense DoD (1994): DoD Directive No. 5000.59: Modeling and Simulation (M&S) Management, US Department of Defense.

Verein Deutscher Ingenieure (2001a): VDI 4640, Blatt 1: Thermische Nutzung des Untergrundes - Grundlagen, Genehmigungen, Umweltaspekte, Volume 4640/2.

Verein Deutscher Ingenieure (2001b): VDI 4640, Blatt 2: Thermische Nutzung des Untergrundes - Erdgekoppelte Wärmepumpenanlagen, Volume 4640/2.

Verein Deutscher Ingenieure (2001c): VDI 4640, Blatt 3: Thermische Nutzung des Untergrundes - Unterirdische Thermische Energiespeicher, Volume 4640/2.

Wassara (2016): Water Powered Drilling - The water hydraulic DTH technology (technology brochure: www.wassara.com, accessed 09/2016), LKAB Wassara AB.

Welsch B, Rühaak W, Schulte DO, Bär K and Sass I (2016a): Characteristics of Medium Deep Borehole Thermal Energy Storage, International Journal of Energy Research, v. 40, no. 13, p. 1855-1868.

Welsch B, Rühaak W, Schulte DO, Bär K and Sass I (2016b): Coupled Modelling and Optimization of Borehole Thermal Energy Storage and Above Ground Installations, *in* Proceedings 67. Berg- und Hüttenmännischer Tag, TU Bergakademie Freiberg, Germany, 8-10 June 2016.

Wiener N (1938): The Homogeneous Chaos, American Journal of Mathematics, v. 60, no. 4, p. 897-936.

Wittig V, Bracke R and Hyun-Ick Y (2015): Hydraulic DTH Fluid / Mud Hammers with Recirculation Capabilities to Improve ROP and Hole Cleaning For Deep, Hard Rock Geothermal Drilling, *in* Proceedings World Geothermal Congress, Melbourne, Australia, 19-25 April 2015.

Xu J, Wang RZ and Li Y (2014): A review of available technologies for seasonal thermal energy storage, Solar Energy, v. 103, p. 610-638.

Yang C, Card C, Nghiem LX and Fedutenko E (2011): Robust Optimization of SAGD Operations under Geological Uncertainties, *at* SPE Reservoir Simulation Symposium, The Woodlands, Texas, USA, 21-23 February 2011, Society of Petroleum Engineers.

Yang W, Shi M, Liu G and Chen Z (2009): A two-region simulation model of vertical U-tube ground heat exchanger and its experimental verification, Applied Energy, v. 86, no. 10, p. 2005-2012.

Zawislanski PT and Faybishenko B (1999): New Casing and Backfill Design for Neutron Logging Access Boreholes, Ground Water, v. 37, no. 1, p. 33-37.

Zeng HY, Diao NR and Fang ZH (2002): A finite line-source model for boreholes in geothermal heat exchangers, Heat Transfer—Asian Research, v. 31, no. 7, p. 558-567.

Zienkiewicz OC, Taylor RL and Zhu JZ (2013): The Finite Element Method: its Basis and Fundamentals (Seventh Edition), Oxford, Butterworth-Heinemann, 756 p.

Appendix

Appendix A:
Seasonal high temperature storage with medium deep borehole heat exchangers

Published as:

European Geosciences Union General Assembly 2015, EGU

Division Energy, Resources & Environment, ERE

Seasonal high temperature heat storage with medium deep borehole heat exchangers

Kristian Bär[a]*, Wolfram Rühaak[a,b], Bastian Welsch[a,b], Daniel Schulte[a,b], Sebastian Homuth[c], Ingo Sass[a,b]

[a]*Technische Universität Darmstadt, Institute of Applied Geosciences, Department of Geothermal Science and Technology, Schnittspahnstrasse 9, 64287 Darmstadt, Germany*
[b]*Darmstadt Graduate School of Excellence Energy Science and Engineering, Technische Universität Darmstadt, Jovanka-Bontschits-Straße 2, 64287 Darmstadt, Germany*
[c]*Züblin Spezialtiefbau GmbH Ground Engineering, Europa-Allee 50, 60327 Frankfurt a.M., Germany*

Abstract

Heating of buildings requires more than 25 % of the total end energy consumption in Germany. By storing excess heat from solar panels or thermal power stations of more than 110 °C in summer, a medium deep borehole thermal energy storage (MD-BTES) can be operated on temperature levels above 45 °C. Storage depths of 500 m to 1,500 m below surface avoid conflicts with groundwater use. Groundwater flow is decreasing with depth, making conduction the dominant heat transport process. Feasibility and design criteria of a coupled geothermal-solarthermal case study in crystalline bedrock for an office building are presented and discussed.

* Corresponding author. Tel.: +49-6151-16-70953; fax: +49-6151-16-6539.
  E-mail address: baer@geo.tu-darmstadt.de

1. Introduction

More than 50 % of the overall energy demand in Germany is due to heating and cooling purposes [1]. Therefore, groundbreaking techniques are needed to save energy and reduce greenhouse gas emissions especially in this low exergy sector. The combination of different renewable energy sources – solar thermal and geothermal – with already existing district heating systems fed by combined heat and power stations (CHP) is a promising new approach.

In summer, excess solar thermal energy is available, while in winter when thermal energy is needed for heating systems its quantity is usually not sufficient. There are different options to cope with the seasonal offset of thermal energy supply and demand. Besides traditional storage tanks at the surface, thermal storage in shallow aquifers and shallow borehole thermal energy storage (BTES, [2, 3]), geothermal heat storage in moderate depths is an innovative and yet barely tested concept. In difference to shallow heat storage systems, the proposed approach upgrades the naturally available geothermal energy in the subsurface by means of external heat input. This is done in summer when no space heating is required or at times when surplus energy from nearby sources is available. In winter when other sources of energy are not sufficiently and cheaply available, the thermal energy from the geothermal storage is used for heating purposes.

The focus of the presented study is the environmentally friendly and energy efficient redesigning of a more than 50 years old office and laboratory building. A BTES system [4] as well as an energy efficient building design will help to use sustainable energy sources for the next period of the building's lifetime.

2. High Temperature Borehole Thermal Energy Storage

The proposed system of a MD-BTES [5] consists of multiple boreholes with depths of 100 m – 1,000 m. Coaxial borehole heat exchangers (BHE) are implemented in the boreholes. The surrounding rock is utilized as a heat storage, the cementation and borehole wall function as heat exchanger. Typically, water (in some cases with refrigerant or other additives to prevent corrosion) is used as heat carrier fluid.

For the design of a MD-BTES two separate phases have to be considered. These phases are the charging phase and the extraction phase. During the charging phase hot water is injected into the BHE to heat up the reservoir. For heat extraction, cold water is pumped into the BHE in order to retrieve the stored thermal energy from the relatively hot formation. It is important to consider the two possible flow directions in a coaxial BHE. The inlet can be either the central pipe (CXC, Figure 1a) or the annulus (CXA, Figure 1b). Flow direction and inlet temperature influence the heat transfer between working fluid and subsurface. In the charging phase, the working fluid should reach the bottom of the wellbore in the insulated inner pipe before discharging the bulk of its heat into the surrounding rock at maximum depth. In the extraction phase, the cold fluid should be injected into the outer pipe to utilize the borehole wall as heat exchanger surface at full length. Furthermore, this reduces heat losses of the working fluid by circulating it back to the surface through the insulated central pipe after it reached its peak temperature at the bottom of the borehole. Consequently, seasonally alternating flow directions in the BHE are beneficial (Figure 1).

The advantage of BTES systems over open systems is the closed circulation system, which is not allowing a direct contact or mass transfer of heat carrier fluids with the groundwater or subsurface. Geochemical alteration processes and a direct hydrochemical or biological influence on the groundwater will be prevented. Furthermore, this protects auxiliaries like pumps, etc. on the surface against scaling and corrosion. This results in a higher lifetime expectancy of such systems and a more constant and therefore more economical operation.

Deep BHEs can be constructed almost everywhere, due to the fact that neither naturally occurring thermal aquifer systems nor special geological structures are needed. The only requirement for heat storage is a location with negligible groundwater flow at reservoir depth so that the induced thermal plume is not dissipated.

In contrast to conventional shallow BTES systems the mandatory heat pump is not necessarily needed due to the higher operation temperature levels [6]. Consequently, the electric power needed to run the system is reduced and thus the profitability of the system is increased. Additionally, deep BTES have a much smaller surface footprint than shallow BTES with the same capacity and are therefore a viable option in densely urbanized areas.
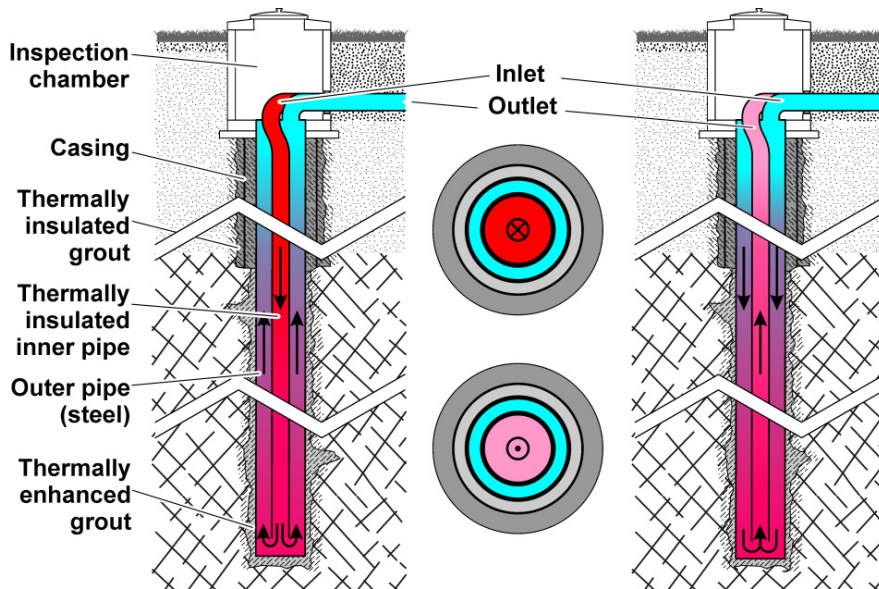
Fig. 1. Schematic horizontal and vertical cross sections of a deep coaxial borehole heat exchanger used as heat storage in summer (charge of the storage as CXC flow, left side and upper middle) and winter (discharge of the storage as CXA flow, right side and lower middle), respectively. Note that only the crystalline bedrock is used as heat storage while the caprock including possible aquifers are thermally insulated.

The completion depth of about 100 m – 1,000 m with higher underground temperatures compared to shallow systems results in a lower lateral temperature gradient between the heat carrier fluid and the surrounding rock. This means a notable decrease of heat losses, which additionally enhances system efficiency.

Charging the BTES with temperatures of up to 110 °C supplied by various heat sources in combination with greater depths can allow for return temperatures of the BTES of 45 °C – 75 °C after an initial charging phase of 3 to 5 years. This is highly depending on the setup of the storage and utilization scenarios [7]. The constant supply of such high heating temperatures allows for applications with conventional radiator-based high-temperature heating systems commonly installed in older buildings. This makes MD-BTES systems even an option for old buildings without low temperature heating systems not meeting the actual energy efficiency levels. Another option is to directly feed in to district heating systems and supply heat for multiple uses possibly even at cascading temperature levels.

For the dimensioning and operation of a BTES, good knowledge of the petrophysical (conductive heat transfer) and the hydraulic (convective heat transfer) properties as well as of the initial subsurface temperature regime is mandatory [8]. Additionally, important design parameters are the heat demand and the required temperature levels of the installed heating systems.

Different kinds of energy flows as well as different storage and utilization scenarios have to be assessed in the simulation and feasibility studies of such systems. Specific user profiles and economic frameworks have to be considered along with local heat sources and sinks.

3. Site Description

The planned drill site (Darmstadt, Germany) for the MD-BTES system is located next to the eastern master fault zone of the Upper Rhine Graben, which divides the urban area of Darmstadt in geological and hydrogeological terms (Figure 2a). A crystalline and Permian-Carboniferous fracture controlled aquifer of the Odenwald and Sprendlinger Horst is located in the eastern part of the city whereas the western part is dominated by a Quaternary porous aquifer of the sedimentary graben fill of the Upper Rhine Graben (Figure 2b).

The northern part of the Upper Rhine Graben fault system is characterized by steep faults in N-S to NNE-SSW direction, which show up to 2,000 m of cumulative vertical displacement. Especially in the inner city area a turn in strike direction to NE – SW results in a complex block mosaic structure [9, 10].

The lithology of the proposed MD-BTES site consists from top to bottom of a 4 - 5 m thick Quaternary soil layer, underlain by some 30 – 60 m thick intercalation of Permo-Carboniferous coarse to fine grained siliciclastic sediments, volcanoclastics and partly altered basaltic to andesitic volcanics [11]. Those unconformably overly the crystalline basement with an up to 30 m thick weathered zone at its top (Figure 2, [12]).
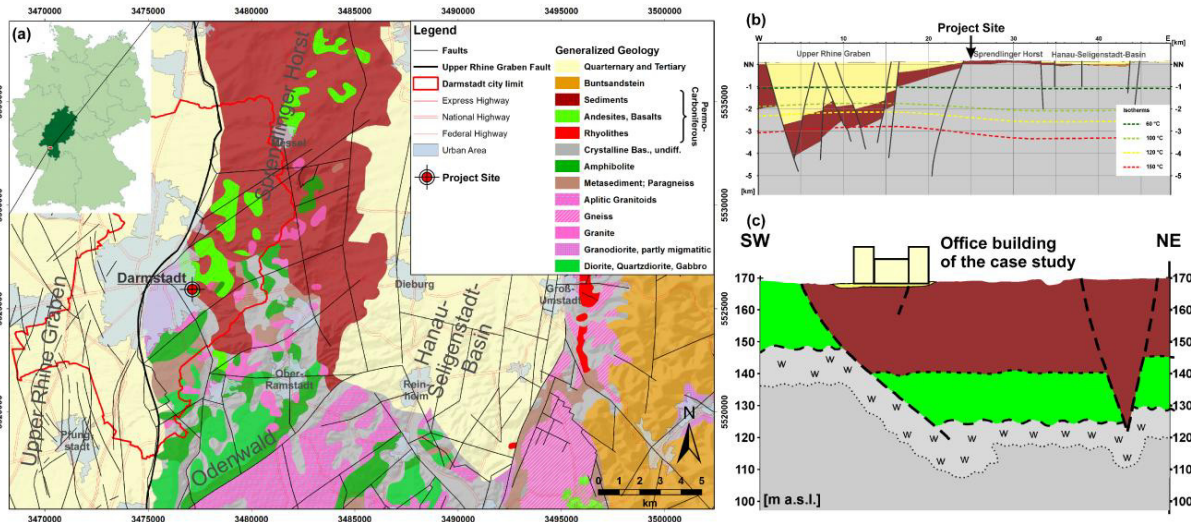

Fig. 2. (a) Simplified geological map of the project site at the eastern Upper Rhine Graben fault, after [13]. (b) Schematic W-E-cross section of the northern Upper Rhine Graben and accompanying graben shoulders including major isotherms [14]. (c) Schematic SW-NE-cross section of the project site, modified from [11], symbol w indicates weathered zone at the top of the crystalline bedrock.

The basement is mainly composed of granodiorite. Additionally, at this northern end of the Odenwald complex amphibolites, diabase, gneiss, granite, diorite, gabbro and hornfels occur [15, 16]. These varying, mostly NE-SW trending, formations are intruded by basic to acidic dyke rocks [17]. The basement is the target of the MD-BTES.

The upper 30 – 40 m of granodiorite are intensely weathered. This is due to its surface exposure during the Permian-Carboniferous, the Upper Cenozoic and the Lower Pleistocene. Near the fracture zone of the Upper Rhine Graben fault systems, weathering is most intensive and results in gravelly layers partially acting as porous aquifers. The hydraulic conductivity of these weathered and fresh rocks are in the range of $10^{-4} – 10^{-5}$ m/s and $10^{-6} – 10^{-7}$ m/s, respectively [12, 17, 18]. Dykes can be either permeable or impermeable [17]. Nonetheless, at depths of more than 100 m the permeability is supposed to be very low making it suitable for a MD-BTES system.

Information about the subsurface temperature result from the 3D geothermal model of Hesse, Germany [19]. Nearby deep drilling sites show that the geothermal gradient ranges between 2.6 and 3.9 °C/100 m.

4. Assessment of Different Heating Scenarios

For this case study two different heat supply scenarios (Figure 3 and 4) were assessed for the office building currently being redesigned in an environmentally friendly and energy efficient way compared to its current system:

1. The use of excess heat from a CHP to charge the MD-BTES system during summer and retrieving all required heat directly from the storage in winter,
2. The combination of scenario 1 with solar thermal collectors on the roof of the building charging the MD-BTES during summer and providing partial direct heat supply during winter. Additional heat demand for charging the MD-BTES is covered by the CHP.

The typical design of a project such as this would not include deep BHEs. Normally a multiple BHE array would be drilled and completed to a depth of not more than 100 – 200 m. At the project site, the boreholes will be placed in a parking lot next to the building. Because of space availability, an array of shallow BHEs large enough to cover the

heat demand is not possible due to the spatial restrictions. Therefore, a layout with a few deeper boreholes and a small surface footprint instead of a multiple borehole array is chosen.
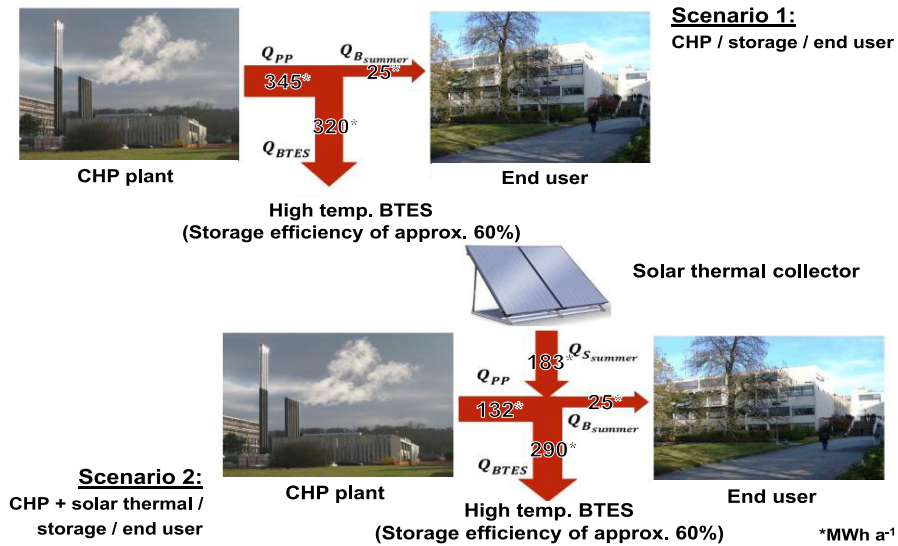
Fig. 3. (top): summer operation mode of scenario 1 with the combined heat and power (CHP) plant covering both the heat demand of the building and the MD-BTES. (bottom): summer operation mode of scenario 2 with the coupling of the CHP and solar thermal collectors to cover the heat demand of the building and the MD-BTES. Numbers are annual heat flows in MWh assuming a storage efficiency of 60%.
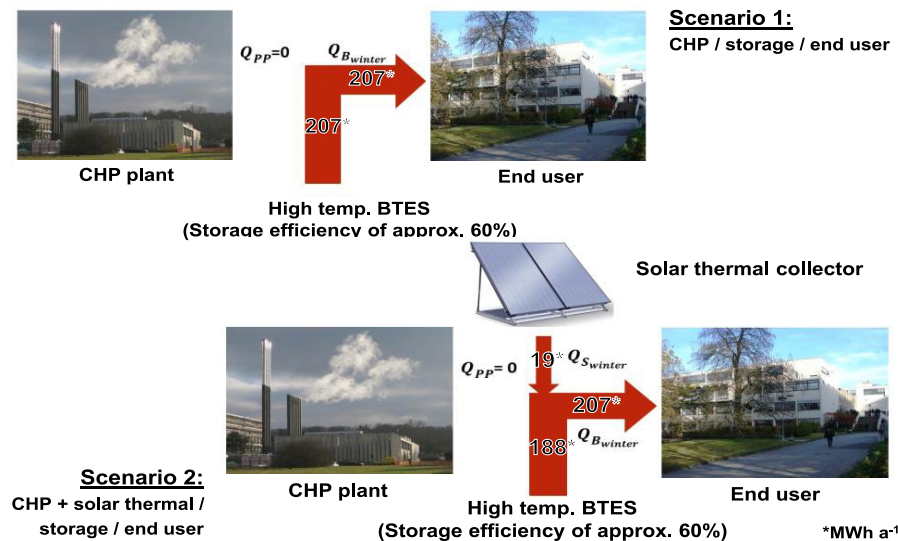
Fig. 4. Winter operation modes for scenarios (1) and (2) respectively with coupling of combined heat and power (CHP) plant, solar thermal collectors and MH-BTES. Numbers are annual heat flows in MWh assuming a storage efficiency of 60%.

In a first step, the building's heat demand and the heat gains of different solar installations were assessed according to national or international standards and requirements. Based on the results, the energy flow demand between the different heat sources and sinks of the three proposed scenarios were evaluated.

4.1. Heat Demand

The building's energy consumption was modelled using a standard software package for precise calculation of energy consumption of every single room inside a building considering the meteorological data of the Test Reference Years (TRY) provided by Germany's National Meteorological Service [20, 21]. All parameters influencing the energy use are defined in the software. The calculations of the required heating load are done according to the standards [22] and [23].

Fig. 5. (left): comparison of the modelled monthly heat demand of the project building before and after the modernization in 2012. (right): amount of solar heat available from the evacuated tube collectors which can be stored in summer and amount of heat needed from the CHP to cover the heat demand of the storage assuming a storage efficiency of 60%.

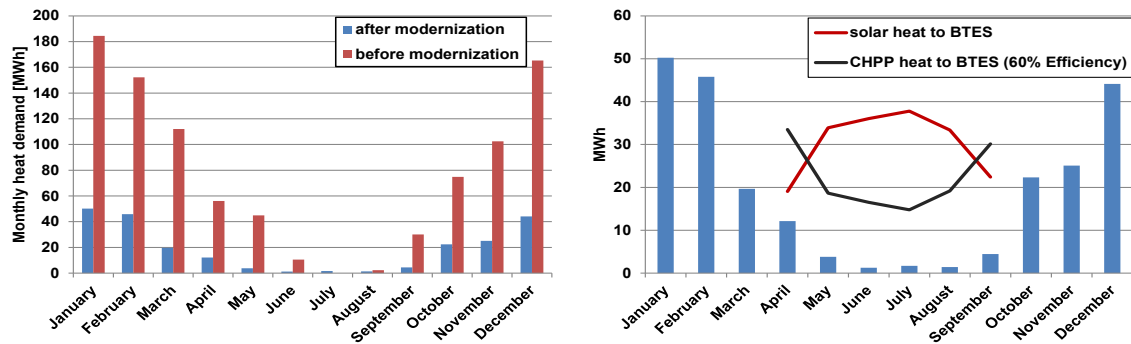Both the heat demand of the building as build in the 1960's and after modernization in 2012 were calculated. Therefore, design construction parameters, the geometry, building service engineering and different space usage were considered. The model of the building was positively validated against measured energy usage in the building with its conditions before modernization. Unfortunately, the modernization is split into two phases. Therefore, a comparison of the actual to the modeled heat demand of the completely modernized building is not yet possible.

The results of the heat demand calculations show a significant reduction after modernization. The modeled value is 232 MWh/a, which represents a reduction of 75 % compared to the measured demand for 2009 of 935 MWh/a (modeled: 916 MWh/a) before the modernization (Figure 5). The calculated characteristic heating energy consumption of the modernized building is 37 kWh/(m²·a) compared to 148 kWh/(m²·a) before modernization, making it one of the most energy efficient buildings for teaching and research purposes of the University.

4.2. Solar Thermal Collectors

For scenario 2 the available roof top area for solar thermal collectors had to be assessed. The building has a flat roof (1,796 m²) easily adaptable for solar installations. The amount of energy produced varies depending on the location, manner of installation and type of the solar collectors. The solar heat gains of the solar thermal system were calculated after [24] for three different types of solar installations: flat plate collectors with an optimized inclination angle of 39º, flat plate collectors with seasonally changing optimized inclination angles of 21º and 57º and evacuated tube collectors situated flat on the roof with tubes tilted 25º. The design arrangement of the solar collectors was based on the limits set by [25] as well as the shading areas of existing construction elements (elevator shafts, ventilation systems) and the solar collectors itself [26].

The biggest amount of solar heat (422 MWh/a) of all considered installations was obtained in the installation with evacuated tube collectors. This is 72 % more than from flat plate collectors with inclination angles of 21º and 57º (114 MWh/a) and 75 % more than from those with an inclination angle of 39º (106 MWh/a). This large contrast between the systems is mainly caused by differences in efficiency of the collectors and in total collector surface area considering the required minimum spacing between collectors. The efficiency used for further calculations of the flat

plate collectors was 25 %, where the efficiency of the evacuated tube collectors was 62 %. The total surface area of evacuated tube collectors was 292 m², 181 m² for the flat plate collectors with 21º/57º inclination angle and 195 m² for those with an inclination angle of 39º (195 m²).

During the winter months, the only time when it's possible to obtain heat from the solar installation is from 12 to 3 pm. This means that the solar installation will be able to provide only a small fraction of a building's heat demand. The solar heat gains for minimum solar insulation (conservative approach) obtained for evacuated tube collectors were used for the calculations.

For the further calculations of the energy flow between the sources and sinks the year was divided into two parts. Charging of the MD-BTES in summer included the months April till September. Extracting heat in winter took place from October till March. The storage efficiency was assumed to be 60 % according to comparable projects [8].

4.3. Results

For scenario 1, the heat demand of the system resulting from the buildings summer heat demand (25 MWh/a) and the energy needed to charge the MD-BTES (345 MWh/a) to meet the buildings winter heating energy demand (207 MWh/a) amounts to 370 MWh/a. This is higher than the annual heat demand supplied by the CHP directly, but still 2.5 times less than what was delivered directly to the building before modernization.

For scenario 2, it was assumed that solar heat is able to meet only about 8 % (17 MWh/a) of the buildings winter heat demand directly because of its short availability and time lag in relation to the buildings heating energy demand. During summer the considered solar thermal installation was able to deliver all of the buildings summer heat demand (25 MWh/a) and supply the MD-BTES with 182 MWh/a of thermal energy. The additional amount of heat from the CHP, which is needed to charge the MD-BTES, was calculated to be 84 MWh/a.

These preliminary results, which do not consider any analytical or numerical analysis of the systems behavior, show that the solar thermal installation is able to deliver 68 % of the required heat of scenario 2. The rest of the heat (84 MWh/a) can be delivered by the CHP and amounts to only 58 % of the heat which was delivered to the building during summer months by the CHP (144 MWh) before its modernization and only 36 % of the total heat demand of the building. The proper design of the solar thermal installation combined with the MD-BTES should therefore be able to significantly reduce or exclude heat provided by the CHP to the project building and will therefore be responsible for a reduction in the CO_2 emissions compared to the current system.

4.4. Drilling Technology

Another important factor for the economic feasibility of MD-BTES systems are the drilling costs. Competitive and cheap drilling technologies are a prerequisite. Because of depth considerations and the geological setting the boreholes for the proposed MD-BTES (100 - 1,000 m b.g.s) shall be drilled with down the hole (DTH) hydraulic hammer drilling technology. Improved cutting transport, increased hole stability and enhanced deviation control (less than 5 to 10 % vertical deviation angle compared to 10 to 40 % with pneumatic hammer [27]) are reasons for the hydraulic hammer. Especially a minimized deviation from the vertical is a crucial prerequisite in BHE fields, where usually less than 10 m spacing between single BHEs is applied. Additionally, CO_2 emission reduction can be achieved since [28] showed that for an equivalent hole of 220 m a pneumatic drilling requires 2.9 l/m of diesel fuel in comparison to 0.7 l/m for the hydraulic hammer drilling process.

5. Design and Numerical Simulation of the System

The BHE completion design has an important influence on the thermal performance of the system. Stainless steel as outer casing material with a thermal conductivity of 54 W/m·K is used to ensure a higher efficiency of heat exchange between the subsurface and the heat carrier fluid in the outer pipe. For the inner pipe pre-insulated steel is recommended to reduce the effective thermal conductivity and thermal bypassing. A 10 mm thick PE foam insulator has a thermal conductivity of 0.026 W/m·K.

The deeper section of the granodiorite is suitable for heat storage whilst the caprock and the weathered zone locally and temporarily may act as an aquifer. Therefore, a thermally and hydraulically insulating backfill material for the shallow wellbore section is required as indicated in Figure 1.

In designing vertical BHEs, the determination of the necessary depth as well as array configuration and amount of boreholes is crucial. Typically, the depth is estimated based on the desired power extraction per unit depth by considering steady state heat transfer. Due to long term and peak power extraction during the operation time, the heat flow will change into transient behavior. In multi BHE systems the degree of geothermal heat enhancement by external heat input depends on various factors such as spacing of boreholes, depth of BHE and amount of heat and frequency of storage phases, etc. These factors affect the level of average output heat during heat extraction depending on the actual heat demand scenario. To find a best fit BHE scenario the consideration of those parameters is necessary but also results in more computation time. Here, best fit scenario means the BHE system with the highest efficiency and highest production capacity possible at minimum total BHE length and economical heat storage conditions.

5.1. Numerical Model

Numerical modeling of the MD-BTES was carried out using FEFLOW [29, 30] to describe the transient behavior of the subsurface and the production characteristics of the system with the set up given in Figure 6. It delivers information about the capacity and sustainability of the BHE system for a given size, depth, flow rate, heat extraction intervals and other factors.
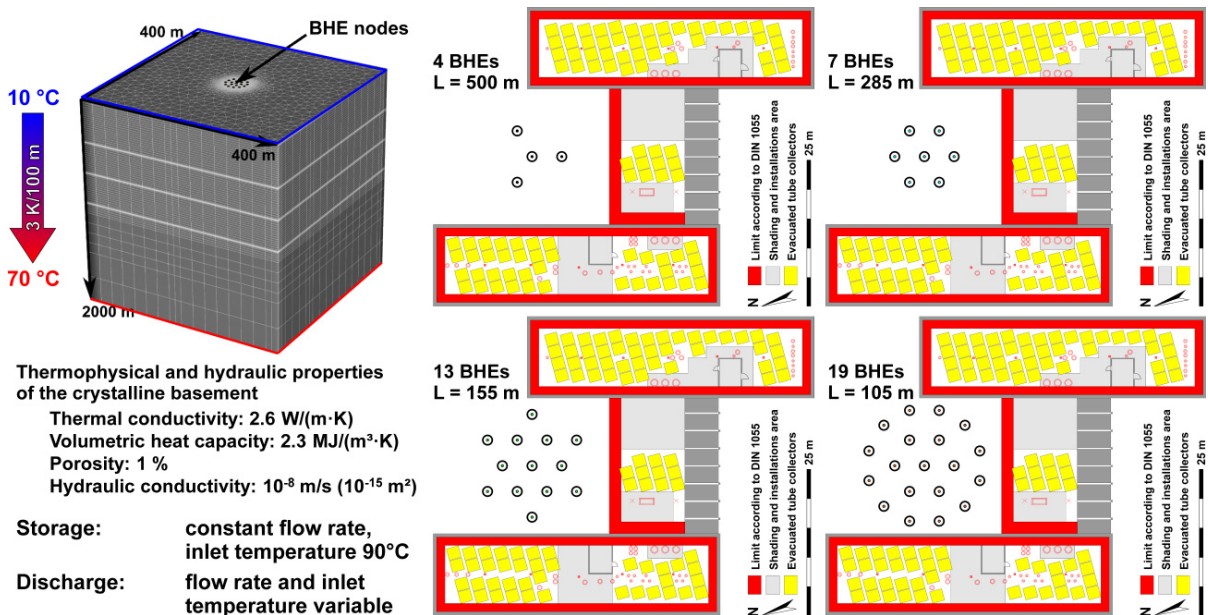
Fig. 6. (left): General set up, parameters, boundary conditions and flow rates and temperature during storage and extraction of the numerical FEFLOW models. (right): Layout of the BHEs in top view of the modelled office building including the position of the evacuated tube collectors installed on the building's roof for the four different preliminary set ups: 4, 7, 13 and 19 BHE's with the same total BHE length for the BTES.

Depending upon the depth of the proposed MD-BTES a vertical extent of the model is defined. The vertical extent is set such that the boundary parameters are kept considerably far from the MD-BTES. For a 1.0 km deep BHE a vertical model extent of 2.0 km has been set so that the 1st kind (temperature) boundary condition or other heat flux boundary conditions may not directly influence the BHEs. Boundary conditions have been set as shown in Figure 6. A subsurface temperature distribution with a geothermal gradient of 3 °C/km is set as initial condition. This model is now used incorporating 4th kind (BHE) boundary conditions at the BHE nodes with the BHE parameter setting and loading cycles for an operation period of 30 years.

5.2. Results

The simulation results (Figure 7) illustrate that the storage efficiency and the outlet temperature are higher if more BHEs can thermally interact with each other. Minimum outlet temperatures range from 40 °C to 60 °C after 30 years of operation. Thus, heat pumps are only needed during the coldest days of the heating period. Storage efficiencies are rather low, illustrating that either the heat demand of the building is too low for the chosen sizes of the different storage set ups and that more heat could be discharged from the storage in winter or that the heat input during summer was too high.

Fig. 6. (From left to right): Stored heat, extracted heat and storage efficiencies of the set up with 19 BHEs; comparison of the outlet tempe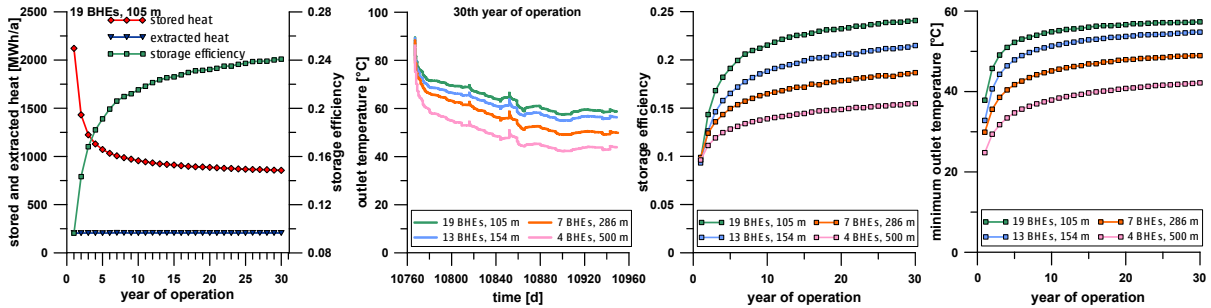ratures in the 30th year of operation and of the storage efficiencies and minimum outlet temperatures (right) for the four different preliminary set ups.

To optimize the design and completion of the MD-BTES to maximize storage efficiency and to reach the desired temperature and power outputs as well as to evaluate the best economic scenario for such a coupled system two approaches are used in ongoing studies. The first approach [7] uses the software FEFLOW to model a variety of different geometrical scenarios as accurately as possible. For the second approach a MATLAB Toolbox [31] is designed to simulate a BHE heat storage system with similar numerical codes as used by FEFLOW but with other gridding and coupling algorithms, supposed to enable much shorter processing times. Furthermore, this toolbox incorporates mathematical optimization algorithms, which allow for an automatic optimization within predefined boundary conditions of each scenario. These parallel approaches are expected to define the best MD-BTES scenario for the project building.

6. Conclusions and Outlook

The largest energy consumer in industrial countries is building infrastructure with its heating and cooling demand. Innovative energy saving concepts in this field will have the biggest impact in terms of reducing CO_2 emissions. Especially the coupling of different renewable energy sources – solar thermal and geothermal – with already existing district heating systems – e.g. combined (biofuel-driven) heat and power stations (CHP) – as presented here, seems to be a very promising approach to cover the heating demand of renovated or old buildings at higher temperature levels with renewable energies. Since conventional heating systems are still installed in approximately more than 90 % of Germany's building stock, the presented concept is a viable option to reduce the heating energy demand and the related greenhouse gas emissions. Consequently, a high temperature storage and heating supply system without the application of a heat pump or specialized heat-pumps with increased coefficients of performance are needed. However, storage configurations like the MD-BTES systems can also be utilized for low temperature heating systems.

The design and completion of MD-BTES systems as described here are strongly depending on the knowledge about the subsurface and the energy flows between the heat source, the storage system and the building. The estimation of the BHE depth and completion design needs some iterative procedures. Coupled numerical-analytical modeling of the whole system combined with mathematical optimization algorithms will be used in future studies to estimate the optimal geometrical setup and depth of the MD-BTES.

Acknowledgements

References

[1] AGEB (ed). Anwendungsbilanzen für die Endenergiesektoren in Deutschland in 2011 und 2012 mit Zeitreihen von 2008 bis 2012. Berlin; 2013

[2] Hellstöm G. Ground Heat Storage, Thermal Analysis of duct Storage Systems. Department of Mathematical Physics, University of Lund; 1991.

[3] Bauer D, Marx R, Nußbicker-Lux J, Ochs F, Heidemann W, Müller-Steinhagen H. German central solar heating plants with seasonal heat storage. Solar Energy 2010:84(4):612-623.

[4] Homuth S, Bär K, Rühaak W, Sass I. Mitteltiefe kristalline Hochtemperaturspeicher – Dimensionierungsgrößen – Übertragbarkeit nördlichen Oberrheingraben (ORG). Proceedings Der Geothermiekongress 2012, Geothermische Vereinigung (GtV-BV e.V.), Essen; 2012.

[5] Homuth S, Rühaak W, Bär K, Sass I. Medium Deep High Temperature Heat Storage. Proceedings, European Geothermal Congress, Pisa, 2013.

[6] Kuntz D, Kübert M, Walker-Hertkorn S, Reisig O.A. Saisonale geothermische Wärmespeicher zur Direktheizung – ein Praxisbeispiel. Geothermische Energie 2013:76.

[7] Welsch B, Rühaak W, Schulte DO, Bär K, Homuth S, Sass I. A Comparative Study of Medium Deep Borehole Thermal Energy Storage Systems Using Numerical Modelling. Proceedings World Geothermal Congress 2015, Melbourne, Australia, 2015:7 p.

[8] Mielke P, Bauer D, Homuth S, Götz AE, Sass I. Thermal Effect of a Borehole Thermal Energy Store on the Subsurface. Geothermal Energy 2014:2,5. Springer, DOI 10.1186/s40517-014- 0005-1 .

[9] Fahlbusch K. Die geologischen Grundlagen der alten Wasserversorgung Darmstadts. Geol. Jb. Hessen 1980:108:223-240.

[10] Hoppe A, Lang S. The eastern master fault of the Upper Rhine Graben below the Science and Conference Centre in Darmstadt (Germany). Z. dt. Ges. Geowiss., 2007:158(1):113-117.

[11] Backhaus E. Die randliche „Rotliegend"-Fazies und die Paläogeographie des Zechsteins im Bereich des nördlichen Odenwaldes. Notizbl. Hess. L.-Amt Bodenforsch. 1965:93:112-140,

[12] Matthess G. Zur Vergrusung der magmatischen Tiefengesteine des Odenwaldes. Notizbl. Hess. L.-Amt Bodenforsch. 1964:92:160-178.

[13] Voges A, Toloczyki M, Trurnit P, Wittekindt H. Geologische Karte der Bundesrepublik Deutschland 1:1.000.000. BGR, Hannover; 1993.

[14] Bär,K. Untersuchung der tiefengeothermischen Potenziale von Hessen. PhD Thesis, TU Darmstadt, 2012:XXVI and 265 p.

[15] Stein E. The Geology of the Odenwald Crystalline Complex. Mineral. Petrol. 2001:72(1-3):7-28.

[16] Mezger JE, Felder M, Harms F-J. Crystalline rocks in the maar deposits of Messel: key to understand the geometries of the Messel Fault Zone and diatreme and the post-eruptional development of the basin fill. Z. dt. Ges. Geowiss. 2013:164(4):639-662.

[17] Beier M. Urbane Beeinflussung des Grundwassers: Stoffemissionen und-immissionen. PhD Thesis, TU Darmstadt; 2007.

[18] Greifenhagen G: Untersuchungen zur Hydrogeologie des Stadtgebietes Darmstadt mit Hilfe eines Grundwasserinformationssystems unter Verwendung von einer Datenbank, Datenmodellierung und ausgewählten statistischen Methoden. PhD Thesis, TU Darmstadt, (2000), 221 p.

[19] Bär K, Arndt D, Fritsche J-G, Götz A E, Kracht M, Hoppe A, Sass I. 3D-Modellierung der tiefengeothermischen Potenziale von Hessen – Eingangsdaten und Potenzialausweisung. Z. dt. Ges. Geowiss. 2011:162(4):371–388.

[20] Deutscher Wetterdienst (DWD), 2004: Testreferenzjahre von Deutschland, viewed 13th December 2010.

[21] Deutscher Wetterdienst (DWD), 2011: Climate data from selected German stations, viewed 13 December 2010.

[22] VDI-Gesellschaft Bauen und Gebäudetechnik, VDI-Fachbereich Facility-Management, VDI Richtlinie 2607 - Wirtschaftlichkeit gebäudetechnischer Anlagen - Blatt 11 - Rechenverfahren zum Energiebedarf beheizter und klimatisierter Gebäude; 2006.

[23] Deutsche Industrie Norm: Energy efficiency of buildings – Calculation of the net, final and primary energy demand for heating, cooling, ventilation, domestic hot water and lighting – Part 100 (18599-100), Deutsches Institut für Normung (DIN), Berlin; 2009.

[24] Honsberg C, Bowden S. Solar Radiation on a tilted Surface. http://pvcdrom.pveducation.org/SUNLIGHT/MODTILT.HTM; 2011.

[25] Deutsche Industrie Norm: Actions on structures - Part 4: Wind loads (1055-4:2005-03). Deutsches Institut für Normung (DIN), Berlin; 2005.

[26] Viessmann: VITOSOL technical guide, Author: Telford; 2006.

[27] Wittig V, Bracke R. Innovative Hydraulic DTH Drilling Technology based on Coiled Tubing for deep, hard rock Geothermal Drilling. Proceedings, European Geosciences Union (EGU) Kongress, Vienna / Wien; 2011.

[28] Riechers J. Wohin bohren wir? Masshaltigkeit konventioneller und innovativer hydraulischer GeoJEtting Bohrtechnik. unpublished BSc Thesis, Internationales Geothermiezentrum, Hochschule Bochum; 2011.

[29] Diersch H-JG, Bauer D, Heidemann W, Rühaak W, Schätzl P. Finite element modeling of borehole heat exchanger systems - Part 1: Fundamentals. Computers & Geosciences 2010a:37(8), DOI:10.1016/j.cageo.2010.08.003.

[30] Diersch H-JG, Bauer D, Heidemann W, Rühaak W, Schätzl P. Finite element modeling of borehole heat exchanger systems - Part 2. Numerical simulation. Computers & Geosciences 2010b:37(8):1136-1147.

[31] Schulte DO, Rühaak W, Chauhan S, Welsch B, Sass I. A MATLAB Toolbox for Optimization of Deep Borehole Heat Exchanger Storage Systems. Proceedings World Geothermal Congress 2015, Melbourne, Australia; 2015:5 p.

Appendix B:
Characteristics of medium deep borehole thermal energy storage

Published as:

Characteristics of medium deep borehole thermal energy storage

Bastian Welsch[1,2,*,†], Wolfram Rühaak[1,2], Daniel O. Schulte[1,2], Kristian Bär[1] and Ingo Sass[1,2]

[1]Department of Geothermal Science and Technology, Technische Universität Darmstadt, Darmstadt, Germany
[2]Darmstadt Graduate School of Excellence Energy Science and Engineering, Darmstadt, Germany

SUMMARY

Seasonal energy storage is an important component to cope with the challenges resulting from fluctuating renewable energy sources and the corresponding mismatch of energy demand and supply. The storage of heat via medium deep borehole heat exchangers is a new approach in the field of Borehole Thermal Energy Storage. In contrast to conventional borehole storages, fewer, but deeper borehole heat exchangers tap into the subsurface, which serves as the storage medium. As a result, the thermal impact on shallow aquifers is strongly reduced mitigating negative effects on the drinking water quality. Furthermore, less surface area is required. However, there are no operational experiences, as the concept has not been put into practice so far. In this study, more than 250 different numerical storage models are compared. The influence of the characteristic design parameters on the storage system's behaviour and performance is analysed by variation of parameters like borefield layout, fluid inlet temperatures and properties of the reservoir rocks. The results indicate that especially larger systems have a high potential for efficient seasonal heat storage. Several GWh of thermal energy can be stored during summertime and extracted during the heating period with a high recovery rate of up to 83%. Medium deep borehole heat exchanger arrays are suitable thermal storages for fluctuating renewable energy sources and waste heat from industrial processes. Copyright © 2016 John Wiley & Sons, Ltd.

Correspondence

*Bastian Welsch, Darmstadt Graduate School of Excellence Energy Science and Engineering, Jovanka-Bontschits-Straße 2, 64287 Darmstadt, Germany.
†E-mail: welsch@geo.tu-darmstadt.de

1. INTRODUCTION

In 2011, about 25% of the global final energy consumption resulted from space heating and domestic hot water production [1]. Most of this heat is required in the winter season while there is a surplus of heat from various sources during summer. For example, solar thermal energy production is characterized by a high seasonality. Exploiting the full potential of solar thermal energy depends on economically competitive and reliable storage systems [2], which are able to bridge the seasonal offset between heat supply and heat demand. Thus, collector stagnation in summer is minimized and solar collector areas could be considerably reduced [3], especially in northern latitudes, where seasonal variations are high [4]. Furthermore, combined heat and power plants (CHP) often have to reduce their energy production because of the low heat demand in summer. Seasonal thermal storages can increase the operating time

and therefore the on-site heat and electricity production of CHPs. This leads to economic benefits and results in further savings of carbon dioxide emissions, compared with a CHP, which is operated without a seasonal storage [5–7]. Thermal energy storage systems can reduce energy costs and energy consumption, reduce equipment size, decrease the initial and maintenance costs and reduce pollutant emissions [8,9].

There are numerous methods for seasonal storage of thermal energy. Good overviews on the available technologies are given, for example, by Pinel *et al.* [2], Dincer and Rosen [8], Schmidt *et al.* [10], Xu *et al.* [11] and Hesaraki *et al.* [12]. Shallow borehole thermal energy storages (BTESs) are a promising technology and have been installed in several locations (e.g. [13–18]). They consist of several boreholes that are usually not deeper than 100 m. Some exceptions are known, for example, from Lund, Sweden [19] or Oshawa, Canada [20], where the

storage systems reach depths of 230 m and 200 m. The boreholes are equipped with borehole heat exchangers (BHEs). A BHE is a closed pipe system, which is embedded in a cement backfilling. A heat transfer fluid is circulated through the pipes. Heat is exchanged with the subsurface by conductive heat transport through the pipe wall and the backfill material. In this way, BTES can access a large storage volume at relatively low expenses [21]. A detailed technology description is given by Reuss [22].

The idea of using the ground as heat storage by shallow BHEs goes back to the 1970s/1980s [23–25]. In the 1980s and early 1990s, intensive research activities on shallow BTES were accomplished, particularly in Sweden and Finland: a first large-scale experimental and demonstration example was built in 1982/1983 at Luleå University of Technology, Sweden, consisting of 120 BHEs with a length of 65 m each [14,15]. Furthermore, the first numerical simulation models for BTES systems were developed (e.g. [26,27]). Lund and Östman [27] created a three-dimensional numerical model for BTES, which already accounted for convective heat flow in the storage region. They studied the behaviour of different BTES models in conjunction with variable dimensioning factors of a solar district heating system. Four different storage volumes were analysed, which all had a cubic geometry and a uniform BHE spacing. The deepest system they considered had a BHE length of 75 m. They also examined the influence of groundwater flow on the storage behaviour by simulating four different hydrogeological conditions. Nordell [28] developed a model for the design optimisation of shallow BTES, which also took account of economic aspects. He analysed sensitivities of different design and operational parameters as well as cost data on the optimum design of a storage system.

Although the viability of shallow BTES systems has been shown in several projects and simulation studies, there are some major difficulties linked to the concept. The major part of drinking water is produced from shallow aquifers. An increase of temperature can change the chemical (e.g. [29,30]) and biological (e.g. [31,32]) properties of the groundwater and thus have a negative impact on its quality [33–35]. Although most countries do not have any legal temperature limits for the heating and cooling of the groundwater [36,37], heat storage in the shallow subsurface is usually very restricted or not approved at all by the responsible water authorities. Furthermore, the return temperatures of shallow BTES are relatively low, and heat pumps are indispensable to provide the required supply temperatures for heating systems.

In contrast, storing heat at temperature levels of 90 °C or even more has a number of advantages compared with low temperature energy storage: higher loading temperatures in the summer season result in higher extraction temperatures during the heating period in winter. Consequently, the coefficient of performance of the heat pump increases, and a higher exergy efficiency of the heating system can be achieved [38]. Low temperature

heating systems, which are characterized by supply temperatures of 25 to 35 °C, could even be supplied directly without the use of a heat pump [39]. To mitigate the potentially hazardous impact on the shallow aquifers, the storage of high temperature heat in greater depths presents a viable alternative: fewer, but deeper BHEs with an insulation in the topmost section can protect the shallow aquifers and store the heat at depths up to several hundred metres [40]. As ground temperature increases with depth, a decreased lateral temperature gradient also reduces thermal losses. Additionally, these medium deep borehole thermal energy storages (MD-BTESs) require less space at the surface, which is especially advantageous in densely populated urban areas.

The dimensions of an MD-BTES differ significantly from those of a shallow BTES. Systems consisting of less than 50 BHEs and drilling depths of 100 m to 1000 m are taken into consideration. Compared with the relatively compact shape of shallow BTES, medium deep systems have an elongated geometry. Furthermore, medium deep systems can be operated at higher temperature levels, which in turn also leads to a different behaviour compared with shallow systems. Hence, the results of former studies are not generally transferable to MD-BTES. The concept has not been put into practice so far. There is no experience in operating an MD-BTES. As drilling costs increase with depth, the construction of an MD-BTES represents a large investment. Consequently, numerical simulations are necessary to predict the system performance and to estimate the influence of key parameters such as the dimension of the storage, the mode of operation and the underground properties.

This study presents comprehensive simulations of different MD-BTES configurations and examines the influence of the BHE length, the number of BHEs, the spacing between the boreholes, the fluid inlet temperatures and the rock properties on the system performance. The sensitivity of the parameters is assessed, and the setup of the simulation experiment is discussed. The study is part of a project, which assesses a potential MD-BTES system to be constructed at the Institute of Applied Geosciences, Technische Universität Darmstadt, Germany as described by Bär *et al.* [41].

2. METHODS

In order to quantify the influence of different design parameters on the performance of MD-BTES, numerical models of different storage setups were simulated, varying the parameters BHE length, number of BHEs and BHE spacing as listed in Table I(a). The simulation of all possible combinations of these parameter variations resulted in 200 different storage geometries. Figure 1 illustrates the five different BHE configurations resulting from the variation of the number of BHEs. In addition to the variation of the storage design, the influence of the heat transfer fluid temperature entering the storage system (inlet temperature)

Table I. Variation of influence parameters applied on the different storage models. Bold print denotes the base case design.

Variable	Value									
(a) Storage configuration										
BHE length [m]	100	200	300	400	500	600	700	800	900	1000
Number of BHEs[1]	7	13	19	28	37					
BHE spacing [m]	2.5	5	7.5	10						
(b) Fluid inlet temperatures										
During charging [°C]	70	80	**90**	100	110					
During discharging [°C]	10	20	**30**	40	50					
(c) Rock properties										
Thermal conductivity [W m^{-1} K^{-1}]	1.4	2	**2.6**	3.2	3.8					
Volumetric heat capacity [MJ m^{-3} K^{-1}]	2	2.15	**2.3**	2.45	2.6					
Hydraulic conductivity [m s^{-1}]	$1\cdot10^{-9}$	$\mathbf{1\cdot10^{-8}}$	$1\cdot10^{-7}$	$5\cdot10^{-7}$	$1\cdot10^{-6}$	$5\cdot10^{-6}$	$1\cdot10^{-5}$	$1\cdot10^{-4}$		

[1]The number of borehole heat exchangers (BHEs) is the only non-continuous variable considered.
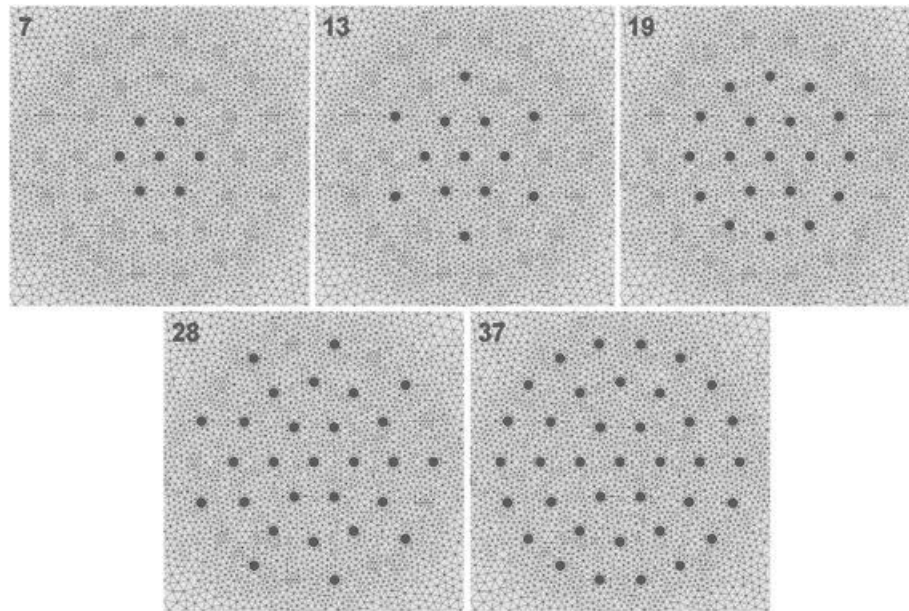
Figure 1. Different storage setups in top view with the corresponding number of borehole heat exchangers.

was studied in one characteristic storage setup by varying the inlet temperature values for the charging and discharging periods (Table I(b)). All possible temperature combinations were simulated. Furthermore, the effect of different geological and hydrogeological conditions was investigated by variation of the thermal conductivity, the volumetric heat capacity and the hydraulic conductivity of the entire model in one characteristic case (Table I(c)). In this partial study, only one parameter was varied, whereas the other parameters were kept at standard values.

In order to investigate the significance of heat losses at the surface and the effect of a hypothetical insulation, an additional set of storage models with an insulating top layer was simulated too.

The numerical simulations of the heat transport processes in the BHEs and in the subsurface were carried out using the finite element programme FEFLOW 6.2 [42,43]. The BHEs were modelled by 1D finite element representations as described by Diersch *et al.* [44]. The analytical BHE solution after Eskilson and Claesson [45] was

applied, as it has shown a high efficiency, robustness and a reasonable accuracy in long-term analyses [44,46]. In a previous study, FEFLOW simulations of the BTES in Crailsheim, Germany were in good agreement with measured data [47].

2.1. General model setup

In this study, all BHEs were implemented as coaxial pipes with annular inlet of the heat transfer fluid and centred outlet (CXA). The borehole diameter was set to 152 mm. For stability reasons, a steel pipe (carbon steel) was chosen as an outer casing with an outer diameter of 127 mm and a wall thickness of 5.6 mm. Furthermore, the relatively high thermal conductivity of the outer pipe ($54\,\mathrm{W\,m^{-1}\,K^{-1}}$) is advantageous for the heat transfer rate between the fluid and the subsurface. Depending on the groundwater properties, low-grade carbon steel might be subject to corrosion. In such a case, more expensive stainless steel pipes should be preferred. Nakevska *et al.* [48] showed that it is advisable to use polyethylene (PE) pipes for the ascending portion of the loop (i.e. the inner pipe) because its relatively low thermal conductivity reduces the heat exchange between the up-streaming and down-streaming fluids. Therefore, the inner pipe was modelled as a PE-X pipe with an outer diameter of 75 mm, a wall thickness of 6.8 mm and a thermal conductivity of $0.4\,\mathrm{W\,m^{-1}\,K^{-1}}$. The aforesaid BHE parameters were used in all considered storage models.

All simulations were run in a simple single-layered block-shaped underground model with the dimensions of $400\,\mathrm{m} \times 400\,\mathrm{m} \times 2000\,\mathrm{m}$. According to Sanner [49], some low permeable sedimentary and crystalline rocks are suitable for the application of high temperature BTES. In this study, the subsurface was assumed to consist of a granodiorite with a thermal conductivity of $2.6\,\mathrm{W\,m^{-1}\,K^{-1}}$, a volumetric heat capacity of $2.3\,\mathrm{MJ\,m^{-3}\,K^{-1}}$ and a porosity of 1%. These are measured values, which were obtained from a field campaign at the proposed location for the study mentioned earlier [40].

In crystalline rock, groundwater flow is primarily restricted to interconnected fracture zones and fissures. MD-BTES tap into large rock volumes for which fracture heterogeneities are smoothed out as a result of spatial averaging. Thus, the subsurface can be treated in the models as a single continuum of porous material [43]. The estimated value for the hydraulic conductivity of the subsurface was $10^{-8}\,\mathrm{m\,s^{-1}}$, which represents a reasonable value for the crystalline basement (cf. [50]). This barely allows for groundwater flow and makes conduction the dominant heat transport process. Hence, the groundwater flow was neglected and eliminated by setting the hydraulic gradient in the model to zero. A temperature boundary condition of 10 °C was set on the uppermost slice as the mean annual surface temperature, whereas a temperature of 70 °C was set on the lowest slice to factor in a geothermal gradient of $3\,\mathrm{K}\,(100\,\mathrm{m})^{-1}$. Before running the actual storage simulations, a steady-state simulation of the underground model

was carried out to guarantee that the temperature boundary conditions are in equilibrium with the geothermal gradient. After the steady-state simulations, the temperature boundary conditions at the top of the model domain were deleted at the BHE positions and their neighbouring nodes to prevent a direct influence of the boundary condition on the BHE fluid temperatures. All parameters for the geological model and the BHEs are summarized in Table II.

To capture high temperature gradients between the BHEs and the surrounding rock during the simulation, the three-dimensional finite element mesh was locally refined: in the horizontal direction around the BHE nodes and in vertical direction close to the surface and close to the endpoints of the BHEs. An optimal mesh refinement around the BHE nodes was realized by using the approach of direct estimation of the nodal distances according to Diersch *et al.* [46]. The grids consist of triangular prisms, which are unstructured in horizontal direction and structured in vertical direction. The horizontal triangles were generated with the Triangle mesh generator [51], which is able to create high quality meshes that fulfil the Delauney criterion. This allows for a sound behaviour of the obtained solution (Galerkin method and upwinding method: shock capturing, iterative solver with a termination criterion of $1 \cdot 10^{-12}$, non-linear coupling with one iteration per time step and an allowed maximum L_∞ error of $1 \cdot 10^{-4}$): a fast convergence was achieved with negligible relative heat balance errors of less than $1 \cdot 10^{-8}$. For the majority of the models, the grid Peclet numbers (cf. [42]) were zero, as no convective heat transport was considered. The models for the groundwater flow variation study constitute an exception: maximum Peclet numbers were in the order of 2–3 for the three systems with the highest groundwater velocities. All remaining systems exhibited Peclet numbers well below 2. Such Peclet numbers are within an unproblematic range. An automatic time step control was applied, using the second-order Adams–Bashforth/trapezoid rule predictor-corrector method [43], which entails a fully implicit time integration scheme.

2.2. Borehole heat exchanger operation scenario

A very simplified loading and unloading scheme was applied in each simulation to simplify the comparison of the MD-BTES performance. Alternating operation between charging and discharging cycles was realized by a change of the inlet temperature every 6 months as shown in Figure 2a. During the charging periods, the inlet temperature was set to 90 °C, as this temperature can easily be supplied by solar thermal collectors but also describes the upper limit of the temperature resistance of the PE-X pipes. During heat extraction, the inlet temperature was set to 30 °C. This ensures that low temperature heating systems can be supplied without the use of a heat pump. The BHEs were connected

Table II. General model parameters for a base case design.

| Underground parameters		Borehole heat exchanger parameters	
Parameter	Value	Parameter	Value
Thermal conductivity of solid	$2.6 \, \text{W m}^{-1} \, \text{K}^{-1}$	Borehole diameter	$0.1522 \, \text{m}$
Volumetric heat capacity of solid	$2.3 \, \text{MJ m}^{-3} \, \text{K}^{-1}$	Outer pipe diameter	$0.127 \, \text{m}$
Thermal conductivity of fluid	$0.65 \, \text{W m}^{-1} \, \text{K}^{-1}$	Outer pipe wall thickness	$0.0056 \, \text{m}$
Volumetric heat capacity of fluid	$4.2 \, \text{MJ m}^{-3} \, \text{K}^{-1}$	Inner pipe diameter	$0.075 \, \text{m}$
Porosity	0.01	Inner pipe wall thickness	$0.0068 \, \text{m}$
Surface temperature	$10 \, ^\circ\text{C}$	Outer pipe thermal conductivity (steel)	$54 \, \text{W m}^{-1} \, \text{K}^{-1}$
Geothermal gradient	$0.03 \, \text{K m}^{-1}$	Inner pipe thermal conductivity (PE-X)	$0.4 \, \text{W m}^{-1} \, \text{K}^{-1}$
Hydraulic conductivity	$10^{-8} \, \text{m s}^{-1}$	Grout thermal conductivity	$2 \, \text{W m}^{-1} \, \text{K}^{-1}$
Hydraulic gradient	0	Heat transfer fluid volumetric heat capacity (water)	$4.145 \, \text{MJ m}^{-3} \, \text{K}^{-1}$
Model length	$400 \, \text{m}$	Heat transfer fluid thermal conductivity (water)	$0.65 \, \text{W m}^{-1} \, \text{K}^{-1}$
Model width	$400 \, \text{m}$	Heat transfer fluid dynamic viscosity (water)	$504 \cdot 10^{-6} \, \text{kg m}^{-1} \, \text{s}^{-1}$
Model depth	$2000 \, \text{m}$	Heat transfer fluid density (water)	$977 \, \text{kg m}^{-3}$
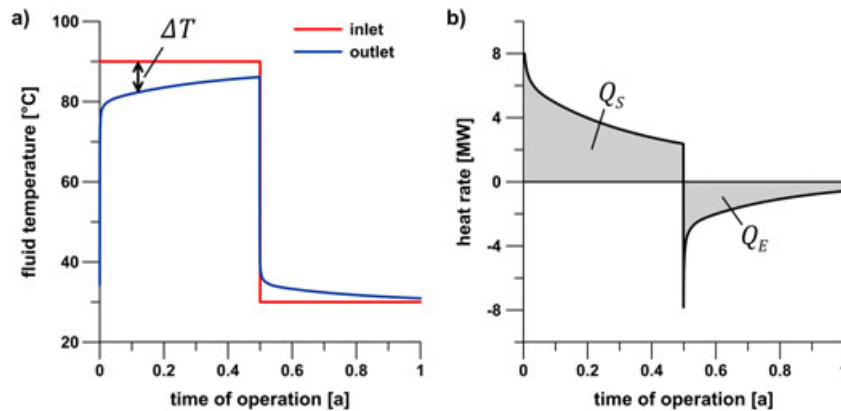
Figure 2. (a) Default inlet temperature and computed outlet temperature and (b) the corresponding calculated heat rate during the first year of operation of a characteristic medium deep borehole thermal energy storage (37 borehole heat exchangers with a length of 500 m and a spacing of 5 m). The hatched areas represent the total heat stored (Q_S) and the total heat extracted (Q_E) during the regarded time span.

to each other in a parallel arrangement, so that all BHEs were supplied with the same inlet temperature. Those temperatures were kept constant during the charging and discharging cycles, respectively. The flow rate for each BHE was set to $4 \, \text{l s}^{-1}$ for the whole simulation time. This value displays a reasonable compromise between a high heat exchange rate and a comparably low pressure drop in the BHEs. The latter depends on the fluid properties, which in turn depend on the fluid temperatures. For the considered inlet temperatures and the assumed pipe configuration, the calculated specific pressure loss (according to, e.g. Yamaguchi [52]) ranges from $295 \, \text{Pa m}^{-1}$ to $385 \, \text{Pa m}^{-1}$. The operation of the storage array is controlled by assigning a variable inlet temperature for a time span of 30 years with one exception: for the simulations of the variation of the underground properties, a time span of just 10 years was regarded.

2.3. Processing and analysis

In order to assess the different storage model setups, several key performance indicators are compared. First of all, the outlet temperatures of the single BHEs calculated during the numerical simulation were averaged to a mean storage outlet temperature. As an example, Figure 2a shows the mean outlet temperature of a high performance storage system. Because of the temperature difference between the heat transfer fluid in the BHEs and the surrounding rock, the subsurface is heated or cooled continuously. Consequently, this temperature difference decreases over time and reduces the BHE's heat transfer rate. The heat rate ΔQ, which is exchanged between the heat carrier fluid and the storage, is calculated as follows:

$$\Delta Q = \Delta T \cdot (\rho c)_f \cdot \dot{V} \tag{1}$$

Where ΔT is the temperature difference between the inlet and the outlet temperature of the fluid, $\dot{V}$ is the flow rate through the BHE array and $(\rho c)_f$ is the volumetric heat capacity of the fluid.

By integrating the heat rate over a charging or discharging cycle, the total heat stored or extracted during this period is calculated (Figure 2b). The ratio of the absolute values of extracted and stored heat, the storage efficiency η is defined by

$$\eta = \left| \frac{Q_E}{Q_S} \right| \qquad (2)$$

Where Q_S is the stored heat and Q_E is the extracted heat during 1 year.

The total BHE length has to be taken into account to compare the total amount of extracted heat of the different systems. Thus, the specific heat extraction rate $\dot{q}$, which is the heat extraction rate referring to one extraction cycle normalized by the BHE length, is calculated as:

$$\dot{q} = Q_E \cdot \frac{1}{\Delta t \cdot L_{tot}} \qquad (3)$$

Where Q_E is the heat extracted from the storage during the considered year, L_{tot} is the total BHE length of the considered storage system and Δt is the length of the heat extraction period.

3. RESULTS

In the simulations of the different storage model setups, the amount of stored heat ranges from about $420\,\mathrm{MWh\,a^{-1}}$ to more than $20\,\mathrm{GWh\,a^{-1}}$ in the 30th year of operation (Figure 3a). The corresponding amount of extracted heat lies between $150\,\mathrm{MWh\,a^{-1}}$ and $17\,\mathrm{GWh\,a^{-1}}$ (Figure 3b). Accordingly, the storage efficiency and the specific heat extraction rate range from 32% to almost 84% (Figure 3 c) and from $49\,\mathrm{W\,m^{-1}}$ to $113\,\mathrm{W\,m^{-1}}$, respectively (Figure 3d).

All simulations display typical BTES long-term behaviour: because of heat diffusion, not all of the stored heat can be recovered during the heat extraction period. A fraction of the stored thermal energy remains in the subsurface generating a heat plume and increasing the storage's average rock temperature. As a consequence, the elevated subsurface temperature leads to a decrease of heat storage and an increase of heat extraction (Figure 4). Thereby, the storage losses shrink and the storage efficiency η grows over time. This effect is especially strong during the first couple of charging and discharging cycles and diminishes later on, but still persists even after 30 years of operation (Figure 4). A complete list of all simulation results is included in the Supporting Information of this paper.

3.1. Influence of storage design

The storage size is determined by the number of BHEs and their length. Both variables correlate almost linearly with
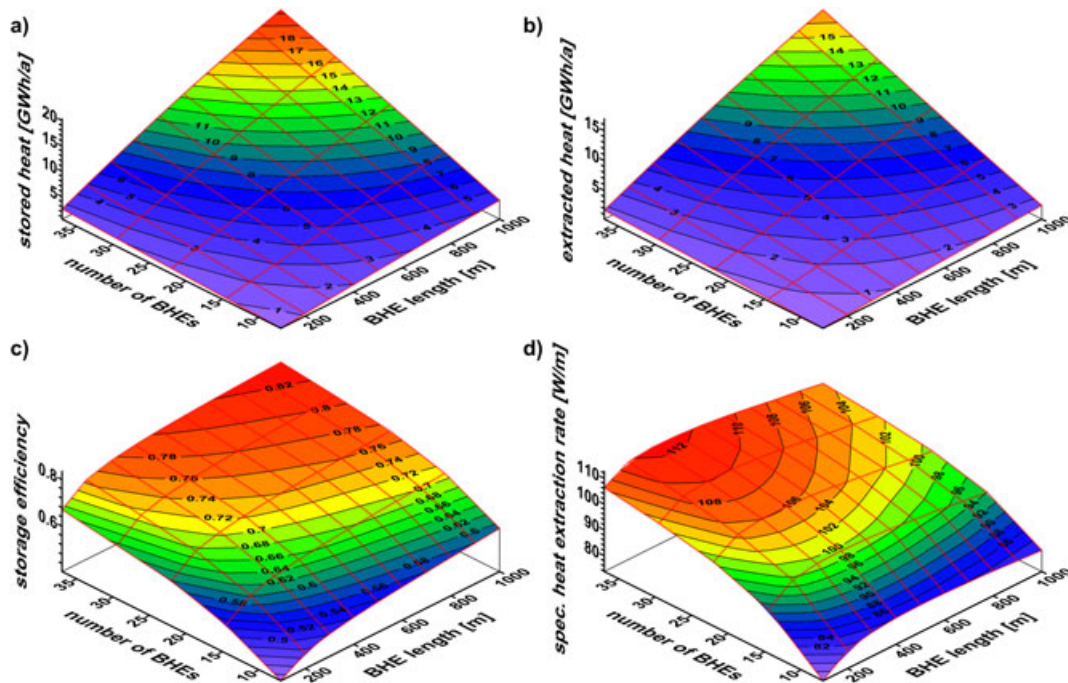

Figure 3. (a) Amount of stored heat, (b) amount of extracted heat, (c) storage efficiency and (d) specific heat extraction rate in the 30th year of operation depending on a change in the number of borehole heat exchangers (BHEs) and the BHE length for storage systems with a BHE spacing of 5 m. The results are illustrated as interpolated surfaces.
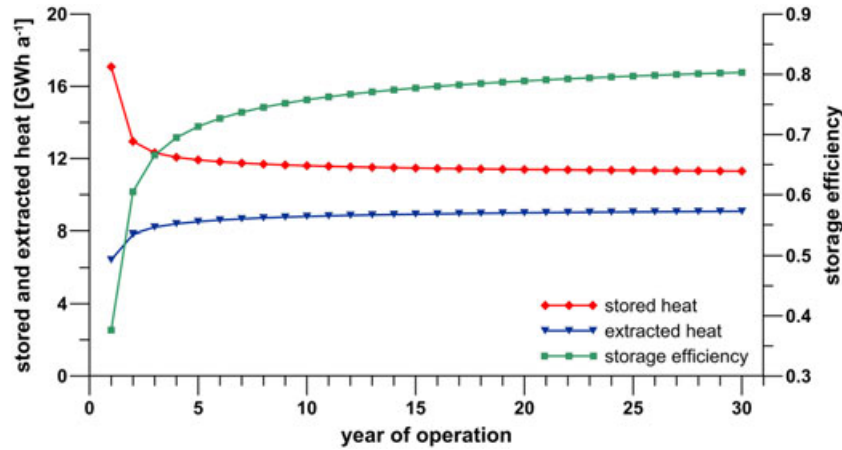
Figure 4. Temporal evolution of storage performance over 30 years of operation for a setup with 37 borehole heat exchangers with a length of 500 m and a spacing of 5 m.

the amounts of stored and extracted heat (cf. Figure 3a and b). Thus, larger storage systems have a higher capacity.

The storage efficiency rises continuously with the storage size, that is, the number of BHEs and their length (cf. Figures 3c, 5a and 6a): heat losses decrease with the increasing ratio of storage volume to storage surface. Furthermore, a higher number of BHEs in an MD-BTES means more thermal interaction between them: thermal energy that is lost due to heat diffusion can be recovered by neighbouring BHEs. Hence, heat losses concentrate on the storage fringe. For this reason, a lateral temperature gradient from the storage centre to the storage fringe develops with time, which leads to higher efficiencies of the inner BHEs compared with the peripheral ones. Moreover, the overall storage efficiency for the layouts of 13 and 28 BHEs is barely increased compared with the respectively next smaller system in the first year of operation (cf. kinks in Figure 5a). These are the borefield layouts, in which the outer BHE ring is occupied only on every second BHE position (Figure 1). As a result, the storage does not match the shape of an ideal circular cylinder, but has an overly

increased envelope area. Only after several years of operation this effect is compensated when a substantial heat plume has developed in the subsurface. This phenomenon has a short-term effect on the specific heat extraction rate as well (Figure 5b).

However, the variables' effect on the specific heat extraction rate and the storage efficiency is more complex. While the specific heat extraction rate generally grows with the number of BHEs, counter-intuitively, it reaches a maximum at a specific BHE length (cf. Figures 3d and 6b). The decrease in the specific heat extraction rate with larger depths can be explained by a prolonged dwell time of the fluid in the BHE pipes. As a result, heat losses increase in the upper parts of the borehole, where thermal energy is transferred back from the heated fluid to the colder subsurface. Beyond a specific depth, this effect outweighs the increased heat extraction in the bottom part of the BHE, which marks the BHE length for the maximum specific heat extraction rate.

Additionally, the non-linear decline in storage efficiency and specific heat extraction rate grows steeper with
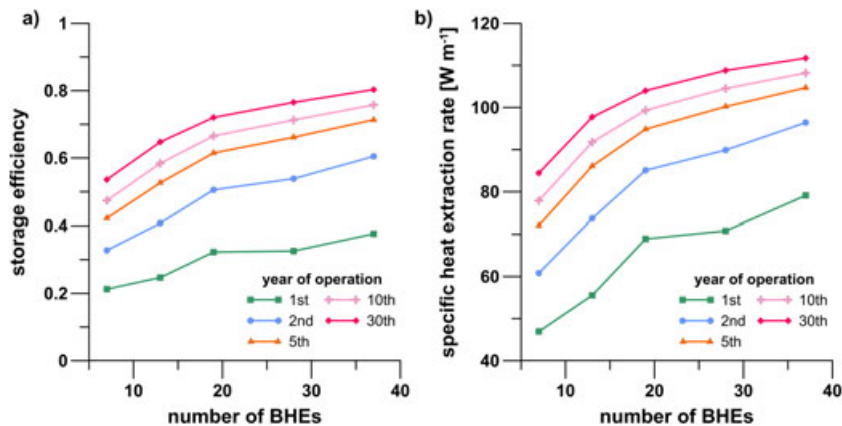

Figure 5. (a) Influence of the number of borehole heat exchangers (BHEs) on the storage efficiency and (b) the specific heat extraction rate in different years of operation, exemplarily illustrated for storage setups with a BHE length of 500 m and a spacing of 5 m.
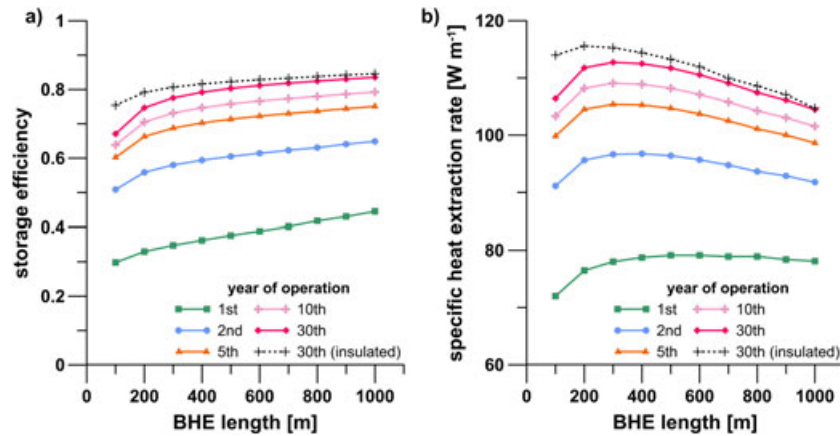
Figure 6. (a) Influence of the borehole heat exchanger (BHE) length on the storage efficiency and (b) specific heat extraction rate in different years of operation for storage setups with 37 BHEs and a spacing of 5 m; insulation layer thickness: 1 m; thermal conductivity of the insulation layer: $0.05 \, \mathrm{W \, m^{-1} \, K^{-1}}$.

decreasing BHE length. The effect of heat losses at the top surface is more significant for shallow systems. Deeper BTES can compensate the heat losses by their higher capacity as the top surface does not increase with BHE length. Consequently, an insulating layer at the top of the storage is most effective for shallow BTES (Figure 6a and b). Furthermore, the specific lateral heat losses diminish with depth because of the geothermal gradient and the thereby reduced temperature difference between BHE fluid and surrounding rock. Insulating the upper portion of the BHEs by a low thermal conductivity grout would further reduce lateral heat losses [41,48]. However, multiple grout sections are not provided in FEFLOWs' analytical BHE solution.

Also, the BHE spacing has an effect on the storage performance. On the one hand, a narrow spacing results in a quick depletion of the storage reservoir during heat extraction. On the other hand, thermal interaction between BHEs is weak for a wide spacing, which equals to an inefficient heat recovery of the neighbouring BHEs. Consequently,

there must be an ideal radial distance between BHEs. The simulation results confirm this hypothesis and show peak specific heat extraction rates for a radial distance of 5 m (Figure 7b). The storage efficiency shows the same effect after a couple of years when the storage is charged and has developed a thermal plume (Figure 7a). A dependency of the optimal spacing on the BHE length cannot be observed.

3.2. Influence of the inlet temperature

The total amounts of stored and extracted heat are strongly dependent on and almost linearly correlated (Figure 8a) with the difference between the charging temperature (i.e. the inlet temperature during the heat storage period) and the discharging temperature (i.e. the inlet temperature during the heat extraction period). This implies that higher temperature differences result in higher specific heat extraction rates and higher storage capacities (Figure 8b). In general, the storage efficiency increases with higher
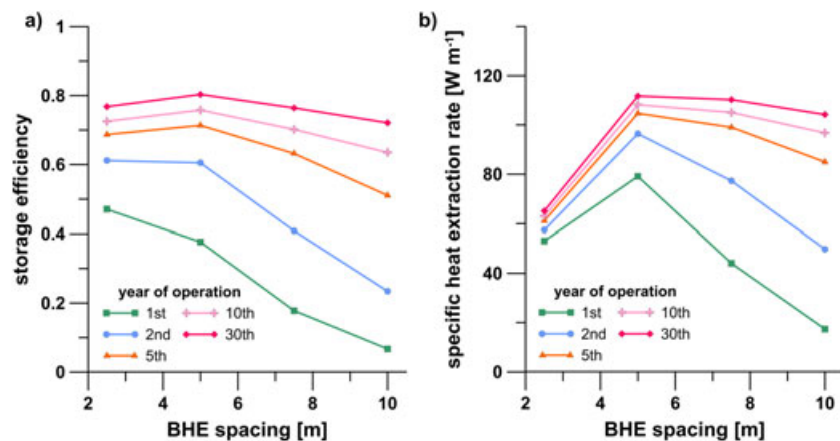

Figure 7. (a) Influence of the borehole heat exchanger (BHE) spacing on the storage efficiency and (b) the specific heat extraction rate in different years of operation, exemplarily illustrated for storage setups with 37 BHEs and a BHE length of 500 m.

charging temperatures and lower discharging temperatures. Yet, the variables' influence on the storage efficiency is interdependent (Figure 8c): While an increase of the charging temperature results in more stored heat, it also causes higher lateral heat losses. For high discharging temperatures and a consequently poor heat recovery, the increase of the charging temperature has a positive effect on the storage efficiency (Figure 8c, 50 °C discharging temperature line). However, if the discharging temperature is low, the positive effect is neutralized by effective heat recovery and the higher heat losses manifest in declining storage efficiencies (Figure 8c, 10 °C discharging temperature line).

3.3. Influence of general model variables

The heat transport processes in the subsurface are controlled by the thermo-physical and hydrogeological framework conditions. Figure 9 illustrates the influence of the variable rock properties on the storage performance in a characteristic storage setup. The thermal conductivity of the reservoir rock not only has a positive and nearly linear influence on the storage capacity but also enhances the lateral heat losses. Consequently, the rising storage capacity is accompanied by a slight decrease of storage efficiency (Figure 9a). In contrast to the thermal conductivity, an increase of the volumetric heat capacity has only a weak positive effect on the amounts of stored and extracted heat (Figure 9b). Thus, the influence of the volumetric heat capacity is considered to be negligible.

As advective dissipation of the stored heat by flowing groundwater has to be prevented, formations with a low hydraulic permeability are suitable reservoirs for BTES applications [48]. Parameter variations show that groundwater flow velocities larger than $2\,\mathrm{m\,a^{-1}}$ lead to considerable advective losses of stored heat. This culminates in the worst case, where the subsurface temperature is set back to undisturbed conditions within the storage, whereas the entire plume of stored heat is displaced by

the groundwater flow. As a consequence, the discharge temperature is too high. Even in the winter period, heat is injected and not extracted resulting in a negative storage coefficient (Figure 9c).

These findings suggest that for locations, where groundwater flow is low, the thermal conductivity, and by extension, the thermal diffusivity of the reservoir rock determine the storage capacity of a given MD-BTES design. Where groundwater flow exceeds a certain level, it can have a strong negative influence on the storage capacity as well as on the storage efficiency.

4. DISCUSSION

Like any other model, the simulations cannot capture every physical detail and are affected by assumptive boundary conditions. Especially the homogeneous geological model and the operational scenario of 6 months of constant inlet temperatures and constant fluid flow rates represent oversimplifications, which certainly do not resemble realistic conditions. However, realistic values for these model parameters would add a lot of noise to the simulation results. Realistic stratigraphic models would have to consider geological uncertainty, while realistic charging and discharging temperature curves have a high temporal resolution and depend on simulation models or measured values, which are specific to a certain building. Consequently, the consideration of realistic values for these parameters would add a lot of complexity and detail to the model response and prevent a conclusive analysis of the other variables' effect. While simulations for the planning of a specific storage should factor in as much detail as possible, these model simplifications are necessary for our study to allow for the investigation of the parameters' sensitivity.

The simulations provide information on the characteristical MD-BTES system responses to the variation of a selection of geological, operational and design
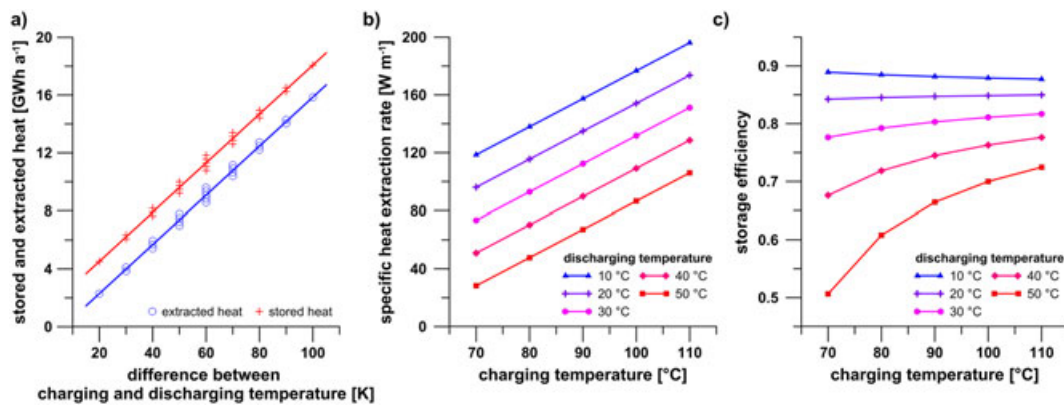
Figure 8. (a) Stored and extracted heat as a function of the difference between the charging temperature and the discharging temperature; correlation of the specific heat extraction rate (b) as well as the storage efficiency (c) and the charging temperature for different discharging temperatures. The results are shown for the storage system with 37 borehole heat exchangers (BHEs), a BHE length of 500 m and a spacing of 5 m in the 30th year of operation.
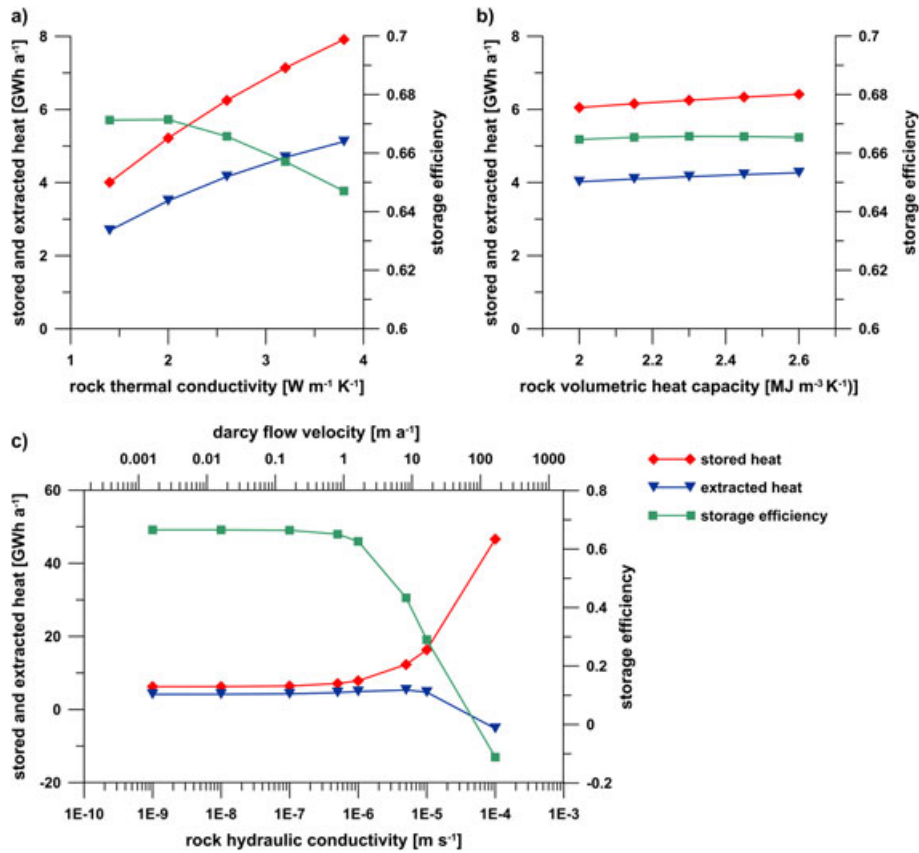
Figure 9. Storage performance in a characteristic storage setup (19 borehole heat exchangers, spacing 5 m and length 500 m) for the variations of (a) the thermal conductivity, (b) the volumetric heat capacity and (c) the hydraulic conductivity of the reservoir rocks. The results for the hydraulic conductivity variations are based on a hydraulic gradient of 5% in the underground model. The corresponding Darcy flow velocities are shown on the upper abscissa.

parameters and show that MD-BTES performance is sensitive to many of these variables. Evidently, many more parameters like thermo-physical properties of BHE materials and flow rates, for example, can have a significant influence. Yet, their number had to be restricted because of the design of the simulation experiments to limit the computational effort. Furthermore, the interdependent influence of variables has only been investigated for the borefield design (i.e. simultaneous change of the number of BHEs, their length and their spacing) and for the inlet temperatures during the charging and discharging cycles. However, the effect of changing charging and discharging temperatures indicates a correlation between several variables. Similarly, the value of the ideal BHE spacing depends on a balance between the thermal BHE interaction and the storage depletion, which is ultimately governed by the duration of the extraction and storage periods in correlation with the thermal diffusivity of the rock [22]. An interdependent effect of these variables on the system performance is obvious, but cannot be quantified because of the setup of variable variation across the simulation experiments. Therefore, future simulations may be based on experimental designs, which allow for the observation of such interdependency effects.

Our results confirm earlier findings (e.g. [10,17,18]) that BTES systems require several years of operation to reach a relatively balanced state. Although the system performance still rises even after 30 years of operation, the annual increase slows down significantly after the first couple of charging and discharging cycles. MD-BTES with a BHE spacing of 5 m achieve 80% of their final storage efficiency (i.e. storage efficiency in the 30th year) after 3–6 years (Figure 10). Furthermore, the strong dependency of the storage performance on its size indicates that under the considered scenario conditions, only large-scale applications are viable. With a heat demand of more than $6\,\mathrm{GWh\,a^{-1}}$, respective MD-BTES can exceed 70% storage efficiency, which is within the range of other underground thermal energy storages: Reuss *et al.* [39] carried out a numerical modelling study on a high temperature BTES, which resulted in a storage efficiency of 64% for the optimal storage design. Analyses of heat budget data of an Aquifer Thermal Energy Storage in Rostock and a BTES in Neckarsulm (both Germany) for the years 2008 to 2012 yielded an average storage efficiency of 69% and 79%, respectively [53]. Efficiencies of 46% are reported for the BTES in Anneberg, Sweden (quasi steady-state
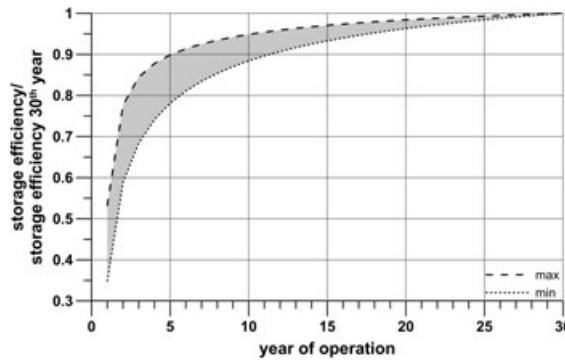
Figure 10. Range of the evolution of storage efficiency related to the storage efficiency in the 30th year of operation (systems with a borehole heat exchanger spacing of 5 m).

conditions, eighth year of operation) [54] and 54% for the BTES of the Drake Landing Solar Community, Okotoks, Canada (fourth year of operation) [17].

The present study emphasizes that higher discharging temperatures result in a significant decrease of the storage capacity and efficiency. Accordingly, the installation of a heat pump can be favourable for heating systems with high return temperatures of more than 50 °C (e.g. conventional radiators) as it reduces discharging temperatures. In contrast, panel heating systems like floor heating with low return temperatures (<30 °C) can reach high storage efficiencies without the utilization of a heat pump. Coupled simulations of all system components are necessary for an optimal fine-tuning of the heating and storage system and a potential heat pump.

5. CONCLUSIONS AND OUTLOOK

In the presented study, numerical simulations of various MD-BTES settings have been carried out. The effects of different storage configurations, fluid temperatures and subsurface properties were compared. The results reveal that with a proper dimensioning of the system and in convenient geological and hydrogeological framework conditions, MD-BTES are eminently suitable for seasonal heat storage. Furthermore, the collected data give reference points for an optimal design, favourable fluid temperatures to operate the storage and appropriate rock properties.

It is clarified that there is an optimal BHE spacing, where the highest storage efficiencies and the highest heat extraction rates are achieved. Increasing the number of BHEs or the BHE length enhances both the storage capacity as well as the storage efficiency. Under the very simplified operating procedure and subsurface conditions, storage efficiencies of up to 83% are reached. By adjusting supply temperatures for the heating system or increasing the loading temperature of the storage, the efficiencies can even be further improved. Groundwater flow has to be limited, as it can significantly affect the performance of MD-BTES by dissipating the stored heat out of the system.

Future work will focus on realistic charging and discharging scenarios to prove that MD-BTES will work not only under simplified assumptions but under realistic conditions as well. Therefore, coupled simulations of the storage system, the heat supply system and the heating system will be implemented. Further studies will be conducted to determine the actual impact on shallow groundwater aquifers to give evidence of the advantages of MD-BTES compared with shallow BTES systems. Moreover, the dependency of the storage performance on the BHE spacing puts high requirements on the verticality of the boreholes. Accordingly, suitable drilling technologies have to be identified and compared from a technical and economical perspective. In addition to that, a detailed economic analysis of the whole storage systems is planned to find an optimal system design from a financial point of view.

NOMENCLATURE

BTES	= borehole thermal energy storage
MD-BTES	= medium deep borehole thermal energy storage
BHE	= borehole heat exchanger
CHP	= combined heat and power plant

ACKNOWLEDGEMENTS

REFERENCES

1. IEA (International Energy Agency). Heating without global warming – market developments and policy considerations for renewable heat. OECD/IEA: Paris, 2014.

2. Pinel P, Cruickshank CA, Beausoleil-Morrison I, Wills A. A review of available methods for seasonal storage of solar thermal energy in residential applications. *Renewable and Sustainable Energy Reviews* 2011; **15** (7):3341–3359. doi:10.1016/j.rser.2011.04.013.

3. Dincer I, Dost S. A perspective on thermal energy storage systems for solar energy applications. *International Journal of Energy Research* 1996; **20**(6):547–557. doi:10.1002/(SICI)1099-114X(199606) 20:6<547::AID-ER173>3.0.CO;2-S.

4. Braun JE, Klein SA, Mitchell JW. Seasonal storage of energy in solar heating. *Solar Energy* 1981; **26** (5):403–411. doi:10.1016/0038-092X(81)90219-X.

5. Raine RD, Sharifi VN, Swithenbank J. Optimisation of combined heat and power production for buildings using heat storage. *Energy Conversion and Management* 2014; **87**:164–174. doi:10.1016/j. enconman.2014.07.022.

6. Mago PJ, Luck R. Evaluation of a base-loaded combined heating and power system with thermal storage for different small building applications. *International Journal of Energy Research* 2013; **37**(2):179–188. doi:10.1002/er.1892.

7. Mago PJ, Luck R, Knizley A. Combined heat and power systems with dual power generation units and thermal storage. *International Journal of Energy Research* 2014; **38**(7):896–907. doi:10.1002/er.3089.

8. Dincer I, Rosen MA. *Thermal Energy Storage: Systems and Applications* (2nd). Wiley: Hoboken, N.J., 2011.

9. Dincer I. Thermal energy storage systems as a key technology in energy conservation. *International Journal of Energy Research* 2002; **26**(7):567–588. doi:10.1002/er.805.

10. Schmidt T, Mangold D, Müller-Steinhagen H. Central solar heating plants with seasonal storage in Germany. *Solar Energy* 2004; **76**(1-3):165–174. doi:10.1016/j. solener.2003.07.025.

11. Xu J, Wang RZ, Li Y. A review of available technologies for seasonal thermal energy storage. *Solar Energy* 2014; **103**:610–638. doi:10.1016/j. solener.2013.06.006.

12. Hesaraki A, Holmberg S, Haghighat F. Seasonal thermal energy storage with heat pumps and low temperatures in building projects – a comparative review. *Renewable and Sustainable Energy Reviews* 2015; **43**:1199–1213. doi:10.1016/j.rser.2014.12.002.

13. Bauer D, Marx R, Nußbicker-Lux J, Ochs F, Heidemann W, Müller-Steinhagen H. German central solar heating plants with seasonal heat storage. *Solar Energy* 2010; **84**(4):612–623. doi:10.1016/j. solener.2009.05.013.

14. Nordell B. *A Borehole Heat Store in Rock at the University of Lulea, The Lulevarme Project 1982–1988*. Swedish Council for Building Research: Stockholm, Sweden, 1990.

15. Nordell B. *The Borehole Heat Store in Rock at the Lulea University of Technology, Constructional and Operational Experience, The Lulevarme Project 1982–1985*. Swedish Council for Building Research: Stockholm, Sweden, 1987.

16. Gao L, Zhao J, Tang Z. A review on borehole seasonal solar thermal energy storage. *Energy Procedia* 2015; **70**:209–218. doi:10.1016/j.egypro.2015.02.117.

17. Sibbitt B, Mcclenahan D, Djebbar R, Thornton J, Wong B, Carriere J, Kokko J. The performance of a high solar fraction seasonal storage district heating system – five years of operation. *Energy Procedia* 2012; **30**:856–865. doi:10.1016/j.egypro.2012.11.097.

18. Lundh M, Dalenbäck JO. Swedish solar heated residential area with seasonal storage in rock: initial evaluation. *Renewable Energy* 2008; **33**(4):703–711. doi:10.1016/j.renene.2007.03.024.

19. Andersson O, Ekkestubbe J, Ekdahl A. UTES (underground thermal energy storage) – applications and market development in Sweden. *Journal of Energy and Power Engineering* 2013; **7**(4):669–678.

20. Dincer I, Rosen MA. A unique borehole thermal storage system at University of Ontario Institute of Technology. In *Thermal Energy Storage for Sustainable Energy Consumption*, Paksoy H (ed.). Springer Netherlands: Dordrecht, 2007; 221–228.

21. Nordell B, Hellström G. High temperature solar heated seasonal storage system for low temperature heating of buildings. *Solar Energy* 2000; **69**(6):511–523. doi:10.1016/S0038-092X(00)00120-1.

22. Reuss M. 6 – the use of borehole thermal energy storage (BTES) systems. In: *Advances in Thermal Energy Storage Systems*, Cabeza LF (ed.), Woodhead Publishing, 2015, 117–147.

23. Andersson S, Eriksson A. Seasonal storage in hard rock – multiple well system. In *Thermal Storage of Solar Energy: Proceedings of an International TNO-*

Symposium Held in Amsterdam, The Netherlands, 5–6 November 1980, Ouden C (ed.). Springer Netherlands: Dordrecht, 1981; 249–258.

24. Beckmann G, Gilli PV. *Thermal Energy Storage: Basics-Design-Applications to Power Generation and Heat Supply*. Springer: Wien; New York, 1984.

25. Givoni B. Underground longterm storage of solar energy – an overview. *Solar Energy* 1977; **19**(6):617–623. doi:10.1016/0038-092X(77)90021-4.

26. Hellström G. *Duct Ground Heat Storage Model – Manual for Computer Code*. Department of Mathematical Physics, University of Lund: Lund, Sweden, 1989.

27. Lund PD, Östman MB. A numerical model for seasonal storage of solar heat in the ground by vertical pipes. *Solar Energy* 1985; **34**(4):351–366. doi:10.1016/0038-092X(85)90048-9.

28. Nordell B. Borehole heat store design optimization, Luleå University of Technology, Dissertation, 1994, 196.

29. Brons HJ, Griffioen J. Appelo CaJ, Zehnder AJB. (Bio)geochemical reactions in aquifer material from a thermal energy storage site. *Water Research* 1991; **25**(6):729–736. doi:10.1016/0043-1354(91)90048-U.

30. Griffioen J. Appelo CaJ. Nature and extent of carbonate precipitation during aquifer thermal energy storage. *Applied Geochemistry* 1993; **8**(2):161–176. doi:10.1016/0883-2927(93)90032-C.

31. Brielmann H, Griebler C, Schmidt SI, Michel R, Lueders T. Effects of thermal energy discharge on shallow groundwater ecosystems. *FEMS Microbiology Ecology* 2009; **68**(3):273–286.

32. Hall EK, Neuhauser C, Cotner JB. Toward a mechanistic understanding of how natural bacterial communities respond to changes in temperature in aquatic ecosystems. *The ISME Journal* 2008; **2**(5):471–481.

33. Hähnlein S, Bayer P, Ferguson G, Blum P. Sustainability and policy for the thermal use of shallow geothermal energy. *Energy Policy* 2013; **59**:914–925. doi:10.1016/j.enpol.2013.04.040.

34. Brielmann H, Lueders T, Schreglmann K, Ferraro F, Avramov M, Hammerl V, Blum P, Bayer P, Griebler C. Oberflächennahe Geothermie und ihre potenziellen Auswirkungen auf Grundwasserökosysteme. *Grundwasser* 2011; **16**(2):77–91. doi:10.1007/s00767-011-0166-9.

35. Bonte M, Stuyfzand PJ, Hulsmann A, Van Beelen P. Underground thermal energy storage: environmental risks and policy developments in the Netherlands and European Union. *Ecology and Society* 2011; **16**.

36. Hähnlein S, Bayer P, Blum P. International legal status of the use of shallow geothermal energy. *Renewable and Sustainable Energy Reviews* 2010; **14**(9):2611–2625. doi:10.1016/j.rser.2010.07.069.

37. Dehkordi SE, Schincariol RA. Guidelines and the design approach for vertical geothermal heat pump systems: current status and perspective. *Canadian Geotechnical Journal* 2014; **51**(6):647–662. doi:10.1139/cgj-2012-0205.

38. Kizilkan O, Dincer I. Borehole thermal energy storage system for heating applications: thermodynamic performance assessment. *Energy Conversion and Management* 2015; **90**:53–61. doi:10.1016/j.enconman.2014.10.043.

39. Reuss M, Beck M, Müller JP. Design of a seasonal thermal energy storage in the ground. *Solar Energy* 1997; **59**(4–6):247–257. doi:10.1016/S0038-092X(97)00011-X.

40. Schulte DO, Welsch B, Boockmeyer A, Rühaak W, Bär K, Bauer S, Sass I. Modeling insulated borehole heat exchangers. *Environmental Earth Sciences* 2016; **75**:1–12. doi:10.1007/s12665-016-5638-x.

41. Bär K, Rühaak W, Welsch B, Schulte D, Homuth S, Sass I. Seasonal high temperature heat storage with medium deep borehole heat exchangers. *Energy Procedia* 2015; **76**:351–360. doi:10.1016/j.egypro.2015.07.841.

42. FEFLOW finite element subsurface flow and transport simulation system – recent release 6.2 (DHI-WASY GmbH, Berlin, 2014).

43. Diersch H-JG. Feflow – finite element modeling of flow, mass and heat transport in porous and fractured media. Springer: Berlin; Heidelberg, 2014.

44. Diersch H-JG, Bauer D, Heidemann W, Rühaak W, Schätzl P. Finite element modeling of borehole heat exchanger systems: part 1. Fundamentals. *Computers & Geosciences* 2011; **37**(8):1122–1135. doi:10.1016/j.cageo.2010.08.003.

45. Eskilson P, Claesson J. Simulation model for thermally interacting heat extraction boreholes. *Numerical Heat Transfer* 1988; **13**(2):149–165. doi:10.1080/10407788808913609.

46. Diersch H-JG, Bauer D, Heidemann W, Rühaak W, Schätzl P. Finite element modeling of borehole heat exchanger systems: part 2. Numerical simulation. *Computers & Geosciences* 2011; **37**(8):1136–1147. doi:10.1016/j.cageo.2010.08.002.

47. Mielke P, Bauer D, Homuth S, Götz A, Sass I. Thermal effect of a borehole thermal energy store on the subsurface. *Geothermal Energy* 2014; **2**(1): 1–15, doi:10.1186/s40517-014-0005-1.

48. Nakevska N, Schincariol RA, Dehkordi SE, Cheadle BA. Geothermal waste heat utilization from in situ thermal bitumen recovery operations. *Groundwater* 2015; **53**(2): 251–260, doi:10.1111/gwat.12196.

49. Sanner B. High temperature underground thermal energy storage – state-of-the-art and prospects. In *Giessener geologische Schriften*, Vol. **67**. 1999; 82.

50. Stober I, Bucher K. Hydraulic properties of the crystalline basement. *Hydrogeology Journal* 2007; **15** (2):213–224. doi:10.1007/s10040-006-0094-4.

51. Shewchuk JR. Triangle: engineering a 2D quality mesh generator and delaunay triangulator. In *Applied Computational Geometry Towards Geometric Engineering: FCRC'96 Workshop, WACG'96 Philadelphia, PA, May 27–28, 1996 Selected Papers*, Lin MC, Manocha D (eds.). Springer: Berlin; Heidelberg, 1996; 203–222.

52. Yamaguchi H. *Engineering Fluid Mechanics*. Springer: Dordrecht, 2008.

53. Bauer D, Drück H, Heidemann W, Marx R, Nußbicker-Lux J, Ochs F. *Solarthermie2000plus: Wissenschaftlich-technische Begleitung des Förderprogramms Solarthermie2000plus zu solar unterstützter Nahwärme und Langzeit-Wärmespeicherung*. Institute of Thermodynamics and Thermal Engineering (ITW): Stuttgart, Germany, 2013.

54. Heier J, Bales C, Sotnikov A, Ponomarova G. Evaluation of a high temperature solar thermal seasonal borehole storage. In: ISES Solar World Congress 2011.

SUPPORTING INFORMATION

Additional supporting information may be found in the online version of this article at the publisher's website:

Appendix C:
Optimization of Medium-Deep Borehole Thermal Energy Storage Systems

Published as:

Optimization of Medium-Deep Borehole Thermal Energy Storage Systems

Daniel Otto Schulte,*[a, b] Wolfram Rühaak,[a, b] Sergey Oladyshkin,[c] Bastian Welsch,[a, b] and Ingo Sass[a, b]

Arrays of medium-deep borehole heat exchangers are characterized by their slow thermal response and large storage capacity. They represent suitable thermal energy storage systems for seasonally fluctuating heat sources such as solar energy or district heating grids. However, the economic feasibility of these systems is compromised by high investment costs, especially by the expensive drilling of the boreholes. This study presents an approach for the simulation and optimization of borehole thermal energy storage systems. To ex-emplify the concept, a software tool is used to optimize the number and length of borehole heat exchangers with regard to a specific annual heat demand. The tool successfully determines the ideal size of the thermal energy storage. Furthermore, the prediction of the system's performance also indicates that borehole thermal energy storage systems only operate efficiently in large-scale applications. With the presented tool, many aspects of borehole thermal energy storage systems can be simulated and optimized.

Introduction

Approximately 65% of the total end energy consumption in private households accounts for heating in Germany.[1] Consequently, there is a high potential for energy conservation in this sector. Renewable energy sources such as solar collectors are increasingly used to cover this heat demand, to reduce the consumption of fossil fuels, and to mitigate CO_2 emissions. In summer, solar thermal collector panels provide excess heat when the heating demand is low. Yet, during the winter time, a secondary system has to provide the heat, as the situation is reversed. Likewise, the increased use of district heating grids is supposed to play an important role in the future of renewable energies.[2,3] They are often powered by combined heat and power plants (CHPs). Whereas electricity is needed throughout the year, the seasonality of the heat demand renders CHPs inefficient during summer when the heat demand is low. Thus, seasonal storage can enhance the efficiency of CHPs in district heating grids and solar collector systems by shifting excess heat to the winter time.

Early considerations for solar thermal energy systems envisaged water tanks for seasonal heat storage. As the water tank is the most expensive component in the system, it is imperative to exploit the decreasing price per storage volume with increasing size.[4] Whereas such water tanks require considerable space on the surface, borehole thermal energy storage (BTES) systems need only a small amount of space to tap into a large volume of subsurface rock, which can serve as the heat storage. Additionally, geothermal heat feeds such a system. This combination of solar heat usage, seasonal storage, and geothermal heat has already been demonstrated in practice to be highly efficient with shallow BTES systems.[5–8] Furthermore, because of this combination, a secondary heating system to back up the solar collectors is rendered dispensable.

However, shallow aquifers are often used for the extraction of drinking water. In Germany and many other countries, legal regulations often restrict alterations of groundwater that may have a negative impact on drinking water quality.[9] Thus, excessive heating, which can induce microbial growth, has to be prevented in these aquifers.[10,11] Given that solar collectors can provide a temperature output of 100°C and above[12] and that district heating grids operate at supply temperatures of approximately ≥80°C,[13] storage of the excess amount of heat in greater depth is favorable. Ideally, a medium-deep borehole thermal energy storage (MD-BTES) system should reach a couple of hundred meters deep and should be thermally insulated at the topmost part. Shallow borehole heat exchangers (BHEs) are often polymer U pipes or double U pipes, whereas deeper BHEs are usually coaxial pipe systems with a high thermal conductivity outer

[a] D. O. Schulte, Dr. W. Rühaak, B. Welsch, Prof. Dr. I. Sass
Graduate School of Excellence Energy Science and Engineering
Technische Universität Darmstadt
Jovanka-Bontschits-Strasse 2, 64287 Darmstadt (Germany)
E-mail: schulte@geo.tu-darmstadt.de

[b] D. O. Schulte, Dr. W. Rühaak, B. Welsch, Prof. Dr. I. Sass
Geothermal Science and Technology
Technische Universität Darmstadt
Schnittspahnstrasse 9, 64287 Darmstadt (Germany)

[c] Dr. S. Oladyshkin
Institute for Modelling Hydraulic and Environmental Systems (LS3)
University of Stuttgart
Pfaffenwaldring 5A, 70569 Stuttgart (Germany)

steel pipe. The inner pipe is insulated to reduce the thermal interaction between the up- and down-streaming fluids. In summer, the warm fluid is injected into the inner pipe for heat storage, whereas in winter the cold fluid is injected into the annular gap for heat extraction.[14]

Typically, permeability decreases with depth, which prevents removal of heat from the storage by ground water flow. Furthermore, the stored heat will not dissipate as fast as in shallow storage systems owing to a reduced lateral temperature gradient. Consequently, the extraction temperatures will be higher than those for shallow BTES systems, which only permit moderate injection temperatures. This increases the performance of the heat pump and possibly allows for use with conventional radiator heating systems, which require a higher supply temperature.[14]

MD-BTES systems are operated in seasonal charging and discharging cycles. Excess thermal energy is stored in summer. During winter, it is extracted again for heating purposes. The performance is quantified by the heat, which is stored and extracted during each cycle [Eq. (1)] (Figure 1).
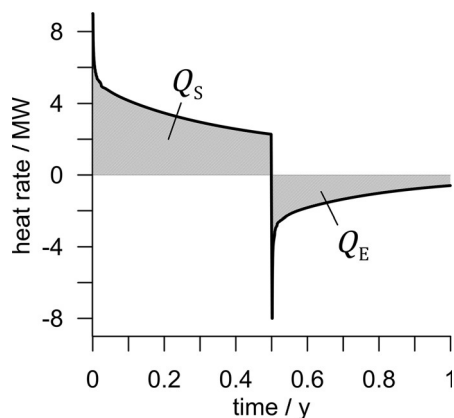

Figure 1. Evolution of heat storage and extraction; Q_S: stored heat, Q_E: extracted heat.

$$Q_{S/E} = \int_t \Delta T \cdot \rho_f \cdot c_f \cdot \dot{V} \, dt \tag{1}$$

in which $Q_{S/E}$ is the stored/extracted heat, ΔT is the temperature difference between the inlet and outlet, ρ_f is the working fluid density, c_f is the specific heat capacity of the working fluid, $\dot{V}$ is the working fluid flow rate, and t is the time of operation.

The ratio of extracted heat to stored heat defines the storage coefficient S [Eq. (2)], whereas the specific heat extraction rate Q_{spec} describes the system's efficiency of heat exchange between BHEs and the subsurface [Eq. (3)]:

$$S = \left| \frac{Q_E}{Q_S} \right| \tag{2}$$

$$Q_{spec} = \frac{Q_E}{l_{tot} \cdot t_E} \tag{3}$$

in which Q_{spec} is the specific heat extraction rate, l_{tot} is the total drilled length, and t_E is the time of operation in the heat extraction mode.

In general, the difference between the inlet and outlet temperatures of the working fluid in the BHEs decreases over the charging or discharging cycle because of continuous heat exchange with the reservoir (Figure 2). Owing to diffu-
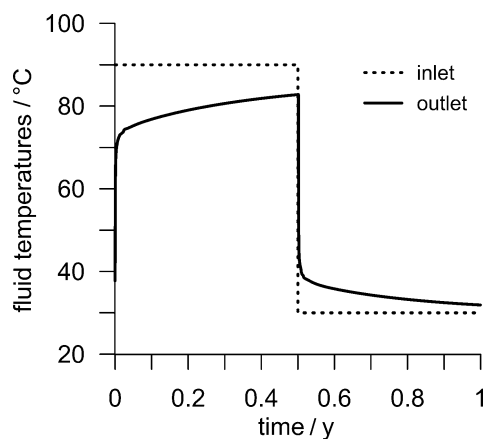
Figure 2. Evolution of the BHE inlet and outlet temperatures.

sion processes, not all of the stored heat can be recovered. Some of the thermal energy remains in the reservoir and begins to create a thermal plume in the subsurface. This thermal plume decreases the lateral temperature gradient between the BHEs and the surrounding rock, which results in declining heat storage over summer, but enhanced heat extraction in winter and increased storage efficiency (Figure 3).

Drilling is the critical cost factor in the development of a geothermal reservoir. Deeper boreholes significantly raise the costs for a high-temperature underground storage system. It is necessary to simulate the performance of a planned system prior to the investment of building a storage platform. The design of the borehole heat exchanger array has
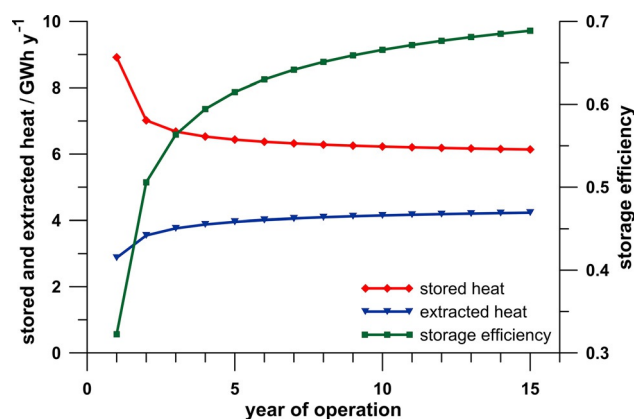
Figure 3. Evolution of storage performance; model: 19 BHEs, BHE length: 500 m, BHE spacing: 5 m, flow rate: 4 L s^{-1}, inlet temperature during storage: 90 °C, inlet temperature during extraction: 30 °C.

to be optimized for the heating purpose to avoid an oversized and, therefore, overpriced system. Earlier optimization approaches used analytical 2D finite line source models.[15,16] We present a MATLAB-based toolbox, which can numerically simulate and optimize the 3D design of an MD-BTES system. Instead of using finite line source models, the thermal interactions of the BHEs are considered by a more detailed solution.

In the proxy model-based optimization section, the basic methods that are used in the optimization process are explained. Afterwards, the optimization of the performance of the MD-BTES system is demonstrated by an arbitrary example. Finally, we discuss the results with respect to real-case applications.

Proxy Model Based Optimization

To optimize the design of an MD-BTES system, many configurations representative for the range of variability of the design parameters have to be evaluated. The seasonal operation is numerically simulated for each configuration to predict the thermal behavior of the MD-BTES system. Given that the performance of an MD-BTES system changes significantly over the first couple of cycles, several years of operation have to be simulated. As a result, the computational time for a simulation is too long to allow the direct use of the numerical model in an optimization algorithm. To bypass this problem, a surrogate proxy model is trained by numerical simulations. The proxy model can be evaluated in a matter of seconds by the optimization algorithm. However, as the proxy model is not exact, the following iterative procedure is performed to assure robustness of the optimization: The best solution for the proxy model is verified by an additional numerical simulation with the parameters found by the optimization algorithm. In case the verification differs too much from the proxy model prediction, the numerical simulation can serve as an additional training simulation to refine the proxy model for a new optimization. This process is repeated until the mismatch of the optimal solution between proxy model and numerical model is sufficiently small (Scheme 1).

Physical model formulation

Simulation of the operation of an MD-BTES system comprises simulation of subsurface heat transport and thermal interaction of the BHEs with the surrounding rock. The transient subsurface heat diffusion is calculated by solving Fourier's law of heat conduction for the model domain [Eq. (4)]:

$$\rho_s c_s \frac{\partial T}{\partial t} = \nabla \cdot \lambda \nabla T + q \tag{4}$$

in which ρ_s is the soil density, c_s is the volumetric heat capacity of soil, T is the temperature, t is the time, λ is the thermal conductivity, and q is the heat sources and sinks. Given that low-permeable rock bodies with negligible ground water
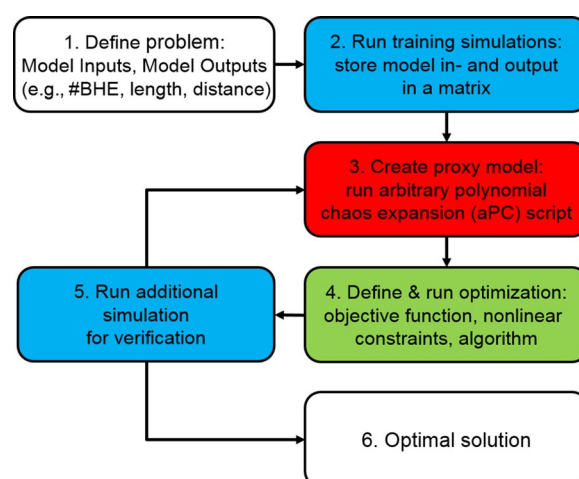
Scheme 1. General process of optimizing the design of an MD-BTES system.

flow are targeted for MD-BTES systems, convective heat transfer is disregarded. Also, temperature dependency of the material parameters is not taken into account. The standard Galerkin method[17] is applied in an adapted MATLAB[18] implementation for finite elements[19] on an unstructured tetrahedron mesh.[20] A predictor–corrector method is used with a second-order Adams–Bashforth predictor and a Crank–Nicolson corrector for automated time stepping.[21]

The thermal interaction of the BHEs is calculated by a 1D analytical thermal-resistance and capacity model.[22–24] Fed with inlet temperature and flow rate data, it provides the temperature distribution in the inlet and outlet pipes in predefined depth levels. The solution takes into account all thermal and hydraulic parameters of the BHE materials and the borehole wall temperature. In the finite element mesh, the BHEs are discretized as vertical lines of mesh nodes. The temperature at these nodes defines the borehole wall temperature and is passed to the analytical solution. In return, the analytical solution sets heat sources on the basis of the thermal resistances within the BHEs and the difference between the borehole wall temperature and the calculated BHE fluid temperature at the corresponding nodes. This results in a contribution to the right-hand side term of the respective equations.[25] As the heat source terms depend on the temperature, which is the solution vector, the system of equations is nonlinear [Eq. (5)]:

$$M\dot{T} + KT = F(T) \tag{5}$$

in which M is the heat capacity matrix, K is the thermal conductivity matrix, F is the right-hand side vector including source terms, and T is the solution vector for temperature. A Picard iteration scheme is applied on the corrector to solve the system of nonlinear equations, whereas the predictor provides a tentative solution to start the iteration loop.[26]

Prior to the study, the code was tested and showed good agreement with FEFLOW[25] in a benchmark simulation. For the benchmark, the BHE outlet temperatures in the
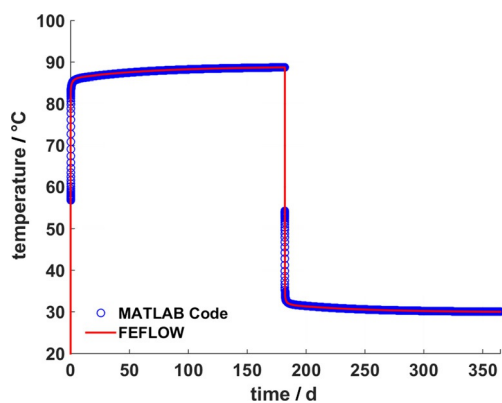
Figure 4. Comparison of BHE outlet temperatures of the central pipe of a BHE array in the MATLAB implementation and in FEFLOW; model: 7 BHEs of 100 length, 182 days of heat storage (90 °C inlet temperature) and 183 days of heat extraction (30 °C inlet temperature) at 2.5 L s^{-1} injection rate.

MATLAB implementation and in FEFLOW were compared against each other (Figure 4).

Proxy model by arbitrary polynomial chaos expansion

The physical model described in the previous section is used to construct a proxy model on the basis of the theory of polynomial chaos expansion (PCE). The basic idea of PCE was introduced by Wiener[27] and consists in the construction of the proxy model (response surface) of the original model with the help of an orthonormal polynomial basis in the parameter space. Simply, the dependency of the model output on all relevant input parameters is approximated by projection onto a high-dimensional polynomial. The key attractive features of all PCE techniques are the high-order approximation of the model combined with its computational speed.

Formally, we will consider the vector of N input parameters $\omega = \{\omega_1, \ldots, \omega_N\}$ for the physical model that is simply denoted as $\Omega = f(\omega)$. Our goal is to capture the influence of all parameters ω on the model output Ω. According to PCE theory, the model output Ω can be approximated by polynomials $\Psi_i(\omega)$ [Eq. (6)]:

$$\Omega(\omega) \approx \sum_{i=1}^{M} c_i(\omega) \Psi_i(\omega) \tag{6}$$

The number M of polynomials $\Psi_i(\omega)$ and the corresponding coefficients c_i depend on the total number of analyzed input parameters N and on the order d of the polynomial representation [Eq. (7)]:

$$M = \frac{(N + d)!}{(N! \cdot d!)} - 1 \tag{7}$$

The coefficients $c_i(\omega)$ quantify the dependency of the model output Ω on the input parameters ω for each desired point in the parameter space, which results in a surrogate for model Ω.

In the current paper, we will apply a recent generalization of the PCE technique known as the arbitrary polynomial chaos (aPC).[28] In aPC, the multidimensional orthonormal polynomial basis can be constructed for arbitrary probability distribution shapes of input parameters and, in addition, can even work with unknown distribution shapes if only a few statistical moments can be inferred from limited data or from expert elicitation. To project the MD-BTES model response onto an orthogonal polynomial basis, a uniform distribution is assumed for the modeling variables, which is simply dictated by equal interest to all possible outcomes of the physical model. The orthogonal polynomial basis of order d can be constructed according to Equation (4) in Oladyshkin and Nowak.[28]

To determine the unknown coefficients $c_i(\omega)$ of the proxy model, the original model is run at least once, but preferably more often, for every input parameter by using so-called training simulations with various sets of the input parameters (see details in the next section). Such training simulations are used to create an initial prediction for the following optimization procedure. However, to assure robustness of the overall modeling procedure, the quality of the proxy model is iteratively improved by incorporating additional simulations indicated by the optimization algorithm: specifically, the performance of the ideal design found by the optimization algorithm is validated by an additional numerical simulation. The approximation error of the proxy model must not be bigger than 1 %. If the verification simulation results in a violation of this criterion, it is used as an additional training simulation for refinement of the proxy model. Thus, a new projection of the model onto the orthonormal basis is performed by using all cumulatively available training simulation within the least-squares collocation method.[29, 30] The optimization is then repeated by using the refined proxy model for the constraint function. From a practical point of view, the computational costs of our framework are dominated by the model calls required for constructing the surrogate model.

Mathematical optimization

Drilling is the cost-critical factor and needs to be optimized. Thus, the fitness function y for this study is the total drilled borehole length, which is simply the product of the number of BHEs and their length [Eq. (8)]. Additionally, the borehole length is penalized against the number of BHEs, because drilling costs rise exponentially with depth:[31]

$$y = x_1 \cdot x_2 \cdot e^{(a \cdot x_2)} \tag{8}$$

in which x_1 is the number of BHEs, x_2 is the BHE length, and a is a scaling factor. The optimization algorithm tries to minimize the value for y by altering the number of BHEs and their length. Each parameter combination represents a certain design for an MD-BTES system, the performance of which has to meet a specific requirement. In the presented

study, it has to cover a building's heat demand after a certain amount of operation time. This represents a constraint to the optimization algorithm: the MD-BTES system cannot be indefinitely small, as this would lead to a vanishingly low performance.

The design parameters for MD-BTES systems can include discrete variables such as the number of BHEs or industrial standard sizes for pipes. Consequently, the optimization algorithm has to be able to handle discrete features. Genetic algorithms[32] can solve mixed integer optimization problems, that is, the variable parameters are real or integer values. Hence, the optimal design for an MD-BTES system is determined with a genetic algorithm, which is included in the MATLAB Global Optimization Toolbox.[33] The integer variables can relate to discrete ordinate values or even categories. Each combination of variables constitutes an individual, whereas a set of individuals represents a population. For every iteration, called generation in genetic algorithm terminology, the individuals of a population are tested by their fitness function score. The algorithm tries to minimize the score partly by combining variable values of individuals with a low score and partly by choosing random values for the individuals of the next population, which are tested in the following generation. A defined number of best individuals, called elite, make it to the next generation unaltered, regardless of the algorithm's choices.

As mentioned before, predicting the performance of an MD-BTES system requires a numerical simulation. The genetic algorithm has to evaluate hundreds of parameter combinations to converge on an optimal solution. It only stops if the best individual's score cannot be improved more than a predefined fitness function tolerance after a predefined number of so-called stall iterations. Given that the performance of each tested configuration has to be checked against the constraint, this results in an enormous computational effort: depending on the model size a single numerical simulation can take a few days up to several weeks. To overcome this problem, we use a proxy model generated from significantly fewer numerical training simulations by arbitrary polynomial chaos expansion,[34] as mentioned in the previous section. Whereas the computational effort for larger models is still high, they have to be rendered only once. The resulting proxy model calculates the performance of the MD-BTES system in a matter of seconds, as only a polynomial function has to be evaluated instead of a numerical model.

Specifically tailored optimization of the simulation model can converge on an optimal solution with less model evaluations without the help of a proxy model. However, the performance of an MD-BTES system depends on many more parameters than the number of BHEs and their length (e.g., thermal properties of rock and BHE materials, radial distance of BHEs, operational parameters such as flow rate, etc.). A pre-existing proxy model can be easily expanded by additional training simulations to incorporate more model parameters. Furthermore, it is possible to formulate more than one optimization objective on the basis of the additional variable parameters. In general, this can be included in the fitness function as well as in the constraints to add to the detail of the model. The genetic algorithm in MATLAB's Global Optimization Toolbox is capable of multiobjective optimization. Whereas renewed optimization under altered considerations requires laborious changes to a specifically tailored solution and profound mathematical knowledge, the rather generic approach of using a genetic algorithm on a proxy model is a ready-to-use tool that allows quick re-evaluations of the optimization problem. Therein lies the main potential of this approach.

Training Model Setup

For the proxy training simulations, the varying MD-BTES configurations are applied to a standard model, which includes constant parameters for the subsurface (Table 1) as well as for the BHE materials (Table 2).

The finite element mesh is 100 m by 100 m wide with the BHE array in its center, whereas the depth of the model is variable and always 50 m more than the BHE length for the considered scenario. An initial temperature field is set, which corresponds to a geothermal gradient of 3 K per 100 m. Dirichlet boundary conditions are defined accordingly: 10 °C as an average annual near-surface temperature at the top,

Table 1. Geological model parameters.

Parameter	Value
thermal conductivity	2.6 W m^{-1} K^{-1}
density	2600 kg m^{-3}
specific heat capacity	800 J kg^{-1} K^{-1}
surface temperature boundary condition	10 °C
geothermal gradient	0.03 K m^{-1}

Table 2. BHE material and operational parameters.

Parameter	Value
radial distance between BHE	5 m
borehole diameter	0.1522 m
outer pipe, outer diameter	0.127 m
outer pipe, wall thickness	0.0056 m
outer pipe, thermal conductivity (steel)	54 W m^{-1} K^{-1}
inner pipe, outer diameter	0.075 m
inner pipe, wall thickness	0.0068 m
inner pipe, thermal conductivity (PE)	0.4 W m^{-1} K^{-1}
grout, thermal conductivity	2 W m^{-1} K^{-1}
working fluid dynamic viscosity (water)	0.000504 kg m^{-1} s^{-1}
working fluid density (water)	977 kg m^{-3}
working fluid specific heat capacity (water)	4145 J kg^{-1} K^{-1}
working fluid thermal conductivity (water)	0.65 W m^{-1} K^{-1}
flow rate	2.5 L s^{-1}
heat storage period	182 days
injection temperature during heat storage	90 °C
heat extraction period	183 days
injection temperature during heat extraction	30 °C
simulated time of operation	7 years

whereas the boundary condition at the bottom depends on the depth of the model for each respective scenario.

Predefined geometric relations determine the layout of the MD-BTES system for the different number of BHEs (Figure 5). The axial reference distance between the BHEs is set to 5 m. Preliminary simulations have shown that the ideal axial distance depends on the thermal properties of the subsurface and the BHE materials rather than the number or length of BHEs.
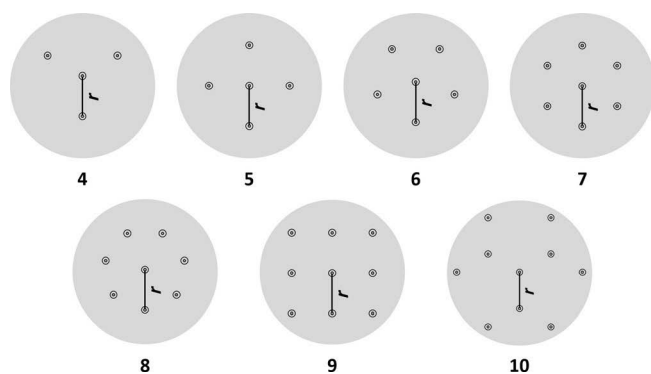

Figure 5. Templates for BHE array layouts, r: axial reference distance.

As a result, only the number and length of the BHEs are variable, and the performance of the MD-BTES system is evaluated on the basis of their variation. For each configuration, the same basic operational scenario is simulated. The MD-BTES system is charged and discharged at constant inlet temperatures and at a constant flow rate (Table 2), whereas the change of flow direction in the coaxial pipe for winter and summer time is accounted for.

To minimize the time for which a redundant heating system is required, an MD-BTES system has to meet the heat demand soon after its construction, which is typically long before the break-even point is reached. Whereas longer simulations would be beneficial for the economical assessment of the long-term operation, they are not necessary for finding the ideal design of an MD-BTES system, which can cover a specified heat demand after a few years. Hence, the basic operational scenario is only simulated for seven years to reduce the computational effort. The long-term operation can be simulated once the ideal design has been determined.

For the numerical simulation of the subsurface heat transport, the initial time step size is set to 1 s and is limited to a maximum of 4 h. It cannot grow by more than 20% per time step. The error tolerances for the time step control and Picard iterations are set to 0.001 and 0.005, respectively. If the Picard scheme fails to converge below the tolerance level within five iterations, the time step size is reduced by 20% and the time step is repeated.

The parameter space is sampled by a full factorial design[35] of experiments with nine levels for the BHE length and seven levels for the number of BHEs (Table 3). The resulting 63 numerical simulations each provide values for stored and extracted heat, storage coefficient, and specific

Table 3. Sampled parameter variations for proxy training.

BHE length [m]	100	133	166	200	233	300	366	433	500
Number of BHEs	4		5	6	7		8	9	10

heat extraction rate for all 7 heat charging/discharging cycles. Including the years of operation as an additional variable parameter, a total of 441 sample points serve as input to the aPC. The polynomial order for the proxy model is chosen in such a way that it is in good agreement with the training data without overfitting them (see the results).

The resulting aPC proxy model is a function of the number of BHEs, their length, and the year of operation and is used to constrain the fitness function as previously mentioned. It returns the value for extracted heat in MWh in the specified extraction cycle. Individuals must yield an aPC function value that satisfies a predefined constraint function to qualify as a possible solution. For the optimization, only the performance after the seventh year of operation is considered. Thus, the operational time is kept constant in the optimization and is only used afterwards with the proxy model to display the temporal evolution of the optimal performance of the MD-BTES system.

Comparably to Tester et al.,[31] the BHE length is penalized in the fitness function exponentially with a scaling factor $a = 7.51 \times 10^{-4}$. In a real case, the scaling factor should be deducted empirically from typical drilling cost data for the local geology.

For this study, two optimization scenarios are considered. In both cases, the constraint for the fitness function is set to 500 MWh minimum heat extraction. This resembles roughly the annual heat demand of a midsized energetically modernized office building. The second scenario includes, in addition, a constraint of 200 m on the minimum BHE depth to take into account a legal requirement (in this case fictional). In both cases, the objective of the genetic algorithm is to determine the smallest possible MD-BTES system that still provides enough heat to cover the annual demand. Preliminary simulations have shown that the increase in the system efficiency slows down after a few years (see Figure 3) Therefore, the requirement has to be met only after seven years of operation to rule out systems that turn out to be oversized later on. All settings for the genetic algorithm are summarized in Table 4.

Optimization of the Performance of the MD-BTES System

All 63 training simulations reflect the typical behavior of BTES systems: the storage efficiency increases over time (Figure 6) and bigger storage systems perform better than smaller ones. After seven years of operation, the storage coefficient ranges from approximately 22 to 50% (Figure 7), and the recovered heat during extraction ranges from approximately 90 to 1800 MWh depending on the storage size

Table 4. Settings for the genetic algorithm.

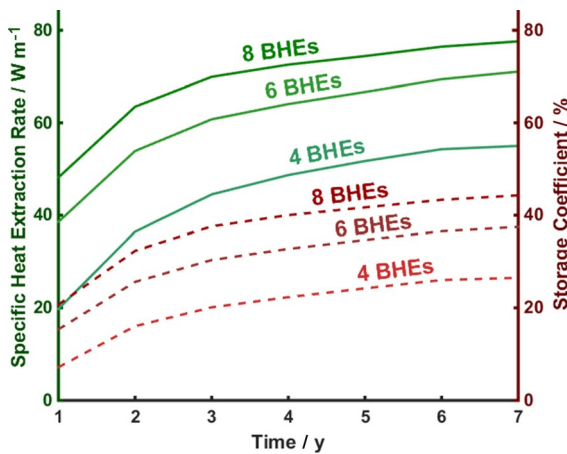| Parameter	Value
number of independent variables	3
integer variables	1, 3
lower bound, number of BHEs	4
upper bound, number of BHEs	10
lower bound, BHE length	100 m
upper bound, BHE length	500 m
lower bound, operational time	7 years
upper bound, operational time	7 years
fitness function	$y = x_1 \cdot x_2 \cdot e^{(a \cdot x_2)}$
scaling factor a	7.51×10^{-4}
population size	200
generations	500
number of elite individuals	3
stall generation limit	20
fitness function tolerance	1×10^{-6}
constraint C_1	500 MWh
constraint C_2	200 m
constraint function for scenario 1 and 2	$0 \geq -a PC \mathrm{proxy}(x_1, x_2)^{[a]} + C_1$
constraint function for scenario 2 only	$0 \geq -x_2 + C_2$
error tolerance (numerical to proxy model)	1%

Figure 7. Response surface of the storage coefficient after seven years of operation as a function of the number of BHEs and BHE length.
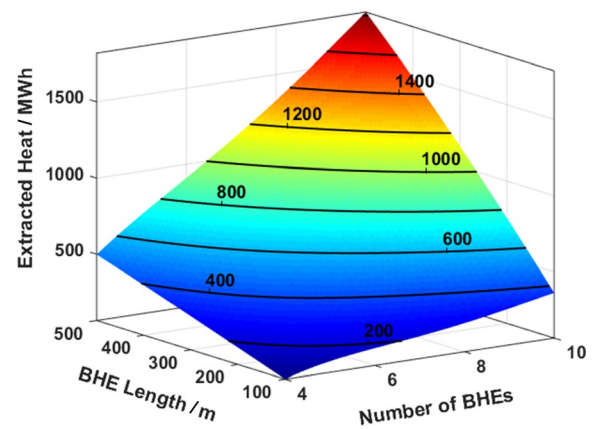
Figure 8. Response surface of extracted heat in the seventh year of operation as a function of the number of BHEs and BHE length.

Figure 6. Temporal evolution of the performance of a 250 m deep MD-BTES system with 4, 6, and 8 BHEs.
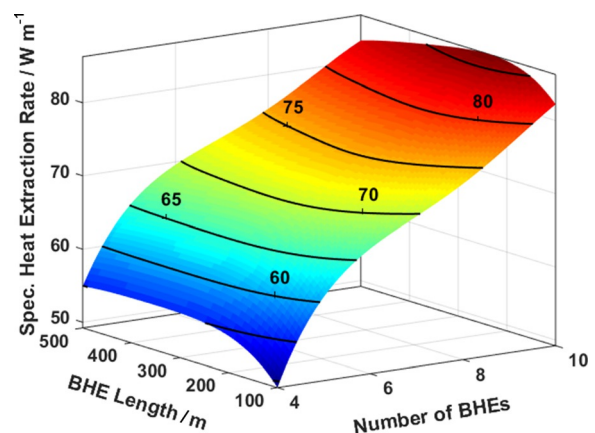
Figure 9. Response surface of specific heat extraction rate after seven years of operation as a function of the number of BHEs and BHE length.

(Figure 8). The specific heat extraction rate reaches values of up to 86 W m^{-1} (Figure 9).

Whereas the MATLAB implementation does not allow for parallel processing, several simulations can be run simultaneously in multiple MATLAB instances depending on the available CPU nodes. The computation time for each simulation ranges from 50 h (smallest model, 4 BHEs of 100 m length) to 95.3 days (biggest model, 10 BHEs of 500 m length), which corresponds to 0.17 and 7.89% of the total computation time of 1208.5 days, respectively. A complete list of all simulation results and the computational time is included in the Supporting Information.

The proxy model allows for fast evaluation in between the sampled training simulations. The quality of the proxy model is quantified by a mean relative approximation error (MRAE), which is the sum of relative approximation errors normalized by the sample size for each model output at the training sample points [Eq. (9)]:

$$\mathrm{MRAE}_i = \left| \frac{\sum_{j=1}^{n} {}^{y_{i,j,\mathrm{numerical}} - y_{i,j,\mathrm{proxy}}} / y_{i,j,\mathrm{numerical}}}{n} \right| \qquad (9)$$

in which y_i is the model output, j is the training simulation index, and n is the number of training simulations. By simple testing the polynomial degree can be set as high as fourth order. All MRAE values are summarized in Table 5. A

Table 5. Approximation errors of the fourth polynomial order proxy model.

Model output	MRAE [%]
specific heat extraction rate	0.0028
storage coefficient	0.0132
stored heat per cycle	0.0279
extracted heat per cycle	0.0868

higher polynomial degree could achieve better MRAE values but would also lead to overfitting owing to the well-known polynomial properties. However, a moderate order of the proxy model such as four is sufficient to capture the model's nonlinearity and also to assure acceptable accuracy with MRAEs below 0.1 %.

In the first optimization scenario, the genetic algorithm fails to improve the solution any further without violating the constraint function after 55 generations and 11 000 evaluations of the fitness function. The second scenario converges on an optimum after 46 generations and 9200 function evaluations. These are approximate numbers as the irreproducible selection of individuals for a new generation involves random processes. Finding the ideal solution, however, is reproducible. For an annual heat demand of 500 MWh extracted in the described operation, the ideal BHE arrays have to have 10 BHEs of 134 m length (total drilled length: 1340 m) for scenario one and 7 BHEs of 220 m length (total drilled length: 1540 m) for scenario two. The MD-BTES system would operate at 43.6 and 40.7 % storage efficiency with a specific heat extraction rate of 84.4 and 74.2 W m^{-1}, respectively, in the seventh year of operation. Any configuration with fewer, but deeper, BHEs also located on the intersection of the model response surface of extracted heat and the 500 MWh plane would provide the required heat as well (Figure 10). However, those solutions have been ruled out by the genetic algorithm, as the increased length is exponentially penalized relative to the number of BHEs in the fitness function.

The ideal MD-BTES designs found by the genetic algorithm are each verified by an additional numerical simulation and are compared against the proxy model prediction with respect to the relative approximation error (RAE) (Table 6). In the second scenario, the RAE does not violate the previously defined tolerance criterion of 1 %. Hence, no further iteration is required and an MD-BTES system with 7 BHEs of 220 m length can be regarded as the solution to the optimization problem of scenario two. However, the verification of the first scenario fails: the numerical simulation of an MD-BTES system with 10 BHEs of 134 m length returns 494 MWh extracted heat in the last cycle, which results in a RAE of 1.2 % and a violation of the 1 % criterion. Consequently, the proxy model is refined with the numerical verifi-
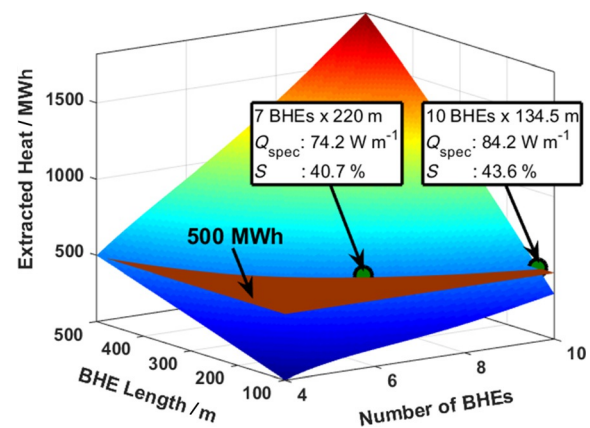
Figure 10. Response surface of extracted heat in the seventh cycle showing the two optimal solutions found by the genetic algorithm.

Table 6. Verification of the optimal solutions on the unrefined proxy model.

Model output	Specific heat extraction rate [W m^{-1}]	Storage coefficient [%]	Heat per cycle [MWh] stored	extracted
Scenario 1				
numerical	83.9	43.5	1136.8	494
proxy	84.3	43.5	1129.9	500
RAE	<1%	<1%	<1%	>1%
Scenario 2				
numerical	74.5	40.7	1238.1	503
proxy	74.2	40.7	1229.6	500
RAE	<1%	<1%	<1%	<1%

cation simulation. Renewed optimization of scenario one with the refined proxy model yields an optimal MD-BTES design of 10 BHEs with 134.5 m. An additional numerical verification shows that the RAE criterion is now satisfied (Table 7).

Discussion

Optimization using a proxy model

The low MRAE values indicate good quality of the proxy model's predictions of the storage performance for low computational costs. This is especially true for the center region of the parameter space. However, as a result of the lack of training points beyond the parameter space boundaries, the proxy model predictions become less accurate at the edges of the response surfaces and even more so in the corners. A corner is a point in multidimensional parameter space at which every variable has its lower or upper boundary value. Therefore, it is important to choose the parameter space for the training simulations in such a way that the optimal solution can be expected to be nowhere close to a corner.

In the first scenario, the optimal solution converges inevitably on the proxy model boundary of two variables. On the one hand, the performance of the MD-BTES system is evalu-

Table 7. Verification of the optimal solutions on the refined proxy model.

Model Output	Specific heat extraction rate [Wm^{-1}]	Storage coefficient [%]	Heat per cycle [MWh] stored	extracted
numerical	84.3	43.5	1143.6	498
proxy	84.2	43.6	1134.4	500
RAE	<1%	<1%	<1%	<1%

ated for the seventh year of operation, which is the upper boundary for the simulation time. On the other hand, because it is unconstrained, it converges at the top boundary for the number of BHEs owing to the fitness penalty on the BHE length. Still, the MRAE compared to verification simulation barely violates the 1% tolerance criterion by 0.2 percentage points and only one refinement iteration of the proxy model is required. However, if more variables are considered, it is advisable to use a more sophisticated experimental design to handle the exponential increase in training simulations. Typically, experimental designs such as the Latin hypercube[35] or Box–Behnken[36] design sample the parameter space much more efficiently but provide proxy models that are less accurate at their boundaries. Therefore, for more complex cases we recommend using wider boundaries for the training simulations than required for the optimization. In this way, the algorithm can converge on an optimization variable's boundary without reaching the edge of the proxy model parameter space.

Implications of the optimal solution for the design of MD-BTES systems

The solutions for both scenarios indicate that storage efficiency increases more quickly with the number of BHEs than with their depth: The proxy model returns a heat supply of nearly 300 MWh for a hypothetical MD-BTES system with 7 BHEs and 134.5 m length. To raise this value to the required 500 MWh, the total drilled borehole length has to be increased by approximately 600 m for the 7 BHEs of 220 m array (i.e., deeper boreholes), but only by approximately 400 m for the 10 BHEs of 134.5 m array (i.e., additional boreholes). However, with only 134.5 m depth the solution of scenario one barely qualifies as a medium-deep BTES system. As a consequence, a possibly decreased efficiency of the MD-BTES system with fewer, but deeper, BHEs has to be accepted to meet legal requirements of minimum depth.

Furthermore, both scenarios are characterized by over 50% storage losses. Although the storage performance would further increase over time, this improvement already slows down significantly after a few years of operation (see Figures 3 and 6). A larger MD-BTES system would operate at higher efficiencies but would also store and extract more heat in each cycle. Hence, a heat demand of 500 MWh can be considered too low for the proposed operational scenario. MD-BTES systems are rather suited for large-scale applications with a heat demand of several GWh. On the basis of

previous estimates,[37] MD-BTES systems are then expected to achieve over 80% storage efficiency.

Extension of the optimal MD-BTES system design to real field

Whereas the genetic algorithm easily determines the ideal design of an MD-BTES system, the actual solution to the optimization problem depends on several assumptive boundary conditions and simplifications. In particular, the operational scenario of continuous storage charging and discharging cycles is unrealistic. In a real case, it should be based on annual heat demand and supply curves with high temporal resolution. Such curves can be provided by comprehensive building model simulations that take into account the interaction of infrastructural installations and weather conditions. This would greatly influence the long-term behavior of MD-BTES systems and possibly lead to a different result even if the total annual heat demand is the same. However, every application requires its own building model, and building models are not the scope of this study. For the sake of simplicity, the presented operational scenario is sufficiently suitable to demonstrate the concept of MD-BTES design optimization.

Another crucial factor is the choice of the parameter space. Many parameters that influence the performance of an MD-BTES system, including thermal conductivities and heat capacities of the BHE materials and the reservoir rock, are kept constant and are not considered as variables. In a real case study, some of the modeling parameters such as subsurface thermal conductivity could also be subject to uncertainty. The aPC method is specially designed to account for uncertain parameters.[34] Hence, the presented procedure could be extended to optimization under geological uncertainty.

Conclusions

We showed in an arbitrary example that the presented software tool can predict the performance of a medium-deep borehole thermal energy storage system and optimize its design efficiently. Careful definition of the problem and selection of the variable parameters and their boundaries is imperative to obtain significant results. The application of a proxy model generated by arbitrary polynomial chaos expansion greatly accelerates the optimization algorithm. The possibility to rerun optimizations considering different boundary conditions with little additional computational cost gives this approach an advantage over simulation codes tailored for a specific optimization problem. Our generic and modular approach allows for easy adaptation to other optimization problems with different objectives.

Acknowledgements

[1] Bundesministerium für Wirtschaft und Energie (Arbeitsgemeinschaft Energiebilanzen e.V.), *Anwendungsbilanzen für die Endenergiesektoren in Deutschland in den Jahren 2011 und 2012 mit Zeitreihen von 2008 bis 2012*, http://www.ag-energiebilanzen.de/, Berlin, **2013**.

[2] H. Lund, B. Möller, B. V. Mathiesen, A. Dyrelund, *Energy* **2010**, *35*, 1381–1390.

[3] I. Sass, R. Bracke, W. Rühaak, *Proceedings World Geothermal Congress*, **2015**, 35014.

[4] D. Lindenberger, T. Bruckner, H. M. Groscurth, R. Kümmel, *Energy* **2000**, *25*, 591–608.

[5] D. Bauer, W. Heidemann, R. Marx, J. Nußbicker-Lux, F. Ochs, V. Panthalookaran, S. Raab, *Forschungsbericht zum BMU-Vorhaben 0329607J (Juni 2005 bis Juli 2008)*, http://www.itw.uni-stuttgart.de/dokumente/Publikationen/publikationen_09-01.pdf, University of Stuttgart, Stuttgart, **2008**.

[6] D. Bauer, R. Marx, J. Nußbicker-Lux, F. Ochs, W. Heidemann, H. Müller-Steinhagen, *Solar Energy* **2010**, *84*, 612–623.

[7] P. Mielke, D. Bauer, S. Homuth, A. Götz, I. Sass, *Geotherm. Energy* **2014**, *2*, 1–15.

[8] B. Sibbitt, D. McClenahan, R. Djebbar, J. Thornton, B. Wong, J. Carriere, J. Kokko, *Energy Procedia* **2012**, *30*, 856–865.

[9] S. Haehnlein, P. Bayer, P. Blum, *Renewable Sustainable Energy Rev.* **2010**, *14*, 2611–2625.

[10] C. Griebler, C. Kellermann, C. Stumpp, F. Hegler, D. Kuntz, S. Walker-Hertkorn, in *54/2015* (Ed.: Umweltbundesamt), http://www.umweltbundesamt.de/sites/default/files/medien/378/publikationen/texte_54_2015_auswirkungen_thermischer_veraenderungen_infolge_der_nutzung_obenflaechennaher_geothermie_0.pdf, **2015**, p. 159.

[11] Guideline 4640/2 of the Society of German Engineers (VDI), https://www.vdi.de/richtlinie/vdi_4640_blatt_2-thermische_nutzung_des_untergrundes_erdgekoppelte_waermepumpenanlagen/, **2001**.

[12] S. A. Kalogirou, *Prog. Energy Combust. Sci.* **2004**, *30*, 231–295.

[13] H. Gadd, S. Werner, *Appl. Energy* **2014**, *136*, 59–67.

[14] K. Bär, W. Rühaak, B. Welsch, D. Schulte, S. Homuth, I. Sass, *Energy Procedia* **2015**, *76*, 351–360.

[15] P. Bayer, M. de Paly, M. Beck, *Appl. Energy* **2014**, *136*, 445–453.

[16] M. de Paly, J. Hecht-Méndez, M. Beck, P. Blum, A. Zell, P. Bayer, *Geothermics* **2012**, *43*, 57–65.

[17] O. C. Zienkiewicz, R. L. Taylor, J. Z. Zhu, *The Finite Element Method: Its Basis and Fundamentals*, 7th ed., Butterworth-Heinemann, Oxford, **2013**.

[18] MATLAB 2014b, The MathWorks, Inc., Natick, MA, **2014**.

[19] J. Alberty, C. Carstensen, S. Funken, *Numer. Algorithms* **1999**, *20*, 117–137.

[20] H. Si, *Finite Elem. Anal. Design* **2010**, *46*, 33–46.

[21] P. M. Gresho, D. F. Griffiths, D. J. Silvester, *SIAM J. Sci. Comput.* **2008**, *30*, 2018–2054.

[22] D. Bauer, W. Heidemann, H. Müller-Steinhagen, H. J. G. Diersch, *Int. J. Energy Res.* **2011**, *35*, 312–320.

[23] H. J. G. Diersch, D. Bauer, W. Heidemann, W. Rühaak, P. Schätzl, *Comput. Geosci.* **2011**, *37*, 1122–1135.

[24] P. Eskilson, J. Claesson, *Numer. Heat Trans.* **1988**, *13*, 149–165.

[25] H. J. G. Diersch, *FEFLOW: Finite Element Modeling of Flow, Mass and Heat Transport on Porous and Fractured Media*, Springer, Berlin, **2014**.

[26] J. N. Reddy, D. K. Gartling, *The Finite Element Method in Heat Transfer and Fluid Dynamics*, 3rd ed., CRC Press, Boca Raton, FL, **2010**.

[27] N. Wiener, *Am. J. Math.* **1938**, *60*, 897–936.

[28] S. Oladyshkin, W. Nowak, *Reliab. Eng. Sys. Saf.* **2012**, *106*, 179–190.

[29] J.-S. Chen, L. Wang, H.-Y. Hu, S.-W. Chi, *Int. J. Numer. Methods Eng.* **2009**, *80*, 163–190.

[30] H. Moritz, *Rev. Geophysics* **1978**, *16*, 421–430.

[31] J. W. Tester, E. M. Drake, M. J. Driscoll, M. W. Golay, W. A. Peters, *Sustainable Energy: Choosing Among Options*, MIT Press, Cambridge, MA, **2005**.

[32] D. E. Goldberg, *Genetic Algorithms in Search, Optimization, and Machine Learning*, Addison-Wesley, Reading, MA, **1989**.

[33] MATLAB 2014b and Global Optimization Toolbox, The MathWorks, Inc., Natick, Ma, **2014**.

[34] S. Oladyshkin, W. Nowak in *Novel Approaches and Their Application in Risk Assessment* (Ed.: Y. Luo), InTech, Rijeka, **2012**.

[35] K. Siebertz, D. van Bebber, T. Hochkirchen, *Statistische Versuchsplanung—Design of Experiments (DoE)*, Springer, Berlin, **2010**.

[36] G. E. P. Box, D. W. Behnken, *Technometrics* **1960**, *2*, 455–475.

[37] B. Welsch, W. Rühaal, D. O. Schulte, K. Bär, S. Homuth, I. Sass, *Proceedings World Geothermal Congress* **2015**, 38006.

Appendix D:
Modeling insulated borehole heat exchangers

Published as:

Schulte DO, Welsch B, Boockmeyer A, Rühaak W, Bär K, Bauer S and Sass I (2016) Modeling insulated borehole heat exchangers, Environmental Earth Sciences, v. 75, p. 1-12, doi:10.1007/s12665-016-5638-x.

CrossMark

Modeling insulated borehole heat exchangers

Daniel Otto Schulte[1,2] · Bastian Welsch[1,2] · Anke Boockmeyer[3] · Wolfram Rühaak[1,2] ·
Kristian Bär[2] · Sebastian Bauer[3] · Ingo Sass[1,2]

Abstract In the heating sector, borehole heat exchangers have become popular for supplying renewable energy. They tap into the subsurface to extract geothermal energy for heating purposes. For advanced applications, borehole heat exchangers require insulation in the upper part of the borehole either to meet legal requirements or to improve their performance. A priori numerical heat transport models of the subsurface are imperative for the systems' planning and design. Only fully discretized models can account for depth-dependent borehole properties like insulated sections, but the model setup is cumbersome and the simulations come at high computational cost. Hence, these models are often not suitable for the simulation of larger installations. This study presents an analytical solution for the simulation of the thermal interactions of partly insulated borehole heat exchangers. A benchmark with a fully discretized OpenGeoSys model confirms sufficient accuracy of the analytical solution. In an application example, the functionality of the tool is demonstrated by finding the ideal length of a borehole insulation using mathematical optimization and by quantifying the effect of the insulation on the borehole heat exchanger performance. The presented method allows for accommodation of future advancements in borehole heat exchangers in numerical simulations at comparatively low computational cost.

Introduction

Public awareness on renewable energies focuses mostly on the electricity supply. Yet, countries in high latitudes spend vast amounts of energy on heating. For example, in Germany, heating purposes alone account for more than half of the total end energy consumption (Ageb 2013). The use of borehole heat exchangers (BHEs) is an increasingly popular way to supply renewable heat all over the world (Angelino et al. 2014; Lund and Freeston 2005). BHEs are typically installed in vertical boreholes; a heat carrier fluid is circulated in closed-loop pipes. A cement grout used as backfill material ensures a good thermal connection to the borehole wall and protects the groundwater from possible contamination by antifreeze contained in the pipes. Heat is extracted from the subsurface rock by thermal conduction in the grout and by convection in the pipes (Sass et al. 2016a). Typically, at the surface a heat pump raises the temperature to the required level for the specific heating purpose. Its efficiency depends on the outlet temperature of the BHE and on the required temperature level for heating. Higher outlet temperatures reduce the required temperature lift and consequently the heat pump's energy consumption.

As the subsurface temperature increases with depth due to the geothermal gradient, deeper BHEs can provide higher outlet temperatures. However, heat losses in the shallow

✉ Daniel Otto Schulte
schulte@geo.tu-darmstadt.de

[1] Graduate School of Excellence Energy Science and Engineering, Technische Universität Darmstadt, Jovanka-Bontschits-Straße 2, 64287 Darmstadt, Germany

[2] Geothermal Science and Technology, Technische Universität Darmstadt, Schnittspahnstraße 9, 64287 Darmstadt, Germany

[3] Geohydromodelling, Christian-Albrechts-Universität zu Kiel, Ludewig-Meyn-Straße 10, 24118 Kiel, Germany

subsurface can eliminate the temperature gains originating from the deeper section of the boreholes (Nakevska et al. 2015) and render the increased investment costs for deeper BHEs worthless. Thus, a thermal insulation in the upper section of a borehole is favorable for deeper BHEs. Furthermore, legal regulations in some countries may restrict the temperature increase of the uppermost aquifer to a certain maximum to protect drinking water from negative biological or chemical alterations (Haehnlein et al. 2010). Hence, a thermal insulation has been proposed for the upper part of medium deep borehole thermal energy storages (BTES) as well (Bär et al. 2015). On the one hand, a backfill material with reduced thermal conductivity and an increased borehole diameter are supposed to reduce the heat losses and the consequent warming of the shallow subsurface due to an increased thermal resistance between the pipes and the borehole wall. On the other hand, a backfill material with a high thermal conductivity can enhance the heat exchange at elevated ambient temperatures in the bottom part of the BHE (Sass et al. 2016a).

In the past, BHEs rarely exceeded 100 m depth. Therefore, no partial thermal insulation was necessary. On the contrary, due to the small temperature differences between the heat carrier fluid and the borehole wall, a high thermal conductivity of a single grout was favorable along the entire borehole. Consequently, simulation models did not need to account for grout thermal conductivities or borehole diameters changing with depth. Based on Eskilson and Claessons's solution (1988), Bauer et al. (2011) and Diersch et al. (2011a) developed a thermal resistance and capacity model (TRCM) which reduces a BHE to a one-dimensional discretization of nodes in a finite element mesh. This model accounts for a detailed description of the geometry of different BHE types and their material parameters. While it is more accurate than many line source models as it calculates depth-dependent grout and fluid temperatures within the BHE, it cannot accommodate changing borehole diameters or backfill material properties along the borehole length. Thus, up to now only fully discretized 3D numerical models have been able to simulate BHEs with vertically varying thermal conductivities. However, these models are laborious to set up, require expensive computations and lack the efficiency of fast analytical solutions, especially for larger models with multiple BHEs as needed for borehole thermal energy storages.

In this paper, Eskilson and Claessons's solution is improved to a model, which considers boreholes with an upper and a bottom section, with both different borehole diameters and different thermal conductivities of the backfill material represented in a TRCM. Our approach is independent from the specific BHE type and can handle coaxial, U-pipe and double U-pipe BHEs. The novel solution is linked to a numerical subsurface heat transport model and tested against a fully discretized numerical benchmark model for a coaxial BHE. Finally, in an application example the model is combined with a mathematical optimization algorithm to determine the ideal length of the insulated section for a double U-pipe BHE.

An extended analytical solution

Eskilson and Claesson's analytical BHE solution (Eskilson and Claesson 1988) describes the fluid temperature in the downstream and upstream pipes T_{in} and T_{out} in °C as two codependent functions of depth z (in the range of $\zeta = 0$ to the total borehole length L) and the current borehole wall temperature T_b at time t.

$$T_{in}(z, t) = T_{in}(0, t)f_1(z) + T_{out}(0, t)f_2(z)$$
$$+ \int_0^z T_b(\zeta, t)f_4(z - \zeta)\, d\zeta \qquad (1)$$

$$T_{out}(z, t) = -T_{in}(0, t)f_2(z) + T_{out}(0, t)f_3(z)$$
$$- \int_0^z T_b(\zeta, t)f_5(z - \zeta)\, d\zeta \qquad (2)$$

The functions f_1, f_2, f_3, f_4 and f_5 are given by the following expressions:

$$f_1(z) = e^{\beta z}[\cosh(\gamma z) - \delta \sinh(\gamma z)]$$
$$f_2(z) = e^{\beta z}\frac{\beta_{12}}{\gamma}\sinh(\gamma z)$$
$$f_3(z) = e^{\beta z}[\cosh(\gamma z) + \delta \sinh(\gamma z)]$$
$$f_4(z) = e^{\beta z}\left[\beta_1 \cosh(\gamma z) - \left(\delta\beta_1 + \frac{\beta_2\beta_{12}}{\gamma}\right)\sinh(\gamma z)\right]$$
$$f_5(z) = e^{\beta z}\left[\beta_2 \cosh(\gamma z) + \left(\delta\beta_2 + \frac{\beta_1\beta_{12}}{\gamma}\right)\sinh(\gamma z)\right]$$

$$(3)$$

The functions' auxiliary variables α, β, β_1, β_2, β_{12}, γ and δ, which are based on the TRCMs of the involved BHE components, are calculated according to the BHE type after Bauer et al. (2011), whereas the derivation of the functions f_1–f_5 can be found in Eskilson and Claesson (1988). Since the solution describes only local steady-state conditions, time t is omitted from the following equations for better readability. The analytical solution has to be linked to a numerical subsurface model by deriving a heat source term from the difference between the borehole wall temperature and the fluid temperature (Diersch et al. 2011a) to account for transient heat transport in the subsurface. Then, the numerical model calls the analytical solution every time step, providing the time-dependent borehole wall temperature.

As the upstream and downstream pipes form a closed loop, the fluid temperature must be the same at the bottom. Hence, Eqs. (1) and (2) can be equalized at $z = L$ and
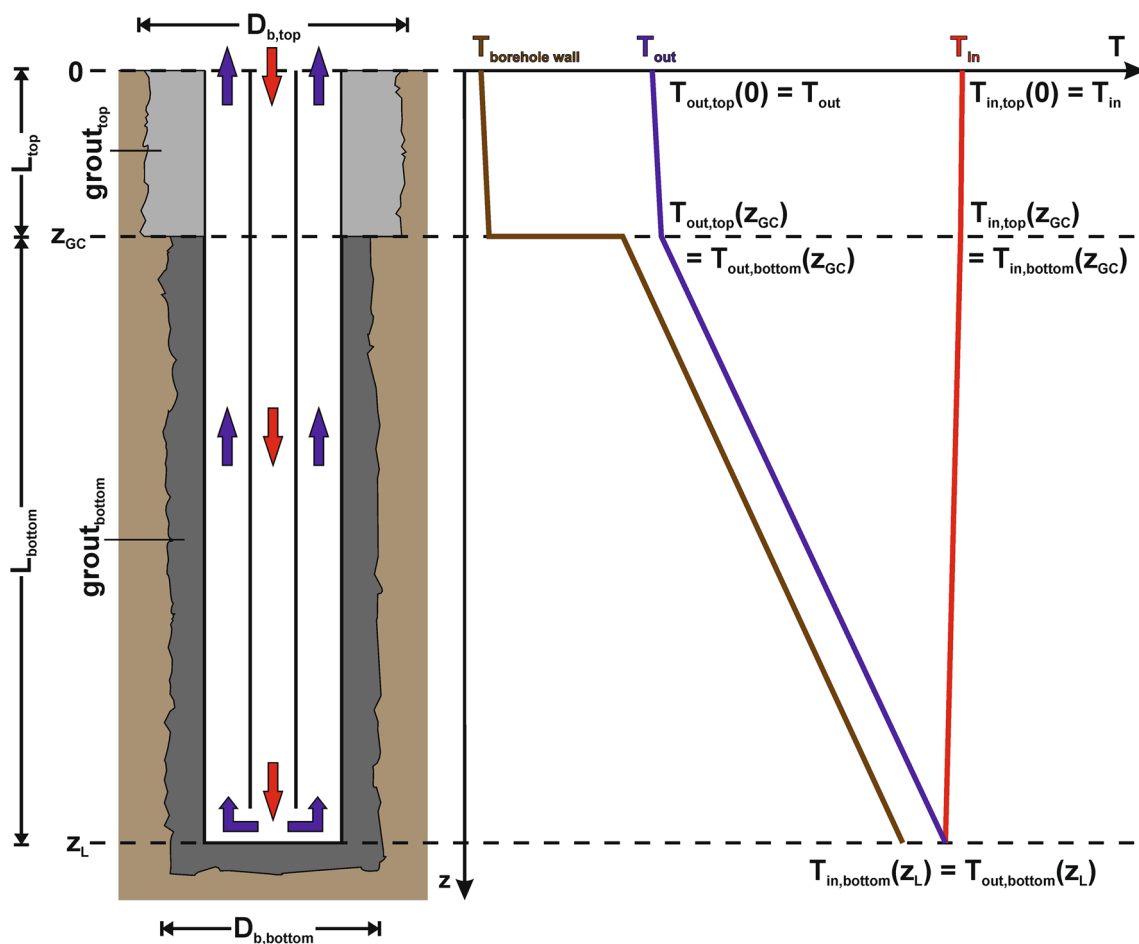
Fig. 1 Sketch of a coaxial BHE (*centered inlet*) with the insulated uppermost borehole section and the initial corresponding temperature profile for heat storage operation. The step-like offset of the borehole wall temperature at z_{gc} is smoothed out after prolonged operation due to vertical heat transport in the subsurface

resolved for $T_{out} = T_{out}(z = 0)$ for a given inlet temperature of the BHE $T_{in} = T_{in}(z = 0)$:

$$T_{out} = T_{in}\frac{f_1(L) + f_2(L)}{f_3(L) - f_2(L)} + \int_0^L \frac{T_s(\zeta)f_4(L - \zeta) + f_5(L - \zeta)}{f_3(L) - f_2(L)}d\zeta \tag{4}$$

Determining the outlet temperature T_{out} is the imperative first step, as Eqs. (1) and (2) require both the inlet and the outlet temperature of the BHE to calculate the depth-dependent temperature profile in the downstream and upstream pipes. However, Eq. (4) shows that the solution for the outlet temperature integrates functions f_4 and f_5 over the entire borehole length L. Likewise, functions f_1, f_2 and f_3 depend on the total borehole length L as well. Hence, borehole properties changing with depth cannot be accounted for in this equation, as they are constants in the auxiliary variables of the functions f_1–f_5. Instead, a BHE with a borehole insulation in the upper part requires a split calculation.

As the design splits the BHE into two sections with different grout properties and drilling diameters (Fig. 1), Eqs. (1) and (2) apply for the upper and lower section separately. This allows for an independent consideration of different TRCMs with different auxiliary variable values for the functions f_1–f_5 in each section. The downstream and upstream pipes are connected in the bottom section. Therefore, Eqs. (1) and (2) cannot be equalized for the bottom of the upper part at the interface between the two different grout types at depth z_{gc} to derive Eq. (4). However, at the interface the fluid temperatures $T_{in, top}(z_{gc})$ and $T_{out, top}(z_{gc})$ of the upper section of the wellbore are equal to the inlet and outlet temperatures $T_{in, bottom}$ and $T_{out, bottom}$ of the bottom section.

$$T_{in, bottom} = T_{in, top}(z_{GC})$$
$$T_{out, bottom} = T_{out, top}(z_{GC}) \tag{5}$$

Equation (4) is still valid for the bottom section, but the inlet and outlet temperatures are unknown. Thus, substitution according to (5) gives

$$T_{\text{out, bottom}} = T_{\text{in, bottom}} \frac{f_{1,\text{bottom}}(L_{\text{bottom}}) + f_{2,\text{bottom}}(L_{\text{bottom}})}{f_{3,\text{bottom}}(L_{\text{bottom}}) - f_{2,\text{bottom}}(L_{\text{bottom}})}$$

$$+ \int_{z_{\text{GC}}}^{z_L} \frac{T_s(\zeta) f_{4,\text{bottom}}(L_{\text{bottom}} - \zeta) + f_{5,\text{bottom}}(L_{\text{bottom}} - \zeta)}{f_{3,\text{bottom}}(L_{\text{bottom}}) - f_{2,\text{bottom}}(L_{\text{bottom}})} d\zeta \equiv$$

$$T_{\text{out, top}}(z_{\text{GC}}) = T_{\text{in, top}}(z_{\text{GC}}) \frac{f_{1,\text{bottom}}(L_{\text{bottom}}) + f_{2,\text{bottom}}(L_{\text{bottom}})}{f_{3,\text{bottom}}(L_{\text{bottom}}) - f_{2,\text{bottom}}(L_{\text{bottom}})} .$$

$$+ \int_{z_{\text{GC}}}^{z_L} \frac{T_s(\zeta) f_{4,\text{bottom}}(L_{\text{bottom}} - \zeta) + f_{5,\text{bottom}}(L_{\text{bottom}} - \zeta)}{f_{3,\text{bottom}}(L_{\text{bottom}}) - f_{2,\text{bottom}}(L_{\text{bottom}})} d\zeta$$

$$(6)$$

Inserting (1) and (2) for $T_{\text{in, top}}(z_{\text{GC}})$ and $T_{\text{out, top}}(z_{\text{GC}})$, the resulting equation can be solved for $T_{\text{out, top}}$:

$$T_{\text{out, top}} = T_{\text{in, top}}$$

$$\times \frac{\kappa + v \int_0^{z_{\text{GC}}} T_b(\zeta) f_{4,\text{top}}(L_{\text{top}}) d\zeta + \int_0^{z_{\text{GC}}} T_b(\zeta) f_{5,\text{top}}(L_{\text{top}}) d\zeta + \mu}{\lambda}$$

$$(7)$$

with

$$\kappa = v f_{1,\text{top}}(L_{\text{top}}) + f_{2,\text{top}}(L_{\text{top}})$$

$$\lambda = f_{3,\text{top}}(L_{\text{top}}) - v f_{2,\text{top}}(L_{\text{top}})$$

$$\mu = \int_{z_{\text{GC}}}^{z_L} \frac{T_b(\zeta) \left(f_{4,\text{bottom}}(L_{\text{bottom}}) + f_{5,\text{bottom}}(L_{\text{bottom}}) \right)}{f_{3,\text{bottom}}(L_{\text{bottom}}) - f_{2,\text{bottom}}(L_{\text{bottom}})} d\zeta$$

$$v = \frac{f_{1,\text{bottom}}(L_{\text{bottom}}) + f_{2,\text{bottom}}(L_{\text{bottom}})}{f_{3,\text{bottom}}(L_{\text{bottom}}) - f_{2,\text{bottom}}(L_{\text{bottom}})}$$

$$(8)$$

Subsequently, the depth-dependent temperature profiles in the downstream and upstream pipes can be calculated with (1) and (2) using $T_{\text{in, top}}$ and $T_{\text{out, top}}$ for the upper insulated section of the wellbore and $T_{\text{in, bottom}} = T_{\text{in, top}}(z_{\text{GC}})$ and $T_{\text{out, bottom}} = T_{\text{out, top}}(z_{\text{GC}})$ for the lower section. The new solution now takes into account borehole properties changing with depth and can be coupled to a numerical subsurface model as described in Diersch et al. (2011a).

Benchmarking

The enhanced analytical solution is integrated in a MATLAB (The MathWorks 2015a) finite element method (FEM)-based simulator called BASIMO (borehole heat exchanger array simulation and optimization tool, Schulte et al. 2016). In a benchmark problem, it is compared against a benchmark simulation of a fully discretized detailed numerical 3D model using OpenGeoSys (OGS; Kolditz et al. 2012). OGS is a process and object-oriented simulator (Kolditz and Bauer 2004) that uses a FEM to solve the arising thermal and hydraulic processes. The OGS model is based on the same principle as introduced in

Boockmeyer and Bauer (2014) and was successfully verified against detailed experimental data for a BHE (Boockmeyer and Bauer 2014). The OGS model can account for spatially varying and temperature–dependent material parameters and is applied for the simulation of heat storage in the subsurface (Bauer et al. 2013, 2015).

A simple heat storage and extraction operation scenario is set up for the benchmark: A partly insulated 100-m coaxial BHE is located in the center of the model domain, which is 100 m by 100 m wide and 150 m deep. The initial temperature distribution corresponds to a geothermal gradient of 0.03 K/m. Dirichlet boundary conditions are set accordingly: 10 °C at the top and 14.5 °C at the bottom. An enlarged drilling diameter and a reduced thermal conductivity of the grout provide a borehole insulation from the surface to 30 m depth (Fig. 2).

Heat is stored for 182 days with an inlet temperature of 90 °C and a flow rate of 2.5 l/s. Subsequently, the heat extraction period lasts 183 days with the same flow rate and an inlet temperature of 5 °C. The change of the flow direction from the centered inlet for heat storage to the inlet through the annular gap for heat extraction is considered. Table 1 summarizes the material properties, the BHE geometry and the according abbreviations used in Fig. 2.

Both simulators are set up with the model described above. In the benchmark, the temporal evolution of the outlet temperatures is compared against each other. As the simulators use independent time-stepping schemes, results are saved after 1 day and after 10 days of storage and extraction operation, respectively, to ensure at least two comparison points per period. The results show that the improved analytical solution lacks in accuracy to match the fully discretized model for the early time steps during transient input situations (Fig. 3a, c), but achieves a very good fit after a few hours of simulation time (Fig. 3b, d). After 10 days of operation, the temperature difference is less than 0.14 °C. At the end of the storage and extraction periods, the BHE outlet temperature differs less than 0.02 °C between the BASIMO and the OGS model.

It is not possible to quantify the difference in the outlet temperature for the entire time domain without interpolation of the results due to the different time-stepping schemes. Instead, the heat balance Q, which represents the heat exchanged with the subsurface and requires the integration for the storage and the extraction period, is considered:

$$Q = \int (T_{\text{in}} - T_{\text{out}}) f \rho_f c_f t \, dt \qquad (9)$$

with T_{in}: inlet temperature, T_{out}: outlet temperature, f: flow rate of the heat carrier fluid, ρ_f: density of the heat carrier fluid, c_f: specific heat capacity of the carrier fluid and t: time. The results of the benchmark and the relative

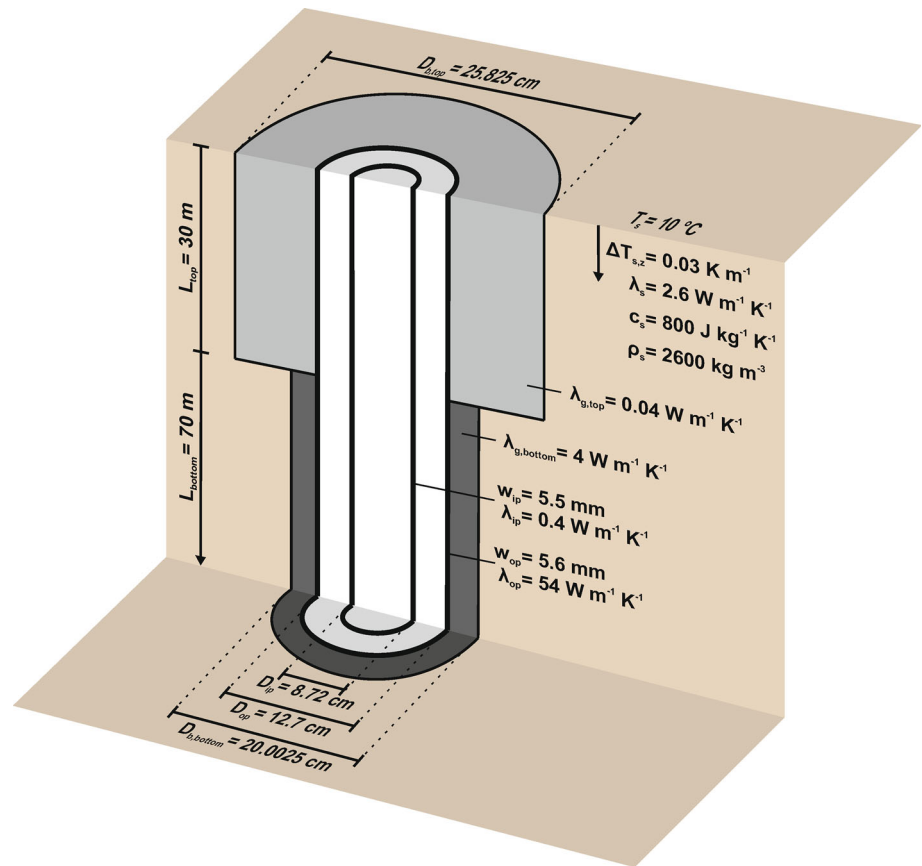**Fig. 2** Schematic of the coaxial BHE used in the benchmark (not to scale)

Table 1 Model parameters and BHE properties for benchmark simulation

| Parameter	Value	Unit	Abbreviation
Rock thermal conductivity	2.6	$W \cdot m^{-1} \cdot K^{-1}$	λ_s
Rock density	2600	$kg \cdot m^{-3}$	ρ_s
Rock specific heat capacity	800	$J \cdot kg^{-1} \cdot K^{-1}$	c_s
Rock volumetric heat capacity	2.08	$MJ \cdot m^{-3} \cdot K^{-1}$	ρc_s
Upper section borehole diameter	0.25825	m	$D_{b, top}$
Upper section grout thermal conductivity	0.04	$W \cdot m^{-1} \cdot K^{-1}$	$\lambda_{g, top}$
Upper section length	30	m	L_{top}
Lower section borehole diameter	0.200025	m	$D_{b, bottom}$
Lower section grout thermal conductivity	4	$W \cdot m^{-1} \cdot K^{-1}$	$\lambda_{g, bottom}$
Lower section length	70	m	L_{bottom}
Outer pipe outer diameter	0.127	m	D_{op}
Outer pipe wall thickness	0.0056	m	w_{op}
Outer pipe thermal conductivity (steel)	54	$W \cdot m^{-1} \cdot K^{-1}$	λ_{op}
Inner pipe outer diameter	0.0872	m	D_{ip}
Inner pipe wall thickness	0.0055	m	w_{ip}
Inner pipe thermal conductivity (polyethylene)	0.4	$W \cdot m^{-1} \cdot K^{-1}$	λ_{ip}
Heat carrier fluid dynamic viscosity (water)	0.000504	$kg \cdot m^{-1} \cdot s^{-1}$	μ
Heat carrier fluid density (water)	977	$kg \cdot m^{-3}$	ρ_f
Heat carrier fluid specific heat capacity (water)	4145	$J \cdot kg^{-1} \cdot K^{-1}$	c_f
Heat carrier fluid thermal conductivity (water)	0.65	$W \cdot m^{-1} \cdot K^{-1}$	λ_f
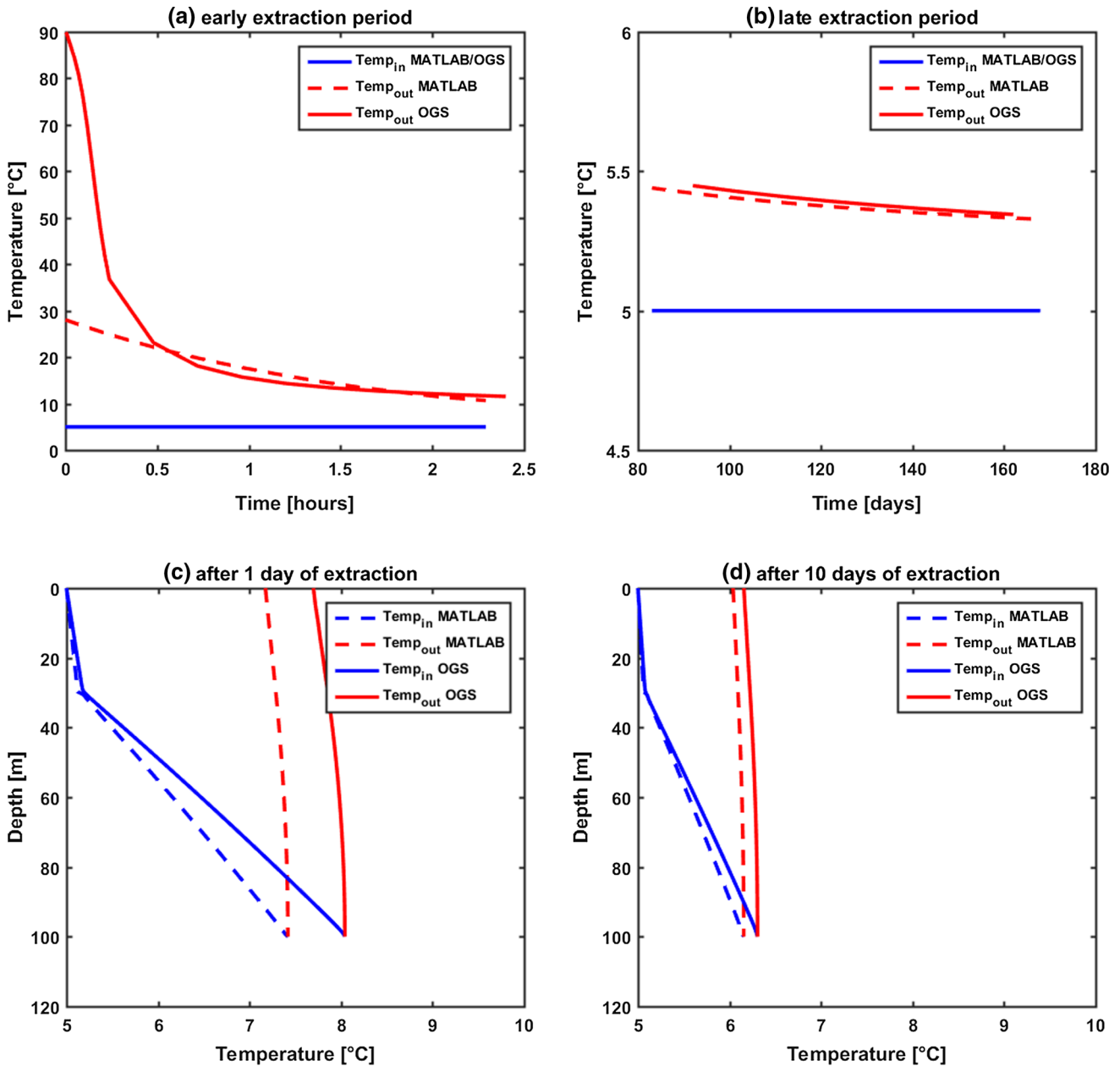
Fig. 3 Comparison of the coaxial BHE model responses. *Top*: **a** short-term and **b** long-term evolution of the BHE outlet temperature. *Bottom*: BHE temperature profiles after **c** 1 day and after **d** 10 days of extraction

difference of the models are summarized in Table 2. The amount of transferred heat differs by 1.6 and 5 % during storage and extraction, respectively. Considering only the first 10 days of the storage and extraction periods, increased errors of 6.8 and 13.54 % indicate the strong influence of the analytical solution's inaccuracy during the first time steps, whereas the remaining storage and extraction periods yield smaller errors (Table 2). The accuracy of the analytical solution and sources for the remaining error are addressed in the "Discussion" section below.

Application example

In most applications, double U-pipe BHEs are coupled with heat pumps (Sass et al. 2016a). Deeper boreholes are often fitted with coaxial BHEs instead (Bär et al. 2015; Schulte et al. 2016; Welsch et al. 2015). They benefit from the fact that the inner pipe is not in contact with the grout and can be designed to have a low thermal conductivity, which can reduce heat losses of the upstream fluid within. For double U-pipe BHEs, the full length of the downstream and upstream pipes acts as a heat exchange surface with the

Table 2 Benchmark results

Period	Q_{MATLAB} (MWh)	Q_{OGS} (MWh)	Error: $(Q_{OGS}-Q_{MATLAB})/Q_{OGS}$ (%)
Storage$_{total}$	106.57	108.29	1.6
Storage$_{0-10 \text{ days}}$	8.34	8.95	6.8
Storage$_{10-182 \text{ days}}$	98.24	99.34	1.1
Extraction$_{total}$	−23.55	−24.77	5.0
Extraction$_{0-10 \text{ days}}$	−3.84	−4.45	13.54
Extraction$_{192-365 \text{ days}}$	−19.70	−20.33	3.1

Table 3 Model parameters and BHE properties for application example

Parameter	Value	Unit	Variable
Rock thermal conductivity	2.6	$W{\cdot}m^{-1}{\cdot}K^{-1}$	λ_s
Rock density	2600	$kg{\cdot}m^{-3}$	ρ_s
Rock specific heat capacity	800	$J{\cdot}kg^{-1}{\cdot}K^{-1}$	c_s
Rock volumetric heat capacity	2.08	$MJ{\cdot}m^{-3}{\cdot}K^{-1}$	ρc_s
Upper section borehole diameter	0.25825	m	$D_{b, \text{top}}$
Upper section grout thermal conductivity	0.04	$W{\cdot}m^{-1}{\cdot}K^{-1}$	$\lambda_{g, \text{top}}$
Lower section borehole diameter	0.13	m	$D_{b, \text{bottom}}$
Lower section grout thermal conductivity	4	$W{\cdot}m^{-1}{\cdot}K^{-1}$	$\lambda_{g, \text{bottom}}$
Depth of diameter and grout change	variable	m	z_{gc}
Pipe outer diameter	0.032	m	D_p
Pipe wall thickness	0.0029	m	w_p
Diagonal shank space	0.06	m	s_p
Pipe thermal conductivity (polyethylene)	0.38	$W{\cdot}m^{-1}{\cdot}K^{-1}$	λ_p
Heat carrier fluid dynamic viscosity (water)	0.000504	$kg{\cdot}m^{-1}{\cdot}s^{-1}$	μ
Heat carrier fluid density (water)	977	$kg{\cdot}m^{-3}$	ρ_f
Heat carrier fluid specific heat capacity (water)	4145	$J{\cdot}kg^{-1}{\cdot}K^{-1}$	c_f
Heat carrier fluid thermal conductivity (water)	0.65	$W{\cdot}m^{-1}{\cdot}K^{-1}$	λ_f

surrounding rock and the grout material. Thus, double U-pipe BHEs suffer growing heat losses in the upstream pipes with increasing borehole length: the heat extracted at the bottom of the BHE is lost to the shallow subsurface and the cooler downstream pipes (so-called thermal short-circuiting) before it reaches the surface. Consequently, only lower inlet temperatures can compensate the heat losses and maintain the required difference between inlet and outlet temperature for the desired heat extraction rate. This, however, directly translates to an increased power consumption of the heat pump and an efficiency loss. Assuming an ideal Carnot process, the efficiency of a heat pump can be calculated by determining the theoretical maximum coefficient of performance (COP):

$$COP_{theor, max} = \frac{T_{hot}}{T_{hot} - T_{cold}} \tag{10}$$

where T_{hot} represents the required temperature level for the specific heating purpose and T_{cold} the outlet temperature of the BHE (all temperatures in Kelvin). Although being a simplification, which neglects internal losses, the theoretical maximum COP reflects the influence of the outlet temperature and can give an estimate on the change of the system performance.

In a synthetic simulation example, a 400-m double U-pipe BHE is to be fitted with a borehole insulation in the upper section. Again, BASIMO (Schulte et al. 2016) is used to simulate the BHE's operation. The vertical BHE is located in the center of the model with a horizontal extension of 100 m by 100 m. The model domain is 450 m deep. Dirichlet boundary conditions and initial conditions concur with a geothermal gradient of 0.03 K/m and a surface temperature of 10 °C. Table 3 and Fig. 4 plot the considered material properties and the BHE specifications. A simple scenario to simulate the BHE operation applies: Heat is extracted at a constant rate of 20 kW for 30 days at a flow rate of 0.5 l/s. For the given fluid heat capacity and density, this equates to a required difference of about 9.88 °C between inlet and outlet temperature. Strong coupling by a Picard iteration loop (Reddy and Gartling 2010) enforces this requirement by altering the inlet temperature for every time step accordingly. The beneficial effect of the insulation is quantified by comparing the outlet temperature against the results of a BHE without insulation, which serves as the base case.

Fig. 4 Schematic of the double U-pipe BHE used in the application example (not to scale)
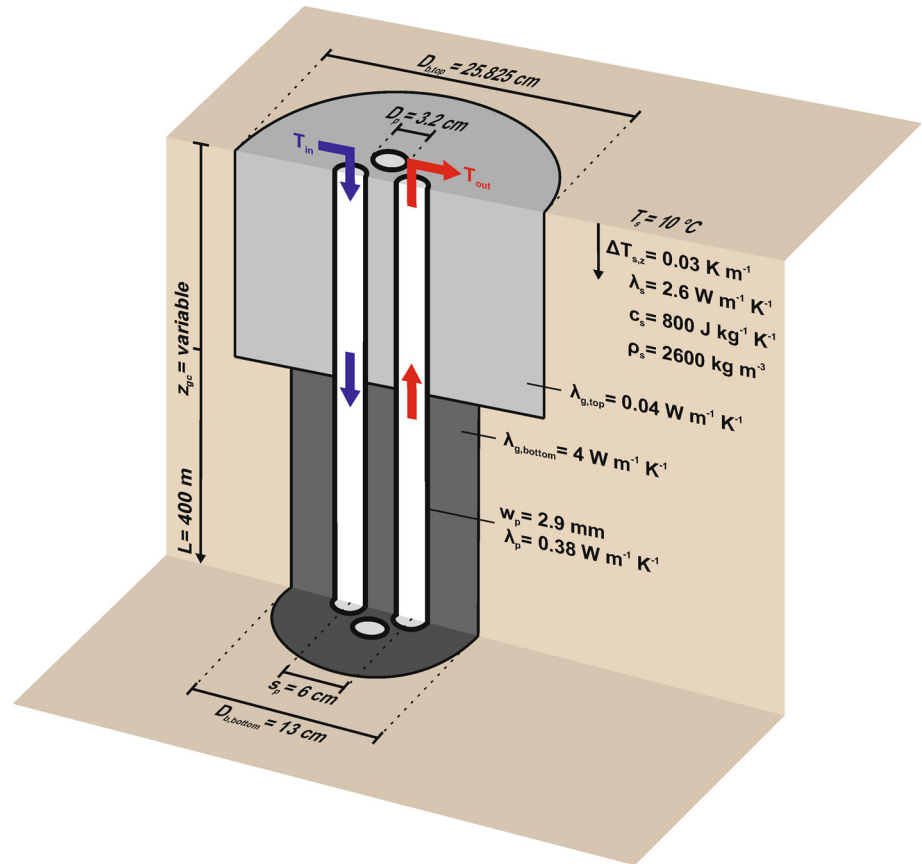
An entirely insulated borehole will perform worse than a BHE without any insulation. Hence, an ideal length of borehole insulation must exist. A basic optimization algorithm contained in the MATLAB Optimization Toolbox (Brent 1973; The MathWorks 2015b) for finding the minimum of a single-variable function on a fixed interval is used to determine the ideal length. The optimization algorithm calls the simulator repeatedly, varying the length of the borehole insulation (i.e., the depth of borehole diameter and grout change) within preset boundaries until it fails to improve the outlet temperature of the BHE with respect to a tolerance criterion for the variable (i.e., length of insulation) or the function value (i.e., the outlet temperature, Table 4).

After 15 iterations, the optimization algorithm converges on an optimal solution of approximately 142 m (Fig. 5a) for the insulation length. At the end of the 30-day period, the outlet temperature of the insulated double U-pipe BHE is 2.36 °C. Compared to the outlet temperature of the same BHE without insulation, this represents an increase of approximately 1.7 °C (Fig. 5b). The effect of the insulation becomes apparent by comparing the temperature profiles of both BHEs after 30 days of operation (Fig. 6a, b). The insulation reduces the heat extraction in the upper section of the downstream pipe. As a result, the

Table 4 Optimization algorithm settings

Parameter	Value	Unit
Lower variable boundary	10	m
Upper variable boundary	390	m
Maximum number of iterations	20	[–]
Variable tolerance	0.1	m
Function tolerance	0.001	°C

heat carrier fluid cannot reach temperatures as high as at the bottom of the uninsulated borehole. However, the insulation also mitigates the heat loss in the upstream pipe, ultimately providing a higher outlet temperature at the top of the insulated borehole.

Assuming an ideal Carnot heat pump, which raises the temperature to a target level of 35 °C (i.e., T_{hot}), the theoretical maximum COP for the insulated BHE is 9.44, whereas the BHE without an insulated borehole only achieves a theoretical COP of 8.97. This equates to a performance increase of about 5 %. Table 5 gives a selection of the optimization iterations' results. The first iteration with an insulation length of 244.85 m shows how an insulation that is too long negatively affects the BHE performance.
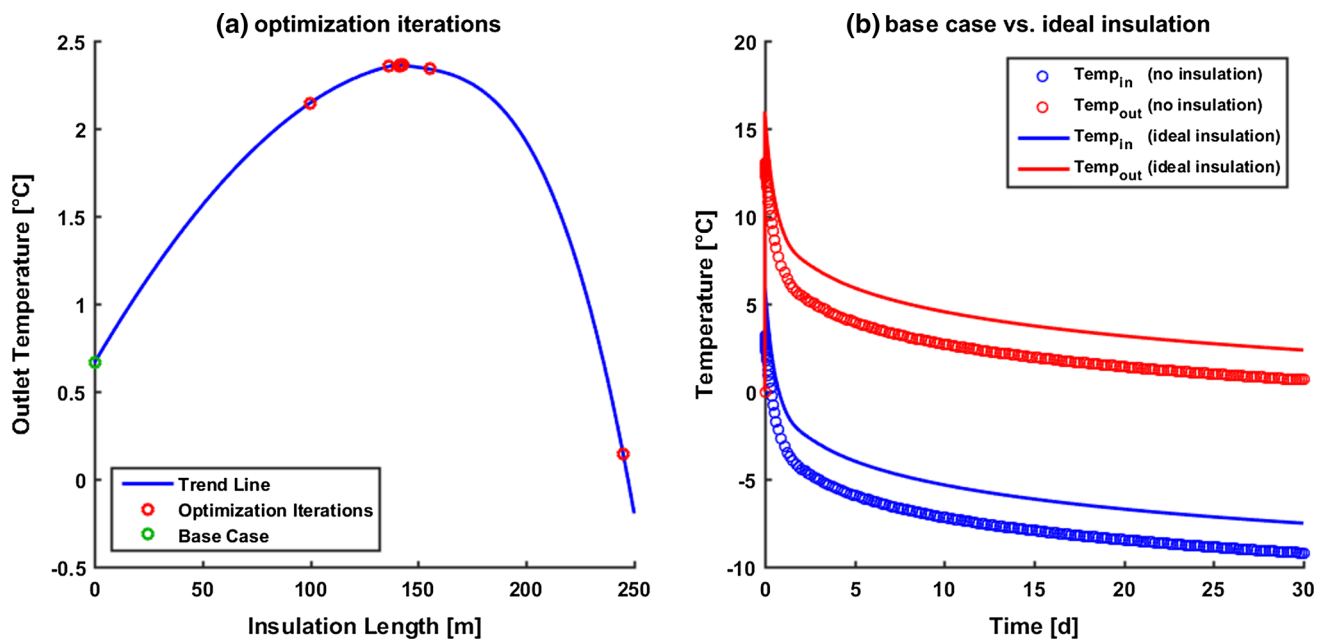
Fig. 5 Optimization results: **a** Temp$_{out}$ after 30 days of operation for each iteration, **b** Temp$_{in}$ and Temp$_{out}$ evolution of the base case and the ideally insulated BHE

Discussion

Although the presented solution only accounts for two borehole sections with different borehole diameters and backfill materials, the method is expandable to any number of segments by further substitution in Eq. (7). Additional segmentation results in nested functions, but is only limited by the increment size of the one-dimensional discretization of the borehole. However, for better readability the calculation rule for two sections sufficiently describes the concept.

In general, any other parameter included in the TRCM (e.g., pipe properties) can be altered as well. Yet, for the purpose of modeling a borehole insulation, the scope in this study is restricted to the borehole diameter and the thermal conductivity of the backfill material. As the solution for modeling insulated BHEs represents an improvement solely on Eskilson and Claesson's work (Eskilson and Claesson 1988), the TRCM providing the parameters for functions (3) is not affected. Consequently, our novel solution can handle improved TRCMs as long as they provide the required parameters for the auxiliary functions (3). For example, future TRCMs can be expanded to include additional standpipes in the thermal resistance network.

Despite the adequate benchmark results, the two simulations still show an observable mismatch. The conceptual differences between the fully discretized OGS model and the FEM-coupled analytical solution can contribute to this error in various ways. Most importantly, the OGS model is

transient, whereas the analytical model is a local steady-state solution coupled to a transient FEM algorithm. Consequently, the FEM-coupled analytical model struggles to match the numerical model in transient input situations on short timescales. Diersch et al. (2011b) have shown that the analytical solution overestimates the outlet temperature during the first time steps of storage operation. However, the errors vanish with increasing time step size until further inlet temperature changes occur. The same is true for the presented analytical solution for insulated BHEs: The outlet temperature difference between the BASIMO and the OGS model decreases to less than 0.02 °C in the long-term prediction. After changing from storage to extraction operation, the difference in outlet temperature soars up before the error diminishes again.

Another source of error in the FEM-coupled analytical model is the grid spacing around the BHE nodes. The nodes representing the BHEs are dimensionless singularities in the finite element mesh, whereas the actual BHE cross section has an extent. Thus, the heat exchange with the FEM model does not occur exactly where the borehole wall would be. In a semi-structured triangular prism mesh, numerical accuracy can be attained by choosing a specific, optimal distance of the horizontally neighboring nodes depending on the borehole diameter (Diersch et al. 2011b). However, the simulator for borehole thermal energy storage (Schulte et al. 2016) uses a tetrahedral finite element mesh. This inhibits the possibility of placing all neighboring nodes at an equal distance. The nodes sharing a tetrahedron element with a BHE node inherently have

Fig. 6 Temperature profiles of **a** the double U-pipe BHE without insulation and **b** the ideally insulated double U-pipe BHE after 30 days of operation
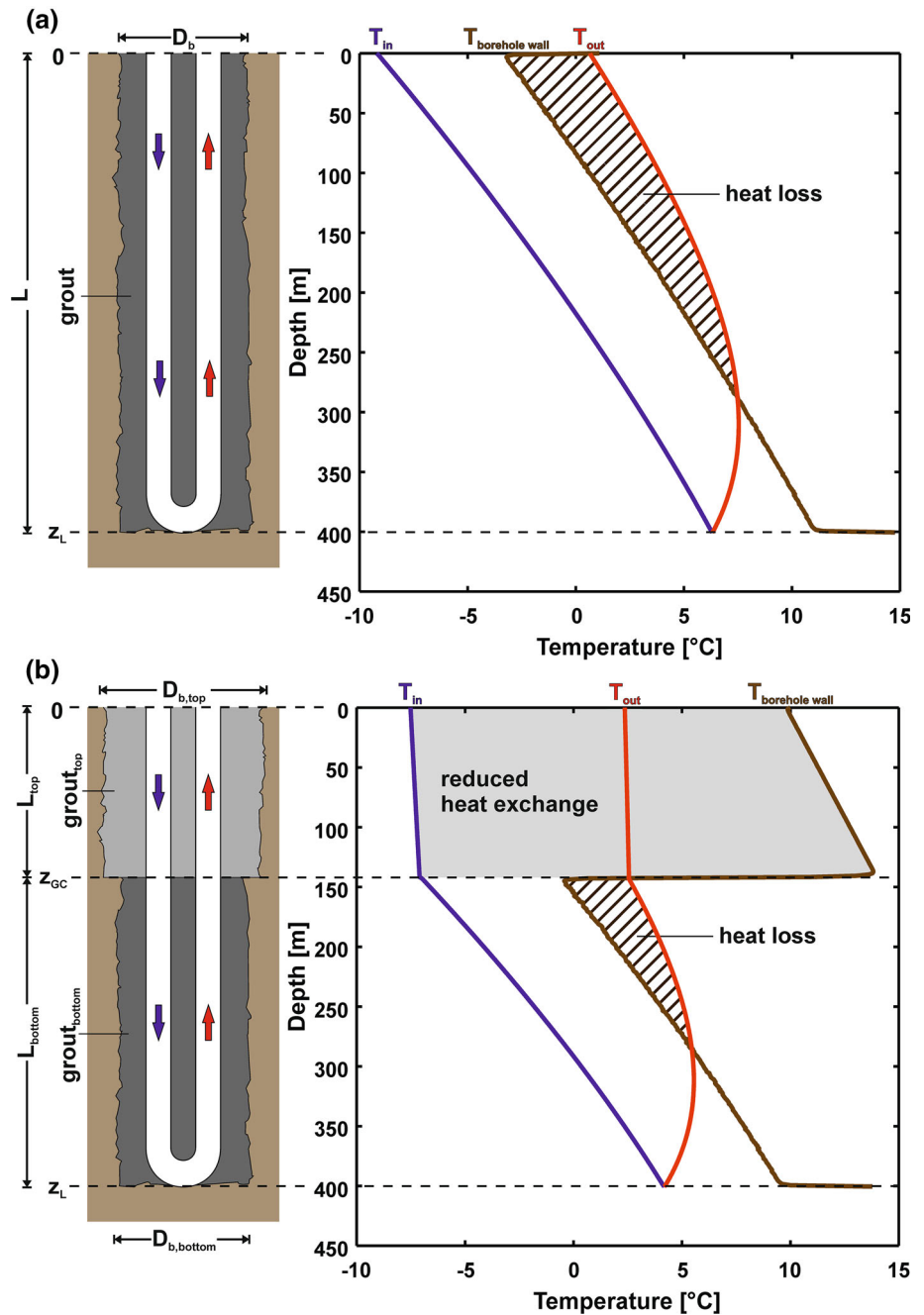
different distances from one another. Consequently, this problem cannot be overcome by optimal conditions of mesh spacing as suggested by Diersch et al. (2011b). Solving this problem to achieve better accuracy is, however, subject of further research. Altogether, the FEM-coupled analytical solution still achieves an acceptable accuracy compared to the fully discretized OGS model. The greater portion of the error can be attributed to the shortcomings in transient situations on short timescales, but since typical simulations of BHE arrays usually span

several years of operation, this deficit is negligible for most applications.

In the past, considerations of insulation focused on the pipes used in BHEs (Acuña et al. 2011; Acuña and Palm 2013) to mitigate thermal short-circuiting. However, the application example shows that an insulation of the borehole can have significant impact on the output temperature of a BHE. Despite its beneficial effect on deep BHEs and although it has been proposed for BTES systems for environmental reasons (Bär et al. 2015), to our knowledge

Table 5 Selection of optimization iteration results (after 30 days of operation)

Iteration	Insulation length (m)	Inlet and Outlet temperature (°C)	Target temperature (°C)	$COP_{theor, max}$	Relative change of $COP_{theor, max}$ compared to base case
0 (base case)	0	−9.21/0.66	35	8.97	not applicable
1	244.85	−9.73/0.15	35	8.84	−1.46 %
2	99.71	−7.73/2.14	35	9.38	+4.50 %
3	155.15	−7.54/2.34	35	9.43	+5.14 %
15 (optimal)	142.15	−7.52/2.36	35	9.44	+5.21 %

thermal borehole insulation has not been put into practice so far. Consequently, the development of grouts for BHEs has focused on enhancing the thermal conductivity (Lee et al. 2010) rather than reducing it. Thus, the thermal conductivity of the insulating grout in the application example does not refer to any available BHE grout, but to polyurethane. Polyurethane may very well be a potential candidate for a BHE insulating grout as it is watertight, has a very low thermal conductivity and is already in use for sealing wellbores in other applications (Mansure 2002; Zawislanski and Faybishenko 1999). Thus, a thermal conductivity as low as 0.04 W m^{-1} K^{-1} is a reasonable assumption.

It is necessary to evaluate the effect of the borehole insulation on the system performance for each scenario specifically. Heat pump specifications, heat losses and the load profile for the heat demand have to be taken into account. As building specifications are beyond the scope of this paper, the performance increase of the synthetic application scenario can only consider the improvement of the theoretical maximum COP neglecting all losses an actual heat pump would have. However, the results still provide a good estimate on the magnitude of a possible performance gain by an insulated borehole.

A gain of 5 % in heat pump performance may appear miniscule considering the increased costs for drilling with a larger borehole diameter and fitting the BHE with the insulation. Simply extending the BHE or adding a second BHE instead of using insulation could achieve the same efficiency gain. At least for U-pipe and double U-pipe BHEs extending the borehole length is not a viable option due to the increased thermal short-circuiting mentioned above. A comparative simulation shows that an uninsulated BHE with the same specifications, but twice the length (i.e., 800 m) provides an outlet temperature of 1.95 °C after 30 days in the described operational scenario. This corresponds to a theoretical maximum COP of 9.32 and a relative COP increase of 3.9 %. Extending the BHE proves to be effective, but even so the borehole insulation provides better results. Furthermore, doubling the borehole length represents a considerable rise in investment costs and does

not even factor in the increased power consumption for the circulation pump, which is about twice as high.

On the other hand, using two BHEs without insulation instead of an ideally insulated one can be a cost-saving alternative. Applying the mathematical optimization algorithm on a system of two identical BHEs without insulation, which are 5 m apart and have the load of 20 kW split equally among them, yields a required length of 162.60 m each to match the outlet temperature of the ideally insulated BHE. While the setup with two shorter BHEs results in saving about 19 % of total borehole length as well as pumping power (considering the described scenario with 0.5 l/s per BHE) compared to the single insulated 400 m BHE, the two BHEs without insulation also require more space at the surface. With only 5 m distance in between, the BHEs will eventually influence each other, which will result in decreasing outlet temperatures. If the reservoir is not replenished by heat storage cycles or prolonged recovery phases, the distance between the BHEs has to be increased even further. For arrays of BHEs this can raise the required surface area significantly. As mentioned before, recharging the reservoir by heat storage cycles can have a negative impact on the drinking water quality in the topmost aquifer and can therefore be legally restricted. BHEs as short as ~160 m are likely to affect this aquifer along a large part of their length, which limits the possibilities of replenishment by heat storage. Therefore, a borehole insulation is a favorable option to increase BHE efficiency where deeper boreholes are required due to limited space in urban areas (Gehlin et al. 2016) or even a necessity, when legal regulations require a reduction of the thermal impact on the topmost aquifer (Bär et al. 2015; Sass et al. 2016b).

Summary and conclusion

Particular advanced applications for borehole heat exchangers require some of the borehole properties to change with depth. This study presents an efficient analytical solution for modeling such depth-dependent

properties. The solution can accommodate future developments on thermal resistance and capacity networks for borehole heat exchangers. If coupled to a transient model for the subsurface heat transport, it is sufficiently accurate to save expensive and cumbersome simulations of fully discretized borehole heat exchangers. This method allows for the implementation of properties like increased borehole diameters and thermal resistances, which can act as borehole insulation, even for simulations of larger arrays of borehole heat exchangers.

References

Acuña J, Palm B (2013) Distributed thermal response tests on pipe-in-pipe borehole heat exchangers. Appl Energy 109:312–320. doi:10.1016/j.apenergy.2013.01.024

Acuña J, Mogensen P, Palm B (2011) Distributed thermal response tests on a multi-pipe coaxial borehole heat exchanger. HVAC&R Res 17:1012–1029. doi:10.1080/10789669.2011.625304

Ageb AE (2013) Anwendungsbilanzen für die Endenergiesektoren in Deutschland in den Jahren 2011 und 2012 mit Zeitreihen von 2008 bis 2012. Bundesministerium für Wirtschaft und Technologie, Berlin

Angelino L, Dumas P, Latham A (2014) EGEC Market Report 2013/2014 Update, 4 edn. European Geothermal Energy Council—EGEC

Bär K, Rühaak W, Welsch B, Schulte D, Homuth S, Sass I (2015) Seasonal high temperature heat storage with medium deep borehole heat exchangers. Energy Procedia 76:351–360. doi:10.1016/j.egypro.2015.07.841

Bauer D, Heidemann W, Müller-Steinhagen H, Diersch HJG (2011) Thermal resistance and capacity models for borehole heat exchangers. Int J Energy Res 35:312–320. doi:10.1002/er.1689

Bauer S, Beyer C, Dethlefsen F, Dietrich P, Duttmann R, Ebert M, Feeser V, Görke U, Köber R, Kolditz O, Rabbel W, Schanz T, Schäfer D, Würdemann H, Dahmke A (2013) Impacts of the use of the geological subsurface for energy storage: an investigation concept. Environ Earth Sci 70:3935–3943. doi:10.1007/s12665-013-2883-0

Bauer S, Pfeiffer T, Boockmeyer A, Dahmke A, Beyer C (2015) Quantifying induced effects of subsurface renewable energy storage. Energy Procedia 76:633–641. doi:10.1016/j.egypro.2015.07.885

Boockmeyer A, Bauer S (2014) High-temperature heat storage in geological media: high-resolution simulation of near-borehole processes. Géotechnique Lett 4:151–156. doi:10.1680/geolett.13.00060

Brent RP (1973) Algorithms for minimization without derivatives. Dover, Mineola

Diersch HJG, Bauer D, Heidemann W, Rühaak W, Schätzl P (2011a) Finite element modeling of borehole heat exchanger systems: part 1. Fundam Comp Geosci 37:1122–1135. doi:10.1016/j.cageo.2010.08.003

Diersch HJG, Bauer D, Heidemann W, Rühaak W, Schätzl P (2011b) Finite element modeling of borehole heat exchanger systems: part 2. Numer Simul Comp Geosci 37:1136–1147. doi:10.1016/j.cageo.2010.08.002

Eskilson P, Claesson J (1988) Simulation model for thermally interacting heat extraction boreholes. Numer Heat Transf 13:149–165

Gehlin SEA, Spitler JD, Hellström G (2016) Deep boreholes for ground source heat pump systems—scandinavian experience and future prospects. Paper presented at the ASHRAE Winter Meeting, Orlando, Florida, 23–27 Jan 2016

Haehnlein S, Bayer P, Blum P (2010) International legal status of the use of shallow geothermal energy. Renew Sustain Energy Rev 14:2611–2625. doi:10.1016/j.rser.2010.07.069

Kolditz O, Bauer S (2004) A process-oriented approach to computing multi-field problems in porous media. J Hydroinformatics 6:225–244

Kolditz O, Bauer S, Bilke L, Böttcher N, Delfs JO, Fischer T, Görke UJ, Kalbacher T, Kosakowski G, McDermott CI, Park CH, Radu F, Rink K, Shao H, Shao HB, Sun F, Sun YY, Singh AK, Taron J, Walther M, Wang W, Watanabe N, Wu Y, Xie M, Xu W, Zehner B (2012) OpenGeoSys: an open-source initiative for numerical simulation of thermo-hydro-mechanical/chemical (THM/C) processes in porous media. Environ Earth Sci 67:589–599. doi:10.1007/s12665-012-1546-x

Lee C, Lee K, Choi H, Choi H-P (2010) Characteristics of thermally-enhanced bentonite grouts for geothermal heat exchanger in South Korea. Sci China Ser E-Technol Sci 53:123–128. doi:10.1007/s11431-009-0413-9

Lund JW, Freeston DH, Boyd TL (2005) Direct application of geothermal energy: 2005 Worldwide review. Geothermics 34:691–727. doi:10.1016/j.geothermics.2005.09.003

Mansure AJ (2002) Polyurethane grouting geothermal lost circulation zones. Paper presented at the IADC/SPE Drilling Conference, Dallas, Texas, 26–28 Feb 2002

Nakevska N, Schincariol RA, Dehkordi SE, Cheadle BA (2015) Geothermal waste heat utilization from in situ thermal bitumen recovery operations. Groundwater 53:251–260. doi:10.1111/gwat.12196

Reddy JN, Gartling DK (2010) The finite element method in heat transfer and fluid dynamics, 3rd edn. CRC Press, Boca Raton

Sass I, Brehm D, Coldewey WG, Dietrich J, Klein R, Kellner T, Kirschbaum B, Lehr C, Marek A, Mielke P, Müller L, Panteleit B, Pohl S, Porada J, Schiessl S, Wedewardt M, Wesche D (2016a) Shallow geothermal systems—recommendations on design, construction, operation and monitoring. Ernst & Sohn, Berlin

Sass I, Welsch B, Schulte DO (2016b) Mitteltiefe Erdwärmesondenspeicher—Lösung für den Nutzungskonflikt Grundwasserschutz versus Geothermienutzung? Paper presented at the 7. Bochumer Grundwassertag, Bochum, 17 Mar 2016

Schulte DO, Rühaak W, Oladyshkin S, Welsch B, Sass I (2016) Optimization of medium-deep borehole thermal energy storage systems. Energy Technol 4:104–113. doi:10.1002/ente.201500254

The MathWorks (2015a) MATLAB 2015b. The MathWorks Inc, Natick

The MathWorks (2015b) MATLAB 2015b Global Optimization Toolbox. The MathWorks Inc, Natick

Welsch B, Rühaak W, Schulte DO, Bär K, Homuth S, Sass I (2015) A comparative study of medium deep borehole thermal energy storage systems using numerical modeling. In: Proceedings World Geothermal Congress, Melbourne, 19–24 Apr 2015

Zawislanski PT, Faybishenko B (1999) New casing and backfill design for neutron logging access boreholes. Ground Water 37:33–37. doi:10.1111/j.1745-6584.1999.tb00955.x

Appendix E:
BASIMO – borehole heat exchanger array simulation and optimization tool

Published as:

Schulte DO, Rühaak W, Welsch B and Sass I (2016): BASIMO – borehole heat exchanger array simulation and optimization tool, Energy Procedia, v. 97, p. 210-217, doi:10.1016/j.egypro.2016.10.057.

European Geosciences Union General Assembly 2016, EGU
Division Energy, Resources & Environment, ERE

BASIMO – borehole heat exchanger array simulation and optimization tool

Daniel Otto Schulte[a,b,]*, Wolfram Rühaak[a,b], Bastian Welsch[a,b], Ingo Sass[a,b]

[a]Technische Universität Darmstadt, Institute of Applied Geosciences, Department of Geothermal Science and Technology, Schnittspahnstrasse 9, 64287 Darmstadt, Germany
[b]Darmstadt Graduate School of Excellence Energy Science and Engineering, Technische Universität Darmstadt, Jovanka-Bontschits-Straße 2, 64287 Darmstadt, Germany

Abstract

Innovative applications and novel modifications of borehole heat exchangers (BHE) require new simulation tools. Currently, features like inclined or partly insulated boreholes necessitate fully discretized models. However, those models come at high computational cost. We present a tool, which uses an analytical solution for the BHE coupled with a numerical solution for the subsurface heat transport. A tetrahedron mesh bypasses the limitations of structured grids for borehole path geometries, while BHE properties changing with depth are considered. The tool benefits from the fast analytical solution of the BHEs while still allowing for a detailed consideration of the BHE properties.

Keywords: borehole heat exchangers; numerical modelling; mathematical optimization; borehole thermal energy storage

1. Introduction

Globally, space heating and domestic hot water production constitute about a quarter of the final energy consumption [1]. In countries, which are affected by winter seasons, this fraction can be substantially higher (cf. [2]). Renewable energy sources like solar collectors are increasingly used to cover the heat demand [3, 4]. They have the

---

* Corresponding author. Tel.: +49-6151-16-25675; fax: +49-6151-16-23601.
  E-mail address: schulte@geo.tu-darmstadt.de

potential to reduce the consumption of fossil fuels and to mitigate the CO_2 emissions. However, like the demand, the renewable heat supply is subject to seasonality in higher latitudes. Excess heat is available in summer, while the heat demand is highest in winter. Consequently, renewable heat sources rely on seasonal storage systems [3-8]. Shallow arrays of borehole heat exchangers are already in use for seasonal heat storage at comparably low temperature levels [9-12]. In many countries legal regulations restrict alterations of the groundwater that may have a negative impact on the drinking water quality [13]. Excessive heating of the shallow subsurface can induce microbial growth and, therefore, has to be prevented in these aquifers [14].

Instead, medium deep borehole thermal energy storage systems (BTES) can store the heat in greater depth at high temperature levels evading the topmost aquifers. For that purpose, medium deep BTES have to be fitted with an insulation in the upper section of the borehole. This can be achieved by larger borehole diameters and the use of insulating grouting material in the regarding borehole section. [15-17]

Compared to shallow installations, drilling is an even more critical cost factor for the construction of a medium deep BTES. Thus, simulations of the storage operation are imperative prior to the investment. Furthermore, the design of the BHE array has to be optimized to avoid badly sized systems. Consequently, a simulator for the BHE array should allow for mathematical optimization [17]. Also, a partly insulated borehole corresponds to depth-dependent BHE properties and implies additional special requirements to numerical models. These requirements rule out most of the available simulation tools like EED [18], FEFLOW [19] or line source-based approaches (e.g. [20, 21]). Up to now, only fully discretized models could fulfill these requirements. However, fully discretized models come at high computational cost and are not a viable option for the simulation of entire arrays of BHEs.

In this paper, we present BASIMO: a **B**orehole heat exchanger **A**rray **SIM**ulation and **O**ptimization tool. It comprises a simulator that employs the finite element method (FEM) to calculate the transient conductive heat transport in the subsurface. The thermal response of the BHEs is calculated using an adapted analytical solution based on thermal resistance and capacity models (TRCM), which allows for the consideration of partly insulated boreholes, but still grants fast computation compared to fully discretized models [22]. As the simulator is MATLAB-based, it can be readily used with the MATLAB Global Optimization Toolbox [23] for the mathematical optimization of the storage performance with respect to variable system parameters. For elaborate optimization problems, the computational time can be reduced using a previously trained proxy model [17]. Furthermore, it is possible to link BASIMO to building models for coupled BTES-building simulations.

2. BASIMO

BASIMO was initially developed for the design optimization of BTES [17]. On the one hand, this determines the required features for the simulator, namely the consideration of borehole insulation and the possibility to couple the simulator to mathematical optimization algorithms. On the other hand, it allows for certain simplifications: BTES systems typically target low permeable rocks for heat storage, as groundwater flow decreases the storage efficiency [15]. Therefore, BASIMO neglects the convective heat transport in the subsurface, which decreases the computational cost significantly. Nevertheless, BASIMO can also be used for the simulation of regular BHE arrays in mere heat extraction scenarios as long as groundwater flow is non-existent. BASIMO applies a dual continuum approach where the numerical calculation of the subsurface heat transport is separated from the simulation of the thermal interactions within the BHEs. The latter can be solved analytically, which significantly saves computation time otherwise required for the full discretization of the borehole. The program structure of the simulator is illustrated in Fig. 1.
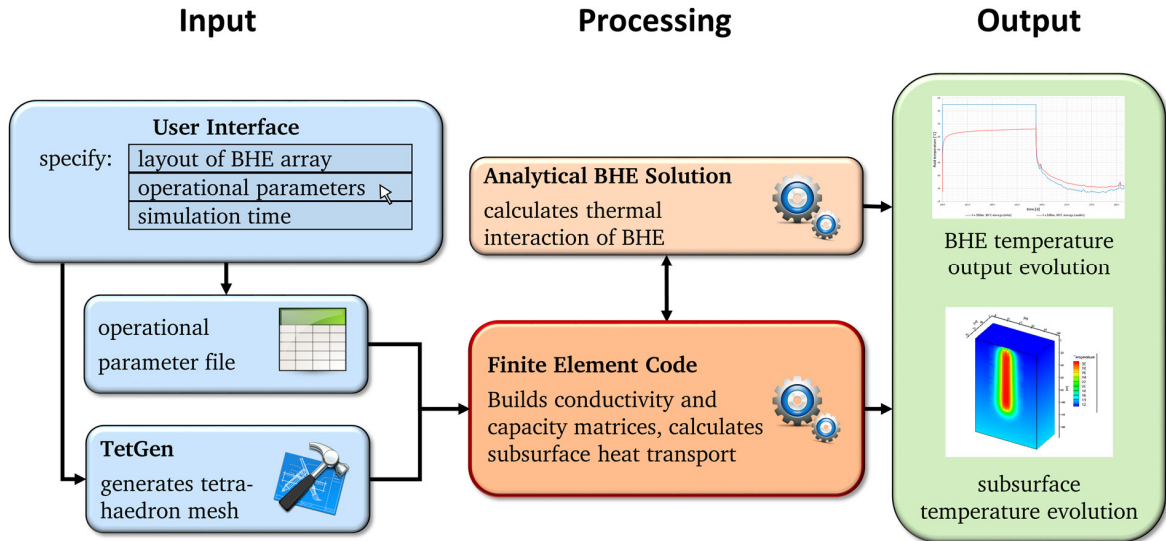
Input **Processing** **Output**

Fig. 1. Schematic of the program structure of the BASIMO simulator, arrows indicate the interaction of the program components.

2.1. Finite Element Method and Tetrahedron Mesh

The core of BASIMO is an improved MATLAB FEM implementation (Galerkin method of weighted residuals [24]) originally developed by Alberty et al. [25]. It calculates the transient heat diffusion in the subsurface by numerically solving Fourier's Law of heat conduction for the model domain, which is discretized as a tetrahedron mesh generated with TetGen [26]:

$$\rho_s c_s \frac{\partial T}{\partial t} = \nabla \cdot \left(\lambda_s \nabla T \right) + q_Q \tag{1}$$

With ρ_s: soil density, c_s: volumetric heat capacity of the soil, T: Temperature, t: time, λ_s: thermal conductivity of the soil and q_Q: heat sources and sinks as internal heat generation per unit volume. The tetrahedron mesh is unstructured and eliminates any restrictions for the bore path geometry. Consequently, inclined BHEs can be modeled in BASIMO (Fig. 2a), whereas semi-structured triangular meshes or fully structured rectangular meshes, typical for most available simulators, only allow for the consideration of vertical boreholes.

The principles of the FEM in heat transfer problems have been described for instance by Reddy and Gartling [27]. Ultimately, the weak formulation of the partial differential equation (1) summarized over the entire model domain can be expressed in a short matrix notation:

$$\mathbf{M\dot{T}} + \mathbf{KT} = \mathbf{F(T)} \tag{2}$$

Where $\mathbf{M}$ represents the heat capacity matrix, $\mathbf{K}$ is the thermal conductivity matrix and $\mathbf{F}$ is the right-hand side vector including source terms, whereas $\mathbf{T}$ is the solution vector, i.e. the subsurface temperature. The BHEs act as heat sources or sinks in the FEM mesh and contribute to the right-hand side $\mathbf{F}$. As the heat transfer from and to the BHEs depends on the temperature of the surrounding reservoir rock, their contribution to the source terms in $\mathbf{F}$ depends on the solution vector $\mathbf{T}$. Consequently, the system of equations (2) is non-linear. A predictor-corrector method is used with a second order Adams-Bashforth predictor and a Crank-Nicolson corrector to solve the system of equations. It

allows for automated time stepping after a few initial time steps provide the acceleration vectors of **T** required for the predictor. A Picard iteration scheme is applied on the corrector to consider the non-linearity. [27]

As MATLAB is an interpreted programming language, the program's execution can have significant performance drawbacks compared to compiled code. Especially the assembly of the conductivity and capacity matrices **M** and **K** becomes very slow for large models. This problem is bypassed using C/C++ code [28], which assembles the matrices outside of MATLAB and speeds up the computation by several orders of magnitude. In the same way, other libraries can be integrated, for example, to replace MATLAB's solver by GPU based routines.

2.2. Analytical Solution for Borehole Heat Exchangers

The thermal interaction of the BHEs is calculated by a one-dimensional analytical thermal resistance and capacity model [29-31]. Fed with inlet temperature and flow rate data, it provides the temperature distribution in the inlet and outlet pipes in predefined depth levels. The solution takes into account all thermal and hydraulic parameters of the BHE materials and the borehole wall temperature. In the finite element mesh, the BHEs are discretized as vertical or inclined (Fig. 2a) lines of mesh nodes. The temperature at these nodes defines the borehole wall temperature and is passed to the analytical solution. In return, the analytical solution sets heat sources based on the thermal resistances within the BHEs and the difference between the borehole wall temperature and the calculated BHE fluid temperature at the corresponding nodes (see above). The same solution is used in the commercial software FEFLOW [19], but has been improved for BASIMO to take into account BHE properties changing with depth [22]. This allows for the consideration of insulation within sections of the borehole (Fig. 2b).
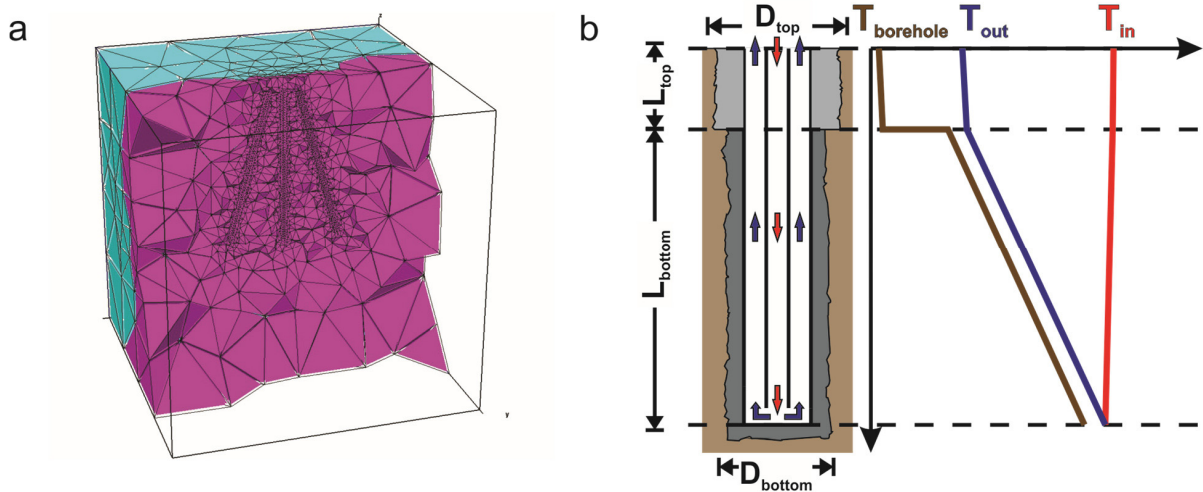

Fig. 2. (a) Cross section of a tetrahedron mesh of a reservoir with inclined BHEs; (b) schematic of an insulated coaxial BHE with centered inlet (not to scale) and the corresponding temperature profiles of the borehole wall and of the fluid in the inlet and the outlet pipe , D: borehole section diameter, L: borehole section length (simplified after [22]).

2.3. User Input and Model Output

BASIMO allows for a detailed model description by the user. Except for the geometry of the BHE array, the model is parametrized by self-explanatory Excel sheets. The user can change the model settings by editing these files without having to tamper with the code. This way, the model can be generated with a simple stratigraphy of the subsurface, where each layer is defined by its bottom depth and can be assigned a different bulk thermal conductivity, density and specific heat capacity.

In a similar manner, the operation of the BHEs is set up by user-defined time steps, for which the BHEs can be assigned a mass flow rate and a corresponding inlet temperature or heat extraction rate. As the analytical solution for the BHEs cannot handle heat extraction rates by itself, an additional Picard iteration loop in BASIMO determines the corresponding inlet temperature. Furthermore, BASIMO allows the user to choose between U-pipe, double U-pipe and coaxial BHEs in the operation setup, which includes the choice between central or annular inlet for coaxial BHEs. These settings apply for all BHEs in the array alike.

The BHEs, on the other hand, are each dealt with independently in a separate file. A detailed configuration allows for the consideration of the following parameters:

- Borehole diameters (two independent sections for possible insulation)
- Pipe diameters
- Pipe wall thicknesses
- Shank space (U-pipe and double U-pipe only)
- Pipe thermal conductivities
- Fluid specific heat capacity
- Fluid thermal conductivity
- Fluid dynamic viscosity
- Fluid density
- Grout thermal conductivities (two independent sections for possible insulation)
- Length of insulation

The temperature dependency of the thermo-physical parameters is not taken into account. The borehole insulation can be disregarded by keeping the borehole diameters and the grout thermal conductivities the same.

Lastly, it is possible, to change a few settings, which concern the numerical calculation and the program output of BASIMO. Depending on the model size and the scheduled operation time, these settings can greatly influence the stability, the accuracy and the simulation time:

- Time integration weighting coefficient of the corrector to change from Crank-Nicolson to fully implicit
- Time stepping control tolerance error
- Picard iteration tolerance error
- Maximum number of Picard iterations
- Initial time step size
- Maximum time step acceleration factor
- Maximum time step size
- Switch for graphical output during the simulation
- Switch for detailed data output for post-processing

BASIMO provides a subroutine for generating the finite element mesh. It first spatially delimits the model domain and then defines the bore paths of the BHEs as lines of nodes in a Cartesian coordinate system before calling TetGen [26] to generate the tetrahedral mesh of finite elements. While the geometrical arrangement of the BHEs is predefined by templates depending on the number of BHEs (Fig. 3), the user can chose their number, their length and their respective distance towards each other. Also, the inclination angle can be defined. In that case, all BHEs radially dip away from the center. If there is a central BHE in the particular arrangement, it remains vertical. The templates try to place the BHEs in a compact arrangement, as a low enveloping surface to storage volume ratio is important for BTES systems. However, BASIMO will also accept user-defined meshes as long as they come with separate files that specify the coordinates of the mesh nodes for each BHE.
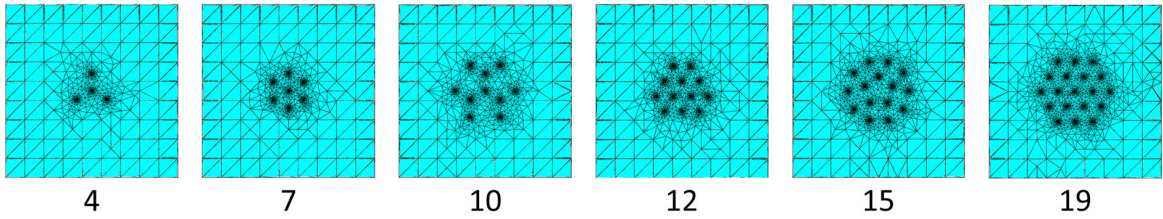
Fig. 3. Exemplary templates for the arrangements of BHEs in the discretized tetrahedron mesh (overhead perspective) and the corresponding number of boreholes, model edge length: 100 m.
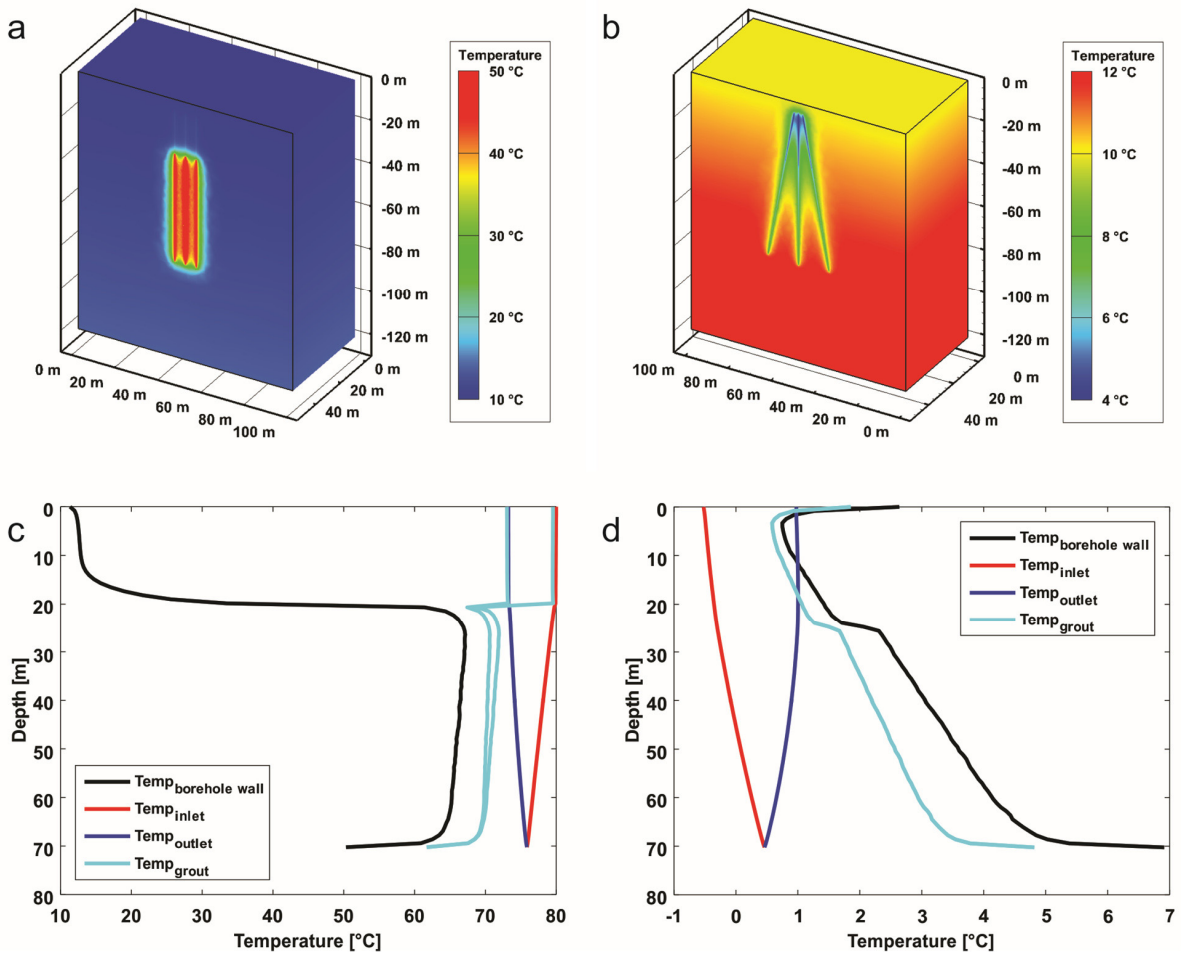

Fig. 4. BASIMO outputs: model cross sections (post-processed) showing the subsurface temperature distribution in a 7 BHE x 70 m array(cf. Fig 3) after 90 days of (a) heat storage in a homogeneous reservoir (granite) with borehole insulation and (b) heat extraction from a stratified reservoir with inclined boreholes (10°); corresponding BHE temperature profiles after 90 days of (c) heat storage in a homogeneous reservoir with borehole insulation and (d) heat extraction from a stratified reservoir with inclined boreholes (10°); stratification: 0-20 m: sandstone, 20-120 m: quartzite.

As mentioned above, BASIMO can return various simulation outputs. Every simulation provides time series of the BHE return temperatures and the final temperature distribution of the subsurface (Fig. 4a & Fig 4b). The latter can also be saved as a time series of distinct time steps for post-processing purposes. Furthermore, it is possible to activate a graphical output during the simulation, which plots the time step size and the inlet and outlet temperature during the simulation, as well as the current temperature profile of the BHE (i.e. borehole wall, downstream pipe and upstream pipe temperature, Fig. 4c & Fig 4d).

2.4. Optimization

Since the code of BASIMO is written in MATLAB, it can be easily embedded in a subroutine called as an objective function or as a nonlinear constraint function in the MATLAB Global Optimization Toolbox [23]. This way, various design or operational parameters can be optimized with regard to characteristic performance indicators. For example, BASIMO can minimize the size of a BHE array for heat storage (i.e. number and length of BHEs), which corresponds to the investment costs, for a specified amount of heat to be provided by the BTES [17]: BASIMO is called as constraint function to ensure sufficient heat provision by the considered array designs. Similarly, the outlet temperature of a single BHE can be optimized by finding the ideal length of borehole insulation [22]. In this case, BASIMO is the objective function called by the optimization algorithm.

Despite the advantages of BASIMO over other programs, simulations of large systems can still be lengthy. This can pose an impasse for some optimization problems that require a large number of function calls to converge on a solution. The problem can be overcome by generating a proxy model from considerably fewer training simulations by arbitrary polynomial chaos expansion [17, 32]. Whereas the computational effort for large models is still high, they only have to be computed once. The resulting proxy model can be evaluated by the optimization algorithm in a matter of seconds, as it consists only of a polynomial instead of a numerical model.

The adaptability of the MATLAB code not only enables its use in optimization algorithms. With only a few simple changes to the code it is possible to couple BASIMO with building models, which consider the heating infrastructure like heat pumps and buffer storages on the surface. Heat demand profiles with a high temporal resolution can be taken into account. This way, the dynamic interplay of the involved system components can be simulated with unprecedented and realistic detail. [33]

3. Outlook

BASIMO is a versatile tool specifically tailored for the simulation and the optimization of BTES systems. It closes capability gaps of currently available simulators like the consideration of borehole insulation and unrestricted bore path geometries, while still maintaining reasonable computational performance. In benchmarks simulations, BASIMO showed good agreement with other simulators [17, 22]. The code is still under development. Future work will focus on the implementation of the transient convective heat transport calculation in the subsurface and on further performance improvements.

Acknowledgements

References

[1] IEA (International Energy Agency). *Heating Without Global Warming – Market Developments and Policy Considerations for Renewable Heat*. Paris: OECD/IAE; 2014.
[2] AGEB (Arbeitsgemeinschaft Energiebilanzen). *Anwendungsbilanzen für die Endenergiesektoren in Deutschland in 2011 und 2012 mit Zeitreihen von 2008 bis 2012*. Berlin: AGEB; 2013.
[3] Schmidt T, Mangold D, Müller-Steinhagen H. Central solar heating plants with seasonal storage in Germany. *Sol Energy* 2004;76:165-174.
[4] Bauer D, Marx R, Nußbicker-Lux J, Ochs F, Heidemann W, Müller-Steinhagen H. German central solar heating plants with seasonal heat storage. *Sol Energy* 2010;84:312-320.

[5] Dinçer İ, Rosen MA. *Thermal Energy Storage*. Hoboken: John Wiley & Sons, Ltd; 2011.

[6] Pine. P, Cruickshank CA, Beausoleil-Morrison I, Wills A. A review of available methods for seasonal storage of solar thermal energy in residential applications. *Renewable and Sustainable Energy Reviews* 2011;15:3341-3359.

[7] Xu J, Wang R, Li Y. A review of available technologies for seasonal thermal energy storage. *Solar Energy* 2014;103:610-638.

[8] Hesaraki A, Holmberg S, Haghighat F. Seasonal thermal energy storage with heat pumps and low temperatures in building projects – A comparative review. *Renew Sust Energ Rev* 2015;43:1199-1213.

[9] Lundh M, Dalenbäck JO. Swedish solar heated residential area with seasonal storage in rock: Initial evaluation. *Renewable Energy* 2008;33:703-711.

[10] Sibbitt B, McClenahan D, Djebbar R, Thornton J, Wong B, Carriere J, Kokko J. The Performance of a High Solar Fraction Seasonal Storage District Heating System – Five Years of Operation. *Energy Procedia* 2012;30:856-865.

[11] Mielke P, Bauer D, Homuth S, Götz A, Sass I. Thermal effect of a borehole thermal energy store on the subsurface. *Geothermal Energy* 2014;2:1-15.

[12] Reuß M. The use of borehole thermal energy storage (BTES) systems. In: *Advances in Thermal Energy Storage Systems*, Cabeza LF editor. Cambridge: Woodhead Publishing; 2015. p. 117-147.

[13] Haehnlein S, Bayer P, Blum P. International legal status of the use of shallow geothermal energy. *Renewable and Sustainable Energy Reviews* 2010;14:2611-2625.

[14] Griebler C, Kellermann C, Stumpp C, Hegler F, Kuntz D Walker-Hertkorn S. *Auswirkungen thermischer Veränderungen infolge der Nutzung oberflächennaher Geothermie auf die Beschaffenheit des Grundwassers und seiner Lebensgemeinschaften – Empfehlungen für eine umweltverträgliche Nutzung, Texte 54/2015*. Dessau-Roßlau: Umweltbundesamt; 2015.

[15] Bär K, Rühaak W, Welsch B, Schulte D, Homuth S, Sass I. Seasonal High Temperature Heat Storage with Medium Deep Borehole Heat Exchangers. *Energy Procedia* 2015;76:351-360.

[16] Sass I, Welsch B, Schulte D. *Mitteltiefe Erdwärmesondenspeicher – Lösungen für den Nutzungskonflikt Grundwasserschutz versus Geothermienutzung?* At: 7. Bochumer Grundwassertag, Bochum, Germany; 17.03.2016.

[17] Schulte DO, Rühaak W, Oladyshkin S, Welsch B, Sass I. Optimization of Medium-Deep Borehole Thermal Energy Storage Systems. *Energy Technology* 2016;4:104-113.

[18] Hellström G, Sanner B. *Software for dimensioning of deep boreholes for heat extraction*. In: Proceedings of the Calorstock'94, Espoo, Finland; 1994.194-200.

[19] Diersch HJG. *FEFLOW Finite Element Modeling of Flow, Mass and Heat Transport on Porous Media*. Berlin, Heidelberg: Springer-Verlag; 2014.

[20] de Paly M, Hecht-Méndez J, Beck M, Blum P, Zell A, Bayer P. Optimization of energy extraction for closed shallow geothermal systems using linear programming. *Geothermics* 2012;43:57-65.

[21] Bayer P, de Paly M, Beck M. Strategic optimization of borehole heat exchanger fields for seasonal geothermal heating and cooling. *Applied Energy* 2014;136:445-453.

[22] Schulte DO, Welsch B, Boockmeyer A, Rühaak W, Bär K, Bauer S, Sass I. Modeling Insulated Borehole Heat Exchangers. *Environmental Earth Sciences* 2016, in press.

[23] The MathWorks. MATLAB 2015b Global Optimization Toolbox. Natick, Massachusetts: The Mathworks, Inc; 2015.

[24] Zienkiewics OC, Taylor RL, Thu JZ. *The Finite Element Method: Its Basis and Fundamentals*. 6th ed. Oxford: Butterworth-Heinemann; 2005.

[25] Alberty J, Carstensen C, Funken SA. Remarks around 50 lines of Matlab: short finite element implementation. *Numerical Algorithms* 1999;20:117-137.

[26] Si H. Constrained Delaunay tetrahedral mesh generation and refinement. *Finite elements in Analysis and Design* 2010;46:33-46.

[27] Reddy JN, Gartling DK. *The Finite Element Method in Heat Transfer and Fluid Dynamics*. 3rd ed. Boca Raton: CDC Press; 2010.

[28] Rühaak W, Bense VF, Sass I. 3D hydro-mechanically coupled groundwater flow modelling of Pleistocene glaciation effects. *Computers & Geosciences* 2014;37:88-99.

[29] Bauer D, Müller-Steinhagen H, Diersch HJG. Thermal resistance and capacity models for borehole heat exchangers. *International Journal of Energy Research* 2011;35:312-320.

[30] Diersch HJG, Bauer D, Heidemann W, Rühaak W, Schätzl P. Finite element modeling of borehole heat exchanger systems: part 1. Fundamentals. *Computers & Geosciences* 2011;37:1122-1135.

[31] Eskilson P, Claesson J. Simulation model for thermally interacting heat extraction boreholes. *Numerical Heat Transfer* 1988;v13:149-165.

[32] Oladyshkin S, Nowak W. Polynomial Response Surfaces for Probabilistic Risk Assessment and Risk Control via Robust Design. In: *Novel Approaches and Their Applications in Risk Assessment*, Luo Y editor. Rijeka: InTech; 2012. p. 317-344.

[33] Welsch B, Rühaak W, Schulte DO, Bär K, Sass I. Advanced Coupled Simulation of Borehole Thermal Energy Storage Systems and Above Ground Installations. At: European Geoscience Union General Assembly 2016, Vienna, Austria; 17.-22.04.2016.

Appendix F:
Digital Supplement

CURRICULUM VITAE

EDUCATION

SCHULTE, DANIEL OTTO
Born on 19.09.1985 in Hagen, Germany

03/2013 – 12/2016
Institute of Applied Geosciences, Technische Universität Darmstadt
Darmstadt Graduate School of Excellence Energy Science and
Engineering
Doctorate studies
towards the degree of Doktor-Ingenieur

04/2010 – 12/2011
University of Canterbury, Christchurch, New Zealand
Studies of Geology
M.Sc. with distinction, grade: A-

10/2005 – 03/2010
Johannes Gutenberg-Universität, Mainz
Studies of Geology
Majors in Tectonics, Geophysics and Sedimentology

04/2005 – 10/2005
Technische Universität Darmstadt
Studies of Physics

09/1996 – 03/2004
Theresianum Mainz
High schoool
High school diploma, grade: 1.5

09/1992 – 07/1996
Deutsche Schule Moskau
Primary school

PROFESSIONAL
AND OTHER
EXPERIENCE

SINCE **09/2016**
Institute of Applied Geosciences, Technische Universität
Darmstadt
Darmstadt Graduate School of Excellence Energy Science and
Engineering
Research assistant

03/2013 – 08/2016
Institute of Applied Geosciences, Technische Universität Darmstadt
Darmstadt Graduate School of Excellence Energy Science and
Engineering
Research fellow

08/2014 – 01/2015
Institute of Petroleum Engineering, Heriot Watt-University, Edinburgh
Visiting scientist

03/2012 – 07/2013
Department of Operative Dentistry, Johannes Gutenberg-Universität,
Mainz
Research assistant

11/2009 – 12/2009
Dyckerhoff Zement AG
Internship

10/2009 – 11/2009
Hessian Agency for Environment and Geology
Internship

03/2007 – 07/2009
Department of Applied and Analytical Paleontology, Johannes
Gutenberg-Universität, Mainz
Student research assistant

04/2004 – 12/2004
Bundeswehr (German armed forces)
Compulsory military service
Enlisted in the reserve since 01/2005, promoted to reserve officer in
12/2008 (1st Lt)

AWARDS

03/2013 – 05/2016
PhD Scholarship of the Darmstadt Graduate School of Excellence
Energy Science and Engineering

2010
Scholarship of the German Academic Exchange Service for abroad
studies in New Zealand

SKILLS

Language skills
German (native), English (fluent), French (basics), Latin (basics),
Bulgarian (basics), Russian (basics)

Programming and computer skills
MATLAB, Python, MS Office, ArcGis, FEFLOW